ADVANCES IN ROCK CORE VOC ANALYSES FOR HIGH RESOLUTION CHARACTERIZATION OF CHLORINATED SOLVENT CONTAMINATION IN A DOLOSTONE AQUIFER

By

Jonathan R. Kennel

A thesis

presented to the University of Waterloo

in fulfillment of the

thesis requirement for the degree of

Master of Science

in

Earth Sciences

Waterloo, Ontario, Canada, 2008

AUTHOR'S DECLARATION

I hereby declare that I am the sole author of this thesis. This is a true copy of the thesis, including any required final revisions, as accepted by my examiners.

Jonathan Kennel

I understand that my thesis may be made electronically available to the public.

ABSTRACT

The current understanding of contaminant migration in fractured sedimentary rock aquifers is inadequate due to the difficulty in describing the geologic and hydrogeologic controls on contaminant fate and transport with appropriate detail. To address contamination at fractured rock sites, multiple methods focusing on different aspects of the hydrologic system are required, and particular emphasis needs to be placed on the rock matrix. This thesis shows the further development and utility of the decade-old rock core VOC method (i.e. CORE™), a rock matrix method, when used in conjunction with multiple high resolution datasets as it applies to a 100 m thick highly productive dolostone aquifer in Guelph, Ontario.

The research site and surrounding area, located in the northwestern quadrant of the city of Guelph, was a productive zone for water supply until the early 1990s when the two closest municipal supply wells (Sacco, Smallfield) were shut down (1991, 1993 respectively) due to volatile organic compounds (VOCs) in the groundwater. Trichloroethene (TCE), a VOC, was used as a degreaser at the Guelph site and likely entered the groundwater more than 20 years ago. The thin overburden, shallow water table, relatively constant dolostone mineralogy, proximity to the UW analytical laboratory, relatively simple plume composition showing minimal degradation, and local importance make this an excellent study site for TCE fate and migration in fractured sedimentary rocks.

This thesis is composed of four chapters. Chapter 1 provides a brief background to the rock core VOC method and gives the conceptual framework for the investigation. Chapter 2 focuses on the further development of the rock core VOC method by providing the field validation of a recently adapted extraction method for VOCs in rock core using microwave assisted extraction (MAE). This chapter also demonstrates the importance of rapid field preservation for samples, and compares MAE to shake-flask extraction and to the industry standard purge and trap method for VOCs on

solid matrices. Results indicate that the microwave assisted extraction (MAE) method typically provides equivalent or higher concentrations when compared with the shake-flask and purge and trap extraction methods, indicating more complete extraction or less loss during transfer and/or storage. The purge and trap method provided false negatives (i.e. non-detects) due to inadequate preservation, incomplete extraction, and the elevated detection limit for TCE. The necessity for field preservation was examined by comparing crushed rock samples preserved in methanol in the field to samples unpreserved in the field with a laboratory addition of methanol less than 12 hours later. Chapter 3 creates high resolution porosity and bulk density logs by using selected geophysical logging tools in combination with core derived physical properties. These logs are then used to calculate porewater concentrations from total contaminant mass concentrations obtained from the rock core VOC method and allows for assigning sample specific rock properties relevant to the conversion. This is beneficial because total mass estimates obtained from the rock core VOC method are not necessarily indicative of the groundwater concentrations given the presence of solid organic carbon controlled sorption. Chapter 4 is a demonstration of the discrete fracture network approach (Parker 2007) applied to the Guelph field site with emphasis on the insights gained through high resolution contaminant profiles generated from cored holes in or near the source area and along a transect. Together, these four chapters present a framework for investigating VOC contamination in fractured sedimentary rocks and with emphasis on evaluating recent advances in the rock core VOC methodology in a field site context.

ACKNOWLEDGEMENTS

I would like to thank my thesis co-supervisor Dr. Beth L. Parker for introducing me to fractured rock hydrogeology. I appreciate the valuable opportunities, insight, and direction she has graciously provided me with over the last few years. In addition, I would like to thank Drs. John A. Cherry and Tadeusz Górecki for serving on my advisory committee and sharing their vast and valuable experience and comments with me. Dr. Cherry's clarity of thought and direction was instrumental to the completion of this degree. I would like to thank my co-supervisor, Dr. Ramon Aravena, for providing administrative assistance for the completion of this degree. I would also like to thank the Natural Sciences and Engineering Research Council (NSERC), the Canadian Foundation for Innovation (CFI), Guelph Tool Inc., Schlumberger Water Services, Solinst Canada Ltd., Flexible Liner Underground Technologies Ltd., Co., and the University of Waterloo for providing funding and services to this research project.

There are many individuals who deserve thanks for making this research possible. First, I would like to thank the field technicians Bob Ingleton, Paul Johnson and Ryan Kroeker for providing knowledge and assistance during these studies. They have not only improved the quality of research but taught me many things. Next, I would like to thank Maria Górecka for her hard work analyzing the myriad of rock core VOC samples and help with the quality assurance and quality control of the samples. Additional samples were analyzed by Wayne Nobel from the University of Waterloo, Shirley Chatten of the University of Waterloo Organic Geochemistry Laboratory, and the Geotechnical Laboratory at Golder Associates. Peeter Pehme deserves the credit for collecting and organizing the majority of geophysical logging events and has helped me immeasurably in this project. Scott Piggot conducted the nuclear logging and provided me with direction on using that data. Mary Anne Hardy has kept everything running smoothly and continues to do so.

Thank you to the members of the research group who were always available to assist and discuss hydrogeology: Jessi Meyer, Dr. Jerome Perrin, Steve Chapman, Dr. Neils Hartog, Ben Swanson, Edison Amirtharaj, Rashmi Jadeja, and Dr. Tariq Cheema.

Chapter two is largely the result of two persons: Clare Stewart and Don Liu. Thank you for your hard work. Cooperation and coordination with Burnside and Gamsby and Mannerow Ltd. and in particular the following employees helped immensely: Dirk Gevaert, Matt Nelson, Matt Ballaban, Mary Kennedy, and Stephanie Goemans.

Thank you to previous and current grad students, Pat Quinn, Ryan Kroeker, Jessi Meyer, James Plett, Diane Austin, and Leanne Burns for friendship and advice.

Next I would like to thank the large number co-op students and other employees that have helped in the creation of this thesis in a variety of capacities, Shannon Robinson, Agata Górecka, Juliusz Górecki, Aaron Vandenhoff, Cameron McNaughton, Will Schinkel, Dave Fox, Reynold Chow, Justin Boudreau, Siavash Parsi, Laura Johnson, Scott Cousins, Kate Dekeyser and any others that I may have forgotten to mention.

TABLE OF CONTENTS

LIST OF TABLES

CHAPTER 2

CHAPTER 3

CHAPTER 4

LIST OF FIGURES

CHAPTER 1

CHAPTER 2

CHAPTER 3

CHAPTER 4

Chapter 1: Thesis Introduction

The predictive capabilities of flow and transport in fractured media are currently inadequate and one of the most challenging problems in hydrogeology (Berkowitz 2002). To address the difficulty inherent to fractured rock sites, Parker [2007] suggests the discrete fracture network (DFN) approach which is based on a suite of complementary high resolution spatial datasets (Figure 1.1). This approach examines individual fractures, fracture sets, and the rock matrix using multiple investigative methods; and in particular, using those methods that minimize the influence of borehole cross-connection. This thesis focuses on one of the fundamental techniques used at fractured rock sites contaminated with chlorinated solvents: the rock core VOC method.

The operating conceptual model for the plume research site is as designed by Parker [2007] and is building off the conceptual model for chlorinated solvent dense non-aqueous phase liquid (DNAPL) source zones in sedimentary rock presented by Parker et al. [1994, 1997](Figure 1.2). Initially, DNAPL contained in fractures dissolves to form aqueous groundwater contamination and migrates by advection in the fractures and also by diffusion into the surrounding rock matrix. Parker et. al. [1994] showed that DNAPL dissolution occurs over relatively short time periods and results in the transformation of DNAPL to aqueous and sorbed phase groundwater and matrix contamination keeping the majority of contaminant mass within or proximal to DNAPL locations in fractured porous media such as clayey deposits and sedimentary rocks (Figure 1.3). Studied for three decades, matrix diffusion conceptual models from Foster [1975] and Freeze and Cherry [1979] illustrate the accumulation of solutes in the rock matrix. However, DNAPL and solute interaction with the rock matrix varies from site to site and therefore requires site specific assessments.

Initially after a contaminant release, the direction of diffusive contaminant flux will be into the rock matrix, but at later times uncontaminated water coming into contact with the contaminated rock matrix will reverse the direction of mass flux to the fracture water (Parker, Gillham, & Cherry 1994;Parker, McWhorter, & Cherry 1997; Mutch, Scott, & Wilson 1993). The rock matrix, which initially acts as a sink for contamination, may slowly release the contamination and act as a long term contaminant source to the groundwater system (Parker, Gillham, & Cherry 1994; Mutch, Scott, & Wilson 1993;Polak et al. 2003) (Figure 1.4). Thus, targeting the rock matrix is a necessary component in fractured rock studies to find the majority of the contaminant mass (Goldstein et al. 2004), but also to be used as a diagnostic tool for understanding advective pathways (fracture network) and interactions with the rock matrix (Goldstein et al. 2004;Lawrence et al. 2006;Lawrence et al. 1990).

The rock core VOC method, with foundations going back more than a decade, relies on sampling the rock matrix in the field concurrently with coring. The relatively rapid dissolution of source zone DNAPL shown in Figure 1.3 allows coring to occur in suspected source zones without the fear of mobilizing NAPL (Figure 1.5). Rock core samples are taken preferentially near fractures and on both sides of the fracture in order to locate diffusion haloes and to determine contaminant migration pathways (Figure 1.6). The first field investigation using a prototype version of the current method occurred in a trichloroethene (TCE) contaminated fractured sandstone located in Simi California as reported by Sterling [1999]. This initial method which is designed from coring to sample and data analysis has evolved and been applied to over 66 coreholes at 14 sites since its inception (Parker 2007).

Turner [2001] applied the method to a fractured dolostone in Cambridge, ON and focused on a comingled metolachlor and TCE plume. Following this, a series of Master's students applied the methodology at 3 research sites (Hurley [2003] (sandstone,

California), Burns [2005] (dolostone, Cambridge), Meyer [2005] (sandstone, Wisconsin), Austin [2005] (sandstone, Wisconsin), Plett [2006] (dolostone, Cambridge)). These theses have helped to refine the conceptual models for contaminated sedimentary rock systems and some of the key points realized are, demonstrating that the majority of contaminant mass resides in the rock matrix, DNAPL is not commonly found even in the release areas, plume retardation and attenuation can be very large, many fractures contribute to the migration of contaminants, and the effects of cross-contamination can provide misleading information (Sterling et al. 2005) and can quickly compromise the quality of data from monitoring wells for a long period.

An integral feature of the rock core VOC method is that it provides data that are minimally influenced by borehole cross-connection. Because many of the methods for characterizing flow in fractured rock sites are done in open boreholes after drilling, they are only sensitive to those features which dominate flow in open boreholes. This oversimplification leads to only two or three active flow regions in a borehole instead of the many interconnected fractures as presented by Parker 2007.

The possibility for large variability of relevant physical, chemical and biological parameters of the fracture network and matrix make it difficult and expensive to characterize each individual feature in sufficient detail. Choosing an appropriate scale of investigation and the correct tools to achieve that scale of investigation for each parameter analyzed is a necessary and a non-trivial decision. Fracture network conditions vary spatially and with different lithologies and thus affect the flow system and hydraulic properties which are fundamental in understanding plume migration. Chemical properties such as reactive minerals and organic carbon control sorption and degradation of contaminants are also expected to vary spatially and can substantially affect contaminant

mobility and fate. To address the highly heterogeneous environment, sample spatial resolution needs to sufficiently match the heterogeneity of the distribution of interest (Lawrence, Stuart, Cheney, Jones, & Moss 2006) and therefore method choice must have the ability to resolve sufficiently this variability on the appropriate scale. This thesis explores not only contaminant variability, but the physical and chemical variability of the system.

This thesis consists of this introductory chapter and three content chapters. Each chapter focuses on a separate but related topic and is meant to be a semi-autonomous unit which may lead to some repetition. The primary purpose of this thesis is threefold: First, to examine extraction and preservation methods for improved rock core VOC analyses, secondly, to examine the relationship between porosity and bulk density with contaminant storage and migration, and also to improve on the method to calculate porewater concentrations from the total mass concentration from rock core; and thirdly, to interpret the rock core contaminant distribution within a multifaceted dataset derived from the Guelph field site where a suite of new, modified and standard data collection approaches have been used. This multiple lines of evidence approach is necessary when characterizing a site, because no single log provides complete characterization of the system.

The research site located in Guelph, ON, consists of middle Silurian age dolostone overlain with 3-5 m of glacial till. This investigation focuses on the Guelph Formation, a tan to grey, fine to medium crystalinity sucrosic dolostone exhibiting a variety of features such as stylolites, vuggy and pinpoint porosity, and fossils. At this site, TCE entered the subsurface more than two decades ago and migrated through the glacial overburden to the dolostone bedrock. Concentrations of tetrachloroethene (PCE) and degradation daughter products of TCE (isomers of DCE) in groundwater and rock core samples are also occasionally detected, but typically much less than the concentrations of TCE. The thin

overburden, shallow water table, relatively constant dolostone mineralogy but variable bulk densities and porosities, high spatial density of rock core VOC holes, and primarily TCE plume make this an excellent research site for the following study.

Chapter 2 focuses on extraction and preservation methods for TCE optimized rock core VOC analyses. Duplicate samples were extracted using a recently developed method for VOCs in crushed rock samples (microwave assisted extraction), the traditional University of Waterloo method (shake-flask), and the conventional industry method (purge and trap). In addition, the necessity of field preservation was examined by comparing the results from field preserved samples with those preserved in the lab fewer than 12 hours later. Statistical analysis was undertaken to compare extraction and preservation methods.

Chapter 3 addresses the uncertainty related to the rock core porewater conversion process due to spatially variable physical properties. To account for the variable bulk density and porosity at the appropriate resolution of the rock core VOC sample size, calibrated geophysical logs were used. Results from three wireline logging probes were calibrated to laboratory derived physical properties: neutron, gamma-gamma, and acoustic televiewer amplitude. The qualitative and quantitative effect of this correction was examined.

Chapter 4 displays the results of the general site investigation for a TCE contaminated site in Guelph, Ontario using the DFN approach. Individual rock core profiles and a transect of rock core profiles provide the basis for interpreting the groundwater flow and contaminant transport in this heterogeneous and dynamic aquifer. In this way the geology, hydrogeology, geophysics are interpreted in the context of the contaminant distribution.

Although the importance of matrix diffusion in the assessment of solute transport in fractured porous media has been known since Foster's landmark paper in 1975, the field-study related literature concerning matrix diffusion has focused almost entirely on fractured clayey deposits (eg Hinsby et al. 1996;Mckay, Gillham, & Cherry 1993;O'Hara et al. 2000;Parker, Cherry, & Chapman 2004) and crystalline rock such as granite (eg Bear, Tsang, & de Marsily 1993;Hadermann & Heer 1996;Mazurek, Jakob, & Bossart 2003). Studies focused on contaminant behavior in hard sedimentary rock (eg sandstone, shale, dolostone, limestone) involving measurements of contaminant mass in the rock matrix are rare. The time scales over which matrix diffusion effects are most apparent are relatively short for fractured clayey deposits and longer for sedimentary rock and longest for crystalline rock. Also, there have been several numerical models developed to simulate solute transport in fractured porous geologic media (eg Grisak & Pickens 1980;Neretnieks 1980;Sudicky & Frind 1982;Tang, Frind, & Sudicky 1981; Sudicky & Mclaren 1992;Therrien & Sudicky 1996) but none of these models have been validated using site specific contaminant distributions (Parker 2007). The major impediment for the collection of the field data to delineate the organic contaminant distributions at sedimentary bedrock sites and to represent the contaminant transport and fate has been the difficulty associated with obtaining representative measurements of the contaminant concentrations in rock core samples at the appropriate scale. However, a suite of methods have been developed and continue to be refined to advance this approach and the subject of this thesis includes the assessment recent advances in the areas of sample collection, extraction, preservation, analysis, and interpretation.

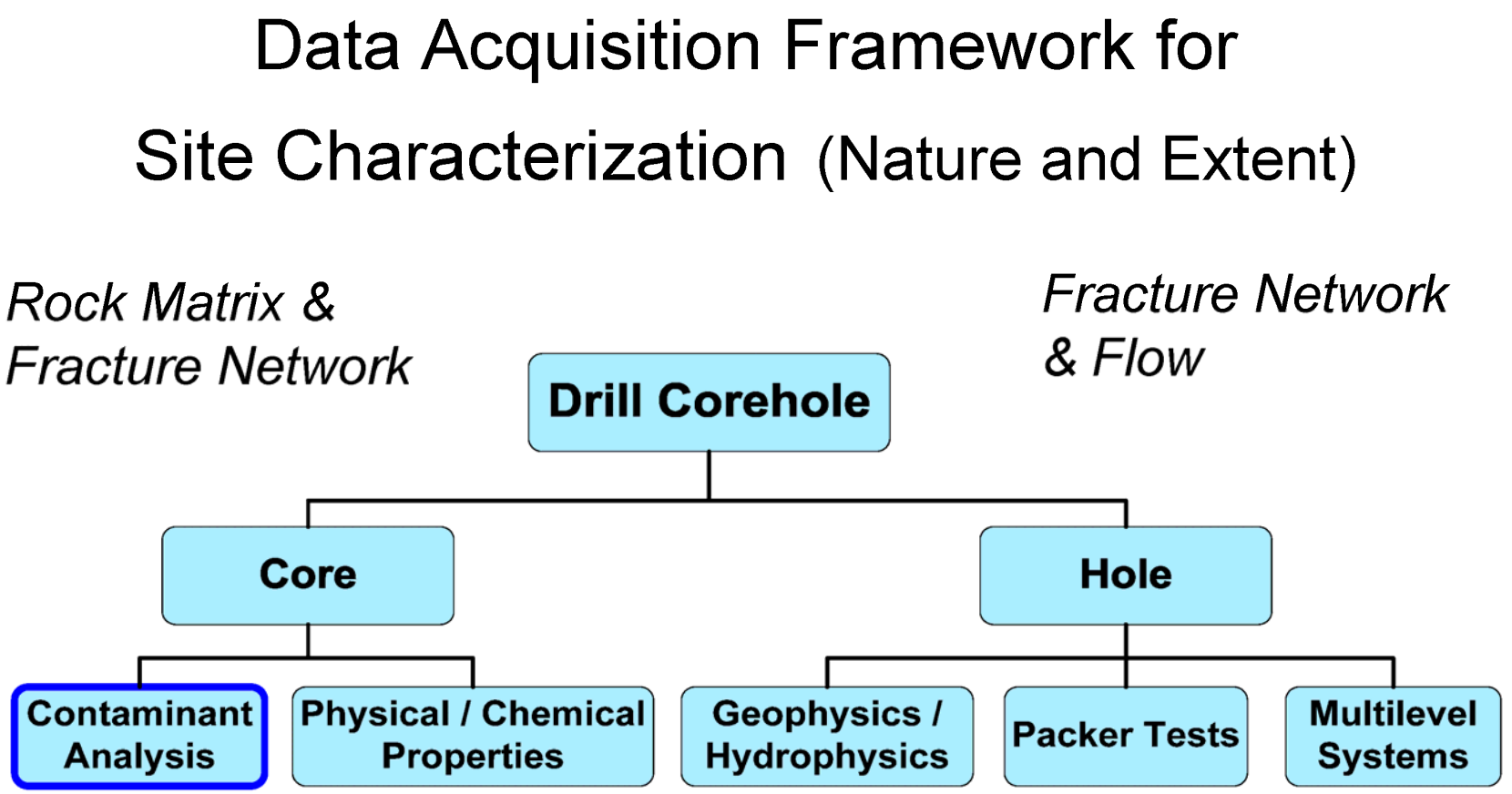

Figure 1.1: Data acquisition framework. Maximizing the information from each corehole by analyzing both the core and the resulting hole (modified from Parker 2004).

Operating Conceptual Model

(Point Source Contamination in Sedimentary Rock)

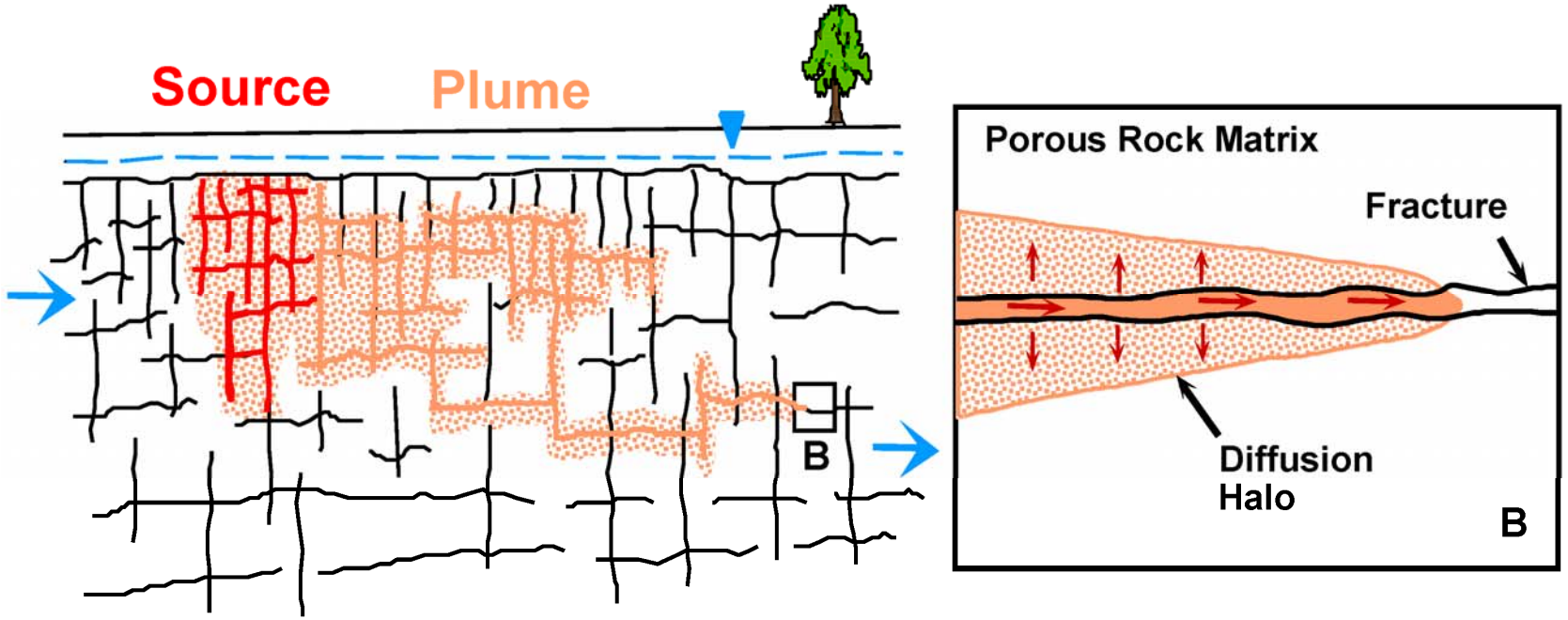

Figure 1.2: Operating conceptual model. DNAPL is released at the surface, migrates through bedrock fractures, and then dissolves, diffuses and advects to create a groundwater plume (Taken from Parker 2007).

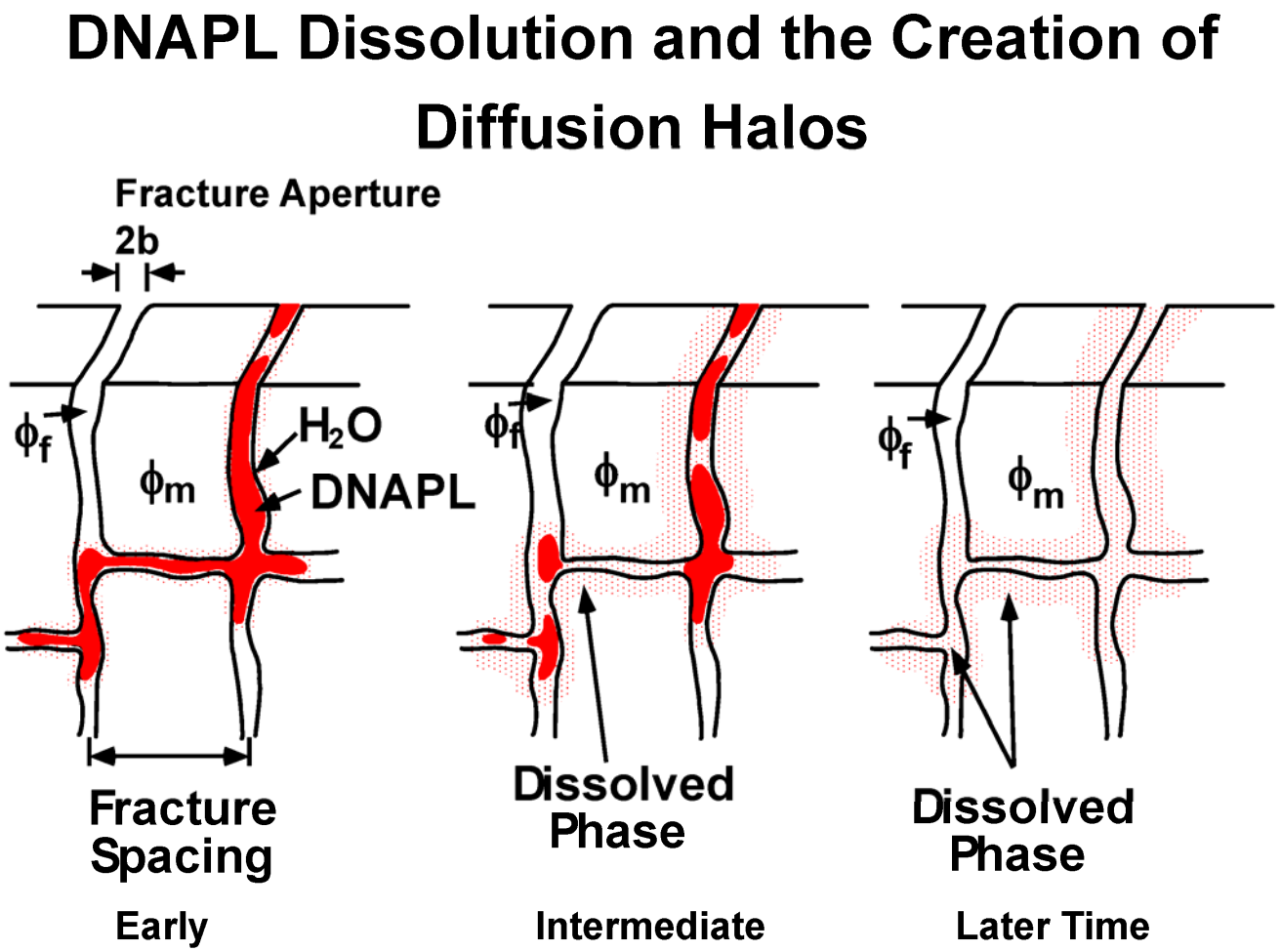

Figure 1.3: DNAPL dissolution and creation of diffusion halos. With time the DNAPL source has totally dissolved and diffused into the rock matrix to become aqueous phase contamination (taken from Parker, Gillham, & Cherry 1994).

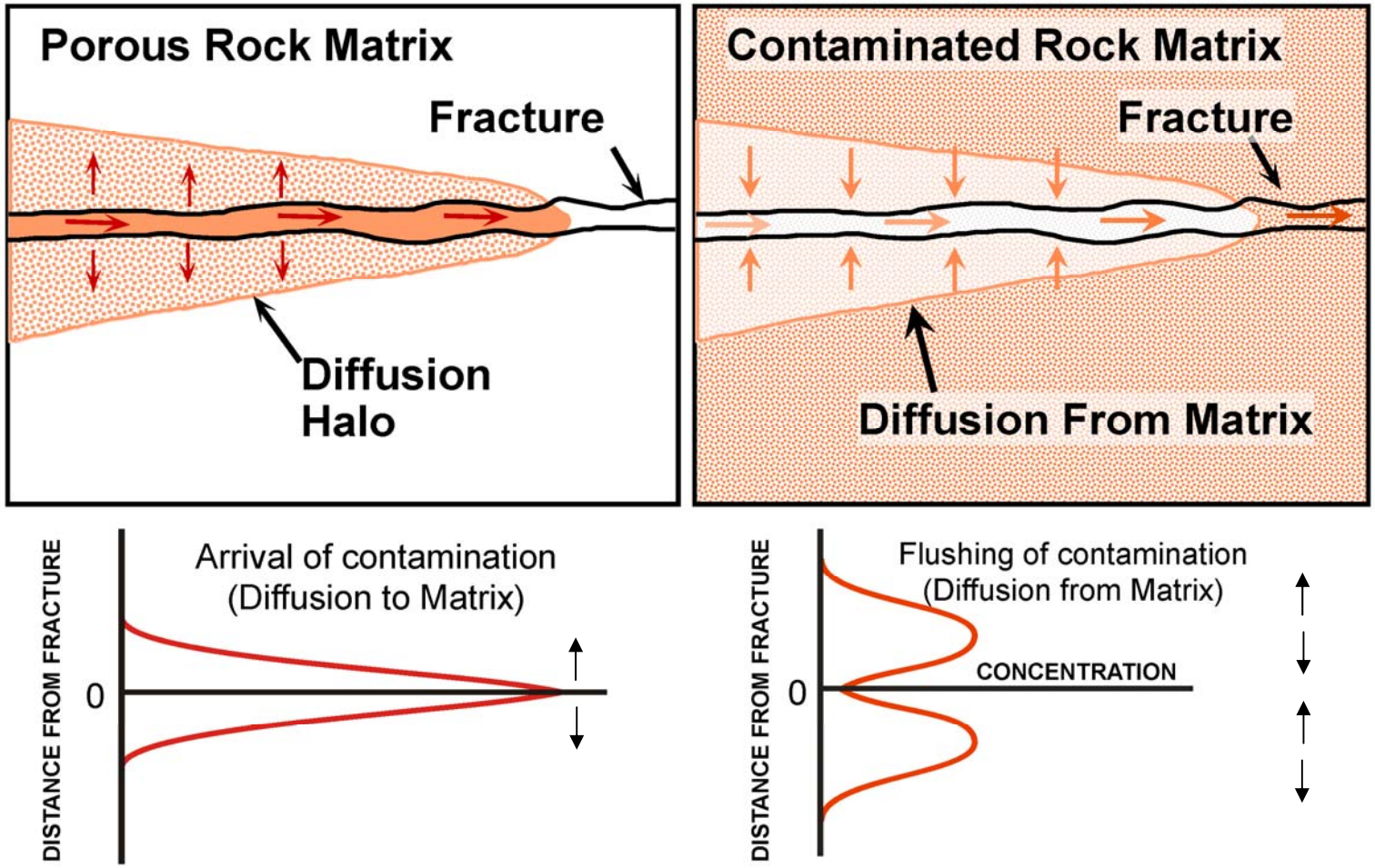

Figure 1.4: Diffusion between the rock matrix and fracture. Concentration gradient causing diffusion from a fracture to the rock matrix and further into the rock matrix (matrix acts as a contaminant sink) (A). Concentration gradient causing diffusion from the rock matrix to the fracture water (matrix acts as a contaminant source) (B) (modified from Parker, 2007).

Core Hole for Rock Core Analyses in Areas of Previous DNAPL Occurrence

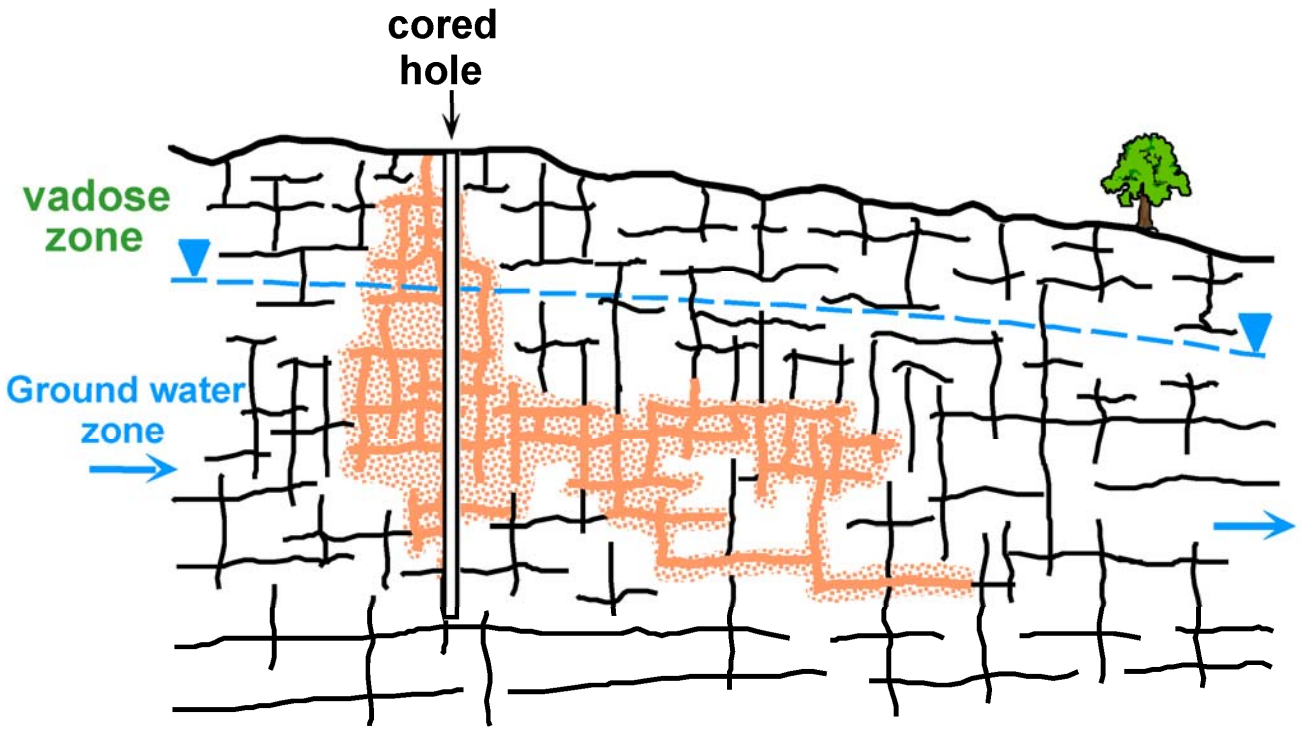

Figure 1.5: Core hole for rock core analyses in areas of previous DNAPL occurrence. DNAPL has dissolved and is no longer present (taken from Parker 2007).

Core Sampling to Identify TCE Migration Pathways

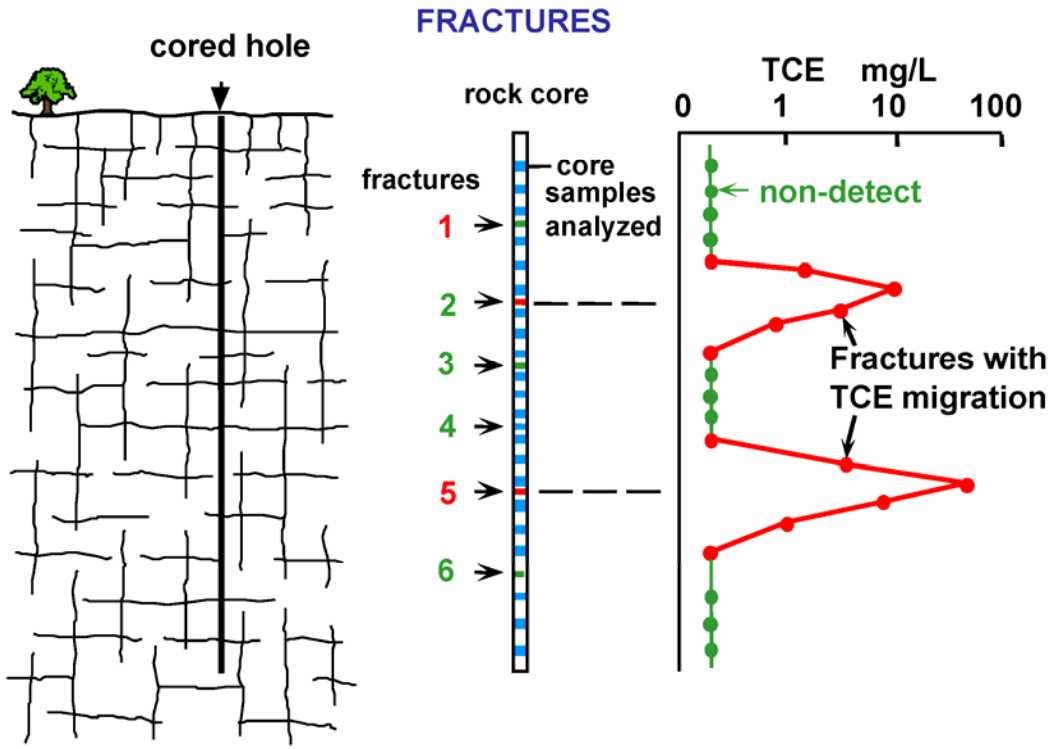

Figure 1.6: Core sampling to identify TCE migration pathways. Hydraulically active fractures are detected by using TCE contaminant haloes (taken from Parker 2007).

Chapter 2: An Advanced Method for Rock Core TCE Contaminant Analysis

2.1 Abstract

Contaminant transport in fractured sedimentary rock typically occurs due to groundwater flow in fractures; however, diffusion-driven mass transfer from the fractures into the rock matrix is also influential in nearly all types of contaminated sedimentary rock. Few investigators have measured contaminant mass distributions in rock core and those that have focused primarily on non-volatile or semi-volatile compounds. The collection, preservation, and extraction of representative rock samples for VOC analysis require further investigation.

This chapter reports on a recently developed method to rapidly extract (microwave assisted extraction) volatile organic compounds (VOCs) from rock samples (Liu 2005) and compares that to the traditional UW method (shake-flask) and the industry standard method (purge and trap), and also demonstrates the sensitivity of crushed rock samples to various preservation techniques. Method testing was performed on core from a dolostone aquifer with long-term TCE contamination (>20 years). Results indicate that the microwave assisted extraction (MAE) method typically provides equivalent or higher concentrations when compared with the shake-flask and purge and trap extraction methods. The purge and trap method provided false negatives (i.e. non-detects) due to inadequate preservation, incomplete extraction, and the elevated detection limit. The necessity for field preservation was examined by comparing crushed rock samples preserved in methanol in the field to samples unpreserved in the field with a laboratory addition of methanol less than 12 hours later. The duplicates subjected to field preservation showed statistically higher

concentrations for TCE thus demonstrating the importance of rapid field preservation for crushed rock samples.

2.2 Introduction

In order to discuss and compare preservation techniques and the microwave assisted extraction (MAE) method with the traditional shake-flask and conventional purge and trap methods, a brief background into the problem this method addresses is important. This chapter will provide a background overview and then move onto an extensive description of the method and the benefits.

To gain insight into contamination in the rock matrix and rock matrix porewater, numerous extraction techniques for an assortment of analytes and solid matrices are available. Depending on the purpose of the investigation, the analyte of concern, and the matrix properties, some of these techniques may be utilized with variable success. Extraction techniques for low volatility and semi-volatile compounds such as polycyclic aromatic hydrocarbons (PAHs), polychlorinated biphenyls (PCBs), organochlorine pesticides (OCPs), and total petroleum hydrocarbons (TPHs) from sediments or interstitial waters (Hewitt 1998;Kinniburgh & Miles 1983;Rawa-Adkonis, Wolska, & Namiesnik 2003;Sporring et al. 2005) are well documented in the literature. Unfortunately, the majority of these modern methods have not been applied to rock matrices and even fewer have focused on VOCs which are often the most common contaminants at industrialized sites. VOCs pose additional difficulties and in future research, some of these methods may be adapted and shown to be suitable for accelerating VOC extraction from rock matrices.

For VOCs in rock matrices, approaches typically are concerned with one or both of the following key components of the matrix: interstitial water (Spence et al. 2005), and the sorbed or total contaminant mass associated with the matrix (Lawrence, Stuart, Cheney, Jones, & Moss 2006;Lawrence, Chilton, Barron, & Thomas 1990;Lawrence et al. 1996;Sterling, Parker, Cherry, Williams, Lane, & Haeni 2005). Chapter 3 shows that with a

knowledge of the physical and chemical properties of the analyte and rock matrix one can estimate the porewater concentration from the total mass concentration.

In the commonly used, but lengthy shake-flask extraction method, samples may require weeks to reach functional contaminant equilibrium with the extracting solvent (Hewitt 1998). This method, implemented for rock samples in the UW Master's theses of Sterling [1999], Turner [2001], Hurley [2003], Burns [2005], Meyer [2005], Austin [2006] and Plett [2006] is a time and labour intensive procedure. This time requirement inhibits the possibility for extraction and analysis in the field.

The industry standard method and EPA recommended method for VOCs in solid matrices is the purge and trap method. This standard purge and trap extraction method has been evaluated for VOCs in soils (fine sands, silty loams, and clayey soils) and was shown to be inadequate for extracting contamination contained in the internal micropores of soils and from strongly sorbed contamination (Askari et al. 1996). Based on particle size alone, crushed rock samples are expected to perform even more poorly than the fine sands and soils used in Askari's study. A variety of established and emerging technologies related to accelerated chemical extraction from solid matrices exist and in particular MAE shows great promise in reducing sample handling, storage, and complete extraction times.

Microwave assisted extraction (MAE), applied to solid matrices by Ganzler et al. as early as 1986, uses non-ionizing electromagnetic waves to impart migrational and rotational energy to microwave absorbing compounds and has achieved success in the extraction of low volatility and semi-volatile compounds from a variety of solid matrices (Bangkedphol et al. 2006;Carro et al. 2006;Letellier et al. 1999;Lopezavila, Young, & Beckert 1994;Pare et al. 1997;Rice & Mitra 2007). Pare et. al [2001] suggest that for the microwave assisted process (MAP™), particle size should fit through a size 10-mesh sieve (Pare et al.

2001). For volatile compounds in lithified materials, grinding each sample to achieve this requirement is not practical and would likely result in volatilization losses.

MAE was shown to be a viable alternative to the traditional shake-flask extraction method for trichloroethene (TCE), a volatile organic compound, in low permeability clay samples while dramatically reducing the extraction time (Dincutoiu, Gorecki, & Parker 2006). MAE was then further developed by Liu [2005] in order to use microwave irradiation to extract TCE from rock matrices using the shake-flask method for comparison. Crushed rock samples have the added difficulty resulting from lower porosity and increased crushed particle sizes when compared to clay samples. Liu [2005] used crushed dolostone and sandstone samples for his method development and also examined the applicability of a variety of polar and non-polar extracting solvents. Extraction times decreased from weeks to less than an hour (Liu 2005) creating the opportunity for on-site extraction and analysis. Beginning with this existing research, this study expands on Dincoutoiu's findings from 2006 and Liu's methodology to examine the application of MAE to rock matrices.

The nature of the matrix determines the effectiveness of extraction procedures (Camel 2001), and, therefore, applying MAE to rock samples requires careful consideration of the partitioning properties of the analyte with the matrix and the ability of the rock matrix to facilitate migration to the extracting solvent. Extraction times and efficiency are sample dependent and are controlled by desorption and diffusion out of the porous diffusion controlled zones. Transport affecting properties such the pore structure tortuosity, the diffusion coefficients in matrix interstices, organic carbon, and the extracting solvent play important roles in the rate of extraction. This study uses MAE to decrease extraction times by promoting desorption and mass transport in crushed rock samples.

2.2.1 Cross-contamination and volatilization losses

Sample handling, extraction, and analysis methodology influence the results of a sampling event. Order of magnitude negative biases may be introduced depending on the sampling and preservation methodologies for VOCs for soil samples (Liikala et al. 1996;Siegrist & Jenssen 1990). Most biases in the collection of rock matrix VOC samples lead to decreased concentrations. Therefore, we operate on the assumption that higher concentrations signify that losses are minimized and/or more complete extraction occurred. This provides a more conservative and accurate assessment of the contamination.

On the other hand, a bias that might lead to false positives is cross-contamination. Rigorous sampling protocols and extensive quality assurance and quality control procedures mitigate complications due to cross-contamination. Throughout the entire collection, extraction, and analysis procedures numerous steps were implemented to minimize exposure, prevent cross-contamination, and ensure valid results (Hurley 2003;Sterling 1999).

2.2.2 Study Description

This study focuses on trichloroethene (TCE), a surrogate for other VOCs showing stability at the elevated temperatures reached during microwave treatment. TCE, a prevalent contaminant in the subsurface, often enters the subsurface as a dense non-aqueous phase liquid (DNAPL) dissolving to cause persistent groundwater plumes having the potential to exist for decades in fractured rock settings (Sterling, Parker, Cherry, Williams, Lane, & Haeni 2005). Low degradation rates, low solubilities, the potential for partitioning with solid phases, and the interplay of fractures with the matrix pore-space govern the migration of aqueous TCE in the saturated subsurface.

The research site is located in Guelph, ON, and consists of middle Silurian age dolostone overlaid with 3-5 m of glacial till. VOC contamination in the Guelph-Amabel aquifer is of importance to the city of Guelph as the two nearest municipal supply wells (Sacco, and Smallfield) have be taken off service since the early 1990's. This investigation focuses on the Guelph Formation, a tan-grey fine to medium crystalinity sucrosic dolostone exhibiting a variety of features such as stylolites, vuggy and pinpoint porosity, and fossils. Porosities are generally between 1 and 20 percent with water saturated bulk densities ranging between 2.42 and 2.89 g/cm^3 and an average percent fraction of organic carbon (% f_{oc}) equal to 0.02. Horizontal fracture spacing varies from centimeters up to 2 meters. A variably saturated region below the bedrock and overburden contact exists for 1-2 meters until the water table is reached.

At this site, TCE entered the subsurface more than two decades ago and migrated through the glacial overburden to the dolostone bedrock. Concentrations of tetrachloroethene (PCE) and degradation daughter products of TCE (isomers of DCE) in groundwater and rock core samples are also occasionally detected, but typically much less than the concentrations of TCE. The thin overburden, relatively constant dolostone mineralogy, proximity to the UW analytical laboratory, relatively simple plume composition showing minimal degradation, and local importance all make this an excellent study site for TCE fate and migration in fractured sedimentary rocks.

2.3 Experimental Methods

The rock core VOC analysis process is outlined in Figure 2.1. To adequately compare extraction and preservation methods, aged field samples were used as they tend to behave differently than laboratory spiked samples (Hatzinger & Alexander 1995;Pavlostathis & Mathavan 1992). However, this means that the true value of

contaminant concentration in the crushed rock samples is not known. For this study, the shake-flask extraction method was used as a benchmark but not considered the definitive method.

In order to expedite the extraction process, rock samples are crushed to increase the surface area available for mass transfer to the extracting solvent, decrease the contaminant travel distances to the extracting solvent, and allow for more rapid solvent penetration into the matrix pores. For the case of non-volatile compounds the rock may be crushed and ground to a fine powder to decrease extraction time. However, for volatile compounds the risk of volatilization losses can be significant and grinding to a fine powder may compromise analyte recovery. Because TCE is a volatile compound, minimizing exposure to air is an important consideration and thus the choice of crushing method is not trivial.

For this study, a hydraulic press was used to crush the samples (Hurley 2003). In less than 5 seconds 4000-7000 psi was applied to each rock sample contained inside a stainless steel cylinder (Figure 2.2). The resulting crushed rock was quantitatively transferred to a 40 mL clear VOA vial with minimal exposure to the atmosphere. Rock particle sizes vary depending on the physical properties and cementation of the rock matrix but typically the crushed rock particles were less than 5 mm at the largest dimension.

For this study, samples were obtained from five coreholes in close proximity (< 130 m); MW-22, MW-23, MW-367-4, MW-367-5, and MW-367-7. Sample collection occurred from the top of bedrock surface until the bottom of the hole. Corehole depths ranged from 25-40 m and all samples came from the Silurian dolostone Guelph formation and the uppermost member of the Amabel formation.

At the research site the water table generally follows a depressed surface of the bedrock and overburden contact. The rock matrix is considered to be saturated below the water table and therefore with the exception of the first few samples of each hole, samples are considered to be water saturated. Samples were preferentially collected on fracture surfaces, at lithology changes, at stylolites, and 15 cm and 30 cm above and below horizontal and moderately inclined fractures. For the case of vertical fractures, a sample in the center of the fracture was taken. When fracture spacing was < 10 cm one sample was taken to be representative of the fracture set. If no targeted features occurred in a core run, 3 evenly spaced samples were taken. The average vertical sample spacing for this study is less than 30 cm.

A wireline rotary coring rig equipped with a diamond impregnated bit and reaming shell was used to obtain continuous HQ sized core (63.5 mm diameter). Prior to each coring run the depth of the corehole was determined using a tagline. A mist of water and compressed air acted as the drilling fluid functioning to remove cuttings and cool the drill bit. To obtain high core recoveries and minimize mechanical breaks a triple-tube coring system was used to collect 1.52 m long core segments. The triple-tube coring system consisted of the outer core barrel attached to the drill bit, an inner core barrel that remains stationary and houses a lengthwise-split, stainless steel tube. Extrusion of the core and stainless steel split-tube from the inner core barrel was accomplished using a piston powered by compressed air. After the removal of the stainless steel split tube, the core was quickly and carefully transferred to a PVC core tray lined with clean aluminum foil that was used to cover the core and prevent exposure to wind and direct sunlight.

The wrapped core and core tray were then transferred to the sampling table where the foil cover was removed. The core was photographed and logged for major geologic and

hydrogeologic features with emphasis on fracture location, lithology changes, porosity changes, and stylolite locations.

Typically 2-5 cm puck shaped samples were taken from the core using a mallet and chisel but some samples were up to 10 cm in length. These samples were then wrapped in aluminum foil, inserted into a clean labeled plastic zip-locking bag, placed in a cooler, and transferred to the crushing station 10 meters away.

At the crushing station, samples were taken from the cooler, aluminum foil removed, and the sample was trimmed inside of a stainless steel, 12 cm diameter basin. Pieces of rock, approximately 2 cm long at the largest dimension, were created to fit into the crushing cell and also to remove the outer portion of the core which had the most potential for contact with the drilling fluids. The sample was placed into the crushing cell and crushed using one stroke of a hydraulic press.

Until this stage the samples were treated identically. The resulting crushed rock was then transferred from the crushing cell to a pre-weighed 40 ml VOA vial using a funnel and spatula. Depending on the extraction method, analysis type, and preservation of the sample the VOA vial either contained 15-20 ml of purge and trap grade methanol or was empty. On average, the time from core recovery to sample bottling took less than 15 min and the time the rock sample was exposed to the atmosphere is considerably less.

In order to prevent cross-contamination all crushing cells, chisels, and equipment coming into direct contact with the rock core was decontaminated after each sample using a six step method. The first step was to remove any particles of rock adhering to the equipment. Next the equipment was immersed into a Fisher Brand Sparkleen 1 detergent and deionized water bath. The equipment was scrubbed using brushes and transferred to a

deionized water bath where the detergent was removed. Following this, the equipment was given a wash grade methanol rinse followed by a deionized water rinse. Finally, the equipment was allowed to air dry before being reused.

Four different types of rock samples for predetermined extraction methods were taken during the 2004 and 2005 rock core sampling episodes (

Figure 2.3, Figure 2.4):

1. Crushed rock samples split in the laboratory (~65 g crushed rock, no headspace)
    a. MAE split (~20 ml purge and trap grade methanol, ~20 g crushed rock)
    b. Shake-flask extraction split (~15 ml purge and trap grade methanol, ~20 g crushed rock)
2. Crushed rock samples preserved in the field for MAE (~15ml purge and trap grade methanol, ~20g crushed rock)
3. Crushed rock samples preserved in the field for shake-flask extraction (~15ml purge and trap grade methanol, ~20g crushed rock)
4. Crushed rock samples to be analyzed by Maxxam Analytics Inc. with SWP-846 EPA Method 8260 (US EPA 1996) (~65 g crushed rock following EPA sample collection and preservation techniques for soil VOC samples).

Samples in categories 1-3 were analyzed at the University of Waterloo Dirt Lab and category 4 was analyzed in a commercial lab. After bottling, the sample and bottle were reweighed to determine the mass of crushed rock added, wrapped with Teflon around the outside of the cap joint, and placed in coolers containing ice.

Sample type 1 (MAE - Lab addition of methanol, shake-flask extraction - Lab addition of methanol)

Approximately 65 g of crushed rock comprised the sample. At the end of the day, samples were transferred to large walk in coolers kept at 4°C used for sample storage. The following day at the lab, the sample was quartered and then split into two ~20 g samples. Care was taken to do this quickly to minimize losses and limit the potential for cross-contamination. In addition, attempts to have similar particle size distributions between the samples were taken and large rock particles were discarded. The samples were then placed into labeled pre-weighed bottles containing approximately ~20 mL of purge and trap grade methanol. Samples marked for MAE were extracted and analyzed the same day whereas the samples marked for shake-flask extraction were shaken on the orbital shaker for 30 min and then placed into storage. Following this, they were shaken for 30 min weekly for 6 weeks.

Sample type 2 and type 3 (MAE - Field addition of methanol, shake-flask extraction - field addition of methanol)

Sample types 2 and 3 were treated identically except for the extraction method. An addition of approximately 20 g of crushed rock went into the vials containing 15-20 mL of methanol. The crushed rock sample was completely immersed in the 15-20 mL of methanol. At the end of the day, samples were transferred to large walk in coolers kept at 4°C. An additional 5 ml of purge and trap methanol was added to the MAE samples for quantitative transfer from the VOA vial to the microwave vessel.

Sample type 4 (EPA Method 8260)

Approximately 65 g of crushed rock comprised the sample. At the end of the day, samples were transferred to large walk-in coolers kept at 4°C used for sample storage. The following work day samples were sent to Maxxam Analytics Inc. in Misssauga, Ontario to be analyzed by EPA method 8260 (US EPA 1996).

2.3.1 Extraction methodology

The MAE and shake-flask extraction procedures occurred according to Liu [2005]. For sample type 2 the comparison of methods was the primary purpose and additional care was taken to ensure that the samples looked visually similar. Larger rock particles were removed and not included in the samples for extraction. This is not achievable for field preserved samples where exposure time is paramount to decrease the potential for volatilization losses.

2.3.2 Sample Analysis

Methanol extracts were taken from the microwave extraction vessels containing the crushed rock samples immersed in methanol. Aliquots from the methanol extracts and laboratory QAQC blanks were taken using an Agilent 7683 automatic sampler. These 1 µl samples were injected into an Agilent 6890 Plus Gas Chromatograph equipped with a µ-ECD detector and a 30 m × 320 µm × 5.0 µm DB-1 capillary fused silica column. Ultra high purity helium functioned as the carrier gas set to flow at 3 mL/min. The column was kept for 3 min at 55°C for 0.5 min, increased to 150°C at the rate of 10°C/min, and finally increased to 200°C at the rate of 35°C/min which was held for 6 minutes. The detector operated at 350°C with nitrogen (TAG grade, Praxair) as the make-up gas and a flow rate of 60 mL/min (Liu 2005).

Trichloroethene results from the UW Lab were reported in µg TCE/L methanol with a method detection limit (MDL) of 0.1 µg TCE/L. For comparison purposes these results were converted to a µg TCE/g rock which gave an average MDL of $1 \cdot 10^{-4}$ µg TCE/g rock for the MAE method and $6 \cdot 10^{-5}$ µg TCE/g rock for the shake-flask method. For the MAE method, additional methanol (~5 mL) was used to ensure quantitative transfer to the microwave extraction vessels. The additional methanol increases the detection limit as the conversion from µg TCE/L methanol to µg TCE/g rock is dependent on both the mass of rock added and the methanol added (Equation 2).

$$C_r = \frac{C_m V}{m} \qquad \textbf{Equation 2-1}$$

Where:

C_r (µg/g rock) is the concentration in the rock

C_m (µg/L methanol) is the concentration in methanol

V (L) is the volume of methanol added

m (g) is the mass of rock (wet)

Samples sent to the commercial lab were analyzed using EPA method 8260 (US EPA 1996). TCE results were reported in µg TCE/g rock with a MDL of 0.01 µg TCE/g rock. This detection limit is two orders of magnitude larger than the detection limit for the samples analyzed in the Dirt Lab.

QAQC measures

Throughout the rock core crushing and extraction procedure samples were taken to test for cross-contamination and ensure confidence in the methodology. The UW analytical lab implemented several techniques for laboratory QAQC measures.

Lab QAQC

1. Methanol bottle blanks consisting of an autosampler vial filled with purge and trap methanol added from the top and bottom of every bottle used for filling up the sample vials.

2. Laboratory blanks consisting of an autosampler vial filled with purge and trap methanol.

3. Matrix spikes and matrix spike-duplicates – Purge and trap methanol spiked with a standard solution of the analytes being tested. Matrix spike duplicates are used for determining method precision.

4. Equipment blank for the TFM Teflon microwave vessels – Purge and trap methanol added to the microwave vessel and microwaved along with the other samples.

5. Laboratory duplicates – Two methanol extracts taken from the same methanol and rock sample

In addition to the rigorous laboratory QAQC measures, several types of field blanks and also field duplicate samples were collected.

Field Blank types

1. Equipment blank consisting of a kimwipe® sprayed with the rinse methanol and wiped on the decontaminated sampling equipment, placed in 40 ml VOA vial, and immersed in 15 mL purge and trap grade methanol (taken every 20 samples)

2. Trip blank consisting of a 40 ml VOA vial containing 15 ml of purge and trap grade methanol. These samples traveled with the other samples and were placed in the

coolers used to transport them to the laboratory from the field site. They were removed when the lab processed the samples on the following day (at least three per cooler).

3. Storage blanks consisting of a 40 ml VOA vial containing 15 ml of purge and trap grade methanol. Samples undergoing shake-flask extraction are stored for weeks creating an increased potential for cross-contamination. When the lab processed the samples on the following day the trip blanks were removed and storage blanks were added (at least three per storage container).

Qualifiers were applied to samples that showed contamination in the associated blanks, were below the detection limit, and those that were above the method detection limit (MDL) but below the limit of quantitation (LOQ). Detection limit statistics are shown in Table 2.1. If a blank showed contamination, the concentration of the blank was multiplied by 5 and all associated samples below that value were qualified. These values are also considered to be an estimated quantity due to the potential for cross-contamination. For the statistical tests only sample sets with two pairs of quantifiable detects above the LOQ were used. Another important comparison is of the qualified sample results. Table 2.2 provides a comparison of the qualified values in this study.

During the field investigations 5% duplicate samples were collected. Duplicate samples were selected during the trimming stage after the core segment was split lengthwise to ensure samples came from a similar depth. Following this the samples were crushed and bottled separately but extracted and analyzed using identical procedures.

2.3.3 Comparison Technique

Datasets not normally or easily transformed to normally distributed require non-parametric methods for analysis. To compare the distribution of the datasets the Wilcoxon

signed rank / lower tailed test was implemented (Wilcoxon 1945). The null hypothesis for this test stated that the distributions of the two datasets did not significantly differ. The alternative hypothesis states that the distribution of the first dataset is shifted to the left of the second dataset (i.e. higher concentrations for the second dataset). Samples lacking a corresponding pair were not included in the statistical analysis.

Duplicates taken in the field were subjected to the same statistical tests. The null hypothesis for duplicate samples stated that the distributions of the two datasets did not significantly differ with an alternative hypothesis that the distributions of the two datasets are significantly different.

To visualize the difference between methods the relative percent difference (RPD) was used. Because neither extraction method is 100% definitive, an arithmetic mean of the two was used for calculating the RPD. The relative percent difference between the two methods was calculated using:

$$Relative\ Percent\ Difference = 100\% \left[\frac{(A-B)}{\frac{(A+B)}{2}} \right] \qquad \textbf{Equation 2-2}$$

Where:

A is the concentration from extraction method A

B is the concentration from extraction method B

Both samples came from the same depth. Table 2.3 shows the designations used to compare datasets and the polarity of the RPD will be based on which sample set is designated A and B.

2.4 Results and Discussion

The development of a robust and rapid extraction method for crushed rock samples is an imperative step necessary to characterize VOC contaminated fractured rock. The shake-flask extraction method currently provides good contaminant recovery at the expense of protracted extraction times. By applying MAE to crushed dolostone samples, timely extraction was performed and the results suggest the method achieves comparable or increased total recoveries.

The laboratory split samples (Type 1a, 1b) undergoing either MAE or shake-flask extraction consistently yielded higher concentrations for MAE than the corresponding shake-flask samples (Figures 2.5). Statistical analysis using the Wilcoxon signed rank test reinforced the visual comparison and the results are shown in Table 2.4. Of the 144 sample pairs detected using both extraction procedures, 129 showed greater recoveries for MAE than shake-flask. Considering the high inherent geological variability at fractured rock sites the samples corresponded exceptionally well as shown by the lower variance of RPDs in Table 2.5 and the visual comparison shown in Figure 2.6.

The comparison of field duplicate samples (Type 2, 3) served to reinforce that MAE is a viable method for extracting VOCs from rock matrices (Table 2.4). Results show increased scatter around the equivalent extraction line (Figure 2.7) when compared to the lab splits, likely resulting from the following differences between the two methods: first, in the lab methods more care was taken than was taken in the field to achieve similar particle size distributions by removing larger chunks of rock, and second, the laboratory split samples came from the same well-mixed bottle of rock. This results in a larger variance in relative percent differences between the samples for the field splits (Table 2.5). However,

as can be seen in Figure 2.8 samples correlate well and with MAE consistently yielding higher results.

Even though the shake-flask extraction method may require weeks to reach VOC equilibrium with the extracting solvent, volatilization losses are noticeable in sealed VOA vials without preservation in under 12 hours. This suggests that sample preservation is an indispensable component in sample collection for VOCs in crushed rock.

The results of the comparison (1b, 3) of field preserved samples (3) compared with the lab preserved samples (1b) are shown in Table 2.4. Field preservation had a greater magnitude effect on the concentration of the samples than did varying the extraction method as illustrated in Figure 2.9 and by the arithmetic mean of the RPDs (Table 2.5). These samples also show increased variance between the relative percent differences when compared to laboratory split samples (1a, 1b) and are likely due to samples showing increased geologic variability, and particle size distribution variability between pairs. Of the 66 pairs of samples showing quantifiable detects in both samples, only 5 showed concentrations greater for the laboratory preserved samples. In addition, it appears that the relative percent difference is most significant at higher concentrations which is illustrated by the difference and regression plots showing increased spread at high concentrations (Figure 2.10). An important note is that the comparison of the shake-flask extraction method and MAE was the primary purpose for the laboratory preserved samples and therefore additional effort was taken to ensure samples had similar particle size distributions. This increased the handling time and exposed samples to the atmosphere for a longer time than absolutely necessary. This would magnify differences between the field and lab preserved samples.

The recommended purge and trap SWP-846 EPA Method 8260 was not a suitable procedure for the crushed rock samples in this study for two primary reasons: first, the detection limit was elevated greatly so contamination at environmentally relevant concentrations was missed, and secondly, the method likely does not provide complete extraction for crushed rock samples. In addition, the lack of field preservation serves to increase the potential for false-negatives.

The elevated detection limit, compounding with incomplete extraction, and lack of field preservation led to only 3 quantitative hits out of the 101 samples analyzed by EPA Method 8260. Therefore no statistics were applied to these samples but a direct comparison of the hits can be made as shown in Table 2.6. The infrequent number of detects suggests incomplete extraction or contaminant mass loss during the storage, extraction, and analysis procedure. Figure 2.11 provides a profile comparing the purge and trap method with the shake-flask method.

The collection of duplicate samples from heterogeneous media in the field is a difficult procedure as chemical concentrations may vary considerably on small spatial scales. Comparison of duplicates was done using the Wilcoxon ranked sum tests which suggested that the distribution of duplicate values were not shown to be significantly different from one another (Table 2.7). Duplicate values did not show a clear bias and differences are likely due to geologic and contaminant concentration heterogeneity in the subsurface (Figure 2.12, Table 2.8).

The one portion of the corehole where the shake-flask method appeared to outperform MAE was in the variably saturated region. The configuration of the water table near the bedrock contact at this site limited the number of samples taken in this region. As the water table fluctuates in this area, samples undergo drainage and imbibition. Based on

water level data from multilevel monitoring wells installed in coreholes MW-367-4 and MW-367-5 and on-site conventional monitoring wells, the elevation of 337 masl was selected to delineate the variably saturated zone. The RPDs for the 11 samples in this region are shown in Figure 2.13 and Table 2.9. Eight of the 11 sample sets showed decreased concentrations for MAE compared to the shake-flask method. The three sample pairs showing higher concentrations occurred in the samples closest to 337 masl and could be the result of inadequate delineation of the saturated zone. This result is not totally unexpected as the samples split in the lab underwent microwave treatment directly after being separated which may not have allowed an adequate time for solvent penetration into the rock pore space, which, for saturated samples would have been full of water. This could lead to inadequate heating of the rock matrix during microwave treatment. The RPD values are smaller for the field splits which had 24 hours for the methanol to invade the unsaturated pore spaces of the matrix before microwave treatment.

In corehole MW-23, a continuous subset of shake-flask samples showed elevated concentrations at approximately 1.5 μg TCE/L methanol (Figure 2.14). The consistency of these concentrations within the highly variable geologic setting suggests that some form of cross-contamination occurred and therefore these samples were not incorporated into the statistical dataset. In addition, these values showed poor correlation with the MAE values.

2.5 Implications and Conclusions

A novel extraction method for the extraction of VOCs from crushed porous sedimentary rock has recently been developed enabling decreased extraction times from weeks to minutes, leading to increased laboratory efficiency, rapid data acquisition, less potential for cross-contamination during storage, and prospects for analysis in the field.

The added benefit of MAE is that it negates the need for long-term storage which has the associated risks of cross-contamination and volatilization losses.

This chapter provides the field verification of this method and also compares it with the conventional purge and trap method for solid samples. MAE and the shake-flask methods both outperform the purge and trap method providing lower detection limits and fewer false negatives. The standard purge-and-trap method recommended for soil samples provided false negatives (i.e. non-detects) due to incomplete extraction, lack of field preservation, and the elevated detection limit.

Rock core VOC samples unpreserved in the field are not representative of the actual sub-surface contamination and thus should not be treated as accurate quantitative mass estimates. This study shows that differences due to preservation methods are statistically significant and that field preserved values were much higher than lab preserved samples. More research is required to determine the effect of sample water content on the extraction efficiency of MAE for rock samples.

Table 2.1: Method MDL and LOQ Statistics: For MAE the MDL and LOQ tend to be higher due to the fact that additional methanol was used for these samples to achieve quantitative transfer of the VOA vials to the Teflon vials.

Statistic	MAE		Shake-Flask	
	MDL (µg TCE/ g rock)	LOQ (µg TCE/ g rock)	MDL (µg TCE/ g rock)	LOQ (µg TCE/ g rock)
No. of observations	698	698	843	843
Minimum	6.E-05	5.E-04	2.E-05	2.E-04
Maximum	2.E-04	1.E-01	2.E-04	1.E-03
Range	1.4E-04	1.1E-01	1.4E-04	1.1E-03
Median	1.E-04	8.E-04	6.E-05	4.E-04
Mean	1.E-04	1.E-03	6.E-05	5.E-04
Variance (n)	6.E-10	2.E-05	6.E-10	4.E-08
Standard deviation (n)	2.E-05	4.E-03	2.E-05	2.E-04

Table 2.2: Qualifier Comparisions J = detected but not quantifiable, U = Not detected, UJ = detected contamination in the associated blank

Field Splits

Qualifier	Field Shake-flask (# of Samples)	Field MAE (# of Samples)
Not Qualified	122	111
J	88	43
U	0	0
UJ	0	56

Lab Splits (Liu, 2005)

Qualifier	LAB Shake-flask	LAB MAE
Not Qualified	162	150
J	107	148
U	31	3
UJ	1	0

Lab vs. Field Preservation

Qualifier	Lab Shake-flask	Field Shake-flask
Not Qualified	69	90
J	66	62
U	17	0
UJ	1	1

Table 2.3: Sample dataset designation for RPD calculation
RPD = 100 % * (Dataset A – Dataset B)/ (Average of Dataset A and B)

	Field Preserved Shake-Flask vs Field Preserved MAE	Lab Preserved Shake-Flask vs Lab Preserved MAE	Lab Preserved Shake-Flask vs Field Preserved Shake-Flask	Lab Preserved MAE vs Field Preserved Shake-Flask
Sample A	Field Preserved MAE	Lab Preserved MAE	Field Preserved Shake-Flask	Field Preserved Shake-Flask
Sample B	Field Preserved Shake-Flask	Lab Preserved Shake-Flask	Lab Preserved Shake-Flask	Lab Preserved MAE

Table 2.4: Wilcoxon Signed Rank Test for dataset comparison (one tail test)- Null hypothesis rejected. In each of these scenarios method B statistically gave higher concentrations than method A.

V+ - The sum of the ranks of the differences where method A is greater than method B
p-value - If this is less than alpha the null hypothesis is rejected
alpha - Probability significance level

H null: The distribution of the two samples is not significantly different.
H alternative: The distribution of the first sample is shifted to the left of the distribution of the second sample.

Test values	Field Preserved Shake-Flask vs Field Preserved MAE	Lab Preserved Shake-Flask vs Lab Preserved MAE	Lab Preserved Shake-Flask vs Field Preserved Shake-Flask	Lab Preserved Shake-Flask vs Field Preserved MAE
V+	720.000	1110.000	211.000	91.000
V (expected value)	5220.000	2376.500	1139.000	1105.500
V (variance)	251430.000	77236.250	25627.500	24505.250
One-tailed p-value	< 0.0001	< 0.0001	< 0.0001	< 0.0001
Alpha	0.05	0.05	0.05	0.05

Table 2.5: Relative Percent Difference Statistics - The RPD statistics approximately followed a normal distribution. As expected the field duplicate RPDs have a higher standard deviation due to increased variability between the samples split in the lab.

Statistic	Field Preserved Shake-Flask vs Field Preserved MAE (RPD)	Lab Preserved Shake-Flask vs Lab Preserved MAE (RPD)	Lab Preserved Shake-Flask vs Field Preserved Shake-Flask (RPD)	Lab Preserved MAE vs Field Preserved Shake-Flask (RPD)
Number of Values	97	144	66	67
Minimum	-188	-88	-108	-116
Maximum	187	115	191	183
Median	30	38	98	63
Mean	29	41	96	66
Variance	4023	1281	4279	4888
Standard deviation	63	36	65	70
Range	375	202	299	299

Table 2.6: Comparison of EPA Method 8260 Detected Values – Out of the 101 sample there were only 3 detects found for the purge and trap method.

Depth (mbgs)	EPA Method 8260B (µg TCE/ g rock)	Lab Shake-Flask (µg TCE/ g rock)	Lab MAE (µg TCE/ g rock)
335.1	2.0E-02	8.9E-02	1.3E-01
324.6	3.0E-02	6.7E-04	1.1E-03
331.7	5.0E-02	8.7E-03	1.4E-02

Table 2.7: Wilcoxon Signed Rank Test for Duplicate Comparison (two tailed test) – Null hypothesis accepted. The distributions of the two samples are not significantly different.

T+ - The sum of the ranks of the differences where method A is greater than method B
p-value - If this is less than alpha the null hypothesis is rejected
alpha - Probability significance level

H null: The distribution of the two samples is not significantly different.
H alternative: The distributions of the two samples are significantly different.

Test Values	Duplicates
T+	811.000
T (expected value)	826.500
T (variance)	15841.250
Z (observed value)	-0.123
Z (critical value)	1.960
Two-tailed p-value	0.902
Alpha	0.05

Table 2.8: General RPD statistics for duplicate comparison.

The field preserved MAE includes duplicate samples from 2004, 2005, and 2006.

Statistic	All (RPD)	Field Preserved Shake-Flask (RPD)	Field Preserved MAE (RPD)	Lab Preserved Shake-Flask (RPD)	Lab Preserved MAE (RPD)
Number of Values	57	6	38	6	7
Minimum	-141	-17	-141	-123	-131
Maximum	138	42	138	81	73
Range	279	58	279	204	204
Median	-3	-4	6	-17	-17
Mean	-7	4	-2	-18	-32
Variance	3442	390	3515	4108	4104
Standard deviation	59	20	59	64	64

Table 2.9: Relative percent difference statistics for the variably saturated zone – For the 11 samples taken above 337 masl shake-flask extraction tended yield higher results than MAE. This region was also the only region to show detects for the shake-flask method and non-detects for MAE.

Field Splits

	Number of Samples	Minimum (RPD)	Maximum (RPD)	Mean (RPD)	Std. deviation (RPD)
All Elevations	210	-188	198	31	82
Elevation > 337 masl	5	-77	36	-14	41

Lab Splits

	Number of Samples	Minimum (RPD)	Maximum (RPD)	Mean (RPD)	Std. deviation (RPD)
All Elevations	301	-196	191	33	60
Elevation > 337 masl	6	-196	92	-126	109

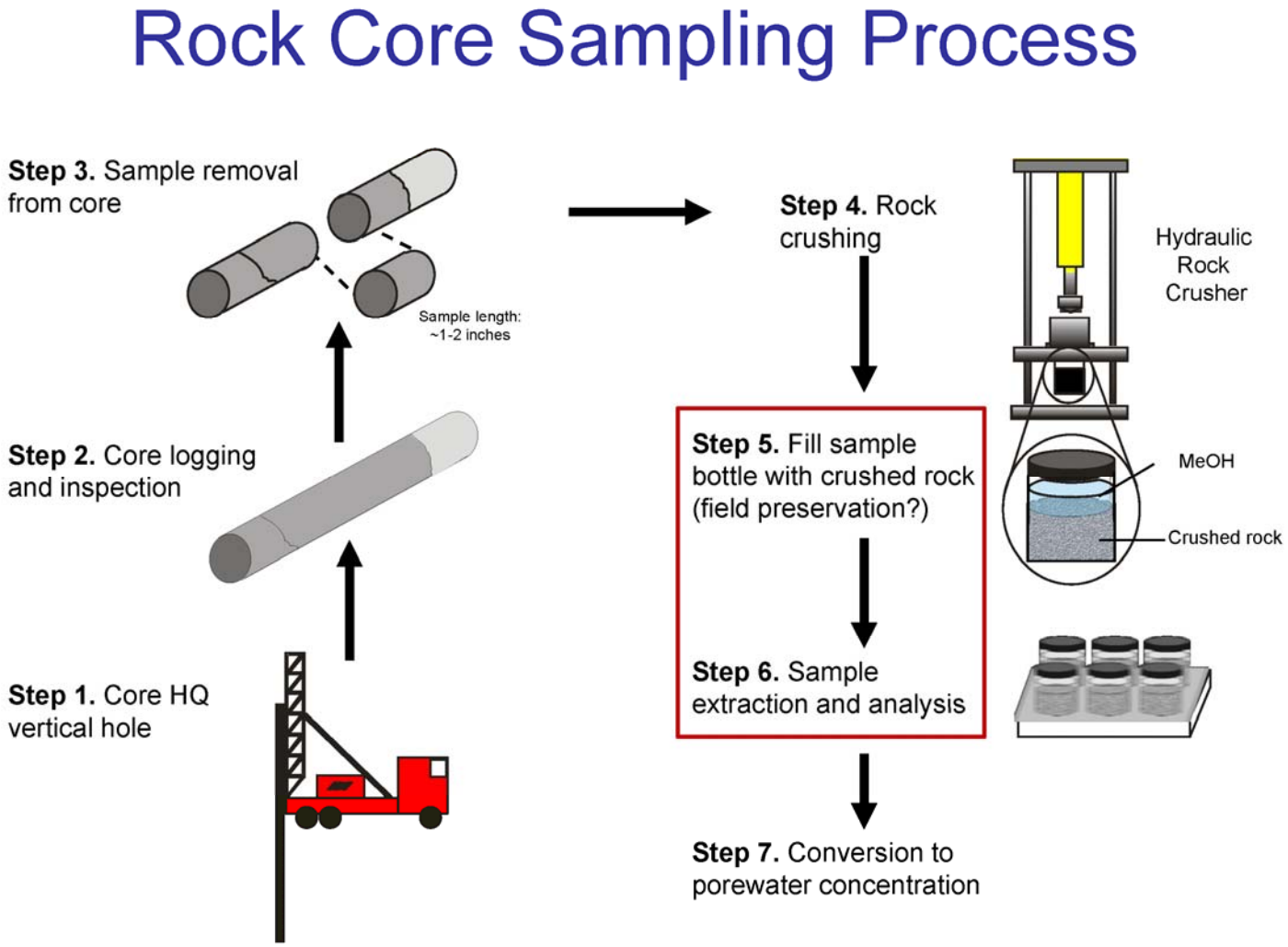

Figure 2.1: Rock core sampling process. Steps 5 and 6 are the focus of this chapter (modified from Sterling [1999], Turner [2001], and Hurley [2003]).

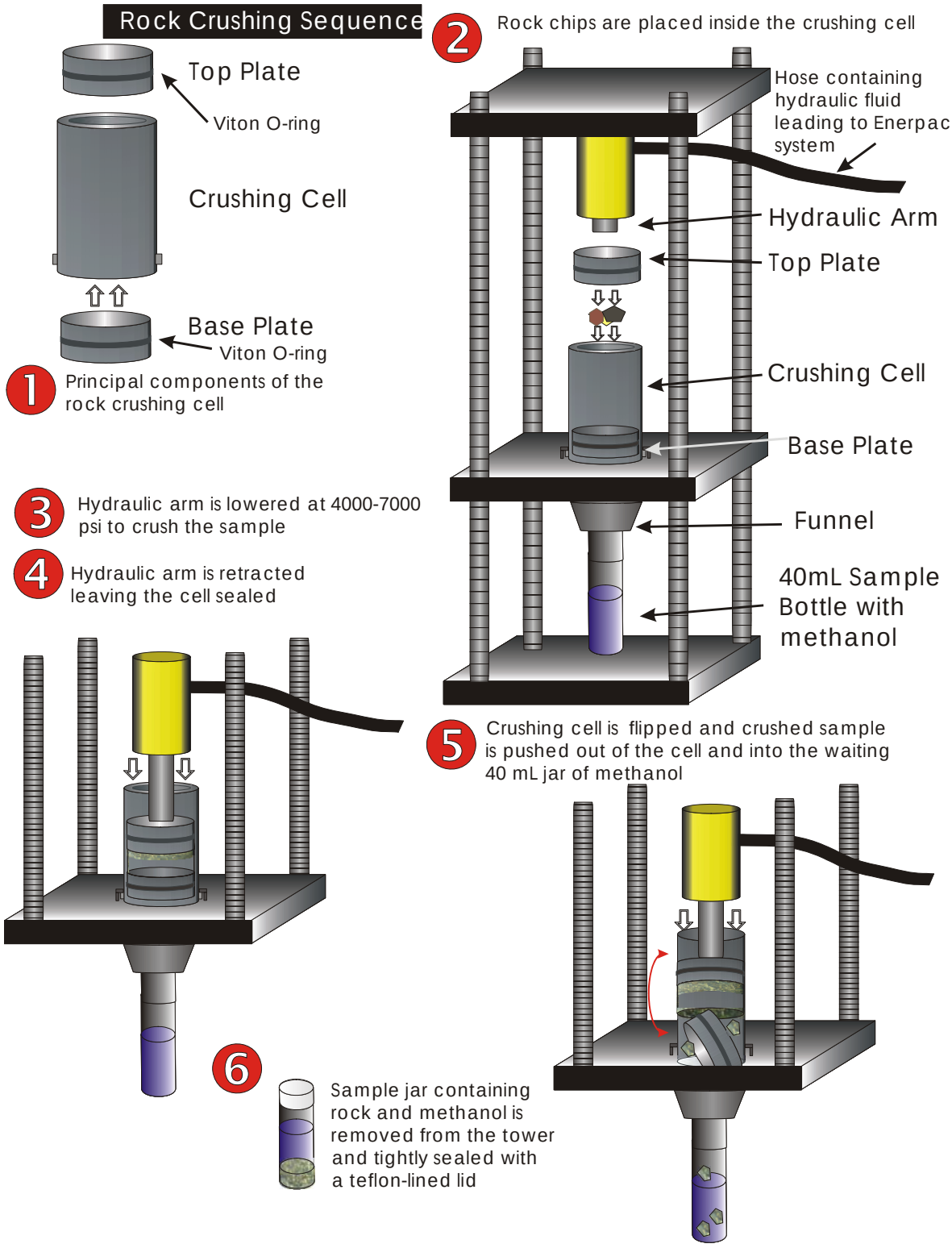

Figure 2.2: Rock Crusher Schematic – (modified figure created by Hurley, 2003 modified by Meyer 2005).

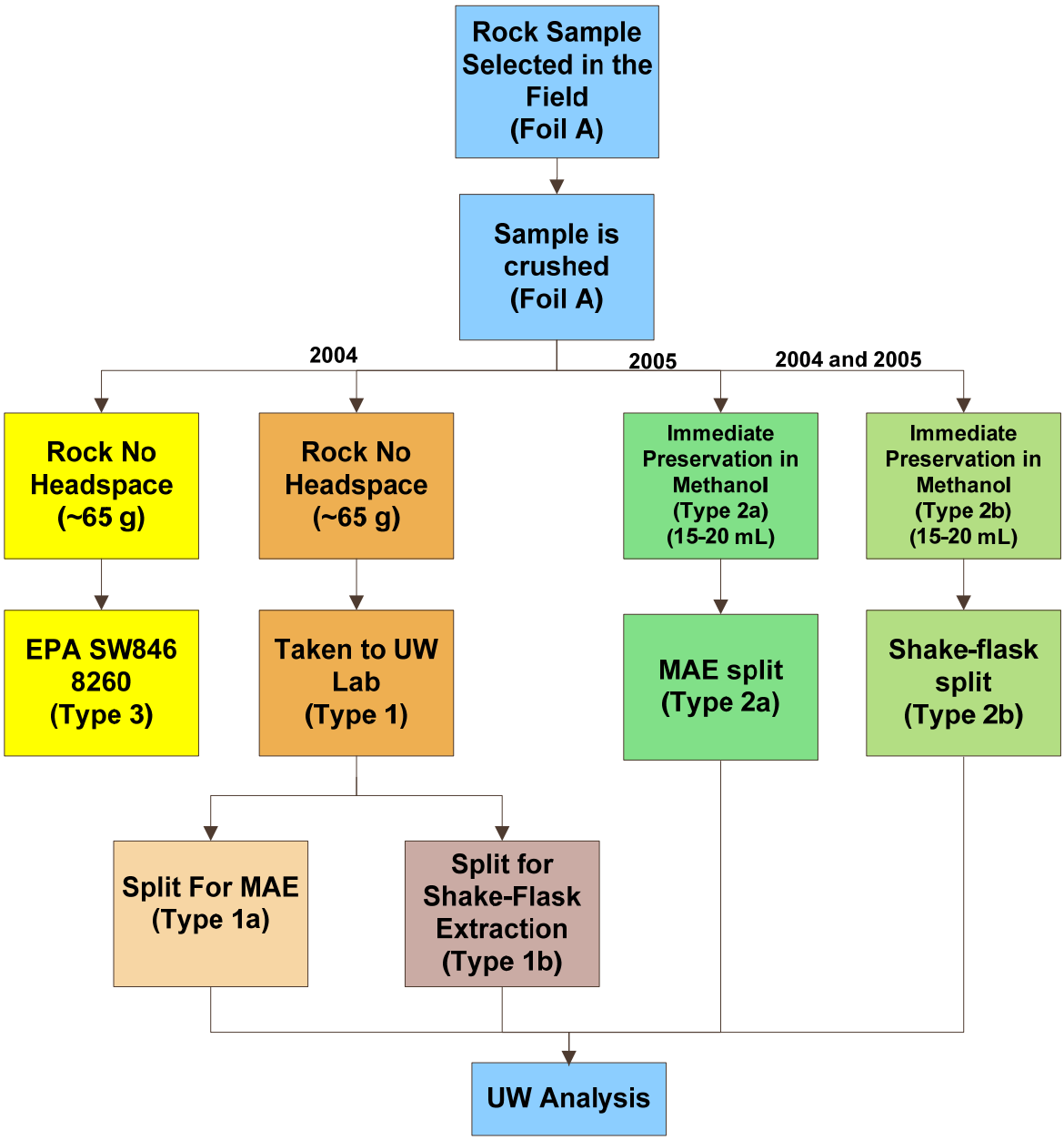

Figure 2.3: Sample collection, extraction and analysis flow chart.

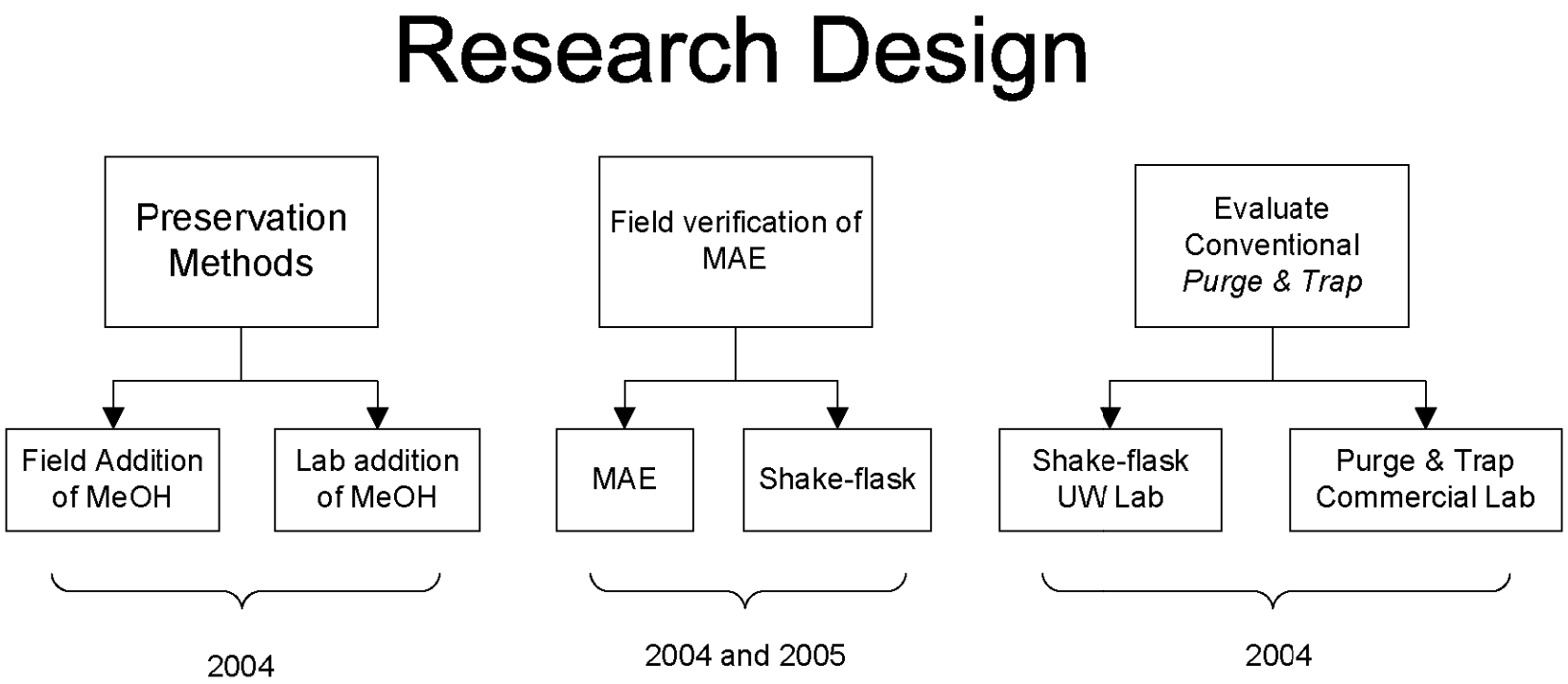

Figure 2.4: Chapter flow diagram showing different extraction comparisons and preservation methods.

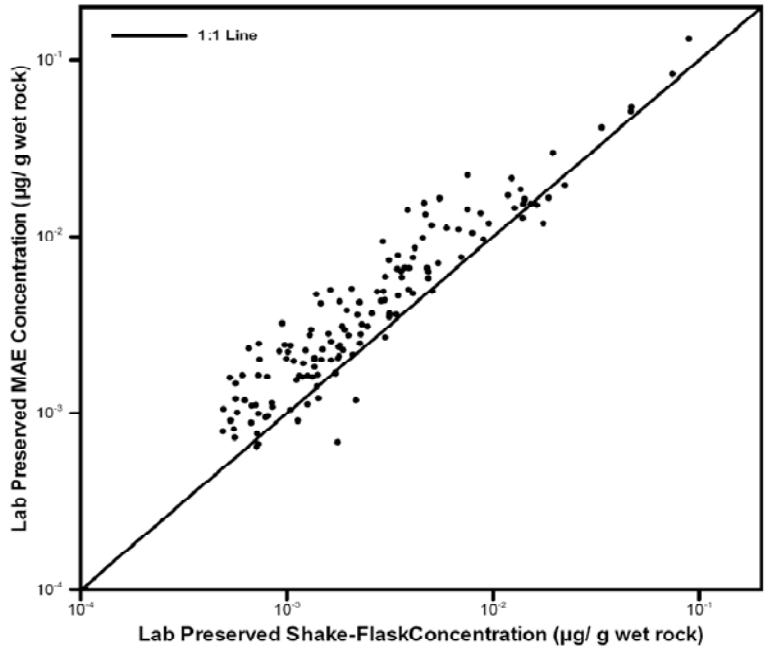

(A)

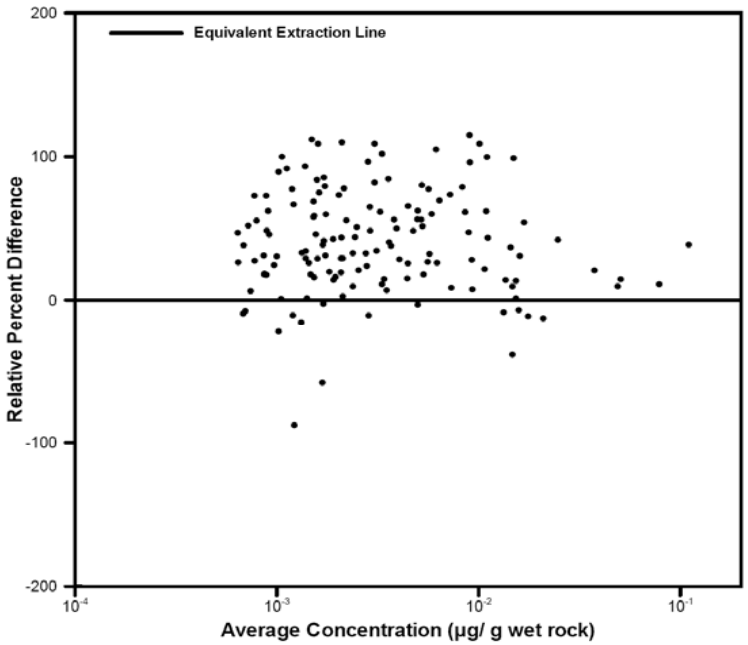

(B)

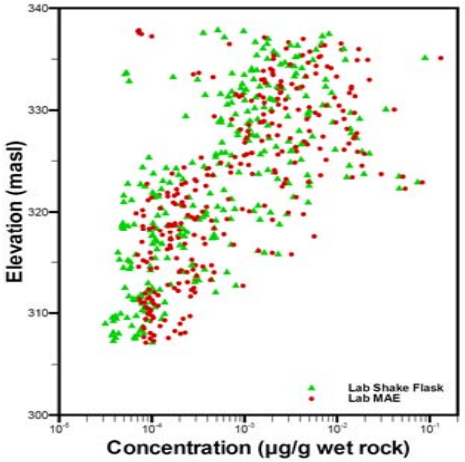

(C)

Figures 2.5: Comparison of shake-flask and MAE (lab addition of methanol): Extraction efficiency for MAE is typically greater than for shake-flask extraction in the laboratory split samples. A – regression plot, B – bias plot, and C – vertical profile

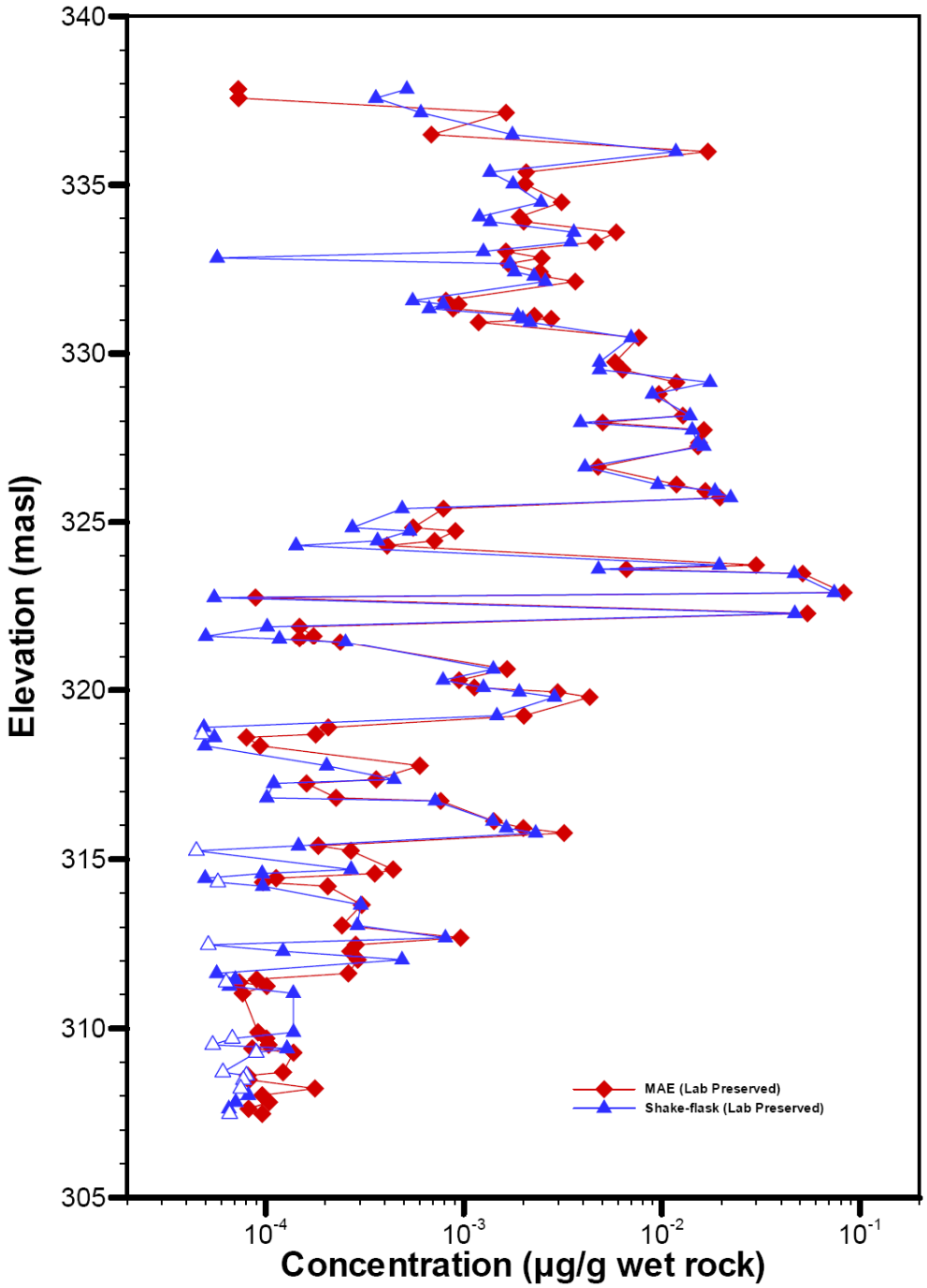

Figure 2.6: MW-367-5 Comparison of shake-flask and MAE (lab addition of methanol). The profiles show excellent correlation with MAE typically yielding slightly higher concentrations. NOTE: x-axis is a log scale

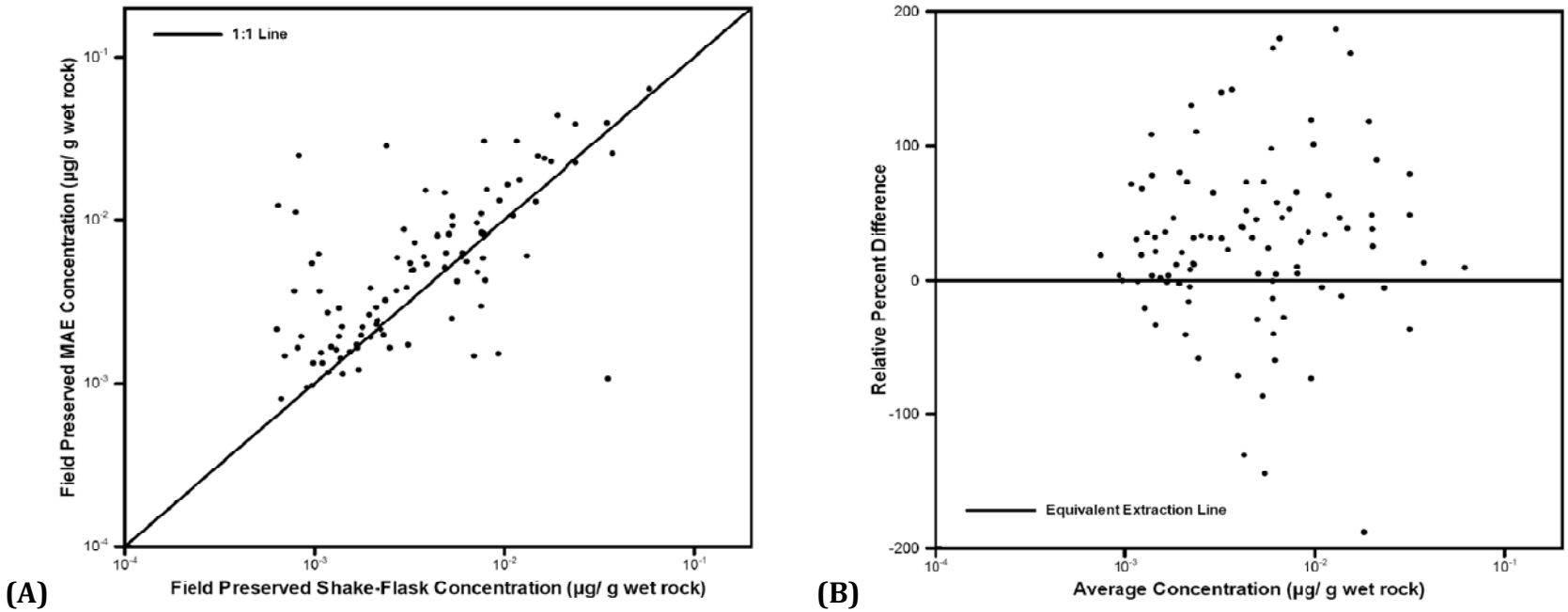

Figure 2.7: Comparison of shake-flask and MAE (field addition of methanol): Extraction efficiency for MAE is typically greater than for shake-flask extraction in the laboratory split samples. A – regression plot, B – bias plot, and C – vertical profile

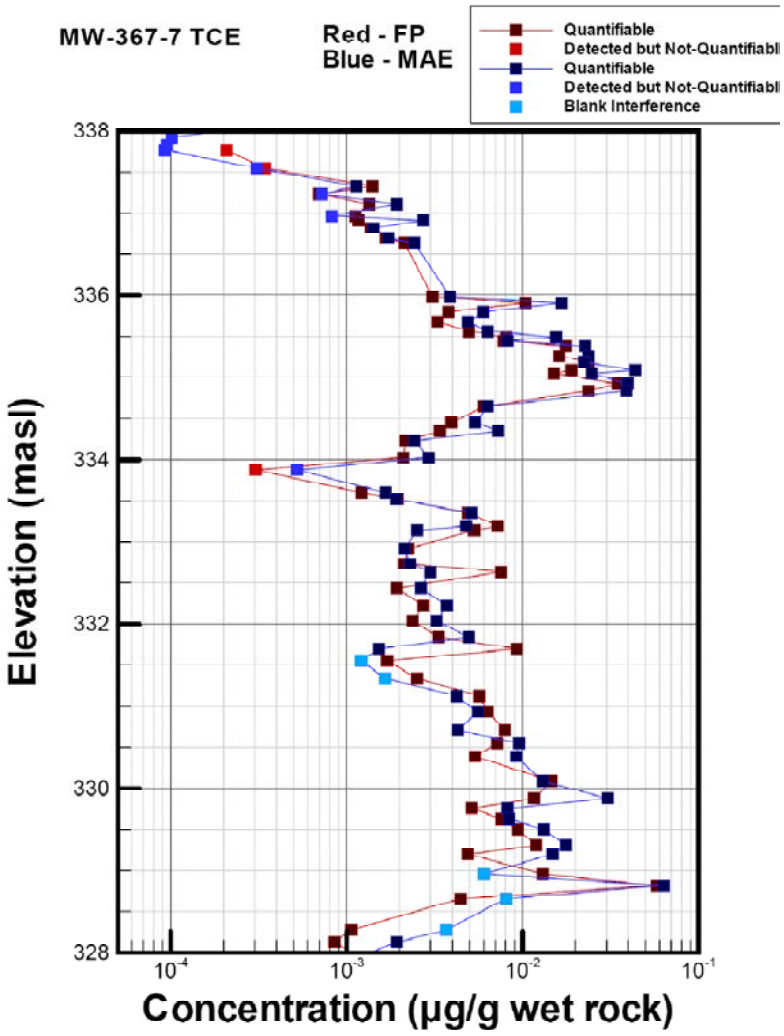

(A)

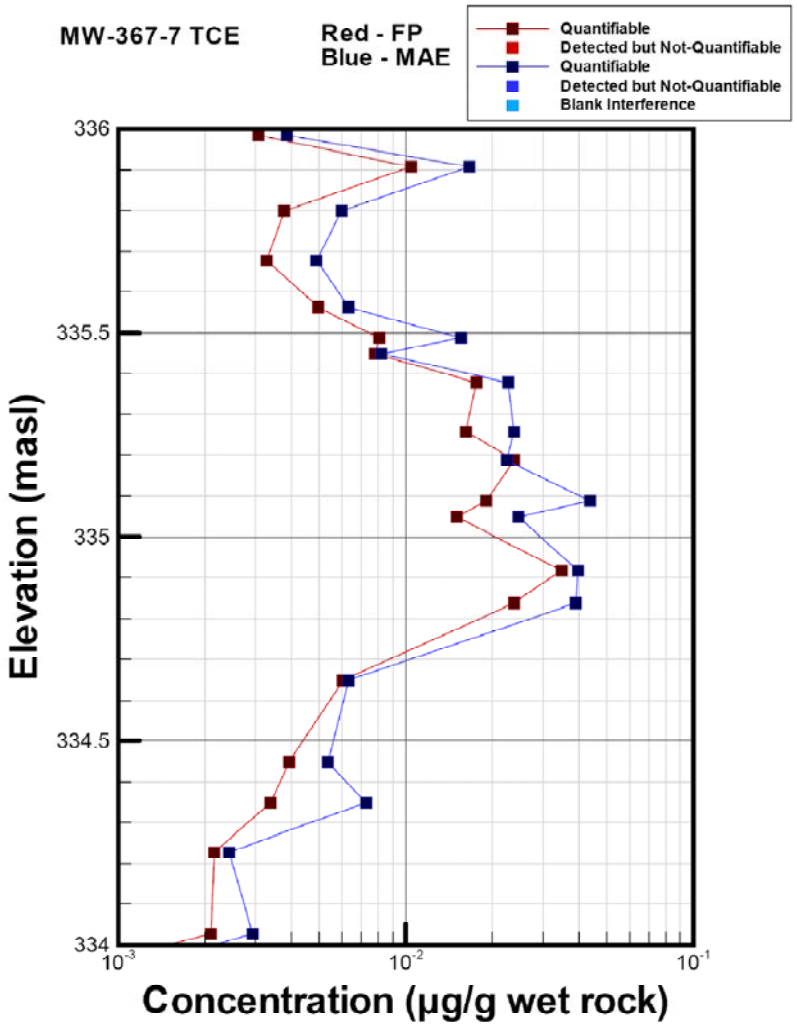

(B)

Figure 2.8: MW-367-7 – Thes plots show the similarities between field preserved MAE (blue) and field preserved shake-flask extraction (red) and the systematic higher recoveries obtained by MAE.

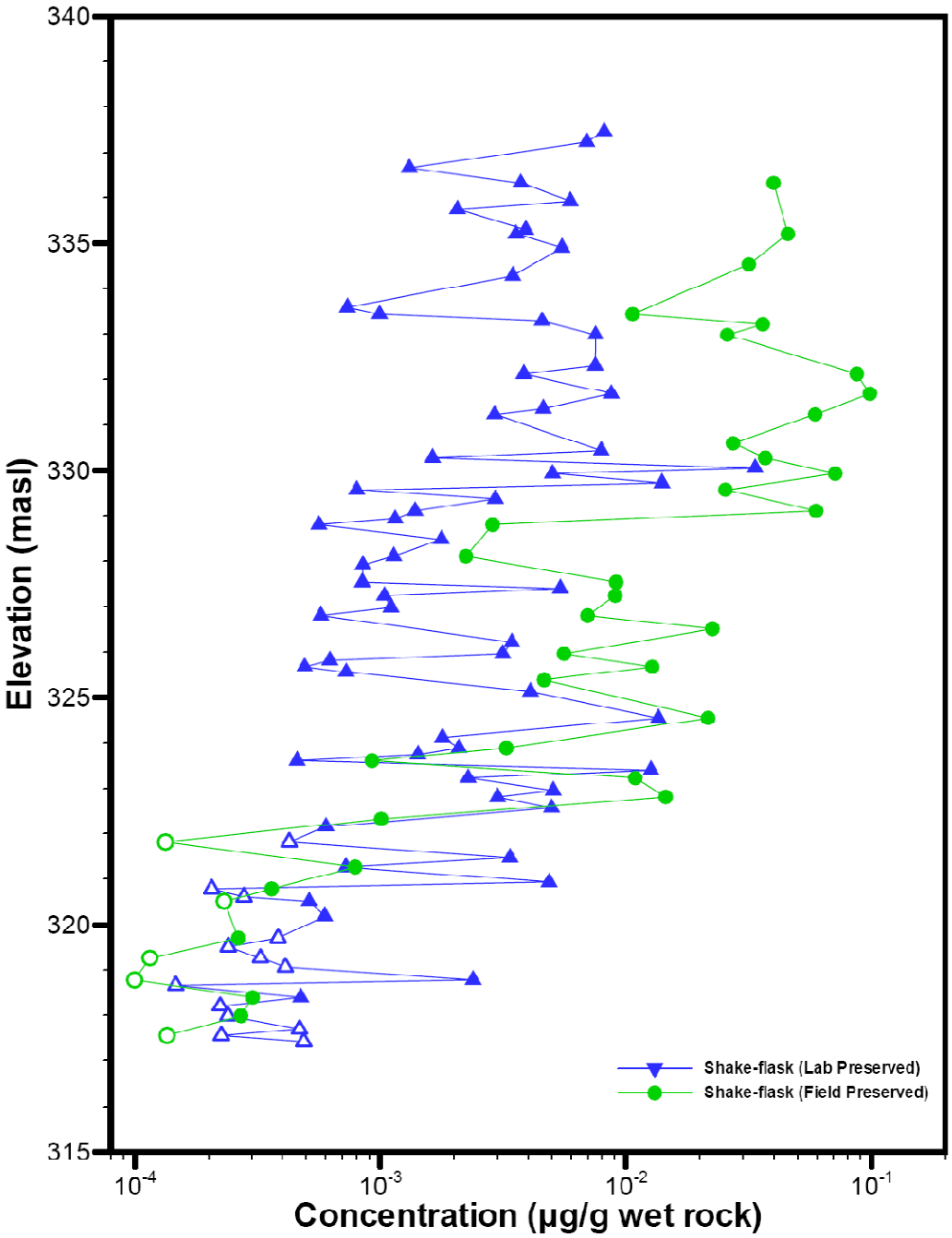

Figure 2.9: MW-22 Comparison of shake-flask (field addition of methanol) and shake-flask (lab addition of methanol). The profiles show the same general trends but with the field preserved shake-flask samples being shifted to higher concentrations. NOTE: x-axis is a log scale

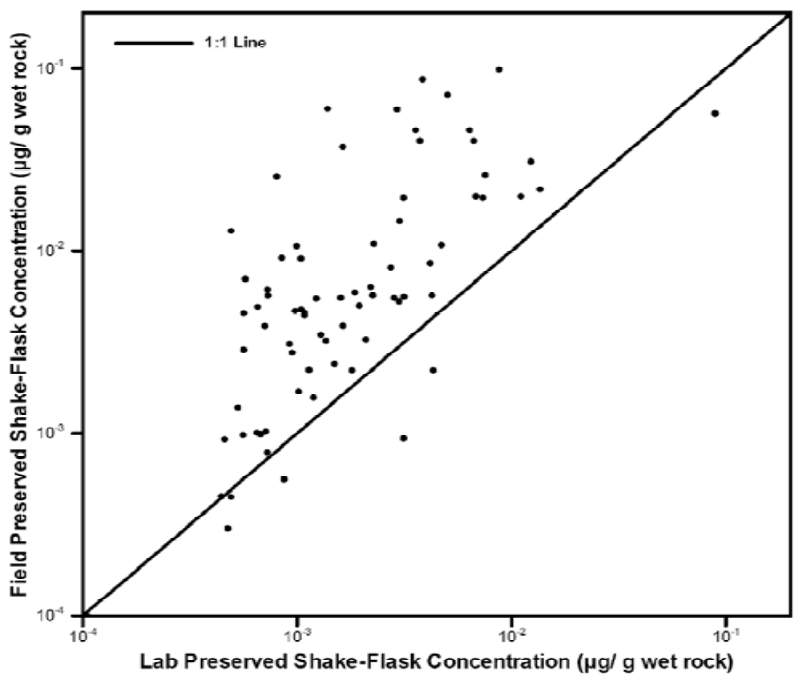

(A)

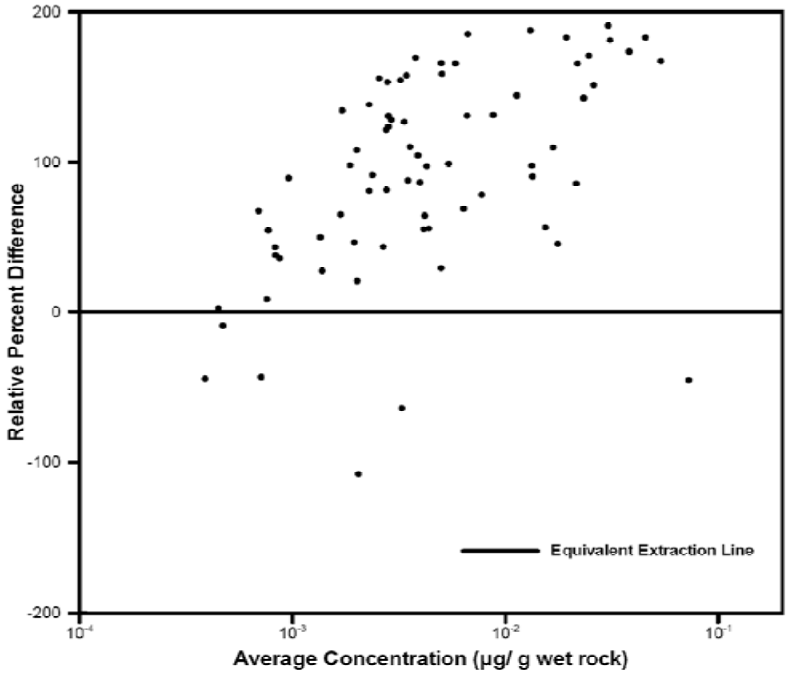

(B)

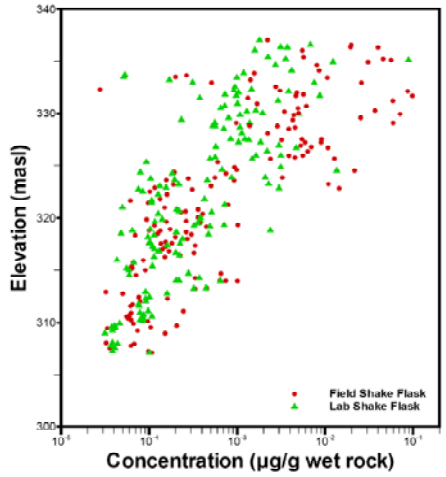

(C)

Figure 2.10: Laboratory addition of methanol (shake-flask extraction) vs. field addition of methanol (shake-flask extraction): Field preservation of rock samples show significant benefits to preserving the rock samples in the lab. At higher concentrations the difference appears more pronounced. A – regression plot, B – bias plot, and C – vertical profile

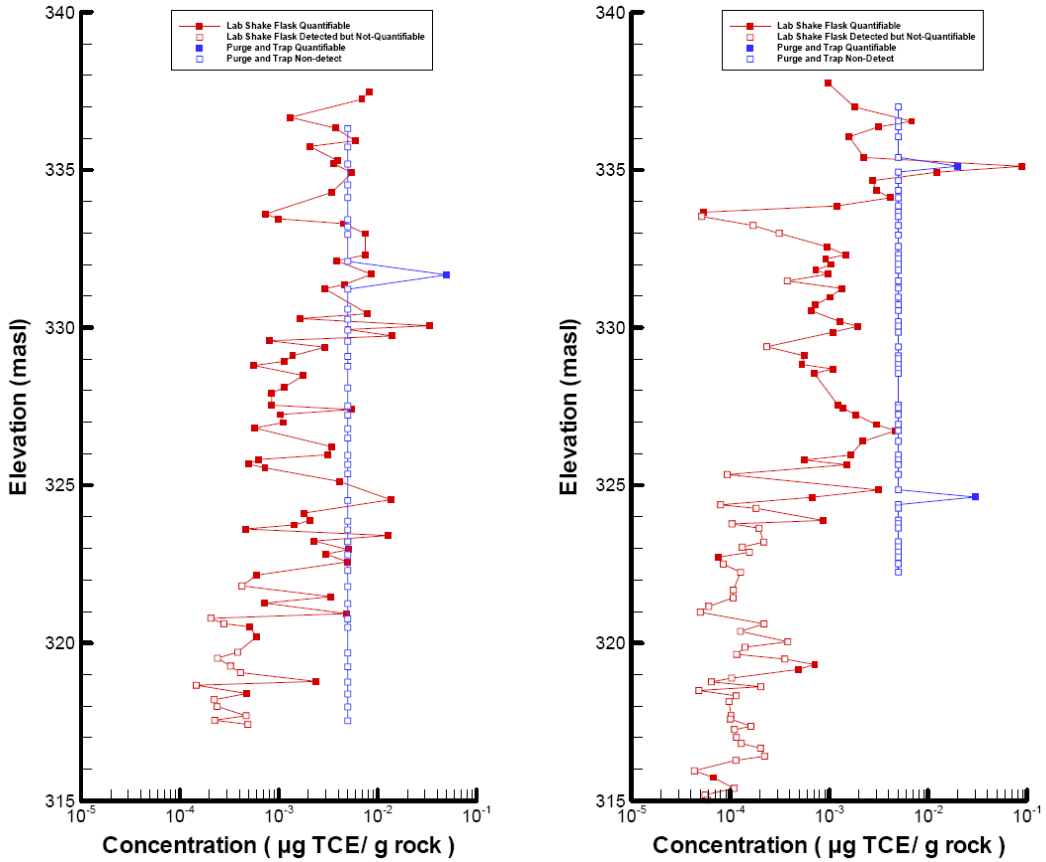

Figure 2.11: Comparison of EPA Method 8260B with laboratory addition of methanol shake-flask samples: Values below their respective detection limits were plotted with open boxes and as 0.5 * MDL. This plot shows that the detection limit for 8260B is typically too large to adequately characterize contamination at the Guelph site. As well, numerous concentrations for the shake-flask extraction above the detection limit for Method 8260B were not detected with this method. This suggests incomplete extraction or additional volatilization losses for this method.

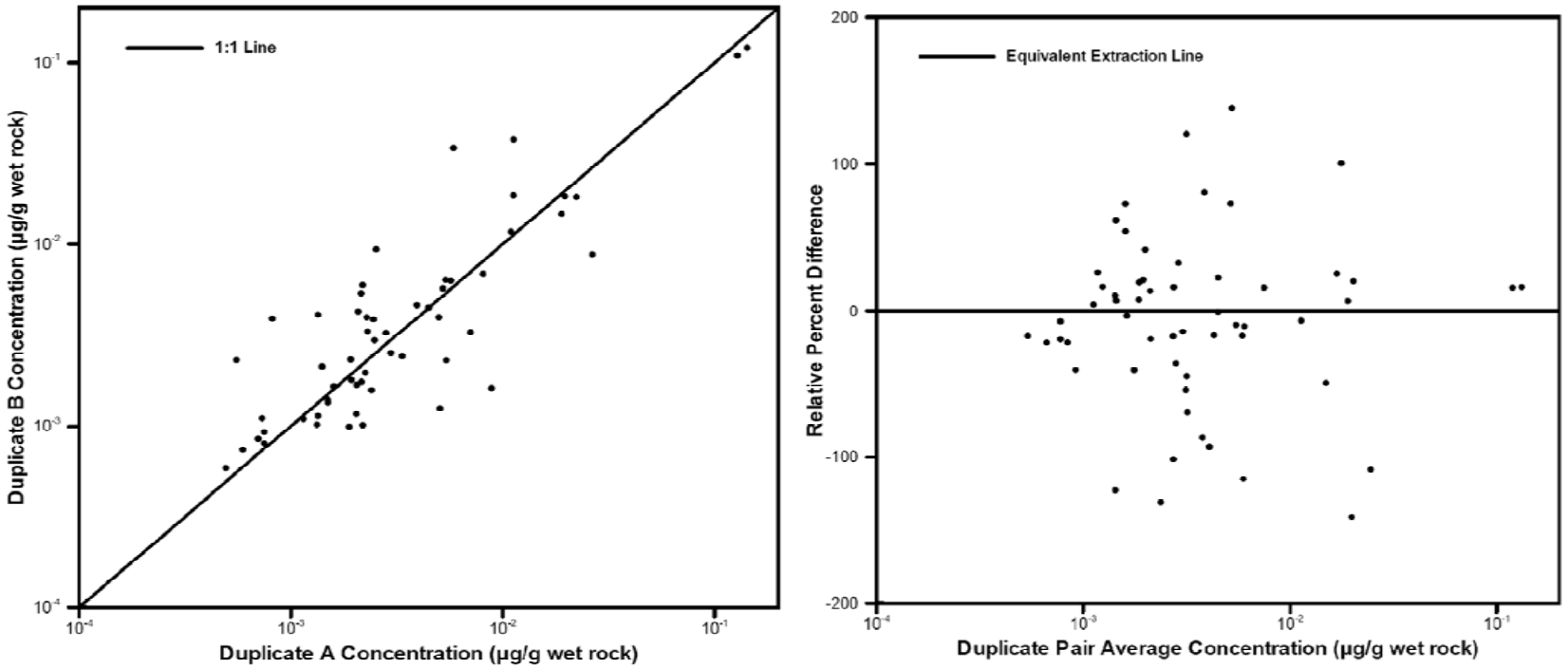

Figure 2.12: Field Duplicate Comparison: The RPD for duplicate field samples extracted using the same method is of similar magnitude to the results from MAE versus shake-flask extraction. There could be potential trends with depth as certain portions of the rock core would give a more variable particle size distribution when crushed. Also certain depths contain more small scale heterogeneities which could influence the partitioning of contaminants. A - regression plot (all duplicates lumped), B – bias plot (all duplicates lumped)

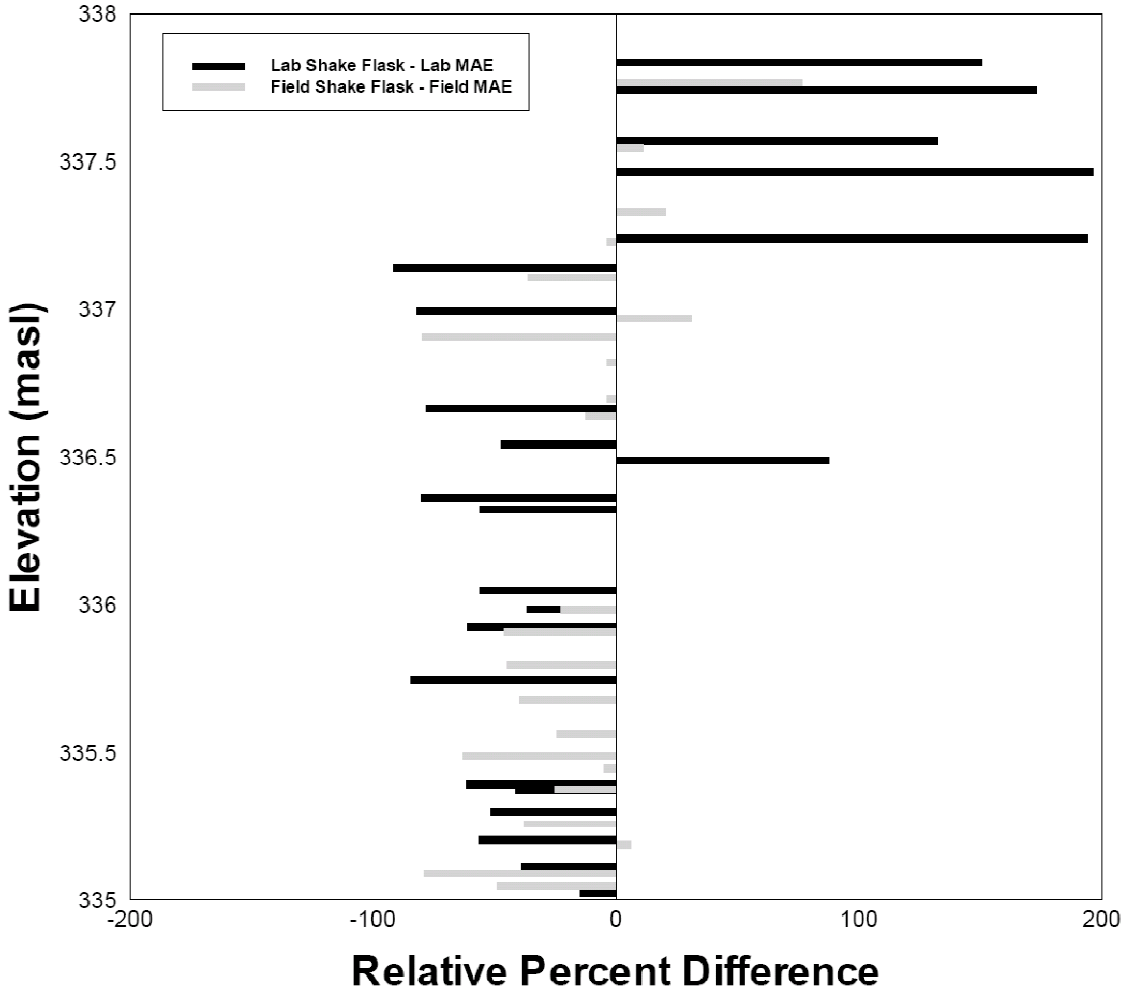

Figure 2.13: Relative percent differences for MAE and shake-flask methods above 335 masl: This plot shows the potential difference in extraction efficiency for the variably saturated zone along with some results in the saturated zone.

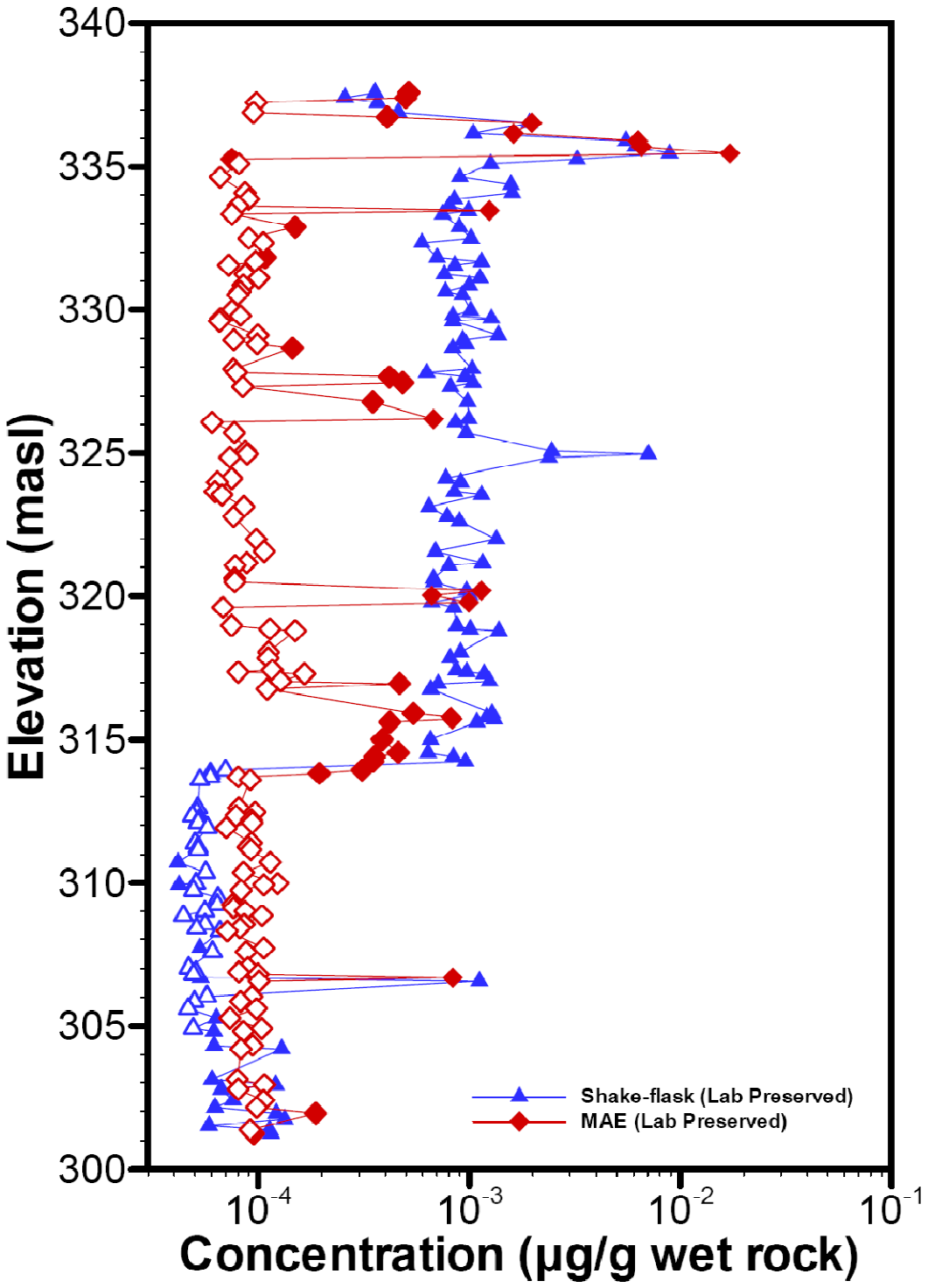

Figure 2.14: MW-23 method comparison - this plot shows the effects of cross-contamination for the shake-flask method.

Chapter 3: The Use of Geophysical Porosity and Bulk Density Estimates to Assist Porewater Conversion

3.1 Abstract

In the method for rock core VOC analyses developed by Parker/Górecki for delineating VOC distributions in sedimentary rock, rock samples from continuous rock core through zones of suspected contamination are collected at mean spacings of 0.3 m and the analytical results for total concentrations are corrected to equivalent equilibrium porewater concentrations using estimated values of the physical properties: rock matrix porosity, dry bulk density and fraction of organic carbon (f_{oc}). These estimated values are derived from measured values on visually representative rock core samples collected at average spacing of 1 per 3 m along the core. The measurements of physical properties are not continuous in order to minimize cost. In this chapter, geophysical logs (neutron, gamma-gamma, and the acoustic televiewer amplitude) were examined in the context of the measured physical properties values to determine whether these logs can provide improvements in the selection of physical properties values for the VOC porewater calculated values relative to the standard method. The traditional method employed was based upon assigning core sections (and the VOC samples contained) to lithologies, and then applying the average physical property values from the representative lithology to the porewater conversion equation.

$$C_{pw} = \frac{C_r * \rho_{b(wet)}}{\phi_m \times \left[1 + \left(\frac{\rho_{b(dry)}}{\phi_m} \times K_{oc} \times f_{oc}\right)\right]} \qquad \textbf{Equation 3-1}$$

This is beneficial to assigning one value for porosity, bulk density and f_{oc} to all rock core VOC samples, however it does not describe the variability evident on the cm scale. Large vertical zones of high f_{oc} were not detected in the Guelph rock core which generally exhibited values near the detection limit, however, some isolated features such as fracture infillings and stylolites did show

higher f_{oc}. High resolution porosity and bulk density values were determined with core sample calibrated geophysical logs leading to improved estimates for porewater concentrations.

3.2 Introduction

In the world of fractured rock hydrogeology uncertainty reigns. Uncertainty is involved in almost every aspect of data acquisition, from sample choice to final analysis. In many instances, we operate under the "myth of monocausality", simplifying the situation by suggesting that one factor is the cause of an event or occurrence (Miles & Shevlin 2001). However, for volatile organic compounds in fractured rock multiple variables must be considered during interpretation.

To accurately assess contamination in porous fractured rock aquifers, targeting the rock matrix is a necessary component of study as this is where the majority of contaminant mass resides at many field sites. Total mass concentrations have important implications to the outcome of remediation procedures and provide a time integrated contaminant concentration. The rock matrix is intimately related to the fracture water and acts as a potential source or sink for contamination in the fracture water. Contaminant mass in the rock matrix samples may reside in a number of different forms: sorbed mass, dissolved mass, NAPL, or as a vapor phase. For this study, contamination in the fully saturated rock matrix exists in the first two forms, as dissolved and sorbed phases.

Fundamental to the comparison of rock core VOC results to groundwater VOC results and also groundwater characterization is a conversion of rock matrix total mass to an equivalent porewater concentration. This conversion is based on the physical properties of the rock matrix and the chemical properties of the analytes of concern and uses the method of Pankow and Cherry (1996). Organic carbon may be concentrated in thin serrated pressure solution features called stylolites (Langer, Novakowski, & Woodbury 1999). Because stylolites are not evenly distributed throughout the rock matrix and are very thin but laterally extensive (100 m) (Langer, Novakowski, & Woodbury 1999), describing the sorptive capacity using rock core measurements alone is difficult and often impractical.

To account for the sorbed phase mass, an understanding of the partitioning properties of the contaminant with the rock matrix is required. For hydrophobic organic compounds, sorption is believed to be dominated by solid organic carbon (Karickhoff 1981;Oliver 1985). The solid organic carbon will be dependent on the fraction of organic carbon (f_{oc}) and dry bulk density of the sample. We assume that the dissolved phase and the sorbed phase are in equilibrium and calculate the expected concentration in the dissolved phase based on this partitioning value (Figure 3.2). The total mass in the dissolved phase will be dependent on the porosity of the rock matrix. With these three measurable values: f_{oc}, dry bulk density, and porosity, we can estimate the aqueous phase concentration from the total mass concentration from the rock core.

Taking continuous physical property samples for these variables is not feasible for most investigations and thus averages of the physical properties are typically applied to VOC samples within a particular lithology (Hurley 2003). However, by using specialized geophysical tools we can obtain continuous estimates of porosity (Allen et al. 1967;Ellis 1990;Ellis & Singer 2007;Galle 1994;Smith 1989;Stromswold et al. 1989;Tittle & Allen 1966).

In this chapter, three geophysical logs are investigated to determine if they can provide reliable high resolution estimates of bulk matrix properties for the purpose of porewater conversion calculations; they are the neutron (porosity) log, the gamma-gamma (density) log, and the acoustic televiewer amplitude log. The goal of this is to create a procedure to use these geophysical logs as an objective measurement for assigning bulk density and porosity for individual samples in the porewater conversion process.

The neutron and gamma-gamma logs are nuclear logs that have primarily been used in determining stratigraphy and in the petroleum industry to estimate oil production. The neutron porosity tools in particular, have been used in the petroleum, mineral and water resources industries tracing back to at least the 1940s (Ellis 1990). The neutron porosity probe's principal

uses as defined by Rider [1996] are to estimate porosity, discriminate between oil and gas and to identify subsurface lithologies. The gamma-gamma density log is often used in conjunction with the neutron porosity log to provide additional evidence of these properties. Typically the acoustic televiewer provides data on borehole caliper, geotechnical rock classes, and fracture location and orientation (Advanced Logic Technology 2002).

3.2.1 Site Description

The research site located in Guelph, ON, consists of middle Silurian age dolostone overlaid with 3-5 m of glacial till. This investigation focuses on the Guelph Formation, a tan-grey fine to medium crystalinity sucrosic dolostone exhibiting a variety of features such as stylolites, vuggy and pinpoint porosity, and fossils. The types of porosity present in the Guelph dolostones can be classified according to Choquette and Pray 1970 as interparticle, fenstral, intraskeletal, shelter, intercrystalline, intracrystalline, moldic, vuggy and fracture porosity (Figure 3.1). Horizontal fracture spacing varies from centimeters up to 2 meters. A variably saturated region below the bedrock and overburden contact exists for 1-2 meters until the water table is reached.

At this site, TCE entered the subsurface more than two decades ago and migrated through the glacial overburden to the dolostone bedrock. Concentrations of tetrachloroethene (PCE) and degradation daughter products of TCE (isomers of DCE) in groundwater and rock core samples are also occasionally detected, but typically much less than the concentrations of TCE. The thin overburden, shallow water table, relatively constant dolostone mineralogy but variable bulk densities and porosities, high density of rock core VOC holes, and primarily TCE plume make this an excellent research site for the following study.

3.3 Methods

High resolution crushed rock VOC sampling was undertaken in 8 contaminated coreholes. Samples were collected, crushed, bottled, extracted and analyzed according the methods outlined in

chapter 2 and shown in Figure 3.3. As rock core VOC studies gain attention and are more commonly implemented steps need to be taken to ensure appropriate interpretations. The distribution of porosity, fraction of organic carbon, water saturation, the presence of NAPL, and to a lesser extent bulk densities, will affect the results obtained from rock core analysis. In addition the sensitivity of the method will strongly be influenced by these factors.

3.3.1 Physical Property Analysis

Physical property analysis was undertaken to determine and quantify the effect of rock variability on contaminant mass storage. Rock core collected in the field was cut with a diamond studded saw and sub-cored to create 3.8 cm diameter core cylinders. The lengths of the cylinders varied from 1.75 cm to 10.80 cm with an average length of 7.01 cm. Porosity was determined gravimetrically using water imbibitions and bulk densities calculated as the ratio of total mass to volume (equations 1 and 2). The experimental procedure for determining bulk densities and porosity were conducted according to Amirtharaj (2007) except deionized water was substituted for the brine water in the imbibition method to determine porosity.

Dry and wet bulk densities were calculated according to their respective equations.

$$\rho_{b(dry)} = \frac{m_{(dry)}}{V} \qquad \textbf{Equation 3-2}$$

$$\rho_{b(wet)} = \frac{m_{(wet)}}{V} \qquad \textbf{Equation 3-3}$$

Where:

ρ_b (g/cm^3) is the bulk density

m (g) the mass of the bulk sample

V (cm^3) is the bulk sample volume

Particle density was calculated according to the following equations.

$$V_v = \frac{(m_{(wet)} - m_{(dry)})}{\rho_w} \quad \textbf{Equation 3-4}$$

$$V_s = V - V_v \quad \textbf{Equation 3-5}$$

$$\rho_s = \frac{m_{(dry)}}{V_s} \quad \textbf{Equation 3-6}$$

Where:

V (cm^3) is the bulk sample volume

V_v (cm^3) is the volume of voids

V_s (cm^3) is the volume of solids

ρ_w (g/cm^3) is the density of water

ρ_s (g/cm^3) is the particle density

m (g) is the mass of the sample

Porosity was calculated according to the following equation.

$$\phi = \frac{m_{(wet)} - m_{(dry)}}{V \times \rho_w} \quad \textbf{Equation 3-7}$$

Where:

ϕ is the matrix porosity

ρ_w (g/cm^3) is the density of water

m (g) the mass of the bulk sample

V (cm^3) is the bulk sample volume

To determine the fraction of organic carbon (f_{oc}) in the dolostone, samples were first pulverized to a fine powder with a pestle in a ceramic mortar. Next samples were analyzed by the University of Waterloo Organic Geochemisty Laboratory using the method of Churcher and Dickhout [1987]. The f_{oc} method detection limit was 0.007 % for 2004-2006 and 0.015 % for 2007. In addition, 14 samples were analyzed by Golder Associates Ltd. Geotechnical laboratory in December 2007 using the method of Walkley and Black [1934]. Six additional samples from shallow fracture infillings were analyzed by PSC Analytical Services for TOC (LECO). Taking samples of pure stylolites proved to be difficult as most were thin and did not contain enough loose material to collect.

The previously mentioned physical properties are useful in estimating the aqueous contaminant concentration using the following relationships to account for sorbed mass.

$$R = 1 + \frac{\rho_{b(dry)} K_{oc} f_{oc}}{\phi} \qquad \textbf{Equation 3-8}$$

Where:

R is the partitioning coefficient

$\rho_{b(dry)}$ is the dry bulk density (g/cm^3)

K_{oc} is the soil organic carbon/ water partitioning coefficient (cm^3/g)

f_{oc} is the fraction of organic carbon (g organic carbon/g bulk)

ϕ is the matrix porosity

$$C_{aq} = \frac{C_s \rho_{b(wet)}}{\phi R} \qquad \textbf{Equation 3-9}$$

Where:

C_{aq} is the estimated aqueous concentration (g contaminant/cm^3)

C_s is the total matrix mass concentration (g contaminant/g rock)

$\rho_{b(wet)}$ is the wet bulk density (g rock/cm^3)

ϕ is the matrix porosity

R is the partitioning coefficient

The K_{oc} was estimated from Garbarini (1986) as 120 cm^3/g.

3.3.2 Geophysical Logging

Geophysical well logging provides useful information about the stratigraphy and groundwater flow at high resolution (cm scale). Depth accuracy is of paramount importance when working at the cm scale. Logging speed, determination of cable stretch and checking for depth encoding errors all play an important role in the quality and interpretation of the data obtained. Logging too quickly can 'smear' the resulting values which decreases the ability to discern small changes in the formation.

To ensure depths were accurate, geophysical logs were compared and matched to the core photo logs and core fracture logs. By doing this the results of geophysical logs and the rock core show excellent agreement with differences primarily less than 10 cm. When using the geophysical logs quantitatively, depth accuracy is necessary.

Neutron and gamma-gamma geophysical logging was conducted inside FLUTe™ lined coreholes. The FLUTe™ liner consists of urethane coated nylon which is expected to have minimal effects on the results of the nuclear tools. Because these logs use radioactive sources special precautions are taken to avoid losing the tool down the borehole. The FLUTe™ liner helps to

prevent cave in which could cause a tool to become trapped downhole and also acts as a safety net and can aid in tool retrieval in the event of the logging tool becoming detached.

Acoustic Televiewer

Two acoustic televiewers manufactured by Advanced Logic Technology (ALT) were used for this study: the FAC40 and the ABI40. These tools collect oriented caliper and structural data of the borehole wall by using ultrasonic pulses. The centralized probe, employing a rotating mirror and a fixed transducer, emits, digitally records, and processes the responses of the ultrasonic wave train. From the reflected wave train, ultrasonic amplitude and travel time images are created allowing one to determine borehole caliper, geotechnical rock classes, and fracture location and orientation (Advanced Logic Technology 2002). The sampling rate for this tool is 0.2 cm.

Neutron Logging

The neutron tool used is a Comprobe™ (model #2136) which is a centralized tool with dual-spaced He^3 thermal neutron detectors spaced 0.343 m and 0.569 m from a 3 curie americium-beryllium source. When neutrons released from the source collide with nuclei of similar mass to a neutron's mass (hydrogen atoms) the greatest amount of neutron energy is lost which in turn decreases the number of neutrons reaching the detectors (Ellis & Singer 2007). Because hydrogen in the subsurface is most commonly found in water the response is closely related to the water content. Electrochemically bound and unbound water is detected using this tool. In saturated rock of similar mineralogy the correlation to porosity is good. Values were recorded every 2.5 cm with estimated vertical resolutions of 0.343 m and 0.569 m for the near and far detectors respectively.

Gamma-Gamma Logging

The gamma-gamma tool used is a Mineral Logging Systems™ bulk density probe which is a side-collimated tool with a single detector 40 cm from a ^{137}Cs source. Gamma rays from the source are moderated and scattered by electrons between the source and detector due to Compton

scattering (Keys 1997). The resulting gamma rays detected will be attenuated more greatly in higher electron density environments which are proportional to the material bulk density. The resolution for the density log is estimated to be equal to the detector spacing which is 0.475 m with a sampling rate of 2.5 cm.

In addition to the differences in resolution of the geophysical methods there is a difference in the depth of investigation. The nuclear logging tools measure into the formation a few 10s of cm whereas the acoustic televiewer primarily scans the borehole surface and only enters the borehole formation by a few mm. These methods use the formation surrounding the core to infer the core properties thus introducing some error.

3.3.3 Comparison of Geophysical and Core Methods for Porosity and Bulk Density

To yield quantitative estimates for porosity and density the geophysical tools require calibration with core samples. In complex hydrologic systems with highly variable mineralogy this may be a difficult task and multiple correlation equations may be needed. Fortunately, the Guelph site aquifer is composed predominantly of dolostone with very minimal shale content. Also, because the particle density for the core samples does not vary greatly the gamma-gamma log can provide a good estimate for porosity.

Correlation equations for the acoustic televiewer and nuclear logs with core samples were created by cross-plotting the count rate at the detectors against the core derived porosity and bulk densities and using linear regression. Linear regression appears to provide a reasonable fit for the data. The acoustic televiewer amplitude data had a different scale for the response depending on the probe used. Therefore the response was normalized to the maximum response from the log before correlations were done.

3.3.4 Effect on Porewater Concentration Calculation

To determine the effect of using geophysical estimates for porosity and bulk density concentration profiles were converted from µg contaminant/g rock to an equivalent µg contaminant/L porewater using two different estimates for density and porosity. The first conversion used the core derived average values for porosity, wet and dry bulk densities, and f_{oc} for all the dolostone samples. The second method used the estimated porosity and bulk densities from the acoustic televiewer log. To get the value for each core sample, values from the normalized acoustic televiewer amplitude were averaged over an enlarged portion (4 cm on each side) around the VOC sample midpoint. This was done to minimize the effect of a spurious value dominating the calculated physical parameters. Then the correlation equations for porosity and bulk density were applied and finally the conversion to porewater concentration was based on equations 2.7 and 2.8 and using the average f_{oc} for dolostone matrix samples.

The relative percent difference was calculated in the following manner.

$$RPD = \frac{C_{pw(ACTV)} - C_{pw(ave)}}{C_{pw(ACTV)}} \times 100 \qquad \textbf{Equation 3-10}$$

Where:

$C_{pw(ACTV)}$ is the calculated concentration using the ACTV derived physical property values (µg/L porewater)

$C_{pw(ave)}$ is the calculated concentration using the average of the core derived physical property values (µg/L porewater)

RPD is the relative percent difference

3.4 Observations and Results

Core physical properties measurements are summarized in Table 3.1. (for more detailed information see Chapter 4). Porosities are generally between 1 and 20 percent with water

saturated bulk densities ranging between 2.42 and 2.89 g/cm^3 and an average percent fraction of organic carbon (% f_{oc}) equal to 0.02. Samples containing large vugs present more difficulties in measuring porosity. This is due to pores rapidly draining upon the removal from water. Attempts were made to capture this water in a basin during weighing to ensure accurate values.

On the other end of the spectrum, difficulties achieving completely saturated shale samples were encountered. Shale samples tended to crack and degrade during imbibition and thus some samples were lost in this process. Porosity and particle density values for the shale samples should be considered as an estimated quantity.

The calculated particle density for the dolostone core samples remains relatively constant at 2.85 g/cm^3. However porosity and bulk densities (wet and dry) are variable both laterally and vertically. Well MW-22 is more porous than MW-367-9 especially in the Amabel formation as seen in Figure 3.7.

Figure 3.5 - Figure 3.7 show porosity, densities, and f_{oc} with depth. Core derived porosities for the rock matrix range from approximately 1-20 pu (porosity unit – equivalent to % porosity) and high porosity samples show lower values for bulk density and are summarized in Table 3.4. The geophysically derived porosity values do not distinguish between fracture porosity and matrix porosity and therefore will yield an estimate of the total porosity as opposed to solely matrix porosity.

Figure 3.8 shows the relationship between dry bulk density and porosity. The constancy of the particle density is apparent by the low standard deviation of 0.03 and the correlation coefficient of 0.939 between the dry bulk density and porosity. Errors in measuring the fully saturated sample, especially for vuggy or shale samples increases the spread of values for the particle density. Values are centered around 2.85 g/cm^3 which is very close to the specific gravity of 2.87 g/cm^3 cited by the Society for Mining, Metallurgy, and Exploration, Inc. for dolomite (Kennedy 1990).

Figure 3.9 shows the different methods for determining porosity and bulk densities used in this study and also illustrates the resolution for each method, and Figure 3.10 - Figure 3.17 illustrate how well the geophysical logs correlate with the physical property samples and describe the porosity and bulk density distribution across the transect. Figure 3.18 illustrates the different sample resolutions by using values obtained in a cross-section. The cross-sections were kriged in Viewlog using a horizontal exaggeration of 50. The different methods of porosity determination compare well for this transect for most of the depths. Above the water table the geophysically derived porosities are not valid and should not be considered in the comparison. In addition, during the nuclear logging of MW-367-9 an obstruction was encountered limiting the depth of investigation and therefore the results in the lower right portion of the neutron and gamma-gamma cross-section plots are the results of kriging and not MW-367-9 borehole data.

Using the geophysical data we can now use the calibrated porosity and bulk density values in the calculation of porewater concentrations (Figure 3.4 and Table 3.3). Figure 3.19-Figure 3.25 demonstrate the effect that variable porosity and bulk density will have on the porewater concentrations. In general the RPD varies between -100 and 100.

Sorption to organic carbon may be the dominant mass storage mechanism and therefore creates a source for potential error. The results of f_{oc} analyses are shown in Table 3.2. The 74 dolostone matrix f_{oc} samples show that the mass of organic carbon is generally low and close to the detection limit and often below the limit of quantitation. However the shallow fracture infilling f_{oc} values are high averaging 2.3. This value reflects the very high concentrations of the 2003 sampling by PSC where the average f_{oc} was 5.54. The 2007 results for shallow fracture infillings were lower but still higher than the matrix samples with an average of 0.15. One result taken solely from a thick stylolite had an f_{oc} of 3.50. This is in the low end of the range of f_{oc} for stylolitic layers that was recorded by Langer [1999]. In general, Langer [1999] seems to have significantly higher f_{oc} than were detected for the Guelph site. No clear relationships between f_{oc} and lithology are evident

from the samples taken in the Guelph and Amabel formations. However, the shale f_{oc} values do appear to be statistically higher than the Guelph and Amabel dolostone samples. Langer (1999) suggests that stylolites may contain elevated organic carbon content and thus can act as a potential contaminant sink. The range of f_{oc} values suggest that it is an important value in the porewater conversion calculation but not necessarily the dominant parameter, at least for non-stylolitic rock core samples, and non-shallow coated fracture samples.

3.5 Discussion and Conclusion

Selected geophysical methods for determining porosity and bulk density show great promise when calibrated with core derived values. For the fractured dolostone at this site the method shows good correlation for bulk density and porosity with the geophysical logs. Scatter is apparent in the linear correlation plots, however the geophysical tools have high utility. Care must be taken to ensure excellent depth accuracy and also that logging speed is considered and that the core samples obtained are representative of the range of bulk matrix properties found in each corehole. The selection of the core samples used for calibration is also an important factor.

The neutron, gamma-gamma, and acoustic televiewer logs have proven useful for improving confidence in the conversion of rock core VOC profiles from total mass concentrations to equivalent porewater concentrations. Additional logging tools may also be useful for this conversion such as the electromagnetic conductivity, sonic or NMR logs. Another beneficial technique could be to use the multiple geophysical tools in conjunction to calculate the physical properties.

The neutron and gamma-gamma logs are nuclear logs that use a downhole radioactive source. This can present problems due to government regulations restricting the use of such tools in open unlined holes, and the transport of such sources. Performing investigations in holes containing a FLUTe liner minimizes the risk of tools becoming stuck down hole. This is also

advantageous because minimizing the number of logging tools that are run in open contaminated holes minimizes the potential for cross-contamination. The acoustic televiewer can also be run in lined holes but typically logging occurs in the open hole to achieve a clearer picture of the borehole wall.

The fact that these geophysical methods sample both the matrix and fracture porosity may allow one to separate the two by using core samples if the fracture porosity is an important component of the total porosity. However to do this requires exceptionally competent corehole walls that do not exhibit large blowouts or worn regions due to coring.

Having continuous logs of porosity and bulk density are beneficial in overall site characterizations and also for calculating rock core porewater profiles. One benefit is the increased confidence in converted porewater values which can be compared to groundwater samples taken from a multilevel monitoring network. The geophysical logs are independent of personal bias introduced by visual judgments during lithology assignment and thus result in a more objective method for the conversion process. Higher resolution is achieved with the use of geophysical logs to centimeters whereas the traditional method of applying lithologies is commonly on the meter scale. At this site the effect of using the higher resolution physical property measurements on porewater conversions does not appear to qualitatively change the shape of the profile as most of the peaks remain peaks and most of the troughs remain troughs. However, RPD values suggest that the change in concentration due to the more refined porosity measurements is considerable.

Unfortunately for this study, no relationships between core derived f_{oc} values and geophysical logs were evident but there may be a correlation with the gamma ray log, and in particular uranium from a spectral gamma log (Rider 1996). Low masses of organic carbon in dolostone matrices are difficult to measure with laboratory procedures and often involve aggressive sample preparation treatments potentially compromising the resulting organic carbon

analysis (Byers, Mills, & Stewart 1978). Because chemical partitioning to solids is calculated based on porosity and dry bulk density, the variable f_{oc} can greatly magnify the difference between averaged vs. more depth discrete conversions thus making values for the dry bulk density and porosity increasingly important.

The method presented is an attempt to decrease the uncertainty due to the effect of physical property variability on the porewater conversion process. The introduced uncertainty during the conversion process can be larger than an order of magnitude and is dependent on the rock type. This is not a standard method that can be applied at every fractured rock site and it is important to be aware of the geology and purpose of the investigation before applying this method. This method does not consider the assumptions that must be made in order to model sorption using f_{oc} and K_d and thus conceptual uncertainty also exists.

Table 3.1: Summary of lab derived dolostone physical property values

Statistic	Dry Bulk Density (g/cm^3)	Wet Bulk Density (g/cm^3)	Particle Density (g/cm^3)	Porosity (%)
No. of Samples	246	246	246	246
Minimum	2.22	2.43	2.74	1.2
Maximum	2.87	2.89	2.93	20.9
Mean	2.57	2.67	2.85	9.8
Standard deviation	0.12	0.08	0.03	4.3

Table 3.2: Fraction of organic carbon by type of sample

Sample Type	Number of samples	Average	Min	Max
Fracture Surface	15	2.31	0.08	6.36
Stylolite Layer	1	3.50	NA	NA
Shale Transition	6	0.06	0.03	0.11
Dolostone Matrix	74	0.02	0.01	0.10

Table 3.3: Summary of core and geophysical method correlations

Geophysical Method	Parameter	Equation	R^2
Neutron	Dry Bulk Density	y = 844.9x - 1208	0.572
Neutron	Porosity	y = -22.35x + 1182	0.526
Gamma-Gamma	Dry Bulk Density	y = -29.44x + 127.4	0.43
Gamma-Gamma	Porosity	y = 0.811x + 43.72	0.428
ACTV Max Amplitude	Dry Bulk Density	y = 0.441x - 0.341	0.564
ACTV Max Amplitude	Porosity	y = -0.012x + 0.913	0.547

Table 3.4: Summary of lab derived physical properties measurements based on lithology

Lithologic Unit	No. of Samples	Mean Dry Bulk Density (g/cm^3)	Mean Wet Bulk Density (g/cm^3)	Mean Particle Density (g/cm^3)	Mean Porosity (%)
A	8	2.72	2.77	2.87	5.2
B	14	2.71	2.76	2.84	4.5
C	33	2.48	2.61	2.86	13.2
D	21	2.62	2.70	2.85	8.1
E	38	2.54	2.65	2.86	11.1
F	23	2.49	2.61	2.85	12.6
G	6	2.40	2.56	2.86	16.0
H	15	2.49	2.61	2.83	12.2
I	9	2.57	2.68	2.87	10.3
J	19	2.48	2.61	2.86	13.2
K1	6	2.73	2.77	2.85	4.3
K2	14	2.68	2.74	2.85	5.8
K3	6	2.70	2.75	2.86	5.4
L1	5	2.70	2.75	2.85	5.1
L2	6	2.64	2.72	2.88	8.1
M	5	2.57	2.67	2.86	10.1
N	17	2.72	2.77	2.87	5.1
O	9*	2.65	2.71	2.77	2.9
All Samples	254*	2.58	2.67	2.85	9.6

*Transition zone to shale. Some of these samples degraded during imbibition

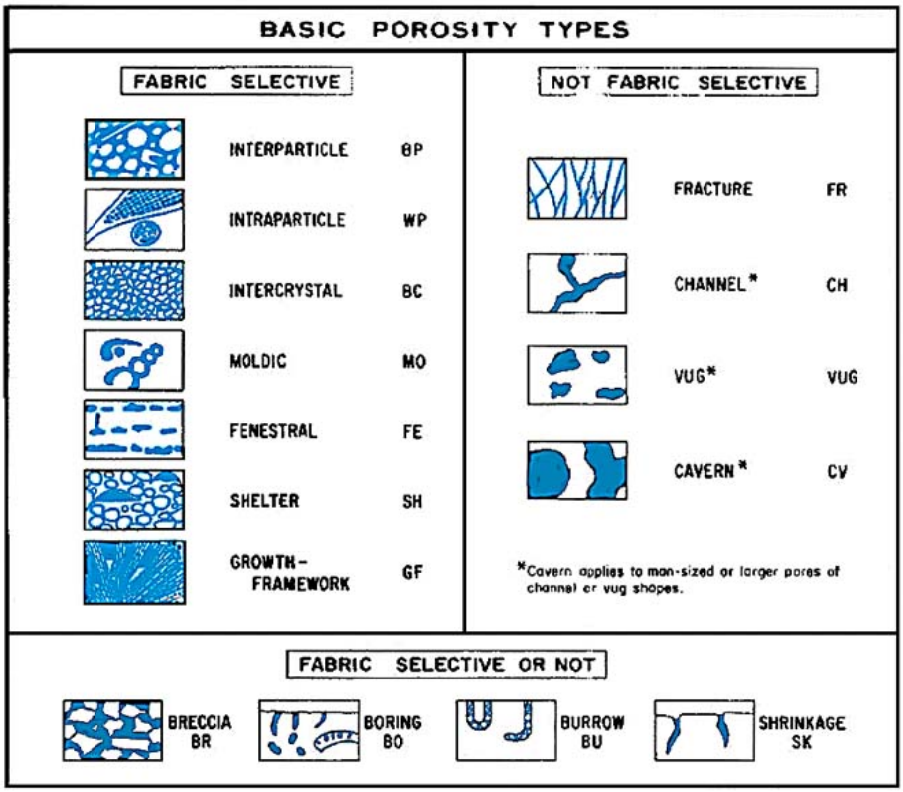

Figure 3.1: Types of porosity encountered in Guelph. (taken from Choquett & Pray 1970)

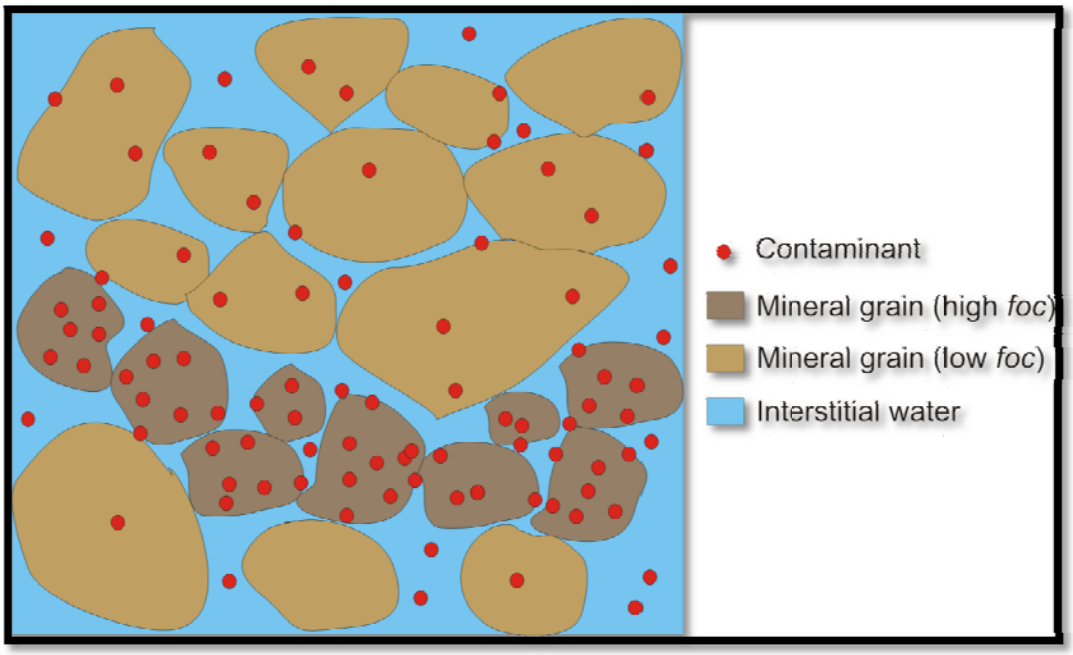

Figure 3.2: Partitioning between sorbed and aqueous phase contamination illustrating increased sorption onto minerals having a higher K_d.

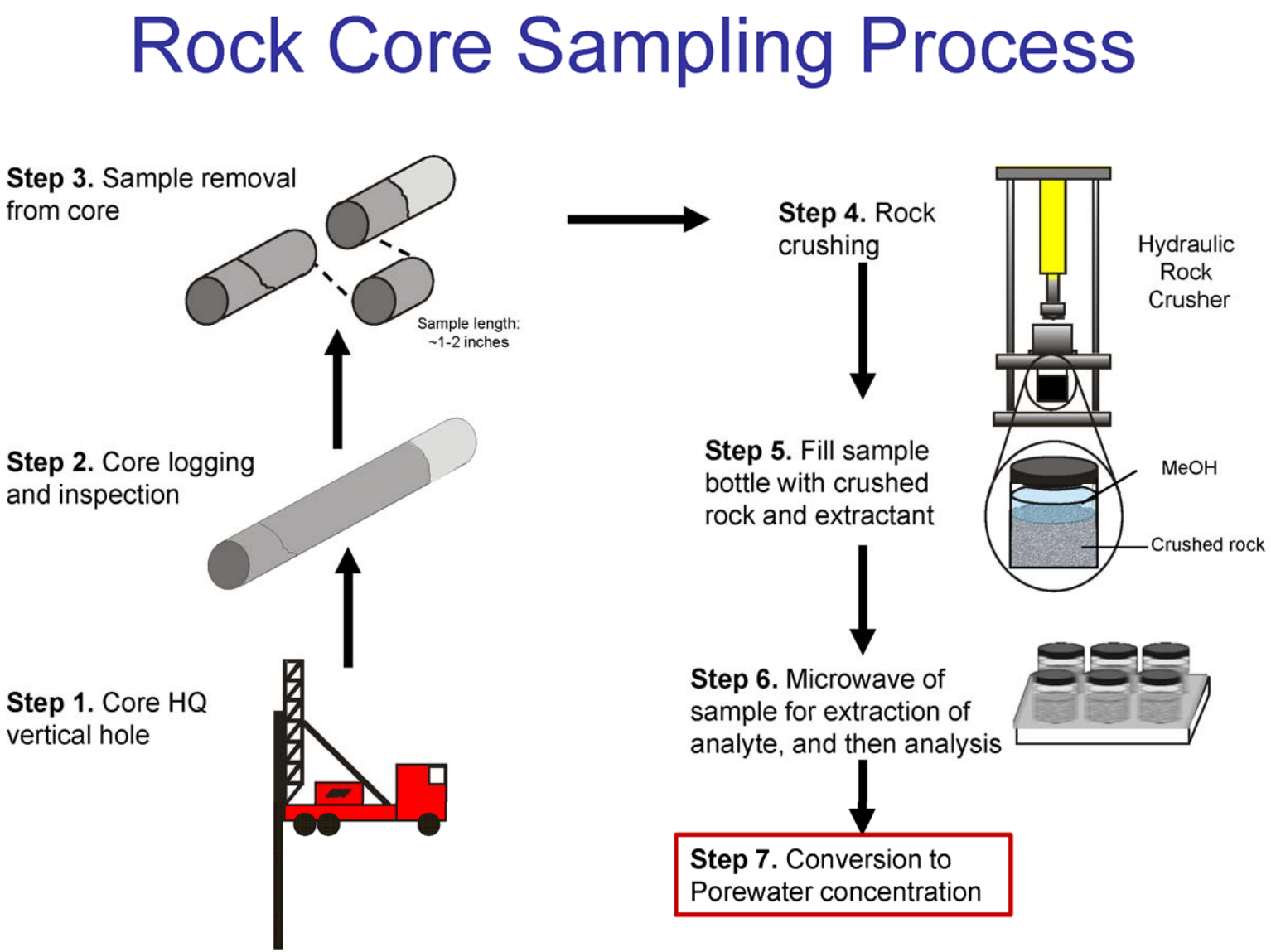

Figure 3.3: Rock core VOC collection, sampling, analysis and interpretation flow diagram (modified from Sterling [1999], Turner [2001], and Hurley [2003]).

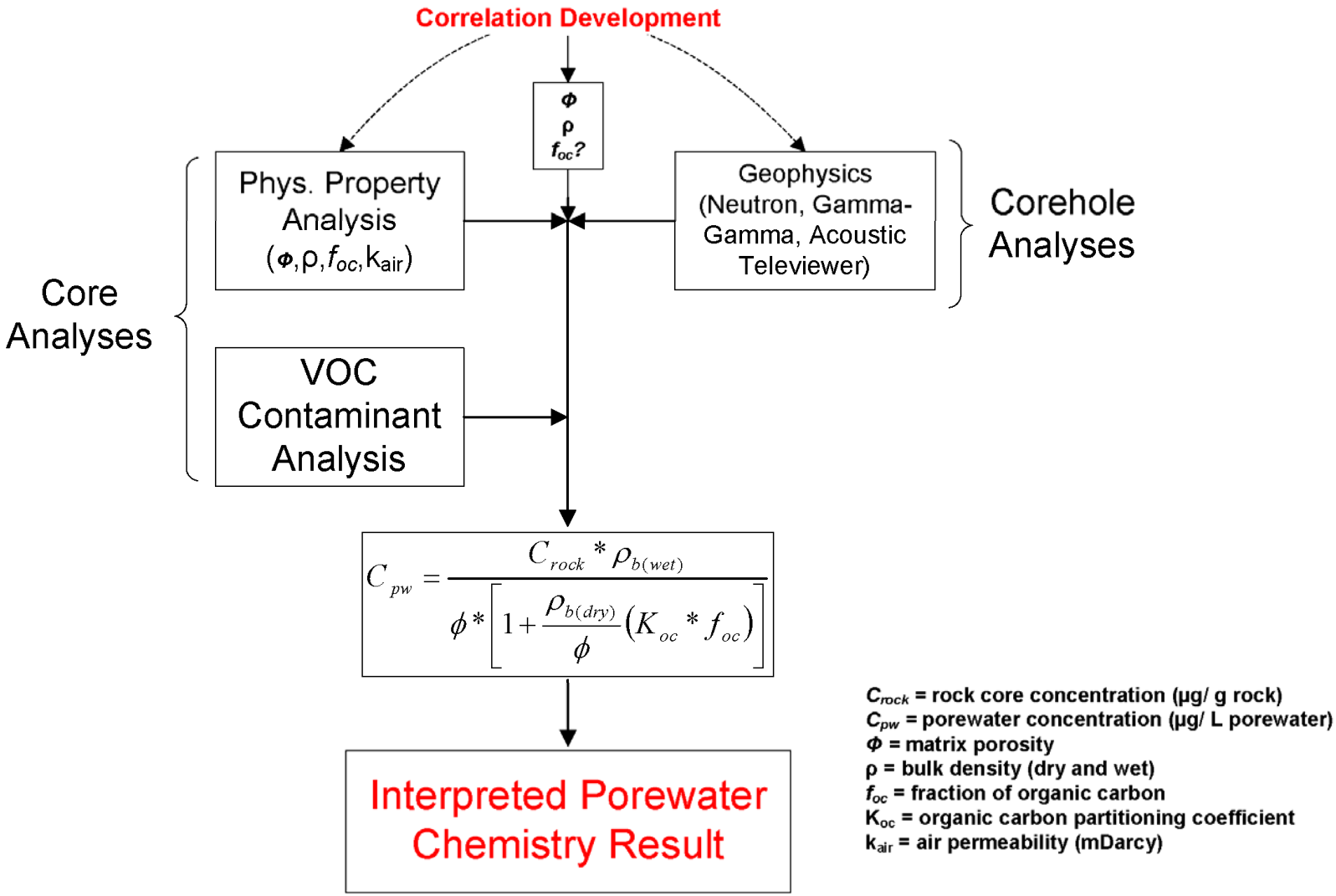

Figure 3.4: Interaction between core analyses and corehole analyses to calculate porewater concentration

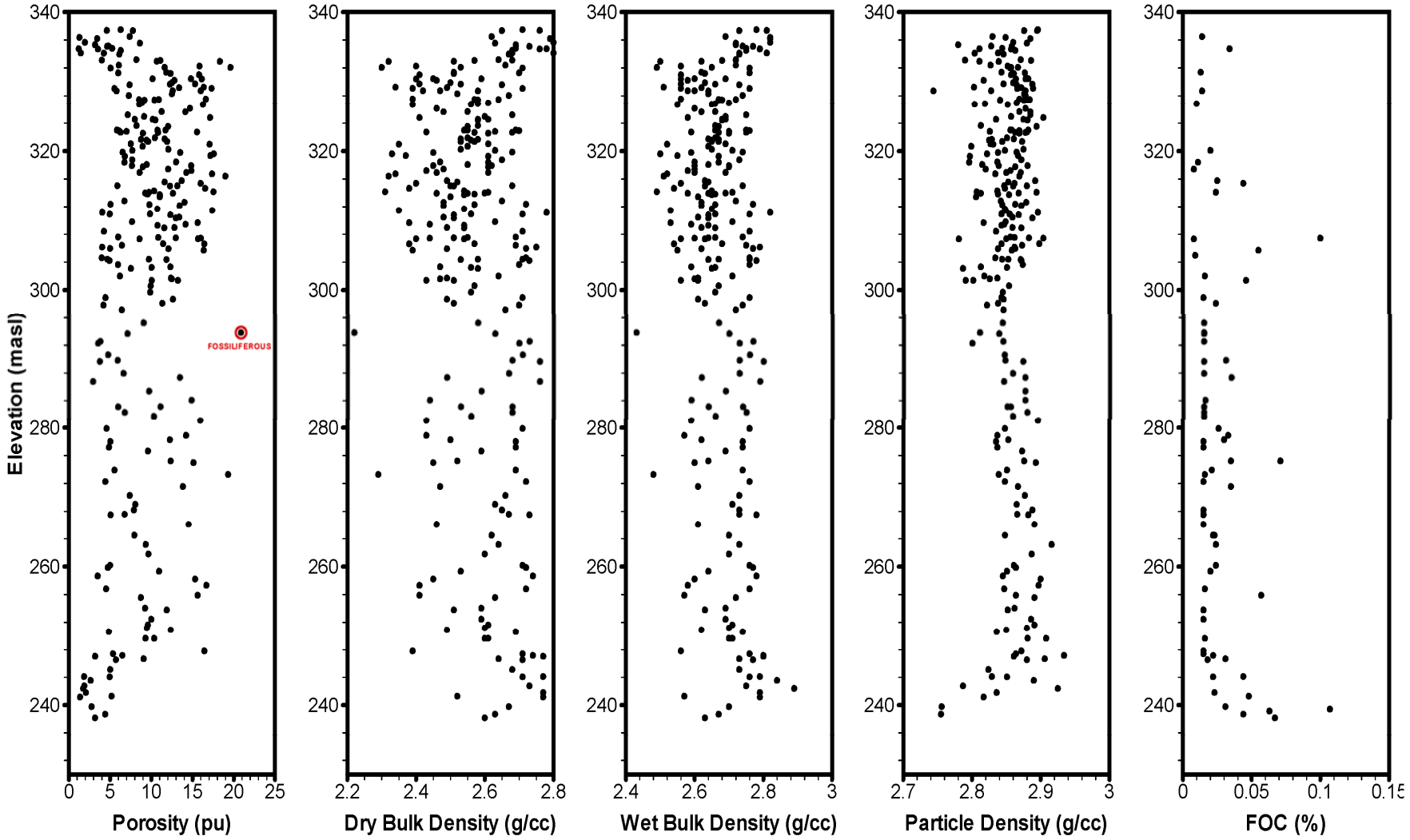

Figure 3.5: Physical properties with depth. Note f_{oc} appears to show a few areas of increased organic carbon but still remains low.

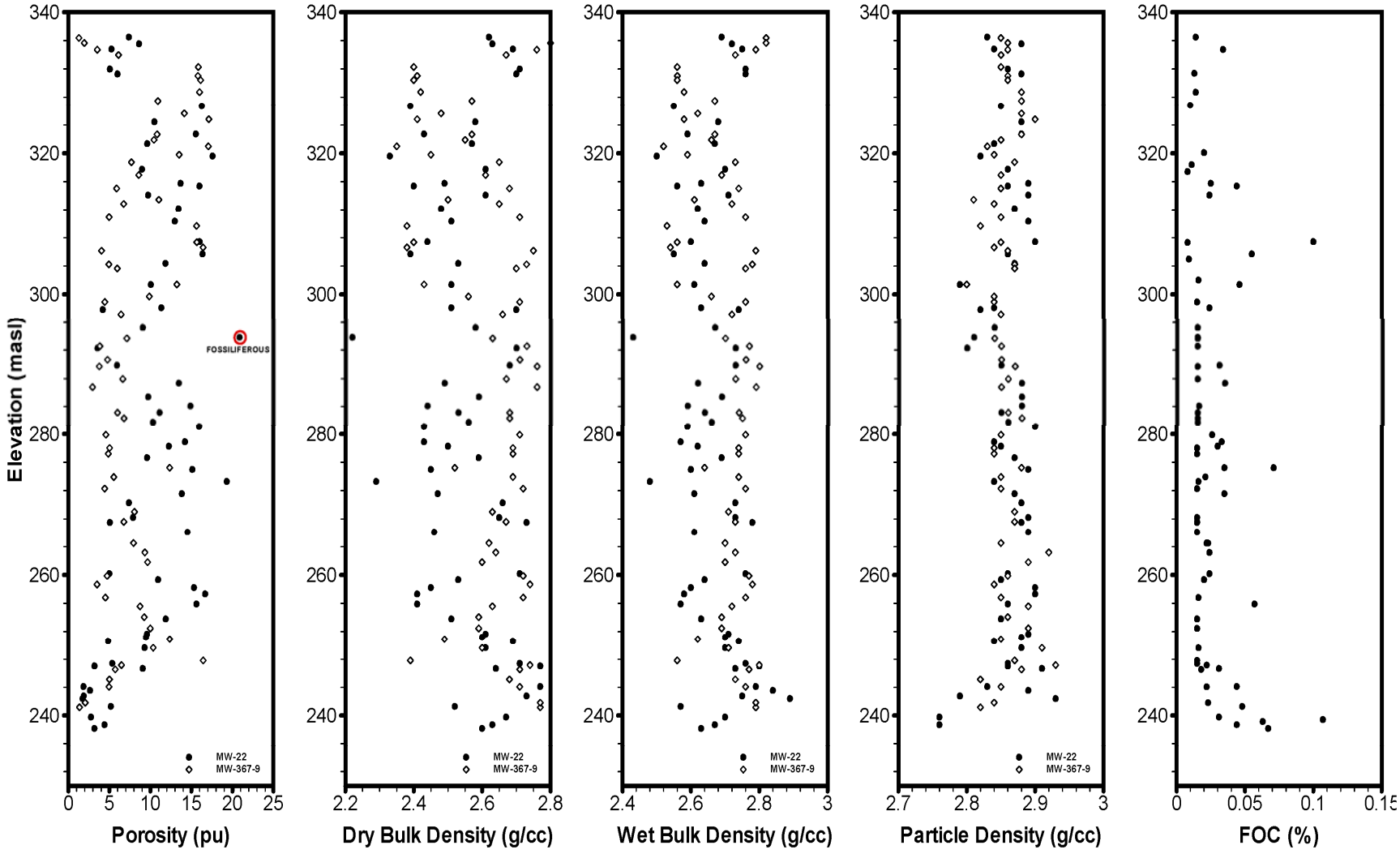

Figure 3.6: Physical properties with depth (wells MW-22 and MW-367-9). MW-22 appears to be more porous below 290 masl

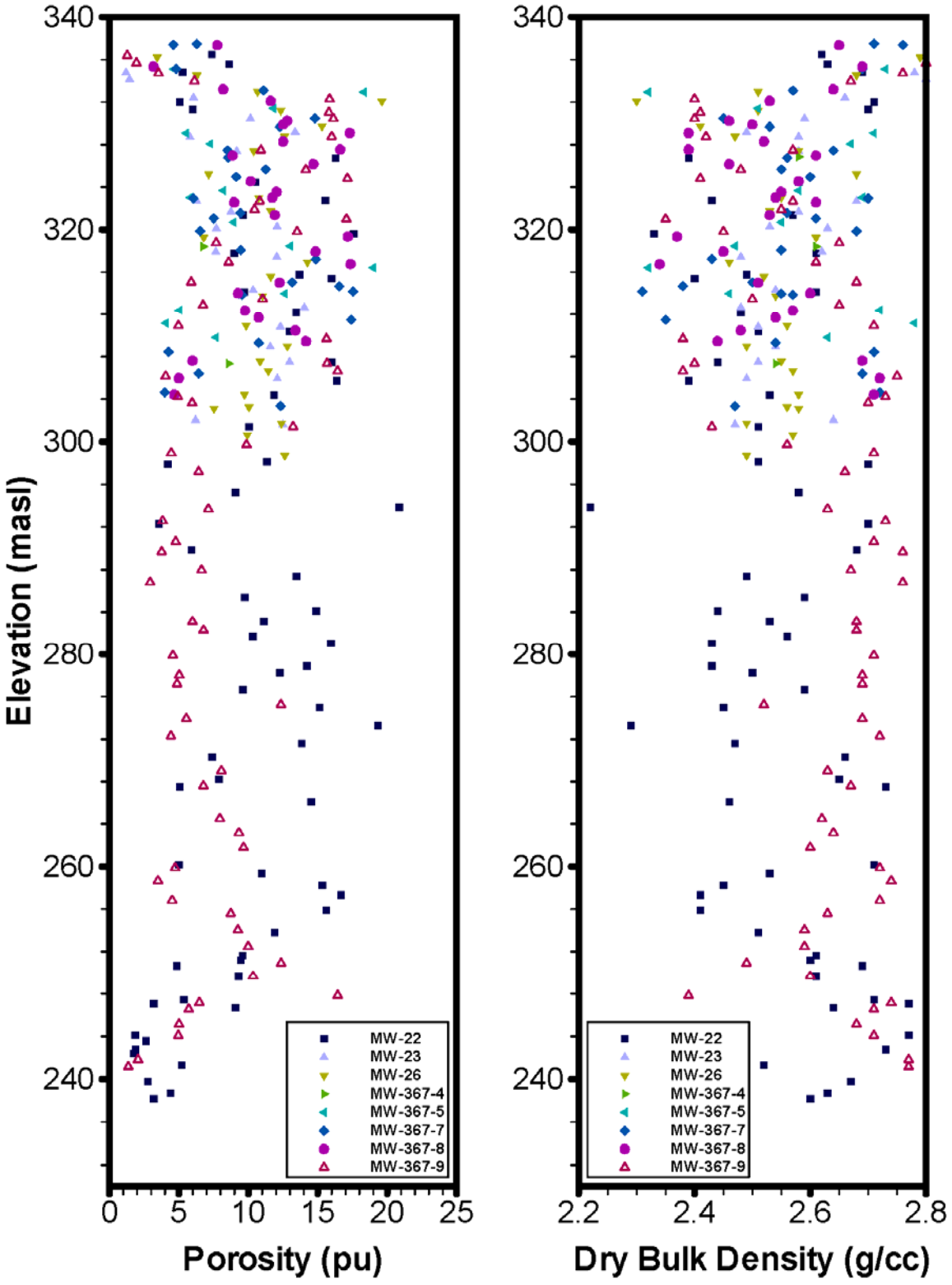

Figure 3.7: Porosity and dry bulk density with depth showing each well. Note the large difference in porosity values between MW-367-9 and MW-22 below 290 masl.

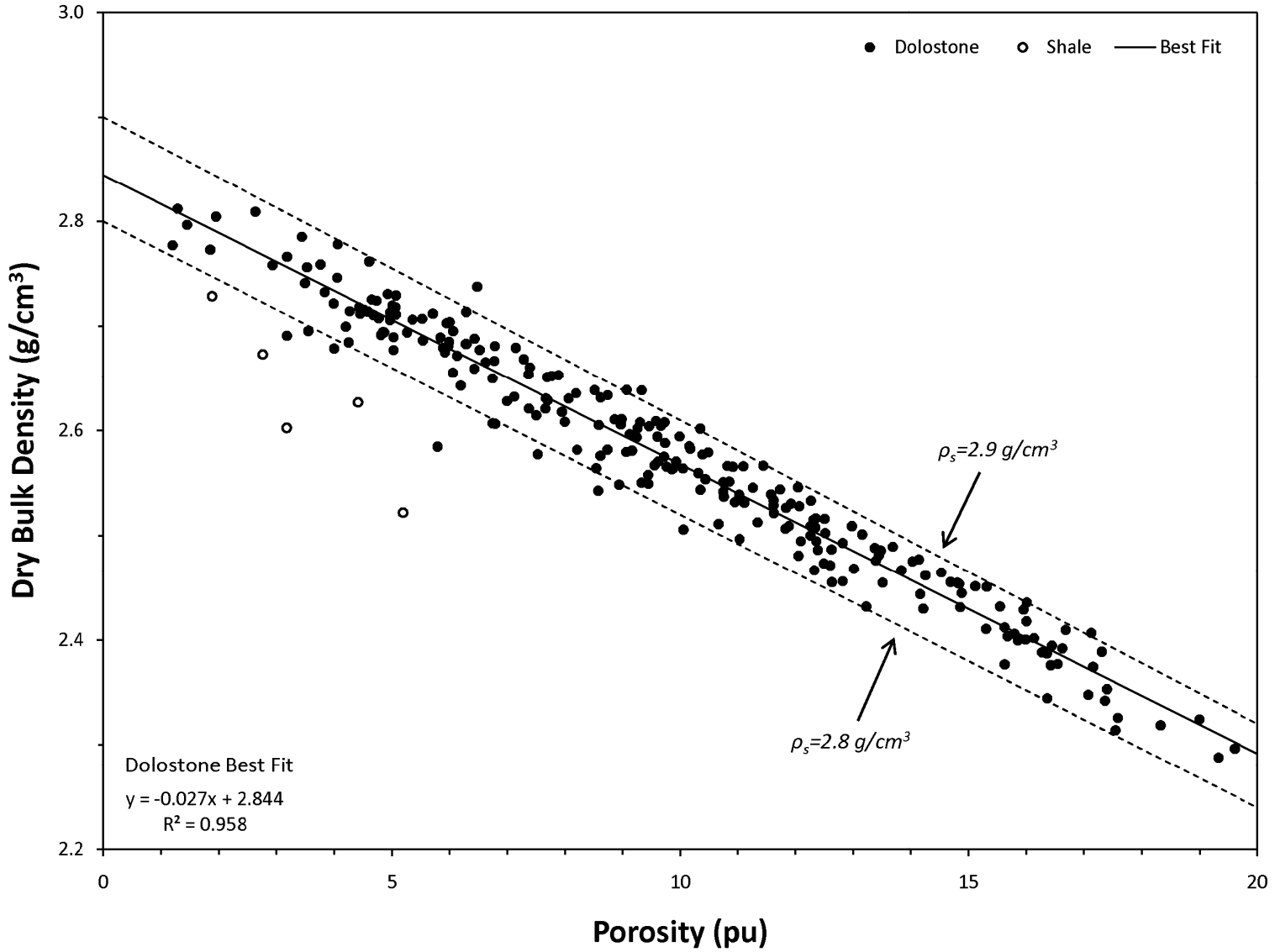

Figure 3.8: Relationship between dry bulk density and porosity. Values not on the line may have a different particle density or be the result of measurement error for porosity.

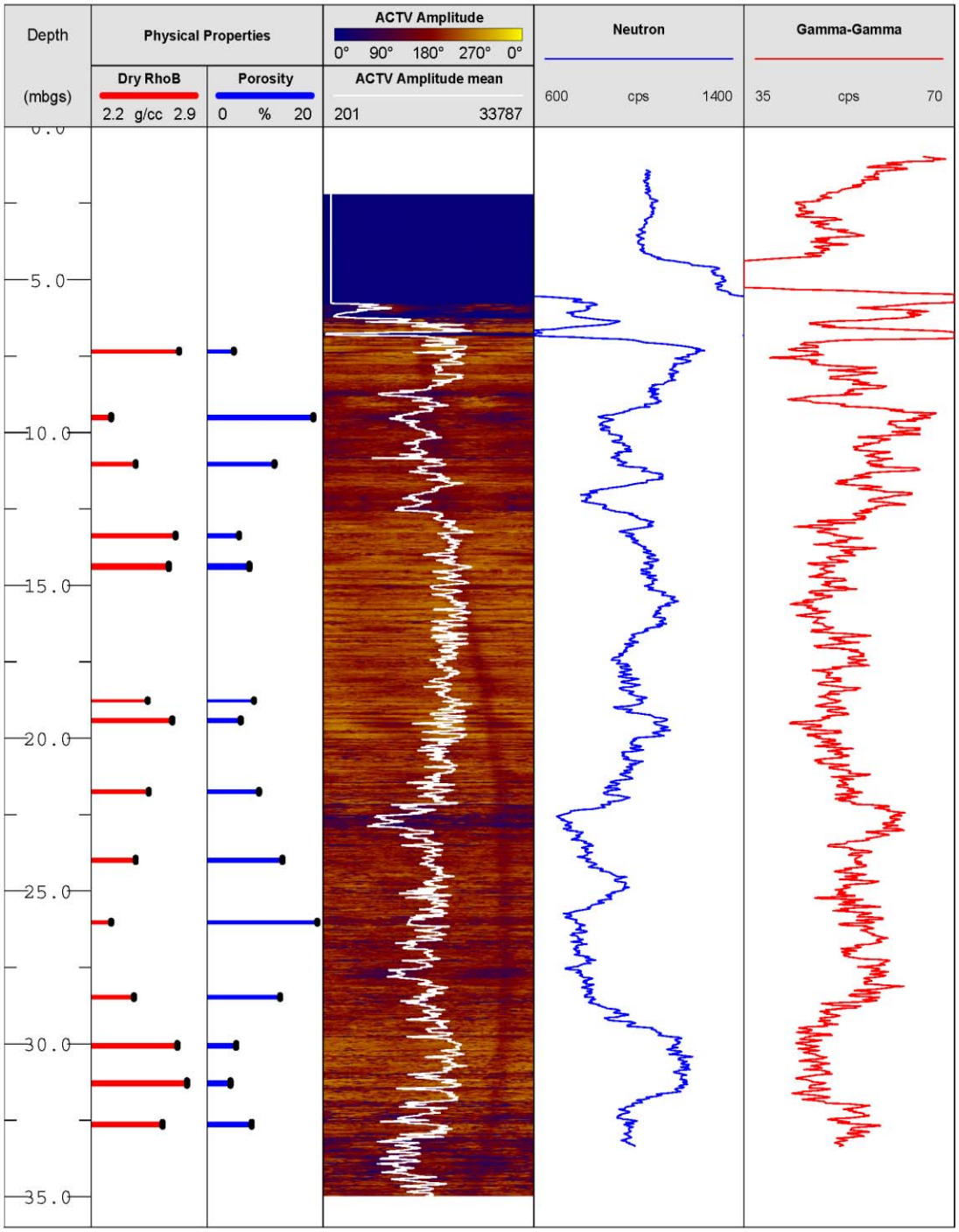

Figure 3.9: Geophysical and rock core profiles for determining porosity and bulk density (core measurements, acoustic televiewer, neutron, gamma-gamma). The white line is the max ACTV amplitude.

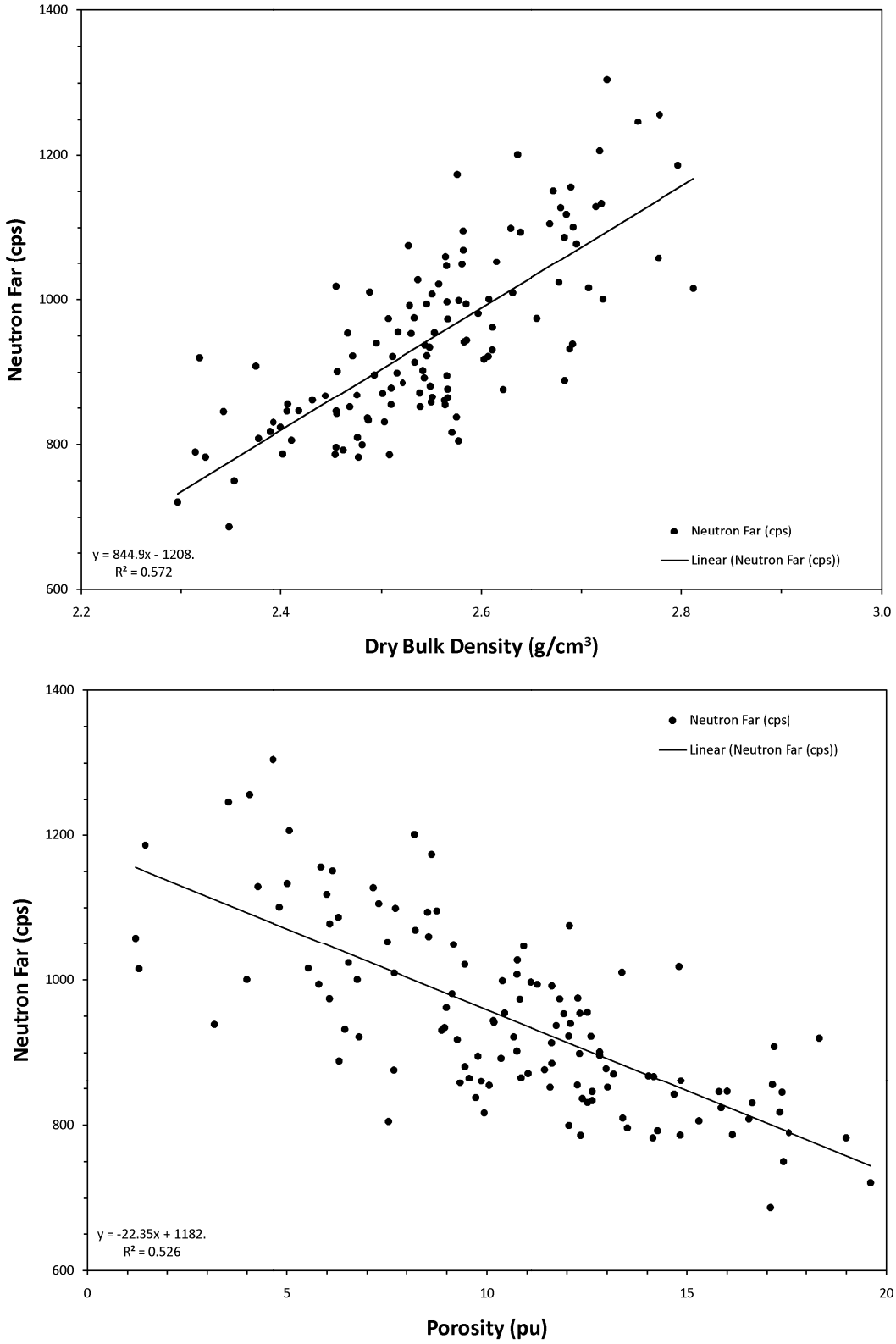

Figure 3.10: Porosity and dry bulk density correlation plots and equations for neutron logs.

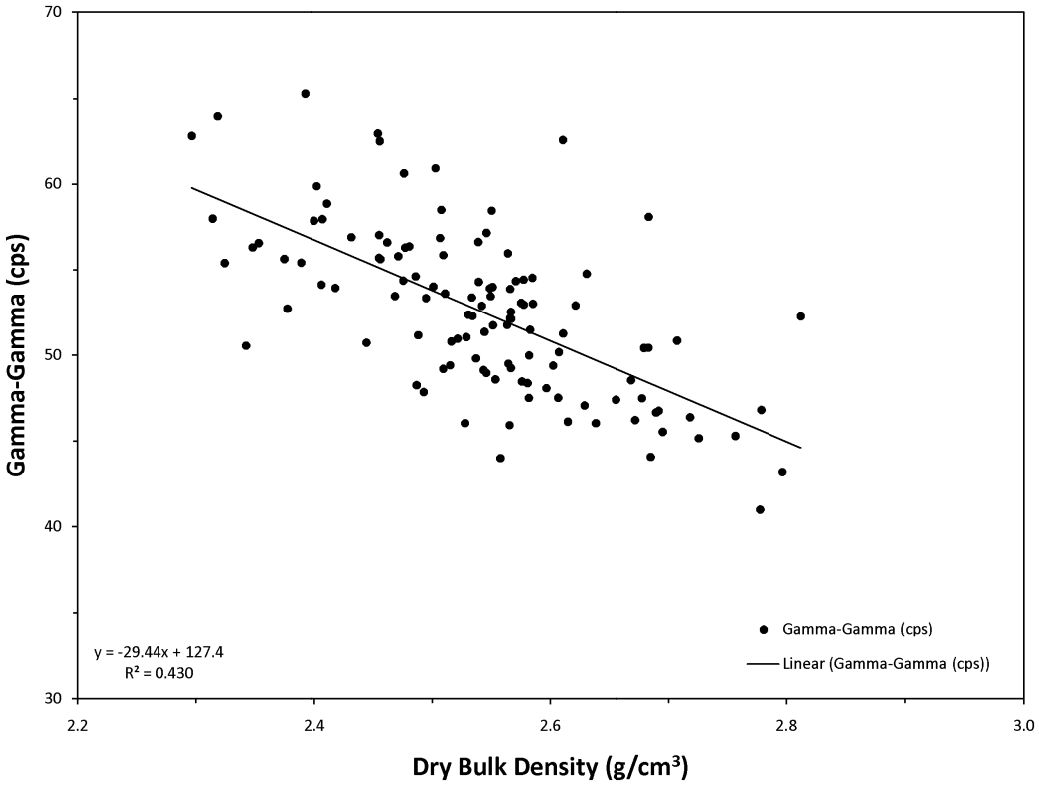

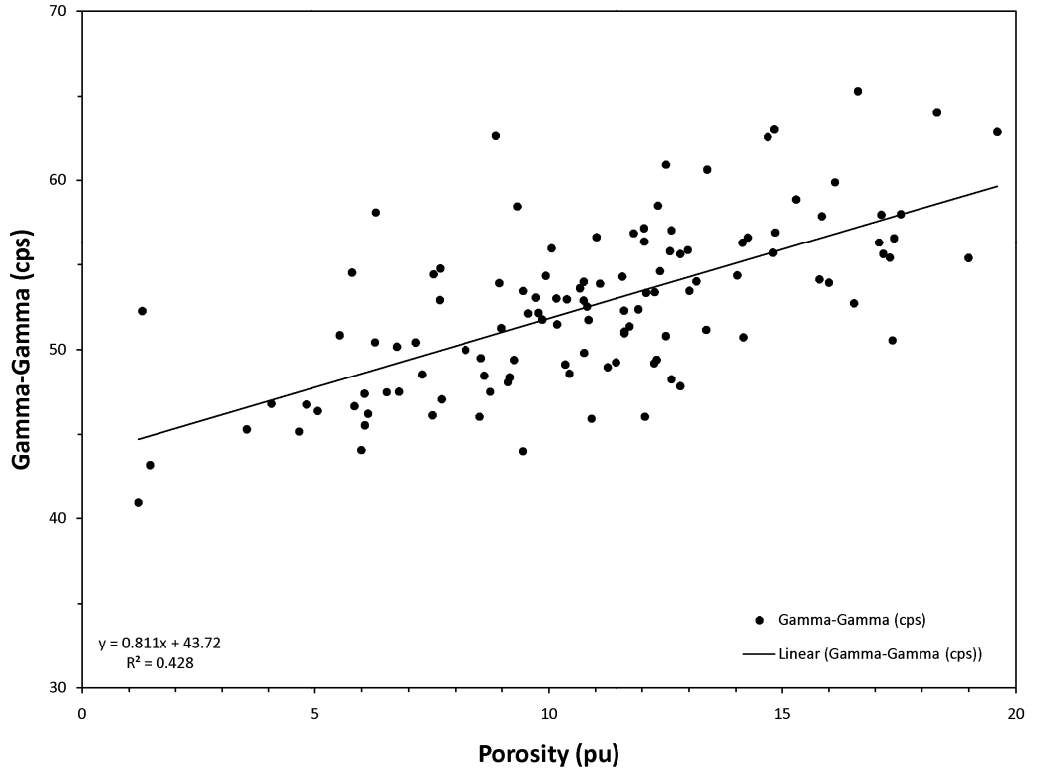

Figure 3.11: Porosity and dry bulk density correlation plots and equations for gamma-gamma logs.

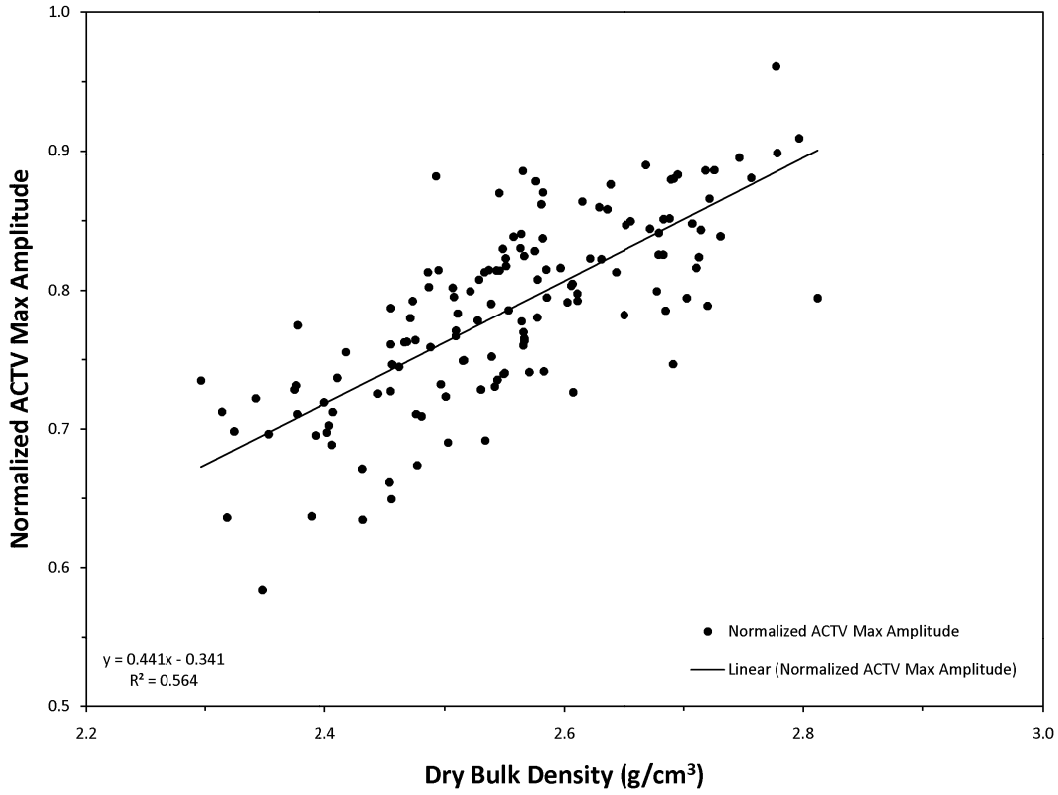

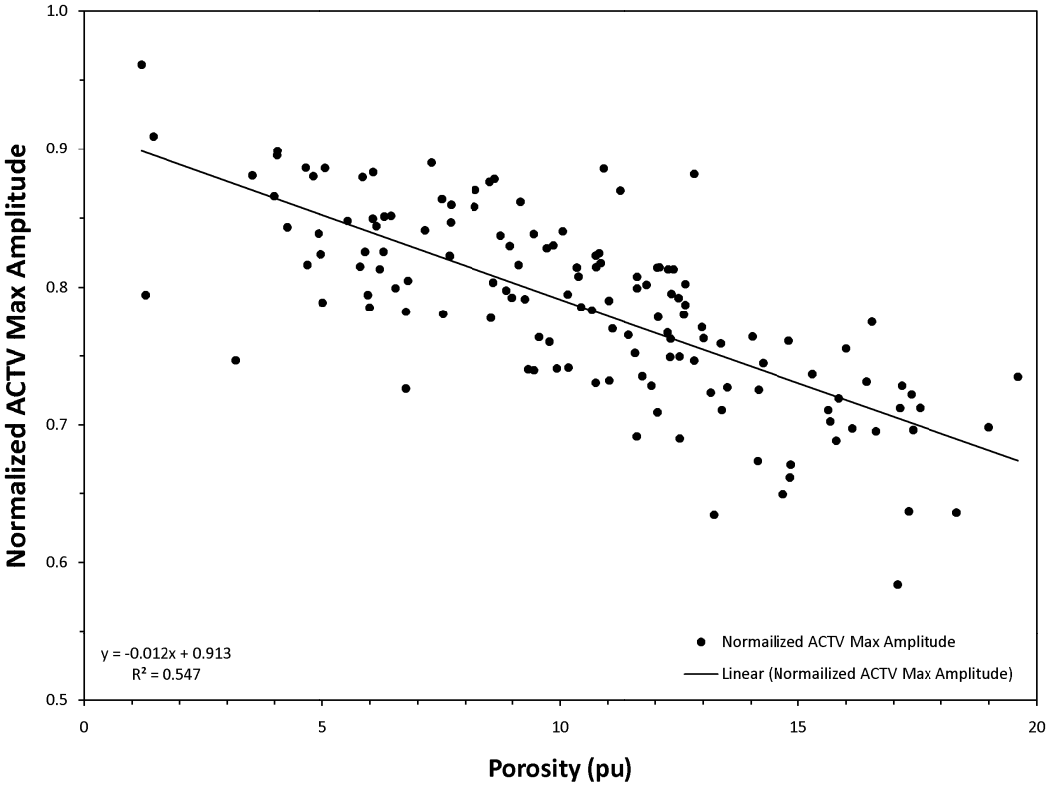

Figure 3.12: Porosity and dry bulk density correlation plots and equations for acoustic televiewer logs.

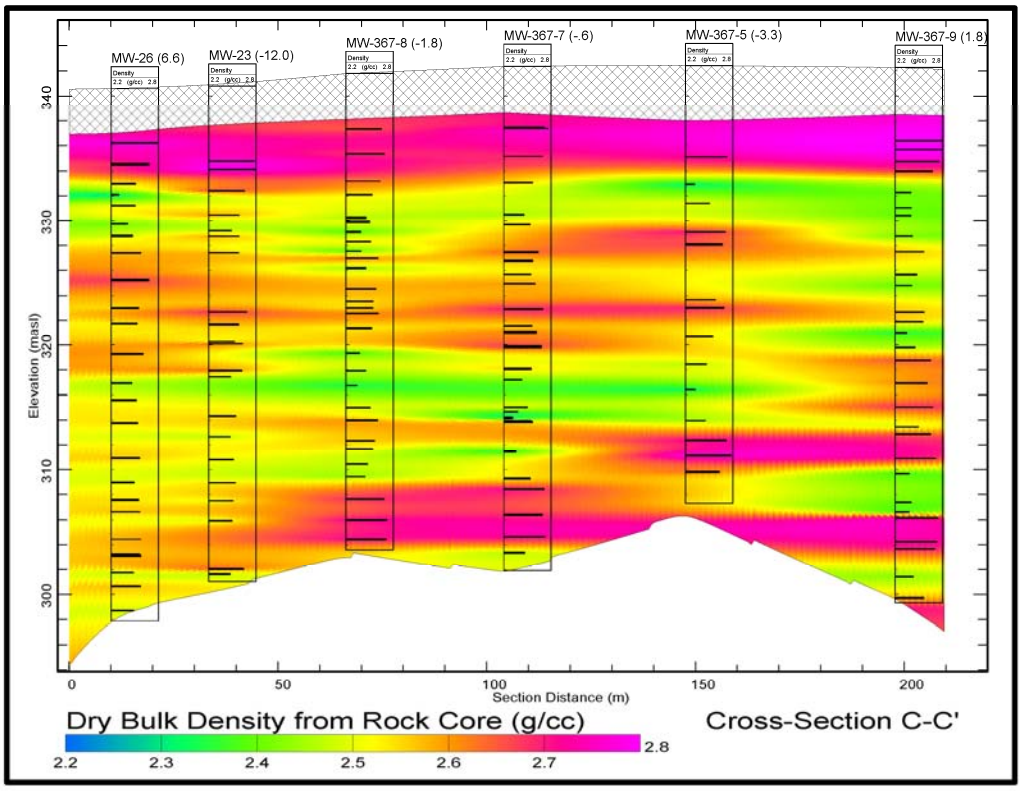

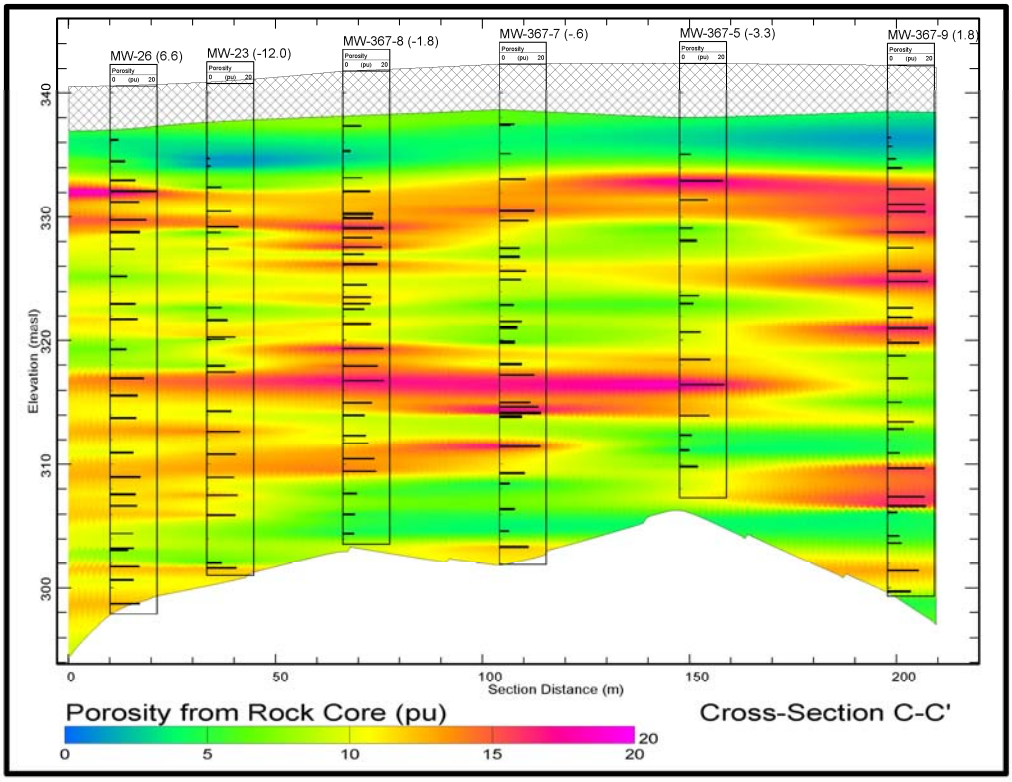

Figure 3.13: Kriged dry bulk density and porosity from core measurements along transect

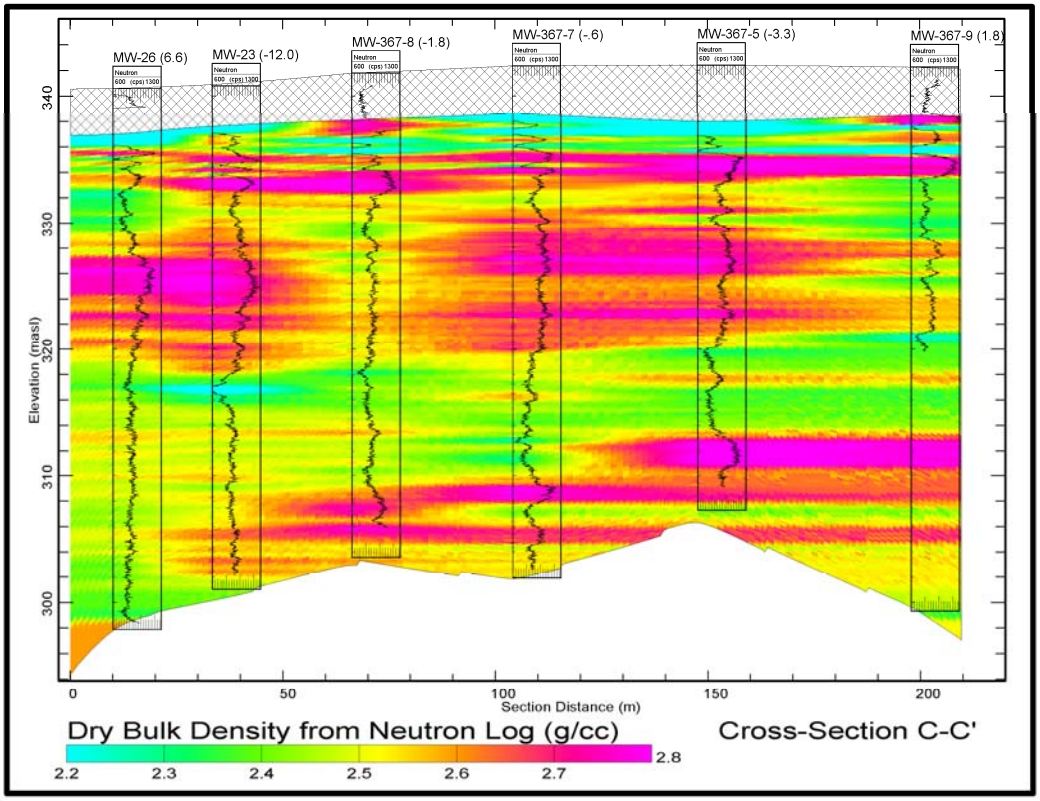

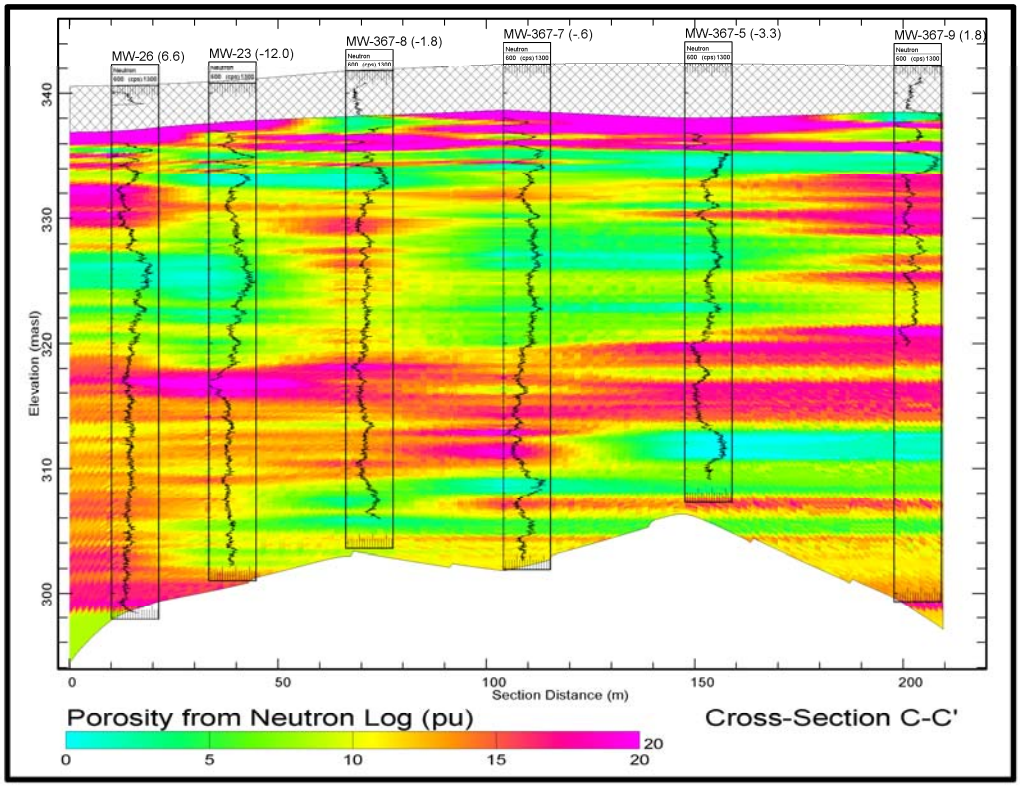

Figure 3.14: Kriged dry bulk density and porosity from neutron log along transect

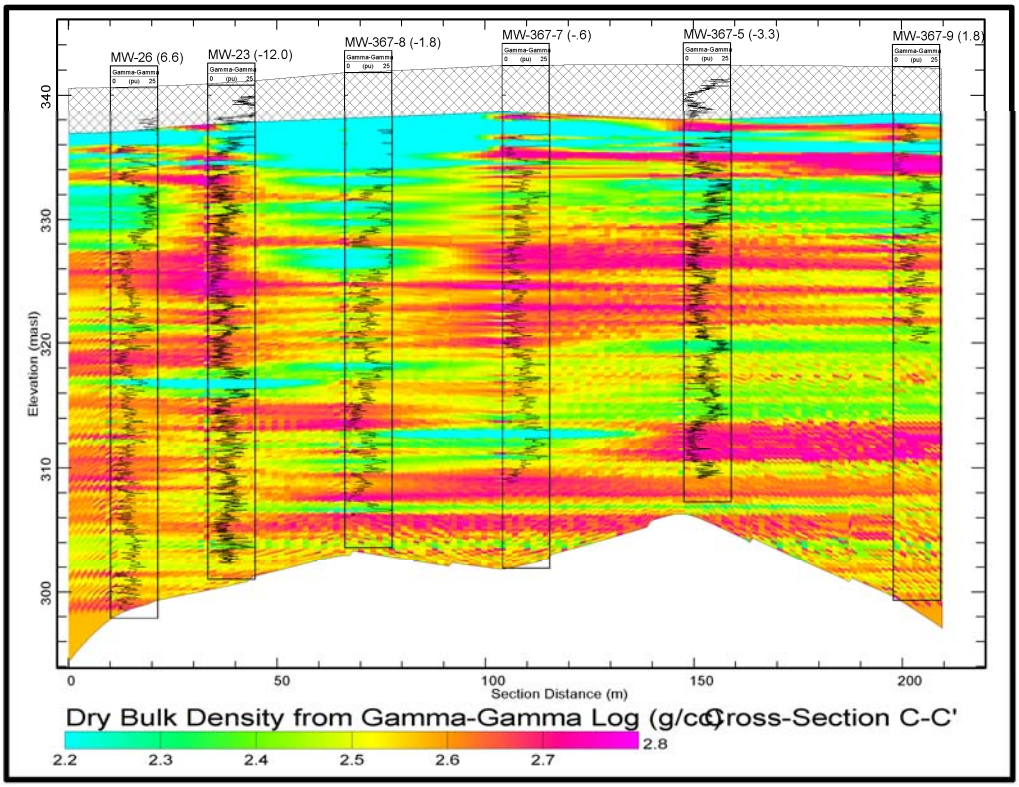

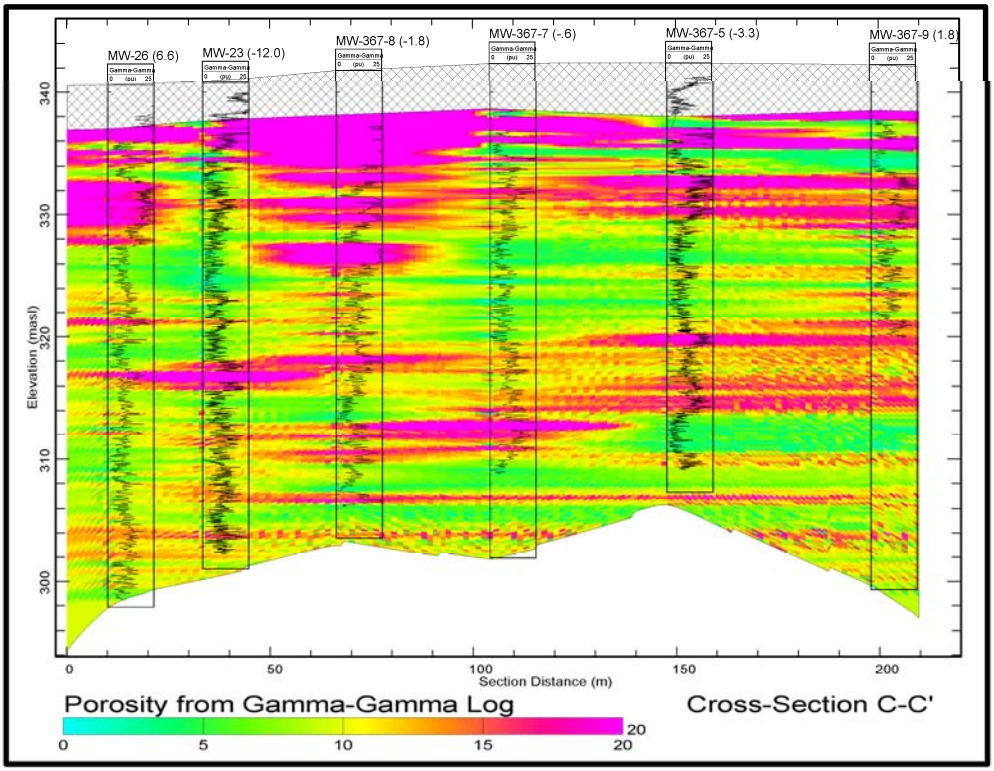

Figure 3.15: Kriged dry bulk density and porosity from gamma-gamma log along transect

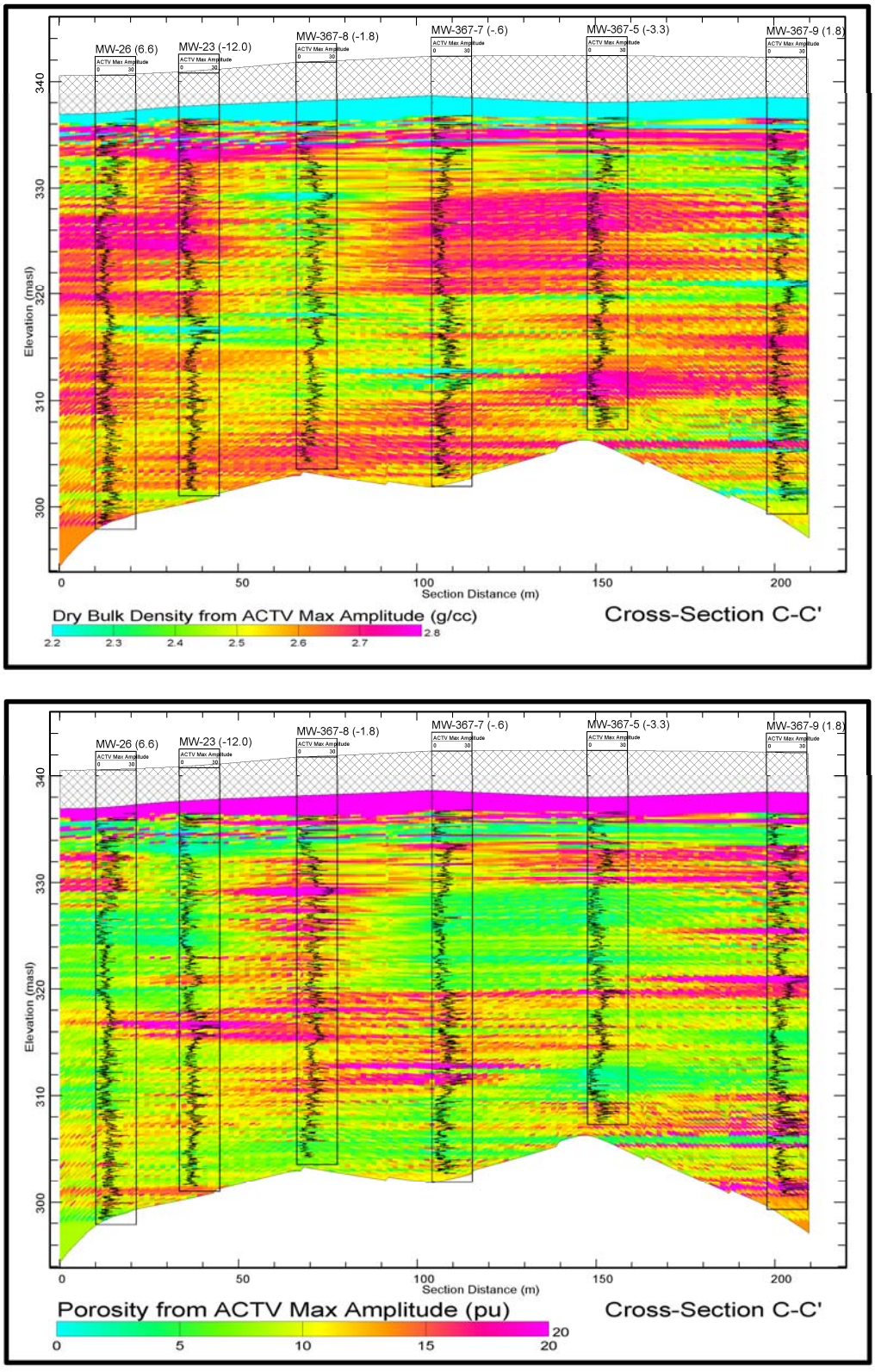

Figure 3.16: Kriged dry bulk density and porosity from acoustic televiewer log along transect

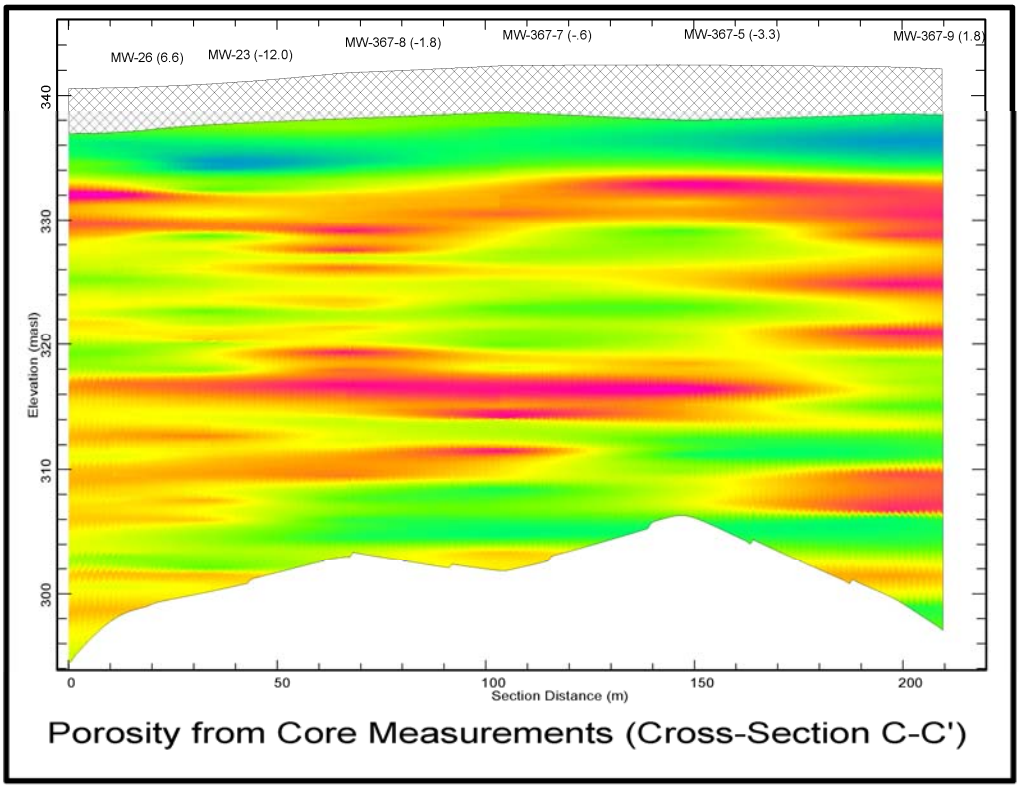

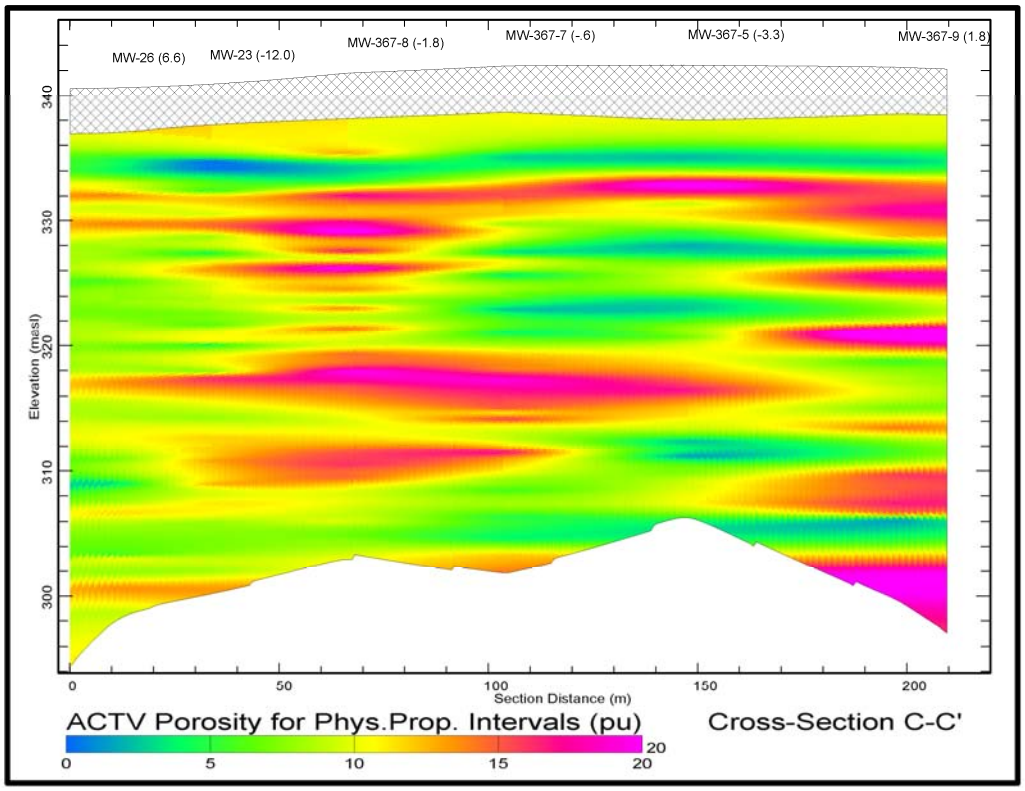

Figure 3.17: Kriged correlation between rock core measurements and acoustic televiewer maximum amplitude porosity over the same intervals along transect

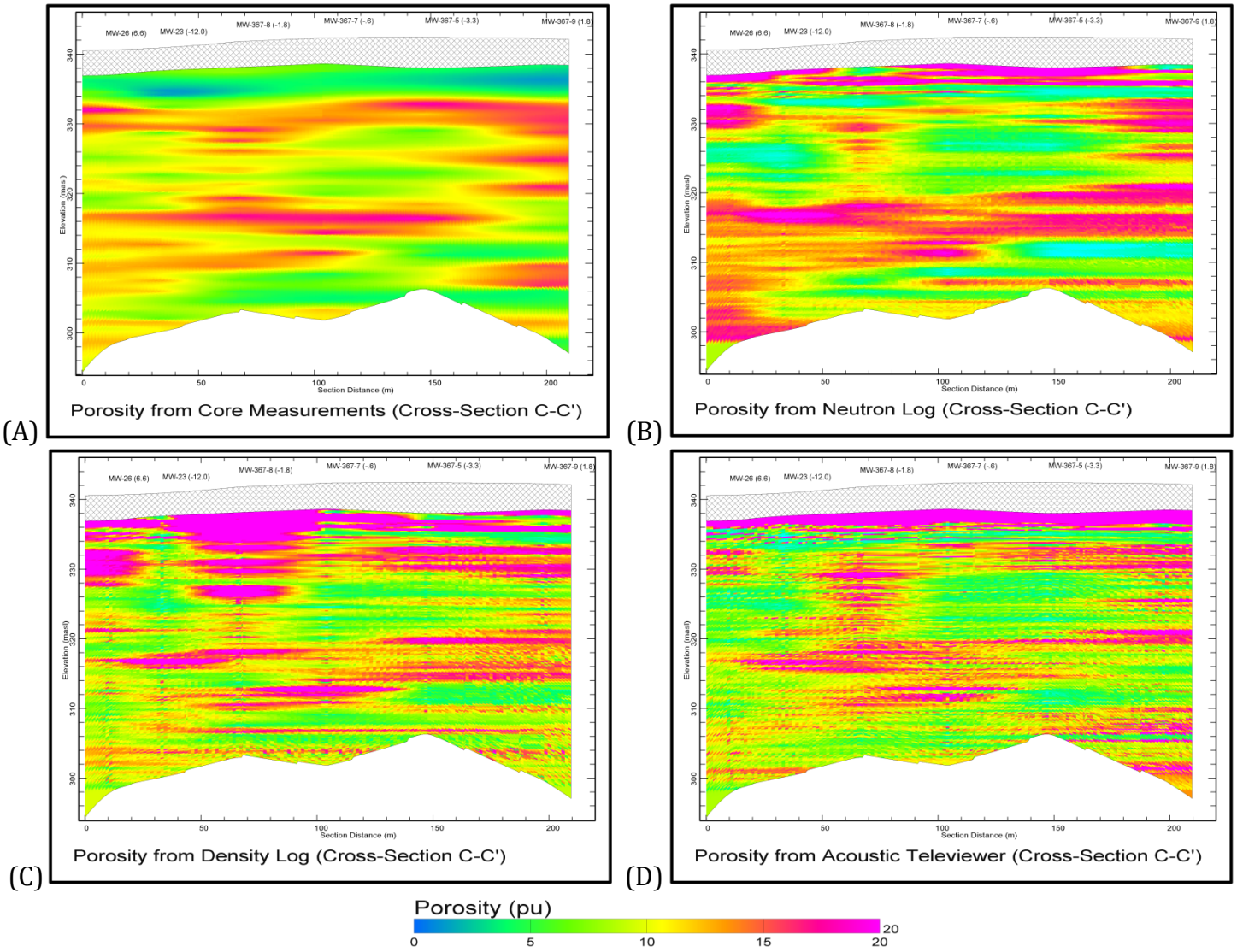

Figure 3.18: Comparison of porosity from calibrated geophysical tools and core matrix porosity. The bottom of hole MW-367-9 was not logged for the neutron and gamma-gamma logs and the values are created from kriging and shouldnot be considered accurate.

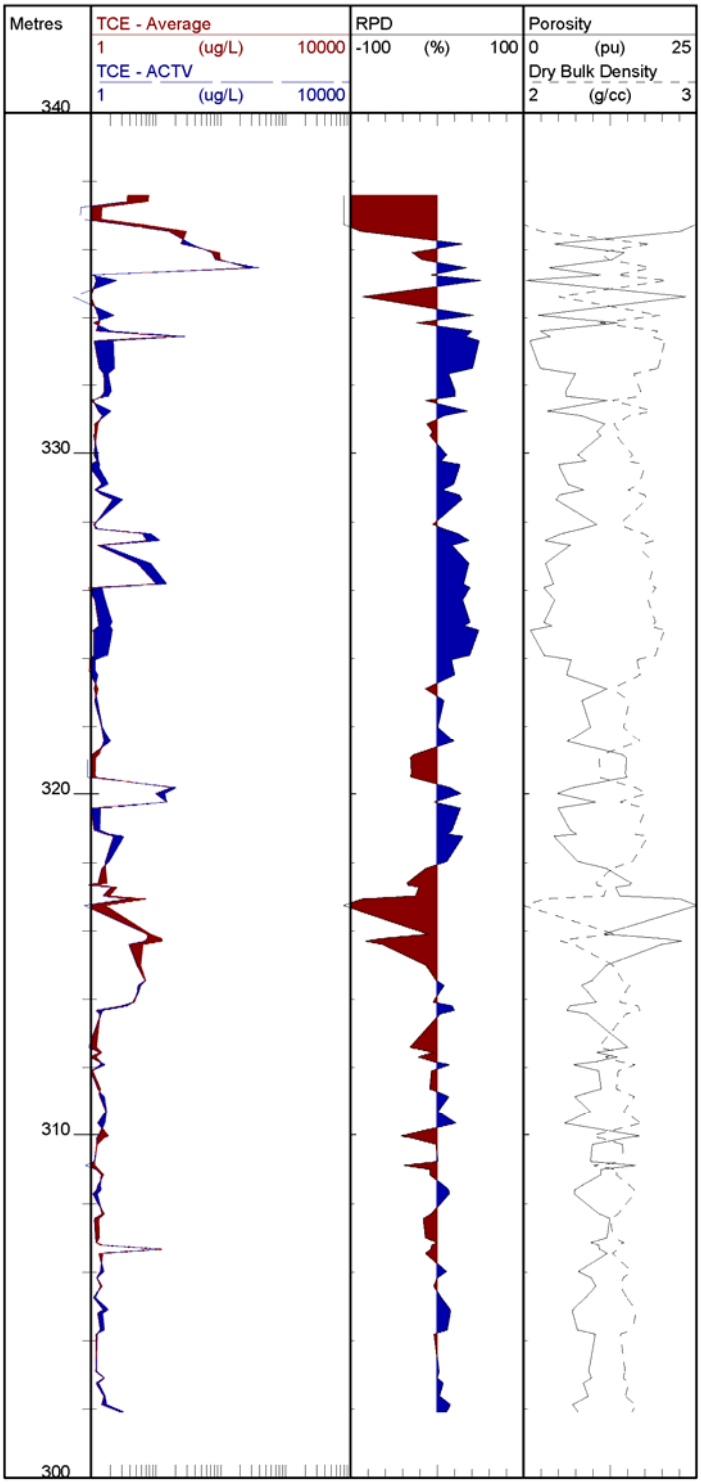

Figure 3.19: MW-23 plot showing the difference between using average values in the porewater conversion or using depth discrete values. Values in red mean that the average value overestimates the concentration and values in blue mean that the average underestimated the concentration. Values in the upper few meters are suspect for the ACTV response due to fractured nature of the borehole and being near the water table.

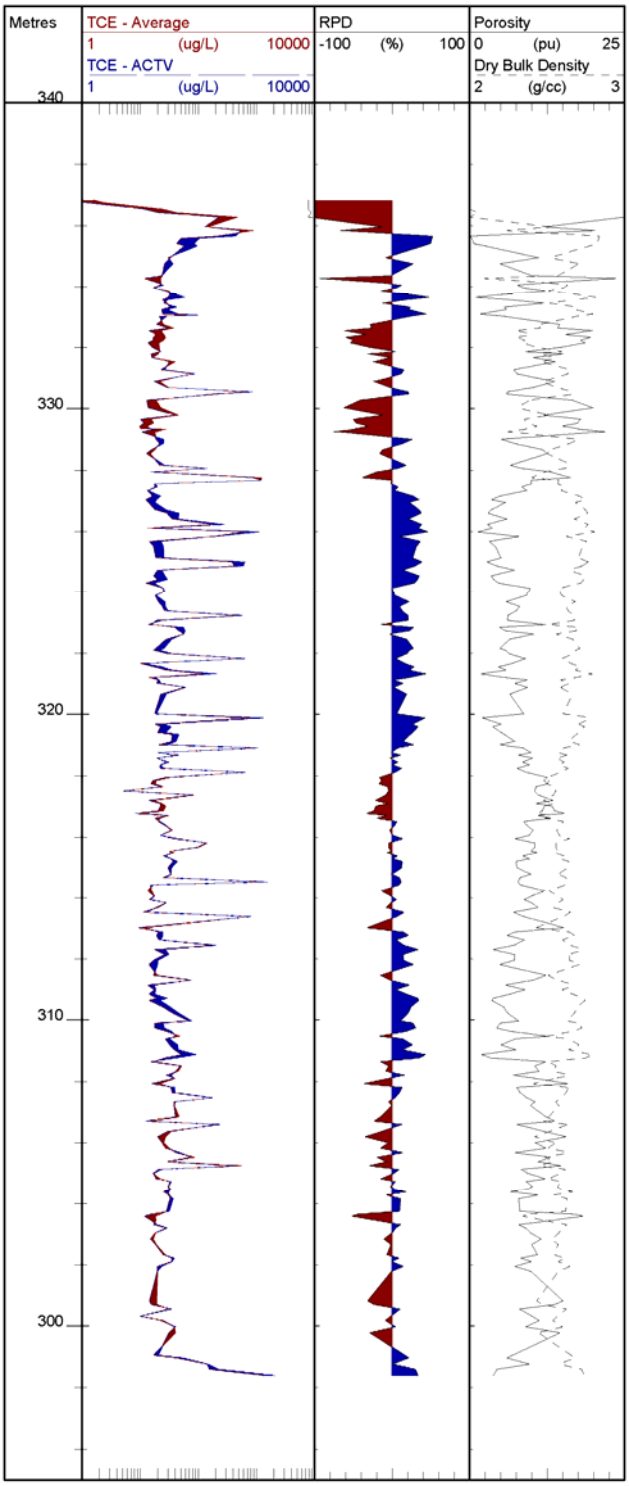

Figure 3.20: MW-26 plot showing the difference between using average values in the porewater conversion or using depth discrete values. Values in red mean that the average value overestimates the concentration and values in blue mean that the average underestimated the concentration. Values in the upper few meters are suspect for the ACTV response due to fractured nature of the borehole and being near the water table.

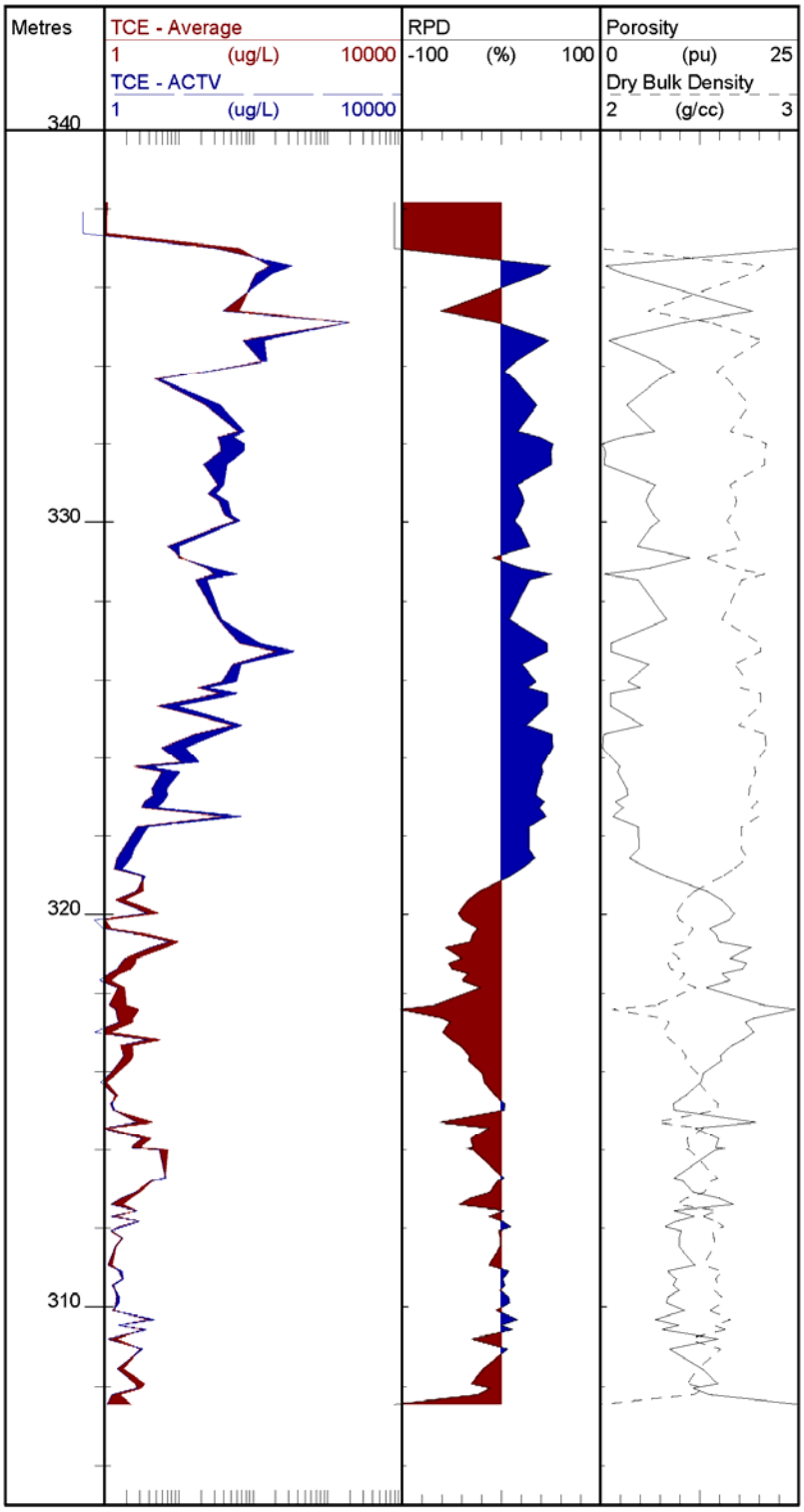

Figure 3.21: MW-367-4 plot showing the difference between using average values in the porewater conversion or using depth discrete values. Values in red mean that the average value overestimates the concentration and values in blue mean that the average underestimated the concentration. Values in the upper few meters are suspect for the ACTV response due to fractured nature of the borehole and being near the water table.

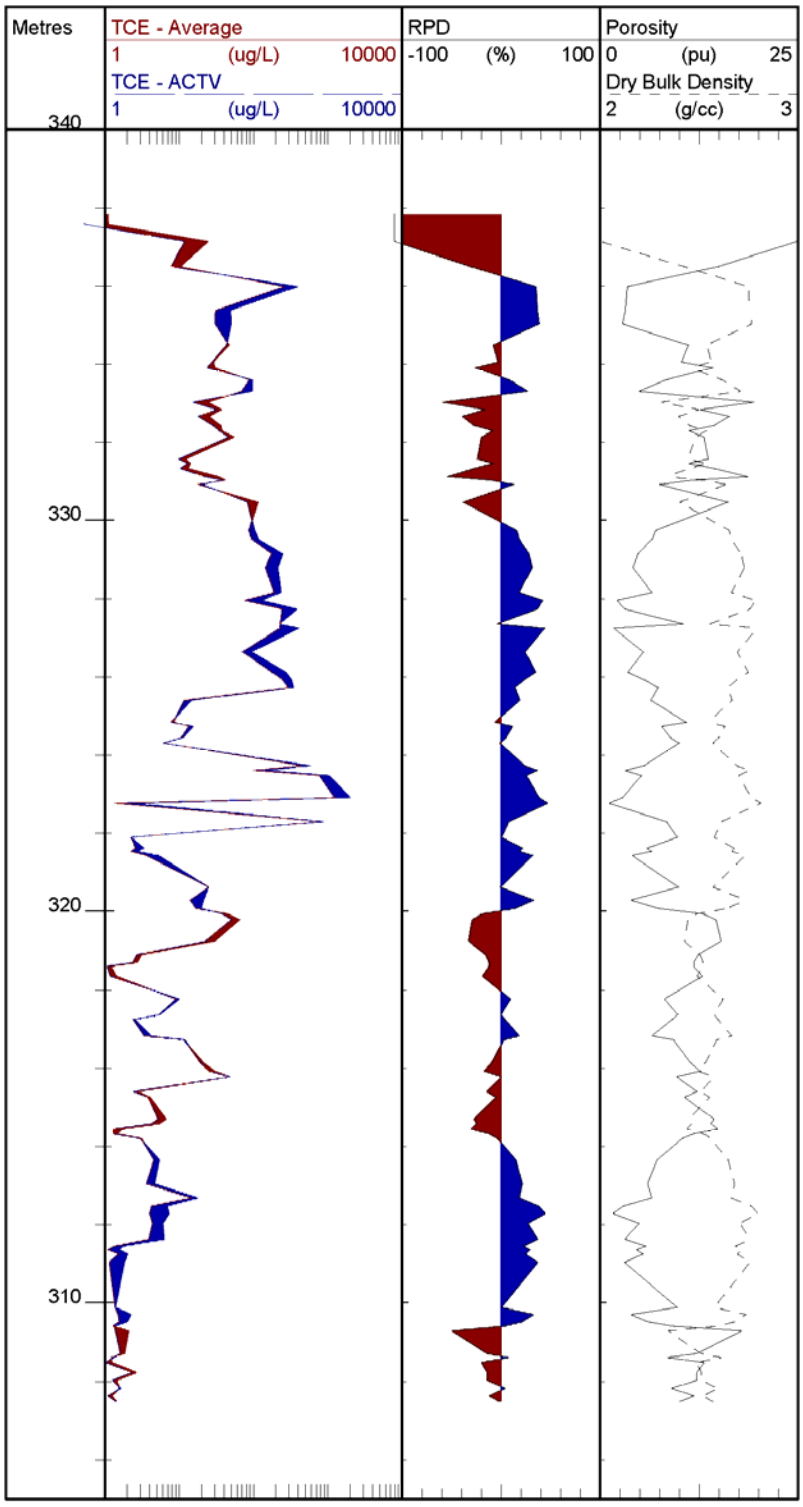

Figure 3.22: MW-367-5 Plot showing the difference between using average values in the porewater conversion or using depth discrete values. Values in red mean that the average value overestimates the concentration and values in blue mean that the average underestimated the concentration. Values in the upper few meters are suspect for the ACTV response due to fractured nature of the borehole and being near the water table.

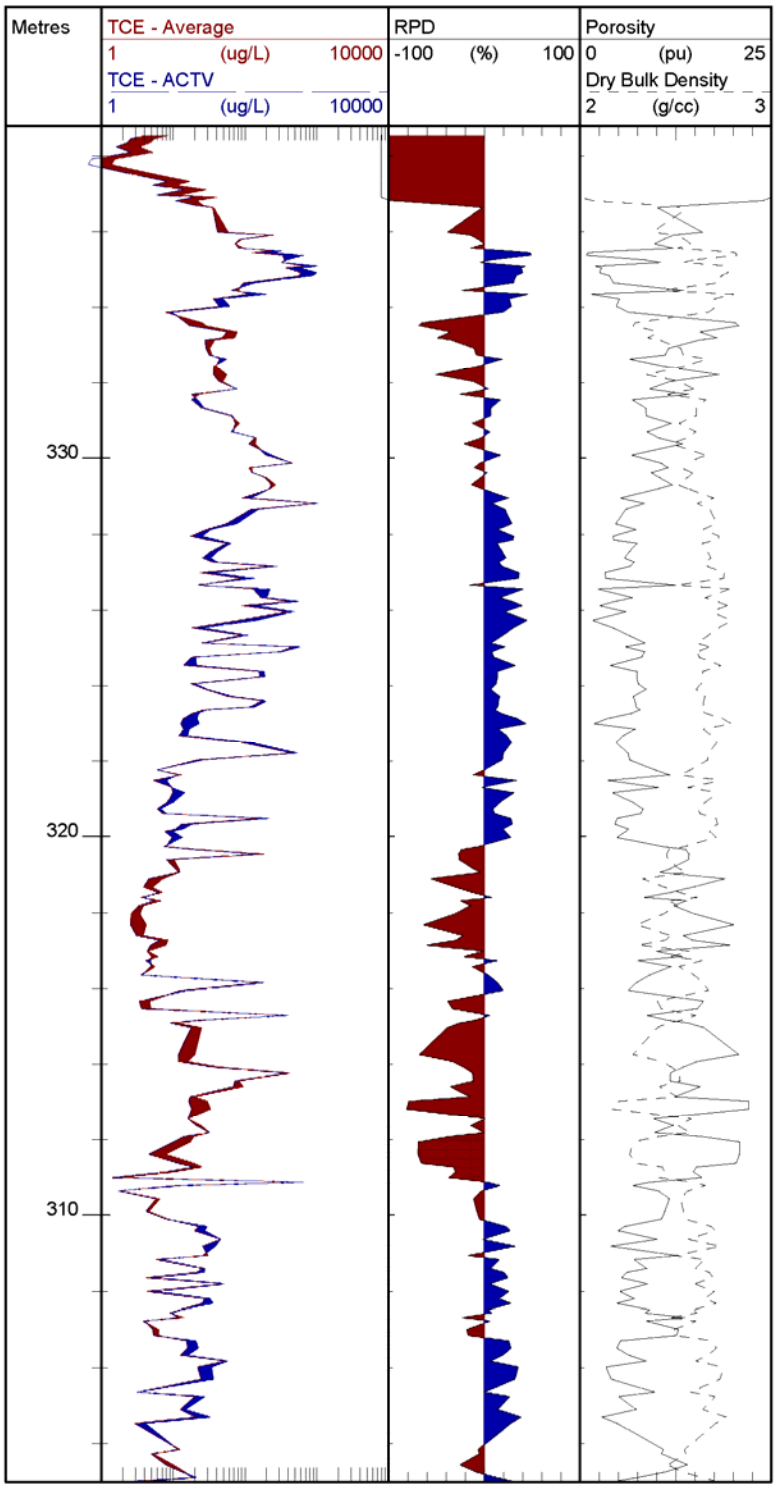

Figure 3.23: MW-367-7 plot showing the difference between using average values in the porewater conversion or using depth discrete values. Values in red mean that the average value overestimates the concentration and values in blue mean that the average underestimated the concentration. Values in the upper few meters are suspect for the ACTV response due to fractured nature of the borehole and being near the water table.

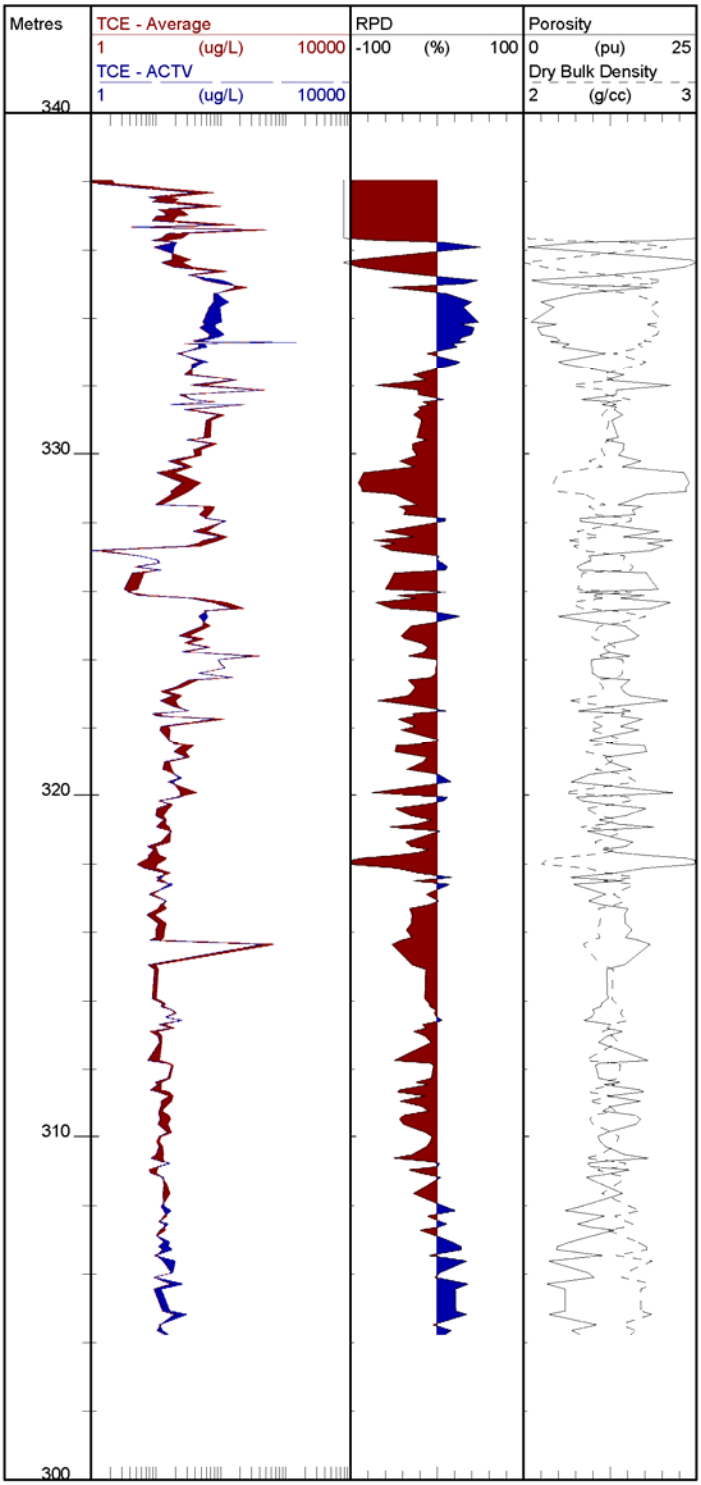

Figure 3.24: MW-367-8 plot showing the difference between using average values in the porewater conversion or using depth discrete values. Values in red mean that the average value overestimates the concentration and values in blue mean that the average underestimated the concentration. Values in the upper few meters are suspect for the ACTV response due to fractured nature of the borehole and being near the water table.

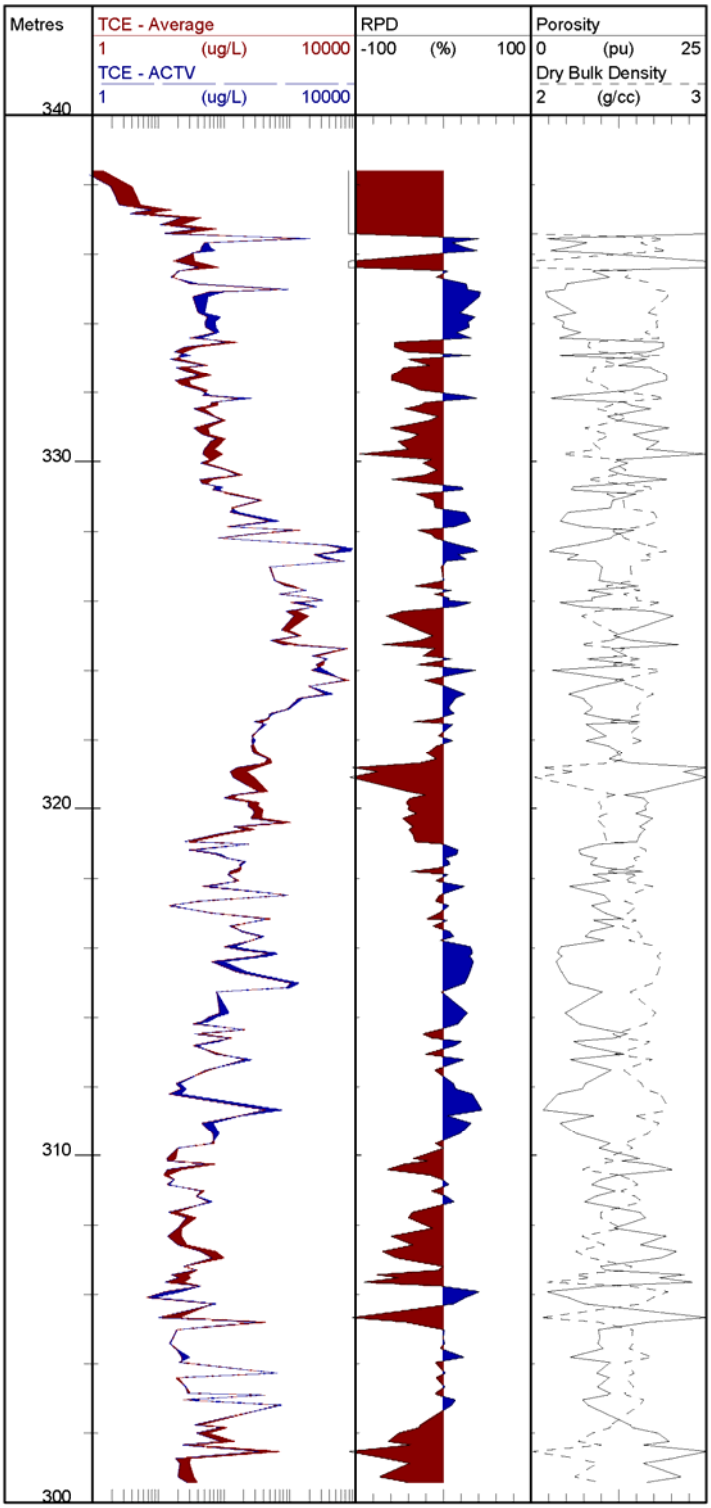

Figure 3.25: MW-367-9 plot showing the difference between using average values in the porewater conversion or using depth discrete values. Values in red mean that the average value overestimates the concentration and values in blue mean that the average underestimated the concentration. Values in the upper few meters are suspect for the ACTV response due to fractured nature of the borehole and being near the water table.

Chapter 4: Site Characterization in the Context of Rock Core VOC Analyses

4.1 Abstract

Contaminated fractured rock aquifers have spatially variable fracture networks and matrix properties which require investigations that rely on multiple lines of evidence for site characterization. This chapter displays a variety of methods for site characterization that are interpreted through the lens of the rock core VOC analysis results. Depth discrete rock core VOC samples were collected at high vertical spatial resolution to allow for correlations with geophysical, geological, and hydrophysical data.

TCE contamination is highly variable with depth and spatially across the research site with the bulk of the contamination existing in the upper 20 m of the Guelph formation, but has been detected throughout the 100 m thick dolostone aquifer and in the underlying shale. Evidence of intermediate degradation daughter products (c-DCE) is only apparent in one of the eight rock core VOC holes and in some samples exceeds the associated TCE concentration. However groundwater samples taken from the conventional monitoring well network show some c-DCE and VC. PCE, 1,1,1-TCA and CF were also detected at the research site but were generally not correlated with the TCE concentrations for rock core VOC samples.

4.2 Scientific Background

Fractured rock aquifers are complex and are associated with a high degree of uncertainty in the field of contaminant hydrogeology. Solutes and water do not migrate identically, a fact that had been recognized since the terminal half of the 19th century (Rolston 2007). The predictive capabilities of flow and transport in fractured media is currently inadequate and one of the most challenging problems in hydrogeology (Berkowitz 2002). Much of the uncertainty stems from the difficulty and expense in characterizing fractured rock sites with enough detail to adequately

describe the variability in the fracture network, and, rock matrix properties, especially for sedimentary rocks where the interplay between fractures and the matrix may be appreciable. Choosing the appropriate areas to focus research on is a difficult task and investigations require multiple lines of evidence to support conclusions. Numerous models exist for fractured rock; including fundamental flow and transport with matrix diffusion principles (Grisak & Pickens 1980;Neretnieks 1980;Sudicky & Frind 1982;Tang, Frind, & Sudicky 1981, Sudicky & Mclaren 1992;Therrien & Sudicky 1996) but calibrating and validating these models has not been done because the appropriate data sets have not been generated (Parker 2007).

Current solute transport models for fractured geologic media realize the importance of matrix diffusion which inherently places emphasis on the rock matrix; however, very few field studies can be found in the literature that have focused on rock core solute concentrations, and fewer yet of these have focused on volatile compounds (VOCs) in the rock matrix. Field studies often rely almost exclusively on groundwater concentrations obtained from wells to characterize the contaminant distribution. Matrix properties are rarely measured so approximate values are used and therefore predictions are not founded on site specific conditions and therefore highly uncertain or the uncertainty isn't known. Field investigations focused on VOCs in fractured sedimentary rock have shown how complex and variable contaminant distributions are in fractured sedimentary rock and present additional tools and techniques as to how fractured rock sites can be characterized (Lawrence, Stuart, Cheney, Jones, & Moss 2006;Lawrence, Chilton, Barron, & Thomas 1990;Lawrence, Geol, Stuart, Barker, & Tester 1996;Sterling 1999;Sterling, Parker, Cherry, Williams, Lane, & Haeni 2005).

4.2.1 Rock Core VOC Analysis Evolution

The importance of interstitial (matrix pore) water composition and its interaction with the soil matrix has been known for more than a century (Cameron & Patten 1907). Because of the

complicated interplay of porewaters with the matrix the quantity measured by different methods also varies. Some methods may focus only on sorbed species, others only on the extractable porewater, and others still focus on a combination of the two.

Coming from the perspective of an ecologist and physiologist, Stiles [1914] presented the commonly used methods of the time for extracting the soil solution: the analysis of drainage water, the lisimetric method, using soil extracts, the centrifuge method, the filter method, and the pressure method. Richards [1941] investigating soil fertility and soil salinity, also lists the commonly used methods of his time (displacement, compaction, centrifugation, molecular adsorption, and suction) and then introduces a modified suction method. A rapid growth of literature based on interstitial analyses occurred in the 1960s , when marine scientists and soil scientists became involved in testing the chemical composition of interstitial waters. Marine scientists applied the methods to deep sediment cores to examine the composition of ancients oceans (Friedman 1965) and the soil scientists, often employing solvent extraction to address sorbed mass, examined the matrix and porewaters contaminated with pesticides (herbicides and insecticides) (Johnsen & Starr, 1967; Mcglamery, Slife, & Butler, 1967; Chiba & Moreley, 1968; Williams, 1968). Squeezers as mentioned in Manheim [1968] had been applied to consolidated sediments such as shales and siltstones for non-volatile constituent analysis. By the 1970's a myriad of approaches for analyzing matrix and porewater concentrations were available and could be chosen based on the type of matrix and analyte of concern. These methods and the increasing body of literature on porewater and matrix chemistry provided the foundation for Foster's [1975] paper on tritium matrix diffusion in the Chalk aquifer, (a relatively soft limestone) which is a fundamental basis of this current study on rock core VOC analyses. Following this, Lawrence [1990] developed a solvent extraction method to analyze VOCs in this Chalk aquifer. Additional studies by Goldstein et. al [2004] and Sterling et al. [2005] show the robustness of the method as it applies to different rock types. Because of the volatility of chlorinated solvents, total matrix and porewater mass concentrations are determined

because removing porewaters without volatile losses is currently impractical. This history has shown the evolution and method development required to analyze more difficult matrices (hard sedimentary rocks) and contaminants (VOCs).

The introduction to tritium matrix diffusion in fractured rock by Foster, 1975 brought attention to the porous matrix between fractures as an important component of the system that would influence contaminant movement in groundwater flowing in fractured porous media. Lawrence, in 1990, using this information as well as other unpublished work in site characterization reports in New York state and Illinois, created a method to assess chlorinated solvent contamination in the Chalk aquifer of the UK which provides the basis for the current work.

4.3 Chapter Focus

This chapter presents discrete fracture network field data sets (vertical profiles of head, rock matrix contamination, porosity, f_{oc}, geophysics, hydrophysics) at high resolution to show the nature of contaminant distribution in the context of the:

1. Flow system
2. Hydraulic conductivity and fracture network characteristics
3. Lithology and stratigraphy

These layers of spatial variability will provide the framework for understanding the source zone condition and plume behavior at this site to create a detailed site conceptual model and parameter estimates for numerical modeling and field verification of the hypothesis for plume behavior in a fractured dolostone aquifer.

4.4 Site Background

Guelph, a city with a population of 115,000 (Statistics Canada 2007), obtains nearly 100% of their drinking water from groundwater and approximately 80% from the dolostone aquifer comprised of the Guelph and Amabel formations (100 m thick). Because of this heavy reliance on

groundwater, steps need to be taken to preserve and maintain this valuable resource. Anthropogenic and natural contamination threaten this local drinking water supply. This aquifer is also used for water supply to other municipalities (e.g. Orangeville, Cambridge, others) and is an important high quality aquifer along the Niagara Escarpment which extends from Niagara Falls to Tobermory serving many smaller towns and private homes (Singer, Cheng, & Scafe 2003).

The research site is located in the industrial north-western quadrant of the City of Guelph which obtains most of its water supply from the Guelph and Amabel dolostone formations (Jagger Hims Limited 1998). Dolostone is a high magnesium content sedimentary rock composed primarily of the carbonate mineral dolomite, $CaMg(CO_3)_2$ (Kennedy 1990). Numerous industries are present near the research site with the potential for multiple contaminant sources in the close vicinity. Volatile organic compounds (VOCs) have posed a threat to the water supply of the city and in the early 1990s resulted in shutting down the two closest municipal supply wells within 500-800 m of the research site (Sacco well closed in 1991, Smallfield well closed in 1993) (Figure 4.1) (City of Guelph 2005). This has resulted in monitoring programs to delineate contamination at local industrial sites.

Trichloroethene, a chlorinated solvent and VOC, entered the subsurface, likely as a Dense Non-Aqueous Phase Liquid (DNAPL), more than two decades ago and migrated through the thin unsaturated glacial overburden deposits into the saturated dolostone bedrock. The water table fluctuates between 3 and 6 mbgs and is variable across the site. TCE is a suspected carcinogen and because of its abundant use in industry, commercially and domestically since 1940's it is one of the most commonly found contaminants at Superfund sites (Doherty 2000;Moran, Zogorski, & Squillace 2007). Currently a contaminant plume several hundred meters long exists as outlined by the consultant installed monitoring well network. No DNAPL has been found in any of the monitoring wells or during rock coring.

4.4.1 Geology

The research site is located on 3-5 m of quaternary sandy silt glacial till (Port Stanley Till) underlain by approximately 100 m of middle Silurian age dolostone (Guelph and Amabel formations). The Silurian dolostone is found in an outcrop-subcrop belt that extends from the Niagara region to the Bruce peninsula (Figure 4.2)(Resident Geologist Program 2004). This investigation focuses on the Guelph and Amabel Formations which comprise the primary drinking water aquifer for the city. The Guelph and Amabel formations contain a variety of features such as stylolites, vugs, fossils and exhibit secondary minerals such as pyrite, sphalerite, fluorite, and glauconite (Dekeyser 2006). The Amabel formation which is correlated with and grades into the Lockport Formation (Smith & Legault 1985) is composed of four members; the Lions Head member, the Colpoy Bay member, the Wiarton member, and the Eramosa member (Bolton 1953;Bolton 1957). At the Guelph site the gradation to the Lockport formation makes the differentiation of the members difficult and potentially not possible (Bolton 1957). At the research site the Guelph formation is typically 30-40 m thick and the Amabel formation is typically 60-70 m thick.

Historically chosen as the uppermost member of the Amabel formation, the Eramosa member forms the contact between the Guelph and Amabel formations. The Eramosa member is of importance as it has been considered an aquitard and therefore a barrier to downward contaminant migration (Gartner Lee Limited 2004). Liberty and Bolton [1971] described the Eramosa as a “thinly bedded, grey to dark grey and brown dense and often cherty, bituminous and non bituminous dolomite”. The member is the result of biohermal patch accumulations and is not continuous across the study area (Bruce Penninsula) being found as often as not being found (Liberty 1971).

Underneath the Guelph-Amabel aquifer lies the Cabot Head Formation shale (Liberty 1971). The contact between the Cabot Head formation and Amabel formation defines the lower extent of

the aquifer and the current depth of study only reaches the uppermost members of this formation including the Wingfield and Dyer Bay members. A simplified geologic cross-section developed by Gartner Lee Limited for the Guelph area is shown in Figure 4.3 and Figure 4.4 shows a simplified stratigraphic column.

4.4.2 Hydrogeology

Porosity and permeability are highly variable both in magnitude and type in fractured dolostone formations. The types of porosity present in the Guelph dolostones can be classified according to Choquette and Pray 1970 as interparticle, fenstral, intraskeletal, shelter, intercrystalline, moldic, intracrystalline, vuggy and fracture porosity (Figure 4.5). All these types of porosity are important to the migration, attenuation, and transport of groundwater contaminants, but it is only the hydraulically active fractures that make the fracture porosity, a small portion of the total porosity, that dominate groundwater flow.

Data obtained from the Grand River Conservation Authority (GRCA) suggest that the groundwater flow direction is primarily to the south-east flowing towards the Speed River for the north-western quadrant of the City of Guelph (Figure 4.6). Previous investigations at the research site suggest that groundwater flow direction may vary with depth (Gamsby and Mannerow Limited 2006).

4.5 Methods

4.5.1 Rock Coring Events

In the summer of 2004, the University of Waterloo began field work at the Guelph site. Since this inception, eleven coreholes have been completed on site with five of them penetrating the entire Guelph-Amabel aquifer (Table 4.1). Prior to this, Gamsby and Mannerow Limited had installed numerous shallow monitoring wells as shown in Table 4.2. A major thrust of the UW investigations was on rock core VOC sampling which occurs concurrently to coring and has been applied to numerous contaminated sedimentary rock sites in Canada and the USA.

Based on groundwater concentrations from conventional wells and water level measurements, locations of four UW holes (MW-22, MW-23, MW-367-4, MW-367-5) were chosen. They were cored in 2004 using air rotary to determine rock core concentrations in the Guelph formation near the source zone, directly down-gradient from the source zone, and near the suspected extent of the contaminant plume. During coring, rock core samples were taken for VOC analysis with the purpose of site characterization and the additional purpose of investigating different extraction and preservation methods examined in chapter 2.

The following winter of 2005 three additional holes (MW-24, MW-25, MW-367-6) were cored through the entire thickness of the Guelph-Amabel aquifer and outside the suspected contaminated zone. These 'regional' holes were primarily for geological, geophysical and hydrophysical logging, with the intent of installing multilevel monitoring wells.

In the summer of 2005 four additional holes (MW-26, MW-367-7, MW-367-8, MW-367-9) were cored in the Guelph formation to complete a transect perpendicular to shallow groundwater flow. These holes were sampled to delineate the VOC contamination in the rock matrix and to compliment the study of extraction methods examined in chapter three.

To determine the maximum depth of contamination in the aquifer, two coreholes (MW-22, MW-367-9) were deepened in November and December of 2006. MW-22 was first cored to below the Eramosa member (44.50 mbgs), in order to isolate the shallow contamination during further drilling. Coreholes were reamed to 6 inches to allow for a removable packer and casing to be installed in order to minimize cross-contamination between the Guelph and Amabel formations. In addition, the increased well diameter increases the number of monitoring ports available for FLUTe™ multilevel monitoring systems. The coreholes were reamed to a diameter of 6 inches using a diamond impregnated reaming shell equipped with a tricone stinger. MW-22 was reamed to 44.50 mbgs and MW-367-9 was reamed to 42.98 mbgs. After reaming, removable packers attached to 5" casing running to the surface were installed in each well. The packers were set at ~40 mbgs and allowed HQ coring to continue to their final completion depths through a central annulus while isolating the Guelph formation from the Amabel formation.

After the completion of each well a blank FLUTe™ liner was used to seal the corehole. During the 2004 coring event Solinst® Continuous Packers or blank FLUTe™ liners were installed in the wells each night to prevent cross-contamination. These seals were removed the morning before drilling continued.

4.5.2 Rock Core Geology

Geological logging occurred alongside rock core VOC sampling. After the core was photographed, an initial overview of the geology was recorded with an emphasis on noting fracture and stylolite positions. The core was then quickly sampled for VOCs to minimize exposure to the atmosphere. After this, more in depth logging occurred which focused on color, fossils, porosity type, crystallinity, mineralogy, and also noting any geological contacts that were visible. The rock quality designation (*RQD*) and percent recovery were determined using the following equations.

$$RQD = \frac{\text{Sum of Core Lengths Greater than 10 cm (m)}}{\text{Length of Core Run (m)}} \qquad \textbf{Equation 4-1}$$

$$\text{Percent Recovery} = \frac{\text{Length of Core Obtained (m)}}{\text{Length of Core Run (m)}} * 100 \qquad \textbf{Equation 4-2}$$

Physical property analysis including porosity, densities and air permeability were performed according to Amirtharaj, 2007. Fraction of organic carbon (f_{oc}) was measured using three different methods and is addressed in Chapter 3.

The core from the three regional holes were not sampled for VOCs and were logged for fracture and stylolite locations in the field and then detailed logging occurred in the summer of 2005.

4.5.3 Rock Core VOC Sampling and Analysis

Rock core VOC sample collection, and analysis methodology is detailed in the methods section of chapter 2. Table 4.3 describes the different collection and extraction methods done for the 2004, 2005, and 2006 rock core sampling events.

Groundwater Chemistry

Groundwater samples were collected from a relatively shallow (typically >320 masl) monitoring network by Gamsby and Mannerow using a waterra pump. Common chlorinated contaminants in the groundwater samples were tetrachloroethene (PCE), trichloroethene (TCE), cis-dichloroethene (c-DCE), and chloroethene (VC). Samples were analyzed according to the procedure outlined in Gamsby and Mannerow Limited, 2003.

4.5.4 Multilevel Montoring Systems

Five multilevel monitoring systems were installed at the Guelph Site for pressure head measurements; three FLUTe™ multilevels and two Westbay Systems. The designs for the systems

are shown in Figure 4.7 and Table 4.4-Table 4.8. Multilevel designs were based on the suite of geological, contaminant, geophysical, and hydrophysical logs.

The Westbay multilevel systems were installed in October 2006 and are described in Westbay Instruments Inc. [1994]. Removable tools interface with pumping/purging and monitoring ports in order to collect data and set up the system. A one-time purge of all the pumping ports using a foot valve attached to waterra tubing and a jerk pump was done in the winter of 2007. This involved pumping each port until at least three well screen volumes were purged and increased water clarity was achieved. After purging, the system is ready for groundwater sampling and no additional purges are necessary.

The fundamentals of FLUTe™ multilevel systems are described in Cherry et al. [2007]. Three 16 port multilevel systems were designed to monitor hydraulic head with depth. Each system was fitted with 16 pressure transducers for temporal hydraulic head monitoring, and were installed in February 2005. MW-23 had difficulties during installation and the lowest port did not evert so only 15 unique monitoring zones are present.

Water Level Monitoring

Hydraulic heads were determined using pressure transducers and validated when possible using manual water level measurements using a water level tape. The locations of the pressure transducers and monitoring wells are shown in Figure 4.7.

Twenty synchronized Solinst® Leveloggers® were installed in the conventional monitoring well network to temporally monitor hydraulic head. A Solinst® Barologger® for measuring atmospheric pressure was necessary to correct for changes in the atmospheric pressure. In addition to recording pressure readings, the Solinst® Leveloggers® also record the groundwater temperature. The 48 transducers installed in the FLUTe™ multilevel systems were manufactured by In-Situ™ (model PXD-261) and vented to the atmosphere and therefore no atmospheric

pressure correction was necessary. Eight transducers were attached to each In-Situ™ Hermit 3000 datalogger for collecting and storing data. Hydraulic head in the two Westbay multilevel systems (MW-24, MW-367-6) were collected by raising and lowering the same unvented pressure transducer to interface with measurement ports (Westbay Instruments Inc. 1994). This procedure typically took two-three hours and an average atmospheric correction for that time interval was applied. Table 4.9 lists the specifications for the different types of pressure transducers.

The transducers were set to record measurements every hour except when pumping or drilling was occurring when readings were recorded every 10 min, or 20 sec respectively. Data were downloaded monthly for the most part but more often during pumping tests and drilling, and less often in the winter.

Vertical hydraulic head profiles are important in determining vertical hydraulic gradients which provide information on the direction, magnitude, and ability for groundwater to flow. The five high resolution multilevel monitoring wells were designed with hydraulic head profiles in mind. Westbay profiles were obtained on 01-11-2006, 05-01-2007, and 10-04-2007 and the FLUTe™ systems continually collected data using the dedicated pressure transducers, however, periods of datalogger failure occasionally occurred where no data were collected.

4.5.5 Hydraulic Testing

Straddle Packer Testing

Straddle packer testing involves temporarily sealing a borehole interval with packers and monitoring the interval response to an induced change in pressure (Lapcevic, Novakowski, & Sudicky 1999). At this site, the change in pressure was created by injecting municipal water into the testing interval and using Environment Canada's National Water Research Institute equipment. By moving up and down the borehole with the straddle packers system the entire borehole can be tested in depth discrete units.

For this study packer test intervals were typically 1.5 or 1.6 meters long resulting in relatively high resolution transmissivity data. The testing apparatus was first lowered to the bottom of the borehole and then raised in 1.5 m intervals. The intervals with the 1.6 m spacing had a 10 cm overlap with the previous interval to ensure that no fractures were missed. Typically three tests were done for each interval by increasing (stepping up) the injection pressures at the start of each test. In general, the differential head applied ranged from 0.06 – 39.74 m with an average of 16.31 m. Some portions of the borehole could not be tested for fear of inadequate packer seating (and resulting packer damage) on the borehole surface due to irregularities caused by intense fracturing.

Transmissivity (T) is calculated using the Theim equation and the measured values for injection flow rate (Q), the differential head (ΔH), the borehole radius (r_w), and estimating the radius of influence to be 10 m (r_e).

$$\boldsymbol{T = \frac{Q}{\Delta H 2\pi} ln\left(\frac{r_e}{r_w}\right)} \qquad \textbf{Equation 4-3}$$

The bulk hydraulic conductivity (K_b) is related to the transmissivity by the testing interval length (b).

$$\boldsymbol{K_b = \frac{T}{b}} \qquad \textbf{Equation 4-4}$$

In addition to the transmissivity data the straddle packer system can get a hydraulic head value for the packed off interval. In low conductivity units it may require hours or longer to achieve equilibrium which isn't practical for testing and yields an unrepresentative head measurement. This introduces error in the calculated differential head value and also the hydraulic head measurements. Straddle packer testing often requires multiple days to collect information about an entire hole which leads to temporal variations in hydraulic head values.

FLUTe™ Transmissivity Profiling

A novel method of determining the transmissivity in a borehole was employed using a blank FLUTe™ liner. Seven coreholes (MW-24, MW-25, MW-26, MW-367-4, MW-367-5, MW-367-6, MW-367-7) were tested using the method described in Keller et. al. [2006]. This method can provide high resolution tranmissivity data. As the liner descends in the borehole fractures providing transsmissivity are covered up, which, in turn results in a decrease in the liner descent velocity. By carefully monitoring the descent velocity, the driving head and depth, a transmissivity profile can be calculated. The resolution of this method is based on the liner descent velocity which is proportional to the transmissivity of the remaining unsealed portion of the hole. Thus, if the bottom of the hole is highly permeable the sample resolution will be coarser. The upper portion of the hole is often coarsely resolved and the velocity data may not be accurate as the borehole adjusts from a transient state to steady state (Keller 2007).

4.5.6 Geophysical and Hydrophysical Methods

Natural Gamma

The natural gamma probe used is an GAMMA39 unit manufactured by Geonics Limited. Natural gamma ray logging is useful for determining lithologies and stratigraphic relationships. As unstable elements decay they may spontaneously emit gamma radiation. The most common of these naturally occurring elements are potassium (^{40}K), uranium (^{238}U) and thorium (^{232}Th) (Keys 1997). This naturally occurring gamma radiation is detected using a thallium activated sodium iodide crystal. The resulting count rate is indicative of the amount of gamma radiation detected. The gamma tool is useful in determining shale content and areas with increasing clay content as these particles are often enriched in the radioactive sediments. Samples were recorded every 0.02 m.

Formation Conductivity

The conductivity probe used is an EM39 manufactured by Geonics Limited. This probe examines the apparent conductivity of the formation by using electromagnetic induction. Primary factors that affect the response of the EM39 are clay content, water content, and groundwater conductivity (Keys 1997). Typically the sampled area is a donut shape 0.1-1.0 meters from the transmitter and the results are recorded in μS/m. The EM39 has an intercoil spacing of 0.50 m and samples were recorded every 0.02 m.

Acoustic Televiewer

Two acoustic televiewers manufactured by Advanced Logic Technology (ALT) were used for this study: the FAC40 and the ABI40. These tools collect oriented caliper and structural data of the borehole wall by using ultrasonic pulses. The centralized probe, employing a rotating mirror and a fixed transducer, emits, digitally records, and processes the responses of the ultrasonic wave train. From the reflected wave train, ultrasonic amplitude and travel time images are created allowing one to determine borehole caliper, geotechnical rock classes, and fracture location and orientation (Advanced Logic Technology 2002). The sampling rate for this tool is 0.2 cm.

Neutron Logging

The neutron tool used is a Comprobe™ (model #2136) which is a centralized tool with dual-spaced He^3 thermal neutron detectors spaced 0.343 m and 0.569 m from a 3 curie Americium-Beryllium source. When neutrons released from the source collide with nuclei of similar mass to a neutron's mass (hydrogen atoms) the greatest amount of neutron energy is lost which in turn decreases the number of neutrons reaching the detectors (Ellis & Singer 2007). Because hydrogen in the subsurface is most commonly found in water the response is closely related to the water content. Electrochemically bound and unbound water is detected using this tool. In saturated rock

of similar mineralogy the correlation to porosity is good. Values were recorded every 2.5 cm with estimated vertical resolutions of 0.343 m and 0.569 m for the near and far detectors respectively.

Gamma-Gamma Logging

The gamma-gamma tool used is a Mineral Logging Systems™ bulk density probe which is a side-collimated tool with a single detector 40 cm from a ^{137}Cs source. Gamma rays from the source are moderated and scattered by electrons between the source and detector due to Compton scattering (Keys 1997). The resulting gamma rays detected will be attenuated more greatly in higher electron density environments which are proportional to the material bulk density. The resolution for the density log is estimated to be equal to the detector spacing which is 0.475 m with a sampling rate of 2.5 cm.

Temperature Logging

High resolution temperature logging was conducted inside open and FLUTe™ lined coreholes. Logging inside the FLUTe™ liner more accurately simulates the natural groundwater flow environment and allows for the detection of smaller fractures (Pehme et al. 2007). Open hole logging may miss these small but hydraulically important fractures due to cross flow in the open borehole which masks the contributions of smaller fractures.

Passive vs Active

The ability to detect flow zones by using changes in groundwater temperature is dependent on stratified temperature with depth. High flow zones are only detectible in passive logging (no addition or removal of heat) if there is a temperature difference associated with the flow zone. Typically, the temperature stratification is related to tropospheric changes, the geothermal gradient, and source of flowing water. Another way to increase detection of features is by heating (or cooling) the water column in a FLUTe™ liner and measure how rapidly heat is transferred to the formation. Zones with high flow can dissipate heat at a faster rate than low flow zones.

Heat Pulse Flow Metering

The heat pulse flow meter (Mount Sopris Model HFP-2293) tests for vertical flow in an open borehole. Upward and downward flow can be detected with this tool by triggering a change in water temperature that is detected either above or below the heat source (Keys 1997). The transit time of the heat pulse is related to the flow in the open hole. Results are reported in gallons per minute and a qualifier is given to the data to show the quality of the data. Horizontal flow, non-constant flow, and poor seals with the borehole wall can all compromise and influence the data collected. The typical test interval length was 0.2 m.

4.6 Observations and Results

4.6.1 General Observations

Of the eight analytes for this study TCE is the most prevalent and commonly occurring in the rock core samples with a maximum concentration of 3.97E-01 µg/g rock (See Table 4.18). Isolated zones of CF, PCE, c-DCE, CFC-113, and 1,1,1-TCA were also found. Chloroform had the highest concentration of all the samples in MW-367-7 at 335.08 masl with a value of 11.4 µg/g rock. The highest concentrations for the other analytes are 1.41E-02 µg/g rock, 1.49E-01 µg/g rock, 4.01E-03 µg/g rock, and 1.88E-03 µg/g rock for PCE, c-DCE, 1,1,1-TCA, and CFC-113 respectively (See Figure 4.48 - Figure 4.59). Concentrations of tetrachloroethene (PCE) and degradation daughter products of TCE (isomers of DCE) in groundwater and rock core samples are also occasionally detected, but typically much less than the concentrations of TCE.

TCE contamination was found as deep as Cabot head shale aquitard (~100 mbgs) situated below the Guelph-Amabel aquifer. The upper 20 m of investigation typically showed large bulges in TCE contamination with the exception of MW-23 and MW-26 which are on the edge of the plume. Contaminant concentrations generally declined with depth after 320 masl and also became sharper peaks coinciding with an increase in fracture spacing.

Horizontal (bedding parallel) fracture spacing varies from centimeters in the upper weathered portion of the Guelph Formation to two meters in the Amabel formation. Because of the difficulty in intercepting vertical fractures with vertical coreholes, the spacing of vertical features is uncertain, however, vertical and steeply dipping fractures were occasionally detected in the rock core suggesting that they are commonly occurring.

Three distinct zones are apparent in hydrographs, a shallow, intermediate, and a deep zone. The transition from the shallow to intermediate zone corresponds to a stratigraphic transition from G_U1 and G_U2. The transition to the deep hydrograph zone typically occurs within the first 15-20 m below ground surface and roughly coincides to the stratigraphic boundary between units G_U2 and G_U3. In the deep zone, vertical hydraulic gradients are small based on the high resolution Westbay multilevel system.

Lithologies

Eighteen different lithologies were defined from the 11 highly variable boreholes in this study. The lithologic descriptions are shown in Table 4.10. The results of the physical property core analysis and comparison with geophysical tools to estimate physical properties is detailed in Chapter 3. Lithologies were primarily based on color, porosity type, particle size, and the type and number of fossils.

Table 4.11-Table 4.15 provide basic statistics for the physical property samples collected. Air permeability was determined for 27 samples from the Guelph formation and the results are shown in Table 4.16 and Figure 4.8. As expected, higher porosity samples generally gave higher air permeability values but determining a quantitative relationship between the two parameters is beyond the scope of this thesis and requires the additional examination of the pore structure and tortuosity of the dolostone samples.

Coreholes

Summary plots for individual UW coreholes are displayed in Figure 4.37 - Figure 4.47.

Cross-Sections

Four units in the Guelph formation, three units of the Amabel, and the Cabot head formation shales were correlated for the cross-sections. These units are outlined in Table 4.17. Three cross-sections of coreholes were made: A-A', B-B', and C-C'. A-A' is approximately coincident with the direction of groundwater flow, B-B' is parallel to a drainage ditch and railroad, and C-C' is approximately transverse to the groundwater flow direction (Figure 4.9).

4.6.2 Shallow Groundwater Flow Direction

The on-site shallow groundwater flow direction obtained from the conventional monitoring network (Figure 4.10) is primarily to the east with a hydraulic gradient of 0.013 (Figure 4.11). There is an inflection in the water table along the drainage ditch which runs parallel to the Canadian National Railway which intersects the site. Groundwater flow directions in the lower Guelph and Amabel formations are uncertain due to too few monitoring data points.

4.6.3 Temporal Hydraulic Head Fluctuations

Hydrographs were created from the FLUTe™ multilevel systems and Solinst® leveloggers® in conventional monitoring wells. Pressure readings were typically recorded every hour but were adjusted during drilling (5 or 10 min) and aquifer testing (20 sec). All ports were situated in the Guelph formation with the exception of the lowest port in MW-367-5 which was situated in the Eramosa member of the Amabel formation. Results show three distinct hydrograph styles which are dependent on depth and the spatial X, Y coordinates of the monitoring well (Figure 4.12 and Figure 4.13). To the east the deeper hydrograph style occurs closer to ground surface which is also consistent with the bedrock stratigraphy showing G_U1 pinching out.

4.6.4 VOC Groundwater Chemistry

Figure 4.14 to Figure 4.17 show the kriged shallow groundwater concentrations of the 2004 and 2006 groundwater sampling rounds. Concentrations of PCE remain relatively constant and do not appear to be migrating from the 2004 to 2006 groundwater sampling rounds. TCE and c-DCE are increasing in lateral extent but are maintaining relatively constant concentrations near the source zone. Migration is primarily to the east for TCE but c-DCE appears to be increasing to the north and slightly to the west. Whether this spread is the result of migration, degradation, or sampling methods is uncertain. Chloroethene concentrations are low and show different distributions between sampling rounds, however, VC appears to be located mostly around the suspected source zone.

4.6.5 Cabot Head Formation Shales (Wingfield and Dyer Bay members)

Geology

Drilling became noticeably slower after reaching the shale contact requiring approximately 30 min for each core run compared to 10 min for the Guelph and Amabel formations. The drilling fluids also changed in color to a dark grey and occasionally red and green, reflecting the changing lithology. The core was thinly bedded and was primarily grey with dark grey, red, and green interbeds. Peaked stylolites decreased in frequency in the shale, and pyrite, chert and gypsum were evident. Horizontal fracture intensity increased as evident by the RQD and fracture trace (Figure 4.37 Figure 4.39 Figure 4.40 Figure 4.44 Figure 4.47). This fracture intensity may however be the result of shale partings and easily induced fractures during coring and handling due to weaker cementation. Visible porosity declined abruptly and laboratory measurements also suggest low porosity. However, porosity determination was difficult as sample disintegration occurred during imbibition when the very fine grained particles expanded during re-saturation. Mean calculated porosity and density values are found in Table 4.10.

Geophysical and Hydrophysical Testing

The fine-grained and shaley dolostones and shales of the Wingfield member of the Cabot Head Formation, are evident by the increase in the response of the gamma and EM conductivity logs. The Dyer Bay member shows large increases in the gamma response with values close to 200 cps, and the EM conductivity response near 70 μS/m. Acoustic televiewer data show a fractured zone at the shale contact.

Despite the high horizontal fracture intensity at this contact, FLUTe™ transmissivity testing did not show an increase in hydraulic conductivity in this region. Packer testing shows higher hydraulic conductivity at the intensely fractured shale contact but generally low values in the shale.

Multilevel Monitoring Wells

Two Westbay systems have monitoring ports in the shale. Hydraulic head in the shale is higher than the overlying Amabel formation and may still be equilibrating (hydraulic head increasing with time), suggesting that the direction of groundwater flow is upward (Figure 4.20). The maximum hydraulic gradients of 0.42 (MW-367-6) and 0.25 (MW-24) are relatively high and suggest that this unit has low vertical hydraulic conductivity and that upward flow is restricted.

Contaminant Distribution (Rock Core VOC)

The shales of the Cabot Head Formation tend to have a higher fraction of organic carbon (f_{oc}) than the dolostone samples. This increases the sensitivity for contaminant detection by increasing the partitioning factor (see Chapter 3, Table 3.2). The shale unit shows the presence of TCE contamination with multiple quantifiable hits in both MW-367-9 and MW-22. To enter the shale, contamination would have to overcome the hydraulic gradient that suggests upward flow (or no flow). To do this, two hypotheses or a combination of the two are suggested: First DNAPL could have penetrated the shale through vertical fractures and then was shunted or transported laterally, and second, aqueous contamination diffused into the shale against the hydraulic gradient. This

means that diffusive mass flux would have occurred at a faster rate than the advective flow of water to the Amabel. In the first hypothesis, a large source (or mobile) or multiple sources would be required to contaminate MW-22 and MW-367-9 as they are approximately 120 m apart. The shale contact for MW-22 is 2.0 m higher than in MW-367-9 which could result in DNAPL migration at the Shale-Amabel contact. Unfortunately the three-dimensional data required to examine the possibility for this is insufficient.

4.6.6 Amabel Formation

Geology

The core from the Amabel formation was bluish grey dolostone containing zones of highly vuggy and pinpoint porosity. Portions of the core were fossil supported with crinoids making up the majority of matrix. Porosity from core samples (MW-22, MW-36-9) showed vertical trends extending over many meters. Stylolites are variable in frequency with depth from hole to hole but present throughout the thickness of the Amabel. Two zones which show increased stylolite frequency are just above the shale contact and in the Eramosa. MW-24, MW-25, and MW-367-6 show fewer stylolites in the field geological logs but Dekeyser's (2005) work suggest that more are present.

A more intensely fractured zone between 250 and 270 masl was found in each of the deep holes except for MW-367-9 which generally showed lower porosity and number of fractures throughout the Amabel. The region corresponds to one of the production zones outlined in Jagger Hims Limited, 1998.

The upper contact with the Guelph formation was defined by the Eramosa member which was highly variable across the site. This member was determined from the rock core by color, grain size, and porosity changes. The color became darker grey and was described as bituminous with an increasing number of stylolites. The porosity became more vuggy and declined in pinpoint

porosity. Grain size was slightly smaller in the Eramosa member. The typical Eramosa containing interbedded shale layers was not present at the site but a more bituminous layer that gave off a petroliferous odor when struck was encountered at the site. Correlations with other members of the Amabel are presented in Perrin 2007 and Dekeyser 2005.

Geophysical and Hydrophysical Testing

Natural gamma values are typically between 10 and 60 cps throughout this unit. The gamma log was used to aid in the determination of the Eramosa unit which typically has a higher gamma signature due to increased clay content. The style of the gamma peak varies from hole to hole: in MW-367-6 it appears as a single sharp peak, in MW-25 it appears to be more like a band, and in MW-367-9 and MW-24 it appears as multiple peaks.

Eramosa

The EM conductivity is also not consistent across the site for the Eramosa member and in some wells shows an increased response signifying increasing water content and clay content but in other wells the response is lower indicating a decrease in water content and clays.

The Neutron log showed a decrease in porosity in the three regional holes for the lower portion of the Eramosa and just below the Eramosa.

Deep production zone (250-270 masl)

The FLUTe™ transmissivity profiles and straddle packer testing results show increased transmissivity in the porous and fractured zones between 250 and 270 masl. Multiple zones in this region had flow rates greater than could accurately be tested using the current straddle packer design.

A temperature bulge in the lined temperature log of MW-367-6 corresponding to the hydraulic conductivity zone suggests that this region is a very active flow zone with connection to

zones at higher elevations (higher temperature). MW-24 shows a inflection in the open hole temperature profile which is indicative of water with a different temperature entering or leaving the borehole. This indicates an increase in hydraulic conductivity.

Multilevel Monitoring Wells

The Amabel formation shows a relatively constant and small hydraulic head drop from the Eramosa to the shale. The average hydraulic gradient for MW-24 is 0.002 and for MW-367-6 is 0.003. There is a slight inflection in the MW-367-6 hydraulic head profile at 265 - 270 masl where the hydraulic gradient increases to 0.009. This corresponds to the region just above the production zone indicating that the production zone has a lower hydraulic head which may be the result of pumping.

Contaminant Distribution (Rock Core VOC)

MW-367-9

The TCE concentration profile shows relatively low concentrations for the majority of the Amabel formation and sharp peaks without any bulges. The Eramosa member and upper Amabel is an exception to this which exhibits elevated TCE contamination in peaks and bulges. A bulge is defined as multiple consecutive contamination hits with lower concentration gradients than for sharp isolated peaks. A bulge could be the result of multiple fractures, a vertical fracture, matrix flow, or a single fracture with diffusion occurring over a longer period of time. The formation diffusion coefficient also plays an important role in the shape of the concentration profile. A collection of low TCE concentration peaks occur between 265 and 275 masl with a few associated PCE peaks.

MW-367-9 shows a marked decrease in TCE concentration at 298.4 masl. This roughly corresponds to the end of the hole that was cored in 2005 which ended at 299.3 masl. In 2006, four rock core VOC samples taken in between 298.4 and 299.3 masl had concentrations similar to the

2005 values, but below this point concentrations declined rapidly to non-detect. In this region it is also important to note a decrease in fracture frequency which is apparent in the increased RQD values (Figure 4.18-Figure 4.19 and Figure 4.47).

The Eramosa member shows lower concentrations than the overlying Guelph formation but comparable with the directly underlying Amabel. A group of c-DCE contaminated samples are found in the Eramosa member which indicates that degradation may be occurring in this unit (Figure 4.56). This could be the reason for the decreased TCE concentrations rather than hydraulic controls. In this region c-DCE concentrations surpass TCE concentrations. In addition chloroform is also found in some of the samples from the Eramosa.

MW-22

MW-22 shows higher contamination in the Amabel than does MW-367-9 with more frequent peaks and bulges. The region between 250 and 265 masl shows numerous TCE peaks and bulges and some PCE peaks. There are fewer regions of minimal contamination in MW-22 than MW-367-9 and the largest is from 266.5 - 271.8 masl.

The basal portion of the Eramosa contains a fracture set (297 masl) with the second highest TCE concentration for the corehole in the adjacent matrix. Above this the Eramosa has numerous non-detect values for TCE.

4.6.7 Guelph Formation

Geology

The core from the Guelph formation was thickly bedded tan-grey dolostone. The majority of the porosity above 320 masl was pinpoint porosity with increasing vugginess below until the Eramosa. Four distinct units were encountered in the Guelph formation, G_U1, G_U2, and G_U3, G_U4 which are described in Table 4.17. Fracture frequency, stylolite frequency and stratigraphic

units are shown in Figure 4.18, and Figure 4.19 and cross-sections A-A', B-B', C-C' (Figure 4.22-Figure 4.27).

The upper contact with the Port Stanley till is a highly weathered and fractured zone 0.5-2.0 m thick. Many of the fracture surfaces contain iron oxide coatings and also contain silt and clay infillings from the overburden. The dolostone from this region was only partially saturated with wet and dry zones.

This weathered zone is underlain by fine grained dolostone unit (G_U1) with many fractures and low matrix porosity <5% (~0-8 m). Core samples from this unit tended to have vertical micro-fractures in them but did not cause the core to come apart. These easily visible, but very small fractures could potentially facilitate flow. Increasing water saturation occurs in this unit. In wells MW-367-6 and MW-25 this unit was not found.

The second unit, G_U2 (~8-15 m) consists of high pinpoint porosity sucrosic dolostone with numerous stylolites. Next is unit G_U3 (~15-24 m), having increasing fossil content and vugginess. Fewer stylolites were present in this unit. G_U4 has dark grey banding and clasts across the core and higher porosity including many vugs. The lower contact with the Eramosa was gradual and often hard to distinguish.

Geophysical and Hydrophysical Testing

The overburden and bedrock contact is signaled by a change in the gamma signal with the overburden having a higher gamma response. Typically the gamma signal is between 0 and 40 cps for the Guelph formation. The bottom of G_U1 coincides with a correlatable gamma peak (Figure 4.27, Figure 4.28). Following this, the gamma signal remains relatively constant until the bottom of G_U2. Unit G_U3 is marked by a series of gamma peaks and then G_U4 exhibits a relatively constant response until the Eramosa member of the Amabel formation.

Packer testing shows several extensive high hydraulic conductivity units in the Guelph formation. Typically, the uppermost portion of the Guelph formation was not tested because of extensive fracturing and the variably saturated conditions of the fractures and rock matrix. Three higher hydraulic conductivity correlatable zones are found at 330 masl across the transect, 310–318 (from MW-367-9 to MW-26) masl, and 308-300 at (from MW-367-9 to MW-26) (Figure 4.29).

Matrix porosity and hydraulic conductivity show some similarities in distribution (Figure 4.30). The correlation might suggest the potential for matrix flow, leakage of water around packers may be occurring in the higher porosity zones, the higher porosity unit has more hydraulically active fractures, or that flow in fractures has altered the porosity of the surrounding matrix blocks. Some areas having high core porosity do not show correspondingly higher hydraulic conductivity by straddle packer testing as seen in MW-367-9 at 326 masl thus indicating fewer fractures.

Multilevel Monitoring

Three FLUTe™ multilevels (MW-23, MW-367-4, MW-367-5) and two Westbay Systems (MW-24, MW-367-6) monitoring wells are screened in the Guelph formation on site. Hydraulic head profiles for MW-23, MW-24, and MW-367-6 have similar shapes with large hydraulic gradients in the upper Guelph formation followed by slowly declining head for the rest of the Guelph formation. MW-367-4 and MW-367-5 show a decline in hydraulic head initially but show more variability with depth as seen by the undulating nature of the profile. Profile shapes are very constant with time but in general show overall shifts for all the ports to higher or lower hydraulic heads. The exception to this is after a recharge event when the shallow ports in the heavily fractured zone respond much quicker and to a higher degree than the deeper ports.

The static hydraulic head profiles found in MW-367-4 and MW-367-5 are interesting for a few reasons: First the values at depth approach the water table hydraulic head, secondly, it suggests

the presence of confining units, thirdly, there is potential for divergent flow, and finally the contrasting profile shapes suggest vertical hydraulic connection is highly variable across the site.

Figure 4.31 shows the response of MW-23 multilevel monitoring wells during the drilling of MW-26, a well 30 m to the north-east. The response can be generally characterized with three distinct styles. The upper two ports show similar hydrograph shapes and are minimally affected by drilling. The third port shows a transition between the upper two ports and the rest of the monitoring ports. The shapes of the hydrographs are similar for the deeper ports, however, the magnitude of the response is varied in each port suggesting different degrees of connection to the well being drilled.

Figure 4.32 shows the response of MW-23 and MW-367-4 to an isolated precipitation event on 19-Aug-2005. The majority of rainfall occurred between 5:00 am and 5:00 pm and was very intense (UW Weather Station 2005). The upper ports in each multilevel responded much more rapidly (and with a greater magnitude) to the recharge event and then declined more rapidly than the other ports after precipitation ceased. MW-23 shows an especially interesting response in the upper two ports. The hydraulic gradient between ports 1 and 2 switched polarity during the recharge event. Once rainfall ceased the direction reversed to the pre-event conditions. MW-23 Port 3 shows a slightly elevated response compared to the lower ports which all acted in a similar manner. The response of MW-367-4 was similar to MW-23 with port 2 showing a larger response to heavy rainfall than did port 1. Unfortunately, MW-367-4 ports 3 and 4 had malfunctioning transducers and thus no data could be collected for them. After the rainfall, the deeper ports continued to show increasing hydraulic heads (without any additional precipitation) until 23-Aug-2005 and then began to decline (Figure 4.33).

The head profiles generated during straddle packer testing can be used to describe the spatial head variability as well. It is important to stress that these data were not collected

simultaneously or even in the same year. However, the profiles are in agreement at least with the shallow water levels from the conventional and multilevel monitoring systems showing decreasing hydraulic head to the north-north east Figure 4.34. The cross borehole effects of the temporal variability of hydraulic head can be mitigated by examining hydraulic gradient plots (Figure 4.35). This is achieved because apart from the heads in the uppermost Guelph (> ~330) the hydraulic heads respond uniformly (thus relatively constant hydraulic gradients) as was shown in Figure 4.31-Figure 4.32. The vertical hydraulic gradients may provide insight into lower vertical hydraulic conductivity zones that straddle packer and FLUTe™ hydraulic testing do not detect.

Contaminant Distribution (Rock Core VOC)

The rock core VOC distribution in the Guelph formation is highly variable laterally and with depth. This is clearly evident by comparing MW-23 TCE contamination with MW-367-9 which are at opposite ends of transect C-C'. MW-367-9 shows a broad set (320-330 masl) of highly contaminated rock core with no non-detects, however, MW-23 shows a majority of non-detects for the corresponding interval. A similar difference can be seen by examining only MW-367-9 at different depths. In the Amabel formation, MW-367-9 shows a contaminant distribution more similar to MW-23 than it does to the overlying Guelph formation.

Typically the upper 20 m (>320 masl) of the Guelph formation is described by a series of bulges indicating intense or vertical fracturing, a long term contaminant presence, increased diffusion coefficients, or a combination of these. Intense fracturing effectively decreases diffusion distances and allows a larger area of the rock matrix to be in contact with fracture water thus facilitating contaminant transport to the matrix creating contaminant bulges. Some of these bulges correlate across the cross-section C-C' (Figure 4.36). Better correlation in magnitude may have been realized if all coreholes were drilled the same year and field preserved in methanol (see chapter 2). In general, TCE concentrations decrease along the transect as you go north.

MW-367-9 shows the highest rock core TCE contamination and is also the only well showing quantifiable detects of c-DCE, and 1,1,1-TCA. In one zone of the corehole (Eramosa member) c-DCE contamination is greater than the corresponding TCE contamination (Figure 4.56). Another zone containing c-DCE exists from 324-327.5 masl and contains c-DCE at concentrations lower than one-tenth of the associated TCE concentration. This highly contaminated zone consists of dark grey dolostone and stylolite rich regions and also contains quantifiable detects of PCE, CF and 1,1,1-TCA.

4.7 Summary of Findings

Analyzing total contaminant mass of the rock matrix has many desirable traits and a few undesirable traits some of which are outlined below.

Scientific Benefits

1. Higher resolution than standard water samples.
2. Spatial depth certainty / no pumping required. Contamination in the rock matrix is less easily disturbed
3. Cross-contamination from open holes minimized
4. Isolate specific features, isolate geologic changes
    a. samples low permeability zones
    b. samples high permeability zones
5. Provides information on the current stage of plume with concentration gradients - one snapshot as opposed to long term sampling
6. Sorbed mass may be important for remediation and life of contamination
7. Most mass resides in the matrix
8. Back calculate porewater concentrations
9. Determine maximum depth of contamination
10. Vadose zone sampling

Scientific Difficulties

1. The increased variability of the rock matrix makes interpretation more complex
2. Not a water concentration, total contaminant mass per gram

Depth Certainty

Sample location uncertainty at contaminated sites can have a dramatic impact in highly heterogeneous media. Sampling groundwater in conventional and most multilevel monitoring

wells yields results that are blended over a depth interval that is often much larger than the heterogeneity of the contaminant distribution. Water, being a fluid, is much easier to disturbed than the rock matrix and most sampling methods require purging or the use of a pump disrupting the natural groundwater flow conditions and further increasing spatial uncertainty. These influential problems that we commonly accept are not inherent in all groundwater investigations. By sampling the rock matrix, depth control is ensured to great accuracy and one can be confident in the sample position.

Resolution

When investigating contaminated sites the sample resolution greatly influences the conceptual model for the site (Lawrence, Stuart, Cheney, Jones, & Moss 2006). The spatial resolution for water samples is typically measured in meters. Water samples may be obtained at close depth intervals using double packer equipment but that is often not practical and sampling would be lengthy as the packers may need to be inflated for a lengthy amount of time to remove artifacts due to vertical borehole flow. Another important consideration is how the open borehole conditions may affect the sampling zones contained inside the packed off intervals. In addition, low permeability layers would be difficult to sample as well. Sample resolution for rock samples is on the cm scale.

Feature Isolation

Conventional groundwater sampling obtains bulk samples that may come from multiple fractures, and preferentially samples high conductivity units. This means that many important features to contaminant flow and migration are not sampled, especially low permeability, low diffusion, and high sorptive units. Rock core sampling allows for the isolation and determination of these features and helps to determine relationships for the contaminant distributions.

Stage of Plume

The rock matrix porewater is often in disequilibrium with fractures, high concentration gradients exist at many fractured rock sites. Concentrations in the fractures facilitate migration by diffusion into and out of the rock matrix. Targeting fractures and the matrix in close proximity to the fractures can determine the direction of contaminant flux based on the shape and style of the profile obtained and thus provides insight about the longevity of contamination. In practice, typical water sampling programs assess the contaminant longevity based on temporal sampling programs which may require sampling for many years providing the information that one snapshot may provide.

Maximum Depth of Contamination

The maximum depth of contamination can be obtained using this method without worrying about the effects of "drag-down" or cross-contamination as rock core is less easily contaminated from other sources.

Majority of the Mass is in the Matrix

Most contaminant sources will originate in the fractures as they typically are the primary conduits of flow. Concentration gradients between the rock fractures and rock matrix will promote diffusive transfer with the rock matrix. The high matrix volume and surface area in contact with fractures means that the matrix is capable of storing considerable contaminant mass and often the matrix becomes the primary contaminant storage compartment which can act as a long term source or sink. When the majority of the contaminant mass is in the matrix and is capable of being released with time an accurate understanding is necessary. Rock core provides the tool to examine the portion of the system where the majority of contaminant mass resides.

Estimate Porewater Concentrations for Groundwater Comparisons

The total mass which includes the aqueous mass and the sorbed mass is calculated for this procedure. Based on physical properties an estimate in the groundwater can be obtained. Conceptual models based primarily on fracture water analyses will be biased and could lead to incorrect conclusions as the majority of the subsurface is being neglected.

Interpretation

As rock core VOC studies gain attention steps need to be taken to ensure appropriate interpretations. The distribution of porosity, fraction of organic carbon, water saturation, and the presence of NAPL will significantly affect the results obtained from rock core analysis and need to be considered when forming interpretations or conclusions based on these results. The sensitivity of the method will strongly be influenced by these factors.

List of Findings

- **Rock core VOC contamination**
    - TCE is the primary contaminant in the rock core samples taken.
    - The TCE concentrations vary in both magnitude and profile style with depth and lateral extent.
    - TCE degradation daughter products do not appear to be widespread in the rock core samples.
        - Two primary zones of c-DCE found in MW-367-9 and are associated with darker more bituminous dolostone zones in the borehole one of which is the Eramosa member.
    - On the northern most wells (MW-23, MW-26) of transect C-C' TCE appears primarily as sharp peaks.

- TCE concentrations generally decrease with depth with the majority of the contaminant mass > 320 masl.
- TCE rock core concentrations are higher in the underlying shale.
- CF shows some very large and isolated peaks. The source of this contamination needs to be investigated further.
- Concentrations of TCE and PCE are not always correlated.

- **Groundwater monitoring network**
  - TCE contamination in the shallow zone is spreading to the east but relatively slowly.
  - The c-DCE plume is also spreading to the east.
  - PCE contamination is remaining fairly constant potentially due to higher sorption coefficient.
- **Geology**
  - Four distinct zones were found in the Guelph formation.
  - G_U1 thickness decreases eastward and is non-existent in MW-25 and MW-367-6.
  - The Eramosa member was often difficult to discern visually and gamma logs helped to determine its location.
  - Eramosa thickness and visual appearance is varied throughout the site.
  - Porosity is highly variable from hole to hole and also with depth.
  - Fracture spacing tends to increase in the Amabel formation compared to the Guelph formation.
- **Water level measurements**
  - Hydraulic gradients are generally downward in three of the five multilevel monitoring systems with the majority of the hydraulic head drop occurring above 320 masl. The other two multilevel monitoring systems have undulating hydraulic heads with depth showing reversals of gradients.

- The shallow vertical hydraulic gradient appears to be greatest in the upper portion of G_U3
- Three distinct hydrograph styles are consistent across the site.
- Hydrograph styles appear to be associated with the stratigraphic units, with wells to the east not showing the shallow hydrograph type as G_U1 is not existent.
- Monitoring multilevel responses to drilling and recharge events can provide valuable hydraulic connectivity data.

- **Geophysics and hydraulic testing**
  - The upper highly fractured zone of the Guelph formation appears to exhibit high hydraulic conductivity. Two other zones in the Guelph formation appear to have increased hydraulic conductivity as well.
  - Multiple lines of evidence confirm a laterally extensive production zone at around 250-270 masl.

Table 4.1: UW well drilling investigations

Well	Dates Cored	Depth (mbgs)	Diameter
MW-22	June and July 2004	24.77	HQ
MW-22 Deepened	November and December 2006	103.95	6" < 44.50 mbgs HQ >44.50 mbgs
MW-23	June and July 2004	39.8	HQ
MW-24	February and March 2005	104.69	HQ
MW-25	February and March 2006	103.69	HQ
MW-26	June and July 2004	42.72	HQ
MW-367-4	June and July 2005	35.15	HQ
MW-367-5	June and July 2004	35.15	HQ
MW-367-6	March 2005	103.32	HQ
MW-367-7	June and July 2005	40.46	HQ
MW-367-8	June and July 2006	38.23	HQ
MW-367-9	June and July 2007	42.98	HQ
MW-367-9 Deepened	November and December 2006	105.46	6" < 42.98 mbgs HQ > 42.98 mbgs

Table 4.2: Site drilling investigation history

Year Constructed	Description
2000	4 monitoring screens in 4 holes
2002	19 monitoring screens in 19 holes
2003	15 monitoring screens in 7 holes
2004	4 UW rock core VOC holes
2005	4 UW rock core VOC holes and 3 regional coreholes
2006	2 UW Deepened rock core VOC holes to shale

Table 4.3: VOC Sampling and analysis methods

Well	Extraction Method	Analytical Lab	Preservation	Year
MW-22	Microwave Assisted Extraction	UW Dirt Lab	Field	2004
MW-22	Shake-Flask	UW Dirt Lab	Lab	2004
MW-22	Shake-Flask	UW Dirt Lab	Lab	2004
MW-22	Purge and Trap	Maxxam Analytics Inc	None	2004
MW-23	Microwave Assisted Extraction	UW Dirt Lab	Field	2004
MW-23	Shake-Flask	UW Dirt Lab	Lab	2004
MW-367-4	Microwave Assisted Extraction	UW Dirt Lab	Field	2004
MW-367-4	Shake-Flask	UW Dirt Lab	Lab	2004
MW-367-4	Shake-Flask	UW Dirt Lab	Lab	2004
MW-367-4	Purge and Trap	Maxxam Analytics Inc	None	2004
MW-367-5	Microwave Assisted Extraction	UW Dirt Lab	Field	2004
MW-367-5	Shake-Flask	UW Dirt Lab	Lab	2004
MW-26	Microwave Assisted Extraction	UW Dirt Lab	Field	2005
MW-367-7	Microwave Assisted Extraction	UW Dirt Lab	Field	2005
MW-367-7	Shake-Flask	UW Dirt Lab	Field	2005
MW-367-8	Microwave Assisted Extraction	UW Dirt Lab	Field	2005
MW-367-9	Microwave Assisted Extraction	UW Dirt Lab	Field	2005
MW-22 Deep	Microwave Assisted Extraction	UW Dirt Lab	Field	2006
MW-367-9 Deep	Microwave Assisted Extraction	UW Dirt Lab	Field	2006

Table 4.4: MW-23 FLUTe^{TM} monitoring port locations

Port ID	Screen Elevations (masl)		Port Elevation (masl)	Effective Screen Length (m)
	Top	Bottom		
ML1	336.86	335.34	336.10	1.52
ML2	334.73	333.20	333.97	1.52
ML3	332.59	331.37	331.98	1.22
ML4	330.16	328.33	329.24	1.83
ML5	327.72	326.19	326.95	1.52
ML6	325.28	323.75	324.52	1.52
ML7	323.45	321.93	322.69	1.52
ML8	321.62	320.10	320.86	1.52
ML9	319.79	318.57	319.18	1.22
ML10	317.35	316.44	316.90	0.91
ML12	312.78	311.56	312.17	1.22
ML13	311.26	309.73	310.50	1.52
ML14	309.12	308.21	308.67	0.91
ML15	307.60	301.02	304.31	6.58

Table 4.5: MW-367-4 FLUTe™ monitoring port locations

Port ID	Screen Elevations (masl)		Port Elevation (masl)	Effective Screen Length (m)
	Top	Bottom		
ML1	336.46	334.94	335.70	1.52
ML2	334.33	332.50	333.41	1.83
ML3	331.58	330.67	331.13	0.91
ML5	328.54	327.32	327.93	1.22
ML7	325.49	324.57	325.03	0.91
ML8	323.36	322.44	322.90	0.91
ML9	321.53	320.61	321.07	0.91
ML10	319.39	318.48	318.94	0.91
ML11	317.56	316.65	317.11	0.91
ML12	316.04	315.43	315.74	0.61
ML13	314.82	313.91	314.36	0.91
ML14	312.99	311.47	312.23	1.52
ML15	310.55	309.33	309.94	1.22
ML16	309.03	307.51	308.27	1.52

Table 4.6: MW-367-5 FLUTe™ monitoring port locations

Port ID	Screen Elevations (masl)		Port Elevation (masl)	Effective Screen Length (m)
	Top	Bottom		
ML1	336.95	335.42	336.19	1.52
ML2	334.82	332.99	333.90	1.83
ML3	332.38	331.77	332.07	0.61
ML4	331.46	330.55	331.01	0.91
ML5	329.94	329.02	329.48	0.91
ML7	325.98	324.45	325.21	1.52
ML8	324.15	323.54	323.84	0.61
ML9	322.93	321.71	322.32	1.22
ML10	321.10	320.18	320.64	0.91
ML11	319.58	318.66	319.12	0.91
ML13	315.61	314.39	315.00	1.22
ML14	313.78	312.26	313.02	1.52
ML15	311.35	309.82	310.58	1.52
ML16	309.21	307.99	308.60	1.22

Table 4.7: MW-24 Westbay System port locations

Port ID	Screen Elevations (masl)		Port Elevation (masl)	Effective Screen Length (m)
	Top	Bottom		
ML1	342.04	337.16	N/A	N/A
ML2	336.25	335.03	335.94	1.22
ML3	334.11	332.89	333.20	1.22
ML4	331.98	330.45	331.67	1.52
ML5	329.54	328.93	329.24	0.61
ML6	328.02	325.27	325.58	2.74
ML7	324.36	321.62	321.92	2.74
ML8	320.70	318.26	320.40	2.44
ML9	317.35	316.74	317.04	0.61
ML10	315.82	315.21	315.52	0.61
ML11	314.30	313.39	314.00	0.91
ML12	312.47	311.25	311.56	1.22
ML13	310.34	309.73	310.03	0.61
ML14	308.81	307.90	308.51	0.91
ML15	306.99	305.77	306.68	1.22
ML16	304.85	302.72	303.02	2.13
ML17	301.80	300.28	301.50	1.52
ML18	299.37	298.76	299.06	0.61
ML19	297.84	296.62	296.93	1.22
ML20	295.71	295.10	295.40	0.61
ML21	294.18	292.96	293.88	1.22
ML22	292.05	290.83	291.75	1.22
ML23	289.92	288.70	289.00	1.22
ML24	287.78	286.26	287.48	1.52
ML25	285.34	283.52	283.82	1.83
ML26	282.60	281.38	282.30	1.22
ML27	280.47	279.86	280.16	0.61
ML28	278.94	276.81	278.64	2.13
ML29	275.90	273.76	275.59	2.13
ML30	272.85	271.63	272.54	1.22
ML31	270.71	270.10	270.41	0.61
ML32	269.19	266.45	268.89	2.74
ML33	265.53	262.79	263.09	2.74
ML34	261.87	257.61	261.57	4.27
ML35	256.69	254.86	256.39	1.83
ML36	253.65	253.04	253.34	0.61
ML37	252.12	250.29	250.60	1.83
ML38	249.38	246.63	249.07	2.74
ML39	245.72	244.50	245.42	1.22
ML40	243.59	242.37	243.28	1.22
ML41	241.45	237.49	239.62	3.96
P1	334.11	332.89	333.81	1.22
P2	328.02	325.27	327.71	2.74
P3	324.36	321.62	324.05	2.74
P4	312.47	311.25	312.17	1.22
P5	304.85	302.72	304.55	2.13
P6	297.84	296.62	297.54	1.22
P7	289.92	288.70	289.61	1.22
P8	285.34	283.52	285.04	1.83
P9	265.53	262.79	265.23	2.74
P10	252.12	250.29	251.82	1.83
P11	241.45	237.49	241.15	3.96

Table 4.8: MW-367-6 Westbay System Port Locations

Port ID	Screen Elevations (masl)		Port Elevation (masl)	Effective Screen Length (m)
	Top	Bottom		
ML1	335.47	333.64	333.94	1.83
ML2	332.72	331.50	331.81	1.22
ML3	330.59	329.98	330.29	0.61
ML4	329.07	328.46	328.76	0.61
ML5	327.54	326.32	326.63	1.22
ML6	325.41	324.80	325.10	0.61
ML7	323.88	323.28	323.58	2.44
ML8	322.36	321.75	322.06	0.61
ML9	320.84	320.23	320.53	0.61
ML10	319.31	318.70	319.01	0.61
ML11	317.79	316.57	316.87	1.22
ML12	315.66	313.52	315.35	2.13
ML13	312.61	311.39	312.30	1.22
ML14	310.47	309.25	310.17	1.22
ML15	308.34	307.43	308.04	0.91
ML16	306.51	305.60	306.21	0.91
ML17	304.68	303.46	303.77	1.22
ML18	302.55	301.94	302.24	0.61
ML19	301.02	300.42	300.72	0.61
ML20	299.50	298.28	298.59	1.22
ML21	297.37	296.15	296.45	1.22
ML22	295.23	294.01	294.32	1.22
ML23	293.10	288.83	292.19	4.27
ML24	287.92	286.70	287.00	1.22
ML25	285.78	283.96	284.87	1.22
ML26	283.04	281.82	282.13	1.83
ML27	280.91	279.99	280.60	1.22
ML28	279.08	277.86	278.16	0.91
ML29	276.95	275.73	276.64	1.22
ML30	274.81	273.59	274.51	1.22
ML31	272.68	271.46	271.76	1.22
ML32	270.54	269.94	270.24	1.22
ML33	269.02	268.41	268.72	0.61
ML34	267.50	266.28	266.58	0.61
ML35	265.36	264.14	265.06	1.22
ML36	263.23	262.62	262.92	1.22
ML37	261.71	260.49	260.79	0.61
ML38	259.57	258.96	259.27	1.22
ML39	258.05	257.44	257.74	0.61
ML40	256.52	254.70	255.00	0.61
ML41	253.78	251.04	253.48	1.83
ML42	250.12	248.29	248.60	2.74
ML43	247.38	245.55	245.86	1.83
ML44	244.64	242.81	243.11	1.83
ML45	241.89	238.24	241.59	1.83
P1	335.47	333.64	335.16	1.83
P2	332.72	331.50	332.42	1.22
P3	327.54	326.32	327.24	1.22
P4	317.79	316.57	317.48	1.22
P5	304.68	303.46	304.38	1.22
P6	299.50	298.28	299.20	1.22
P7	295.23	294.01	294.93	1.22
P8	287.92	286.70	287.61	1.22
P9	283.04	281.82	282.74	1.22
P10	279.08	277.86	278.77	0.61
P11	272.68	271.46	272.37	1.22
P12	267.50	266.28	267.19	1.22
P13	261.71	260.49	261.40	1.22
P14	256.52	254.70	256.22	1.83
P15	250.12	248.29	249.82	1.83
P16	244.64	242.81	244.33	1.83

Table 4.9: Pressure Transducer Specifications

Manufacturer	Model	Pressure Range	Accuracy	Vented
Solinst®	Levelogger® Model 3001	5 psig	± 0.7 cm H_20	No
In-situ	PXD-261	100 psig	± 3.5 cm H_20	Yes
Westbay	MOSDAX® Pressure Probe	100 psig	± 7.0 cm H_20	No

Table 4.10: Lithologic designation table

Lithology Class	Color	Crystallinity	Porosity	Bioturbation	Fossils	Notes
A	yellowish grey to grey	medium-fine	medium pinpoint, trace vugs	no	trace fragments	some infilled cracks with diffusion haloes; vugs and pores have new calcite precipitation
B	light grey to grey	fine	low pinpoint, trace vugs	no	no	some large calcite crystals filling trace vugs
C	tan-yellow to grey	medium	high pinpoint, trace vugs	no	trace fragments	some reddish, some dark grey
D	tan-yellowish white to light grey	fine	low pinpoint, few vugs	no	no	
E	tan-yellow to light grey	fine-medium	medium-high pinpoint, some vugs	no	some fossils; corals and fragments	new calcite precipitation in vugs
F	light grey to grey and cream mottled	fine	medium pinpoint, some to many vugs	some	fossiliferous	fine grained calcite/dolomite cement between fossil fragments; vugs and pores have new coarser calcite precipitation
G	tan-yellowish grey to dark grey and cream mottled	medium-fine	high pinpoint, some vugs	no	many fossils; fragments; clasts	medium to fine grained calcite/dolomite cement between large fossil fragments; vugs and pores have new coarser calcite precipitation
H	light grey to dark grey and cream mottled	fine-medium	low-medium pinpoint, vuggy (large)	no	fossiliferous	fine to medium grained calcite/dolomite cement between fossils; most vugs show fresh calcite precipitation (Eramosa)
I	grey to grey and cream mottled	fine-medium	medium-high pinpoint, vuggy (small)	no	some fossils; fragments	new calcite precipitation in vugs
J	light to dark grey and cream mottled	fine-medium	low-medium pinpoint, vuggy (small)	no	fossiliferous	new calcite precipitation in vugs
K1	blue-grey	fine	low pinpoint, few vugs	no	few fossils; fragments	new calcite precipitation in vugs, some well developed, some stylolites
K2	tan blue-grey	fine	low pinpoint, some vugs	no	few fossils	come calcite/dolomite in vugs, some stylolites
K3	darker blue-grey	fine	low pinpoint, some vugs	no	many fossils, crinoids, corals and fragments	some calcite/dolomite in vugs, some stylolites
L1	blue-grey some brown mottling	very fine	low pinpoint, some vugs	no	some fossils, most are structureless clastlike	fine calcite/dolomite cement between fossils, new calcite precipitation in vugs
L2	tan-cream and blue grey mottled	very fine	very low pinpoint, few vugs	no	many small fossils and clasts	Some stylolites
M	grey to dark grey and light grey mottled	very fine	low pinpoint, many vugs (small to very large)	no	no	some very large vugs containing well developed calcite crystals; very distinct mottling at some points
N	grey to dark grey and cream mottled	fine	low-medium pinpoint, trace vugs	no	some fossils; fragments, crinoids	some fine pyrite along seams; new calcite precipitation in vugs
O	dark grey to red	fine	low pinpoint, trace vugs	no	no	some interbedded limestone/dolostone has vugs

Table 4.11: Summary of physical properties based on lithology

Lithologic Unit	No. of Samples	Mean Dry Bulk Density (g/cm^3)	Mean Wet Bulk Density (g/cm^3)	Mean Particle Density (g/cm^3)	Mean Porosity (%)
A	8	2.72	2.77	2.87	5.2
B	14	2.71	2.76	2.84	4.5
C	33	2.48	2.61	2.86	13.2
D	21	2.62	2.70	2.85	8.1
E	38	2.54	2.65	2.86	11.1
F	23	2.49	2.61	2.85	12.6
G	6	2.40	2.56	2.86	16.0
H	15	2.49	2.61	2.83	12.2
I	9	2.57	2.68	2.87	10.3
J	19	2.48	2.61	2.86	13.2
K1	6	2.73	2.77	2.85	4.3
K2	14	2.68	2.74	2.85	5.8
K3	6	2.70	2.75	2.86	5.4
L1	5	2.70	2.75	2.85	5.1
L2	6	2.64	2.72	2.88	8.1
M	5	2.57	2.67	2.86	10.1
N	17	2.72	2.77	2.87	5.1
O*	9	2.65	2.71	2.77	2.9
All Samples	254*	2.58	2.67	2.85	9.6

*Transition zone to shale. Some of these samples degraded during imbibition

Table 4.12: Laboratory determined dry bulk density statistics by lithology

Lithologic Unit	N	Arithmetic Mean (g/cm^3)	Standard Deviation (g/cm^3)	Minimum (g/cm^3)	Maximum (g/cm^3)
A	8	2.72	0.06	2.62	2.79
B	14	2.71	0.06	2.63	2.81
C	33	2.48	0.09	2.30	2.67
D	21	2.62	0.05	2.55	2.71
E	38	2.54	0.07	2.33	2.68
F	23	2.49	0.08	2.31	2.64
G	6	2.40	0.08	2.32	2.50
H	15	2.49	0.12	2.22	2.68
I	9	2.57	0.07	2.45	2.68
J	19	2.48	0.07	2.29	2.60
K1	6	2.73	0.03	2.71	2.78
K2	14	2.68	0.05	2.56	2.75
K3	6	2.70	0.05	2.63	2.76
L1	5	2.70	0.02	2.68	2.72
L2	6	2.64	0.06	2.56	2.73
M	5	2.57	0.12	2.39	2.71
N	17	2.72	0.05	2.64	2.81
O	9	2.65	0.12	2.52	2.87
All Dolostone	246	2.57	0.12	2.22	2.87
All Other	8	2.63	0.10	2.52	2.77

Table 4.13: Laboratory determined wet bulk density statistics by lithology.

Lithologic Unit	N	Arithmetic Mean (g/cm³)	Standard Deviation (g/cm³)	Minimum (g/cm³)	Maximum (g/cm³)
A	8	2.77	0.04	2.69	2.82
B	14	2.76	0.04	2.72	2.82
C	33	2.61	0.06	2.49	2.73
D	21	2.70	0.04	2.65	2.76
E	38	2.65	0.05	2.50	2.74
F	23	2.61	0.05	2.49	2.71
G	6	2.56	0.05	2.51	2.63
H	15	2.61	0.08	2.43	2.74
I	9	2.68	0.05	2.60	2.73
J	19	2.61	0.05	2.48	2.70
K1	6	2.77	0.02	2.76	2.82
K2	14	2.74	0.03	2.66	2.79
K3	6	2.75	0.03	2.70	2.80
L1	5	2.75	0.01	2.74	2.76
L2	6	2.72	0.04	2.66	2.78
M	5	2.67	0.08	2.56	2.76
N	17	2.77	0.03	2.73	2.84
O	7	2.71	0.10	2.57	2.89
All Dolostone	246	2.67	0.08	2.43	2.89
All Other	6	2.69	0.08	2.57	2.79

Table 4.14: Laboratory determined particle density statistics by lithology.

Lithologic Unit	N	Arithmetic Mean (g/cm³)	Standard Deviation (g/cm³)	Minimum (g/cm³)	Maximum (g/cm³)
A	8	2.87	0.03	2.83	2.90
B	14	2.84	0.03	2.78	2.88
C	33	2.86	0.03	2.74	2.90
D	21	2.85	0.03	2.80	2.89
E	38	2.86	0.02	2.80	2.90
F	23	2.85	0.03	2.78	2.90
G	6	2.86	0.02	2.83	2.88
H	15	2.83	0.02	2.80	2.85
I	9	2.87	0.03	2.82	2.91
J	19	2.86	0.03	2.79	2.90
K1	6	2.85	0.02	2.83	2.90
K2	14	2.85	0.02	2.80	2.87
K3	6	2.86	0.02	2.84	2.88
L1	5	2.85	0.01	2.84	2.86
L2	6	2.88	0.02	2.85	2.92
M	5	2.86	0.02	2.85	2.88
N	17	2.87	0.03	2.83	2.93
O	7	2.77	0.08	2.67	2.93
All Dolostone	246	2.85	0.03	2.74	2.93
All Other	6	2.76	0.06	2.67	2.84

Table 4.15: Laboratory determined porosity statistics by lithology

Lithologic Unit	N	Arithmetic Mean (%)	Standard Deviation (%)	Minimum (%)	Maximum (%)
A	8	5.2	1.4	3.4	7.4
B	14	4.5	2.5	1.2	8.6
C	33	13.2	3.4	5.8	19.6
D	21	8.1	1.6	5.5	11.3
E	38	11.1	2.6	6.5	17.6
F	23	12.6	3.1	6.2	17.5
G	6	16.0	2.5	12.8	19.0
H	15	12.2	3.8	5.9	20.9
I	9	10.3	2.9	5.0	15.1
J	19	13.2	2.7	9.5	19.3
K1	6	4.3	0.6	3.5	5.1
K2	14	5.8	1.9	3.6	9.9
K3	6	5.4	1.5	3.8	7.1
L1	5	5.1	0.7	4.4	6.0
L2	6	8.1	2.0	4.9	10.1
M	5	10.1	4.5	4.6	16.4
N	17	5.1	2.1	1.9	9.1
O	7	2.9	1.4	1.4	5.2
All Dolostone	246	9.8	4.3	1.2	20.9
All Other	6	5.2	1.3	1.4	5.2

Table 4.16: Porosity-Air permeability comparison

WellID	Elevation Top (masl)	Elevation Bottom (masl)	Porosity	Permeabiltiy (mDarcy)
MW-13	333.20	333.07	4.00	3.00E-03
MW-21I	324.93	324.17	8.00	2.80E-01
MW-21I	329.35	329.15	16.36	1.87E+00
MW-22	336.54	336.45	7.38	1.60E+00
MW-23	334.81	334.71	1.20	3.00E-03
MW-23	328.76	328.68	5.79	8.30E-01
MW-23	320.16	320.05	7.70	2.15E-01
MW-23	317.46	317.40	12.05	3.14E+00
MW-23	302.10	301.96	6.20	1.10E-01
MW-26	333.04	332.91	10.67	3.77E+01
MW-26	328.85	328.66	12.60	1.02E+01
MW-26	319.34	319.21	6.79	4.37E-01
MW-26	303.19	303.04	7.53	1.24E+00
MW-367-3I	329.68	329.52	7.37	9.11E-01
MW-367-3I	322.90	322.74	7.00	2.75E-01
MW-367-4	307.38	307.28	8.58	3.81E-01
MW-367-4	318.47	318.36	6.75	4.40E-01
MW-367-4	326.90	326.78	8.62	5.21E+00
MW-367-5	323.71	323.64	8.21	2.99E-01
MW-367-5	331.45	331.36	11.82	1.14E+00
MW-367-7	326.85	326.65	8.55	2.13E-01
MW-367-7	321.16	320.94	7.51	5.30E-02
MW-367-7	318.18	317.98	9.45	5.30E-01
MW-367-7	314.27	314.09	17.55	2.80E+01
MW-367-7	313.99	313.93	9.33	9.81E-01
MW-367-8	330.32	330.13	12.81	8.55E+00
TH-1B	334.24	334.01	4.25	3.00E-03

Table 4.17: Stratigraphic unit descriptions

Unit	Description
G_U1	Fine grained, low matrix porosity, light grey/brown, **dolostone,** trace fossils, trace vugs, few stylolites, highly fractured zone in contact with the overburden
G_U2	Fine-medium grained, medium matrix porosity, light grey **dolostone** with spotted appearance, trace fossils, trace vugs, many stylolites
G_U3	Fine grained, medium matrix porosity, grey **dolostone,** some fossils, some vugs with calcite, some stylolites
G_U4	Fine-medium grained, high matrix porosity, grey **dolostone** with dark grey banding, high matrix porosity, many fossils, many vugs, clasts, few stylolites
E_U1	Fine grained, dark grey to grey bituminous **dolostone,** very many fossils, many vugs, many stylolites (Eramosa)
A_U1	Fine grained, medium matrix porosity, mottled white-blue **dolostone,** fossiliferious (crinoid rich), many vugs, many stylolites, few fractures
A_U2	Fine-very fine grained, medium-high matrix porosity, white blue-dark grey mottled **dolostone,** many vugs, many fossils (zones of crinoids), variable stylolite spacing, many fractures, intesely fractured zones, fewer fractures and decreased porosity near the shale interface
S_U1	Very fine grained, very low visible matrix porosity, green, grey and red **shale,** trace fossils, no vugs, no stylolites, intense horizontal fracturing

Table 4.18: Analyte qualifier data

Well	Qualifier	Number of Samples
TCE		
MW-22	Quantifiable Detect	107
MW-22	Non-Quantifiable Detect	91
MW-22	Non-Detect	138
MW-23	Quantifiable Detect	13
MW-23	Non-Quantifiable Detect	21
MW-23	Non-Detect	98
MW-26	Quantifiable Detect	144
MW-26	Non-Quantifiable Detect	3
MW-26	Blank Interference	109
MW-367-4	Quantifiable Detect	43
MW-367-4	Non-Quantifiable Detect	86
MW-367-4	Non-Detect	1
MW-367-5	Quantifiable Detect	55
MW-367-5	Non-Quantifiable Detect	47
MW-367-7	Quantifiable Detect	111
MW-367-7	Non-Quantifiable Detect	51
MW-367-7	Blank Interference	55
MW-367-8	Quantifiable Detect	200
MW-367-8	Non-Quantifiable Detect	16
MW-367-8	Non-Detect	1
MW-367-8	Blank Interference	16
MW-367-9	Quantifiable Detect	205
MW-367-9	Non-Quantifiable Detect	33
MW-367-9	Non-Detect	154
MW-367-9	Blank Interference	39
c-DCE		
MW-22	Non-Detect	140
MW-26	Non-Detect	256
MW-367-7	Non-Quantifiable Detect	65
MW-367-7	Non-Detect	149
MW-367-8	Non-Quantifiable Detect	7
MW-367-8	Non-Detect	126
MW-367-9	Quantifiable Detect	11
MW-367-9	Non-Quantifiable Detect	32
MW-367-9	Non-Detect	160
MW-367-9	Blank Interference	9

Well	Qualifier	Number of Samples
PCE		
MW-22	Quantifiable Detect	13
MW-22	Non-Quantifiable Detect	69
MW-22	Non-Detect	174
MW-22	Blank Interference	78
MW-23	Quantifiable Detect	6
MW-23	Non-Quantifiable Detect	76
MW-23	Non-Detect	50
MW-26	Non-Quantifiable Detect	137
MW-26	Non-Detect	87
MW-26	Blank Interference	32
MW-367-4	Quantifiable Detect	4
MW-367-4	Non-Quantifiable Detect	83
MW-367-4	Non-Detect	40
MW-367-5	Quantifiable Detect	1
MW-367-5	Non-Detect	76
MW-367-5	Blank Interference	22
MW-367-7	Non-Quantifiable Detect	193
MW-367-7	Non-Detect	24
MW-367-8	Non-Quantifiable Detect	139
MW-367-8	Non-Detect	82
MW-367-8	Blank Interference	13
MW-367-9	Quantifiable Detect	5
MW-367-9	Non-Quantifiable Detect	173
MW-367-9	Non-Detect	203
MW-367-9	Blank Interference	51
t-DCE		
MW-22	Non-Detect	336
MW-23	Non-Detect	132
MW-26	Non-Detect	256
MW-367-4	Non-Detect	130
MW-367-5	Non-Detect	102
MW-367-7	Non-Detect	217
MW-367-8	Non-Detect	228
MW-367-9	Non-Detect	431

Table continued on next page

Well	Qualifier	Number of Samples
1,1-DCE		
MW-22	Non-Detect	99
MW-367-9	Non-Detect	36
CT		
MW-22	Quantifiable Detect	1
MW-22	Non-Detect	32
MW-22	Blank Interference	218
MW-367-9	Non-Quantifiable Detect	1
MW-367-9	Non-Detect	88
MW-367-9	Blank Interference	101
CF		
MW-22	Non-Detect	203
MW-22	Blank Interference	1
MW-26	Non-Quantifiable Detect	50
MW-26	Non-Detect	133
MW-26	Blank Interference	73
MW-367-7	Quantifiable Detect	7
MW-367-7	Non-Quantifiable Detect	142
MW-367-7	Non-Detect	6
MW-367-7	Blank Interference	43
MW-367-8	Quantifiable Detect	8
MW-367-8	Non-Quantifiable Detect	127
MW-367-8	Non-Detect	17
MW-367-9	Quantifiable Detect	58
MW-367-9	Non-Quantifiable Detect	139
MW-367-9	Non-Detect	85
MW-367-9	Blank Interference	6

Well	Qualifier	Number of Samples
1,1,1-TCA		
MW-22	Non-Quantifiable Detect	2
MW-22	Non-Detect	332
MW-23	Non-Detect	130
MW-26	Non-Detect	256
MW-367-4	Non-Quantifiable Detect	1
MW-367-4	Non-Detect	122
MW-367-5	Non-Quantifiable Detect	3
MW-367-5	Non-Detect	90
MW-367-7	Non-Quantifiable Detect	3
MW-367-7	Non-Detect	213
MW-367-8	Non-Detect	221
MW-367-9	Quantifiable Detect	7
MW-367-9	Non-Quantifiable Detect	8
MW-367-9	Non-Detect	417
CFC-113		
MW-22	Quantifiable Detect	1
MW-22	Non-Quantifiable Detect	43
MW-22	Non-Detect	263
MW-23	Non-Detect	132
MW-26	Quantifiable Detect	3
MW-26	Non-Quantifiable Detect	5
MW-26	Non-Detect	248
MW-367-4	Non-Detect	129
MW-367-5	Non-Detect	83
MW-367-7	Non-Quantifiable Detect	1
MW-367-7	Non-Detect	212
MW-367-8	Non-Detect	217
MW-367-9	Non-Quantifiable Detect	3
MW-367-9	Non-Detect	346

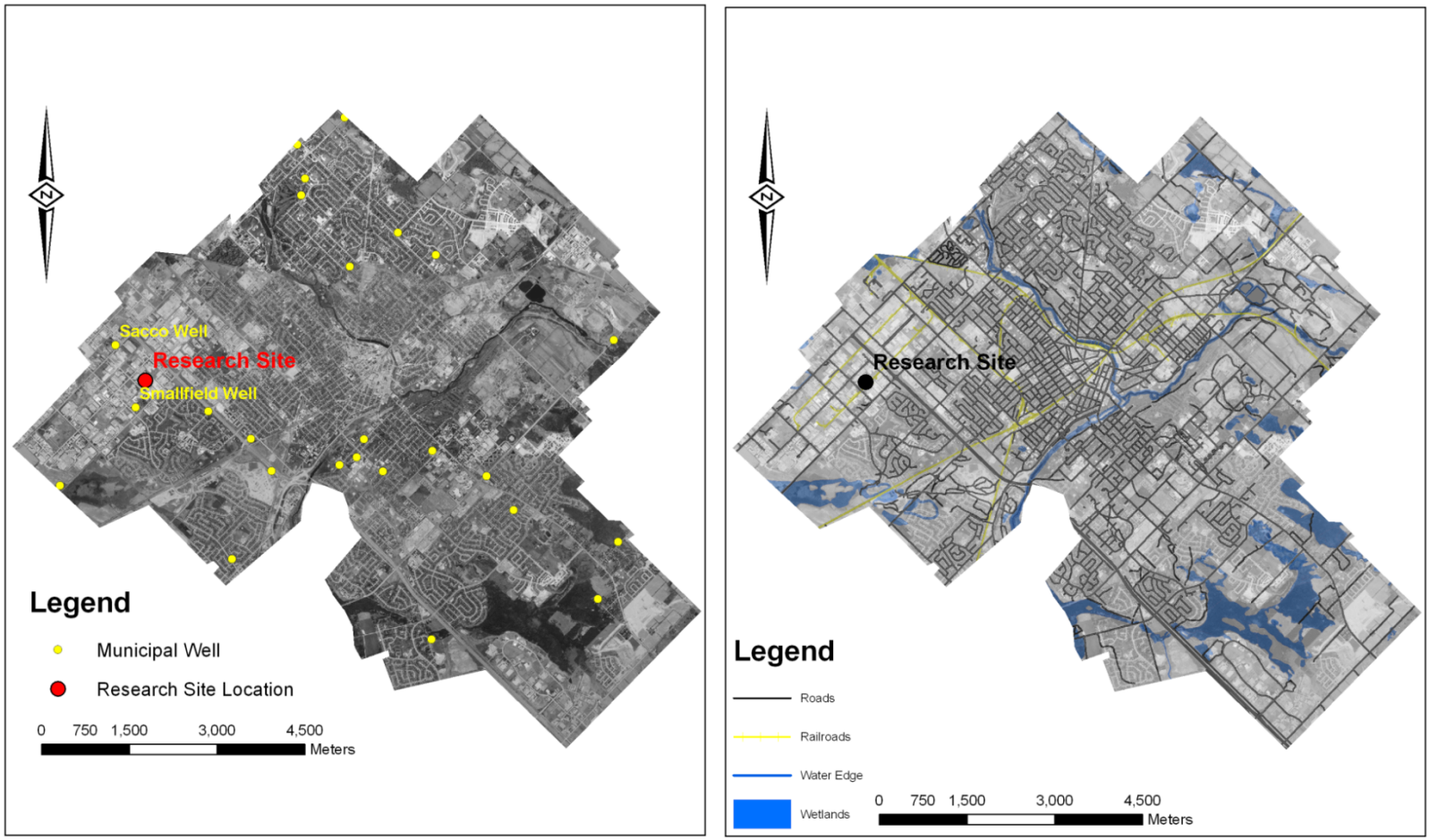

Figure 4.1: Location of municipal pumping wells in Guelph in relation to the research site (A). City of Guelph map showing surface water, roads, and railroads (B) (data from Grand River Conservation Authority 2006).

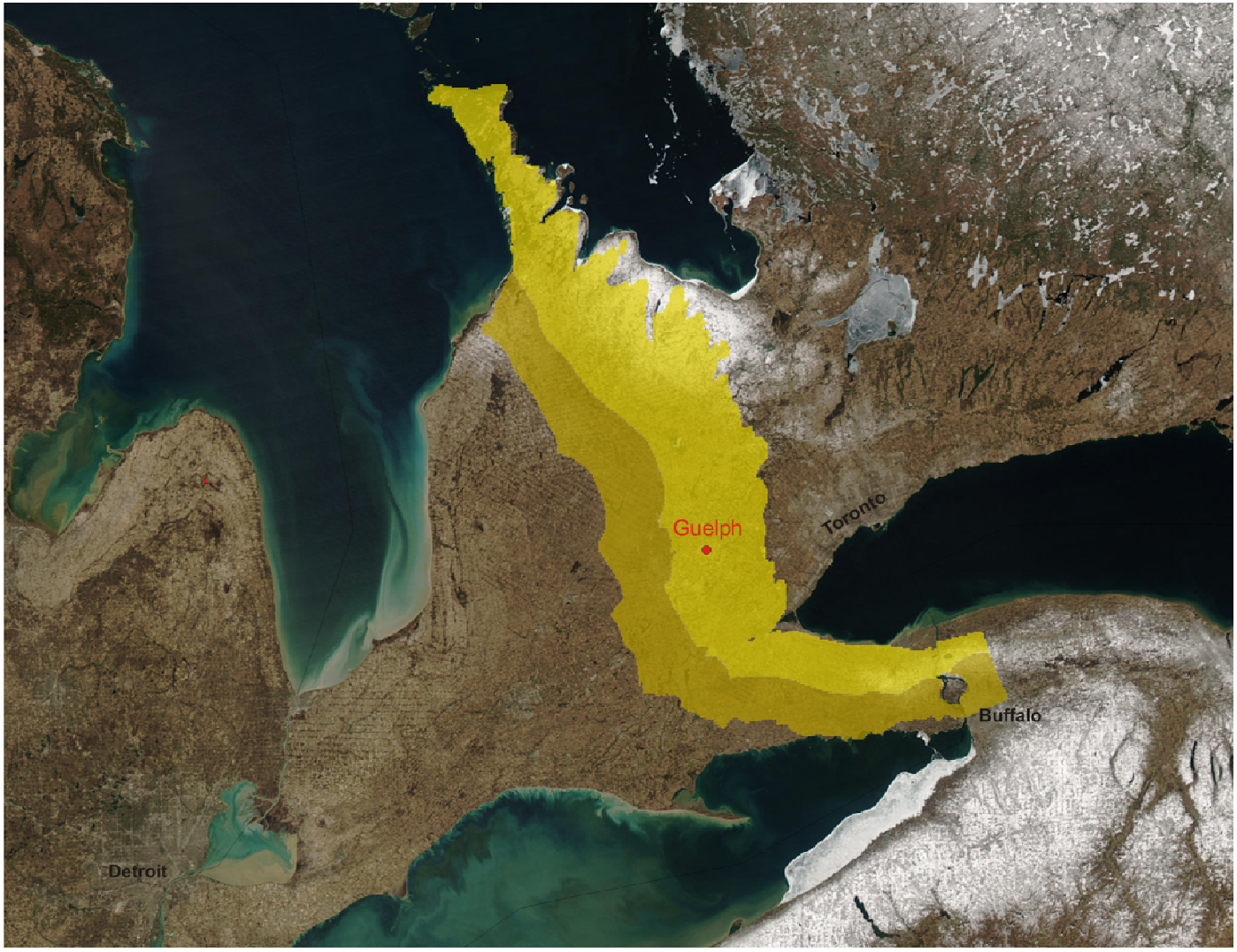

Figure 4.2: Silurian dolostone outcrop and subcrop belt running from Niagara peninsula to the Bruce peninsula. The darker yellow band refers to the upper Silurian rocks and the lighter yellow band is the middle and lower Silurian rocks (air photo from NASA 2007;Resident Geologist Program 2004).

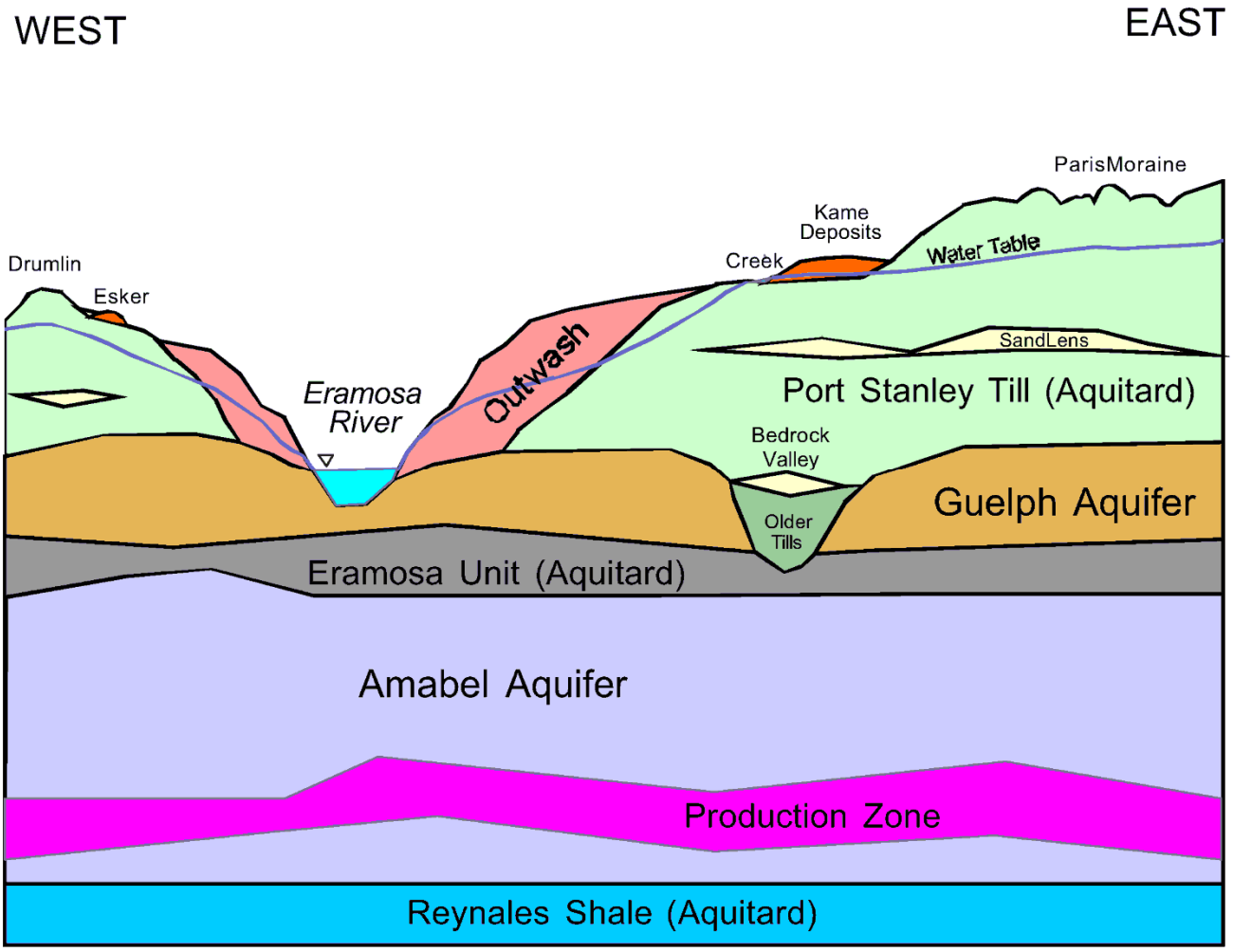

Figure 4.3: Conceptual stratigraphic units for the city of Guelph showing the classification of the Eramosa member as an aquitard (taken from Gartner Lee Limited 2004).

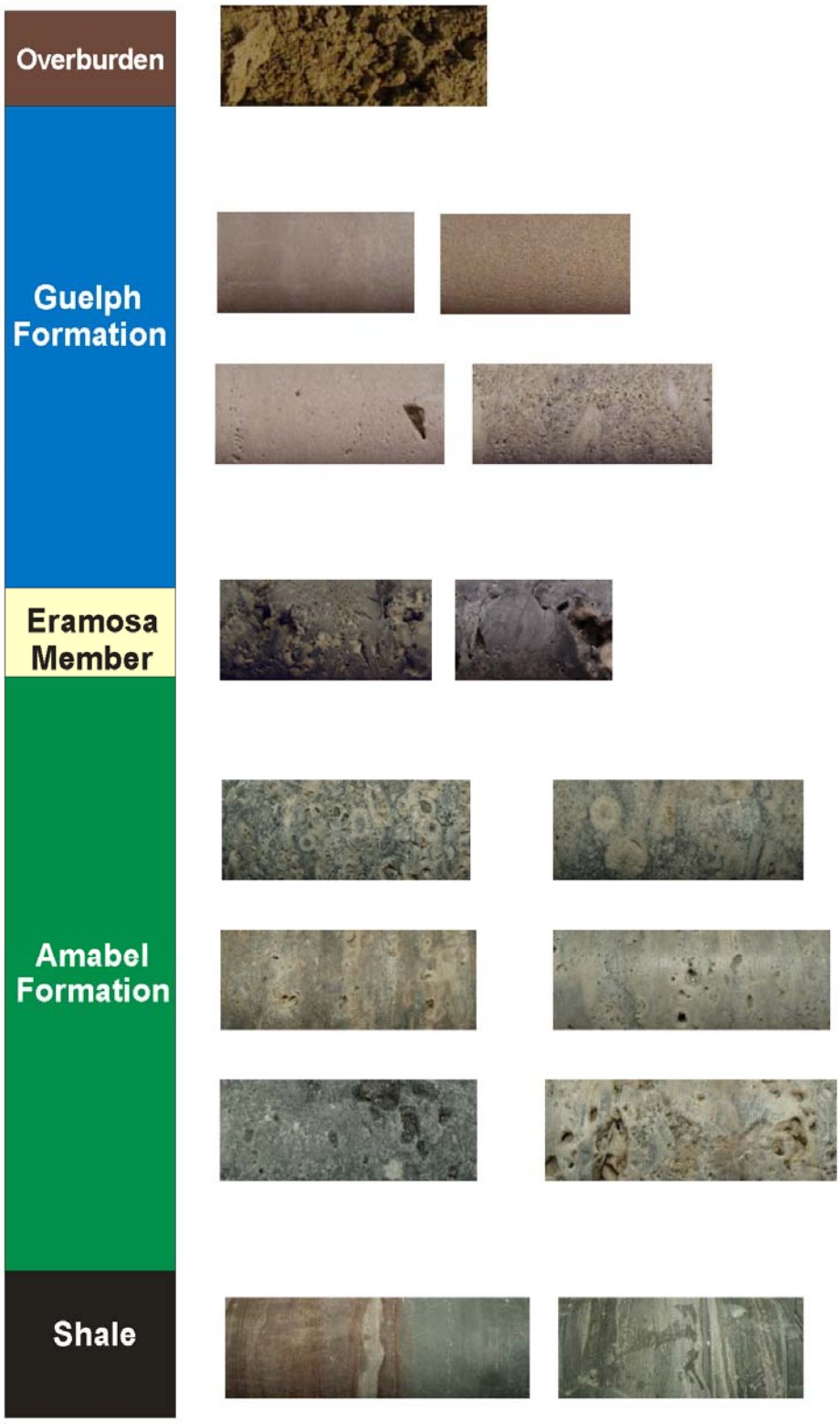

Figure 4.4: Simplified stratigraphic column with example lithologies from rock core.

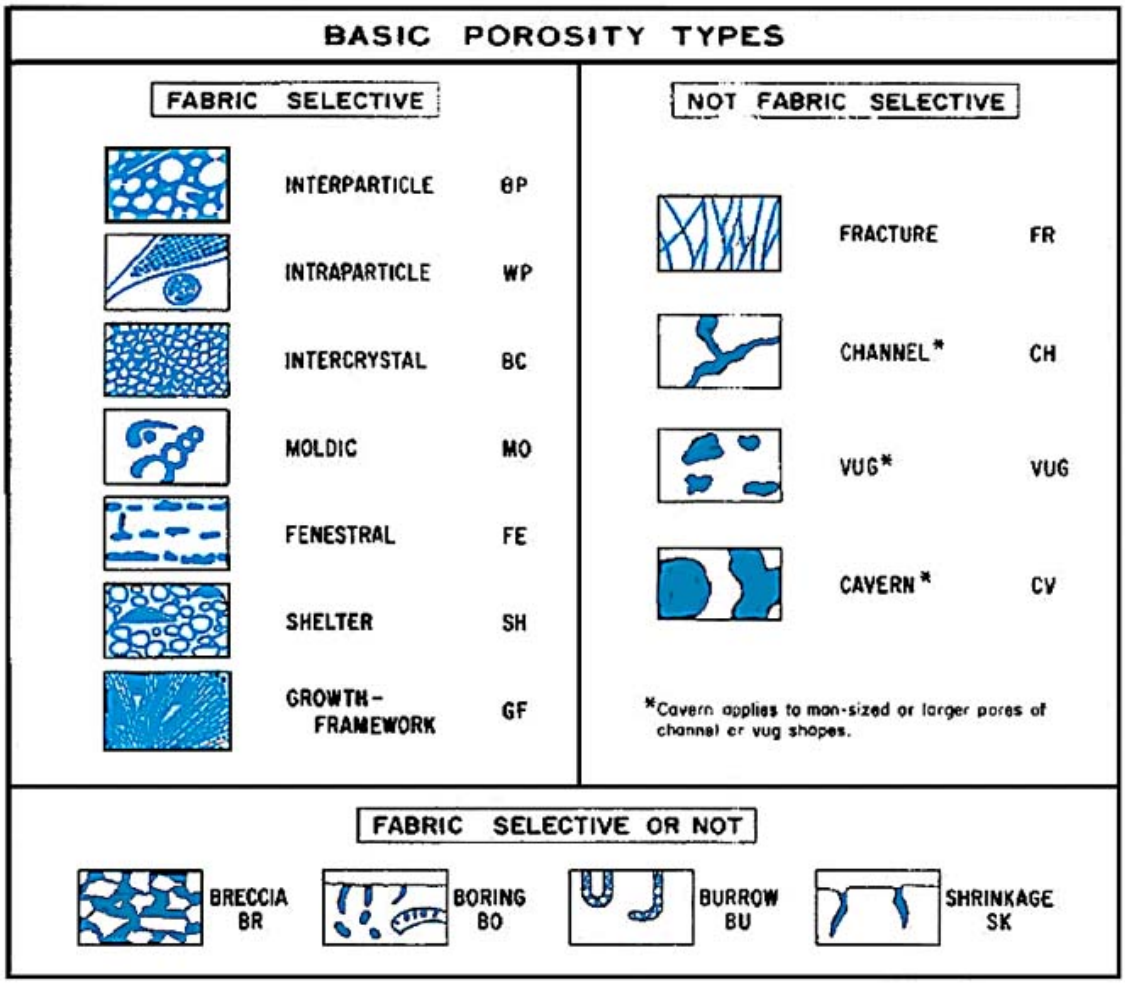

Figure 4.5: Porosity types (taken from Choquett & Pray 1970).

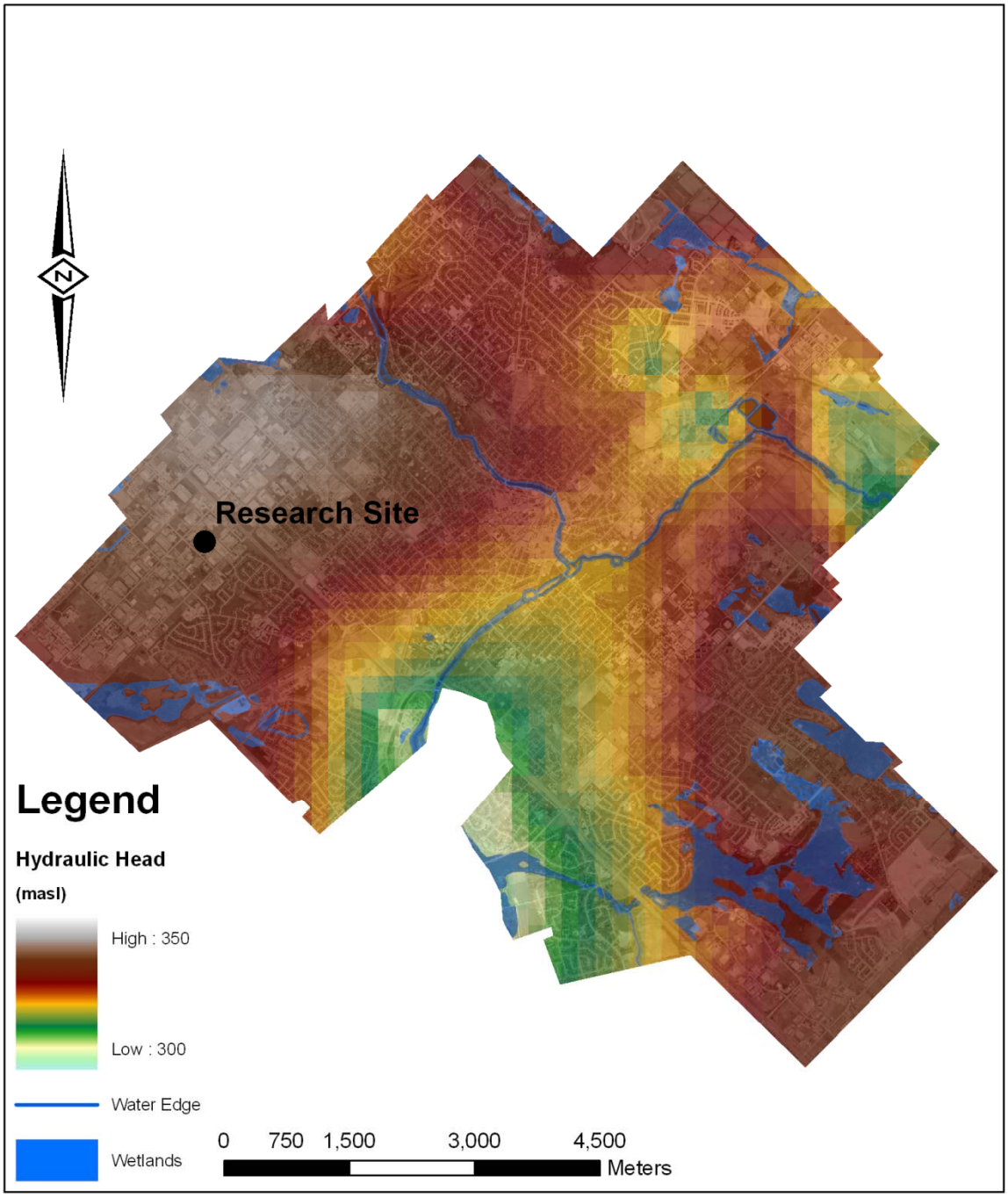

Figure 4.6: Shallow ground water levels for the City of Guelph indicating groundwater flow to the south east from the research site (Data from Grand River Conservation Authority 2006).

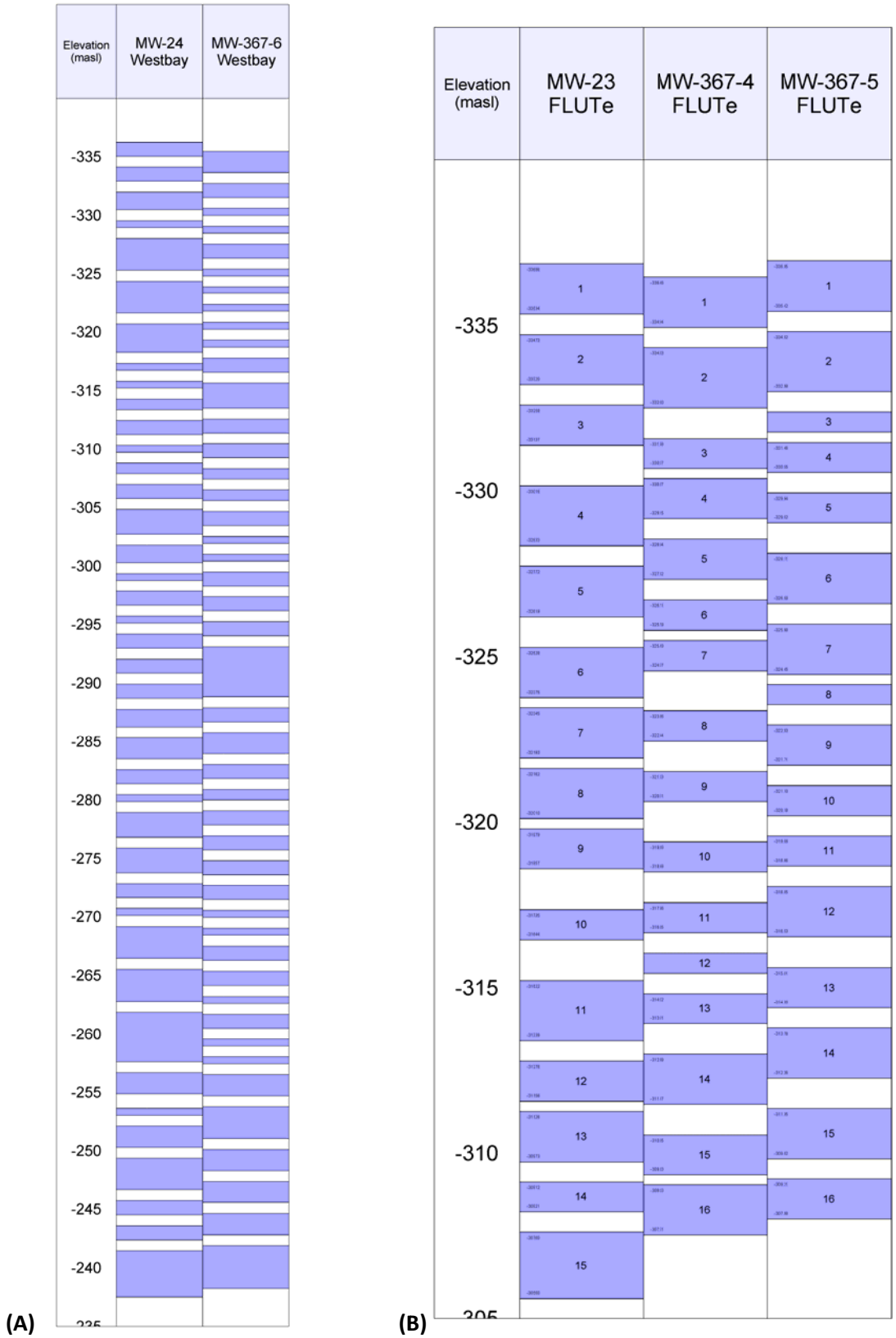

Figure 4.7: Multilevel monitoring well designs (A) Westbay Systems, (B) Water FLUTe™

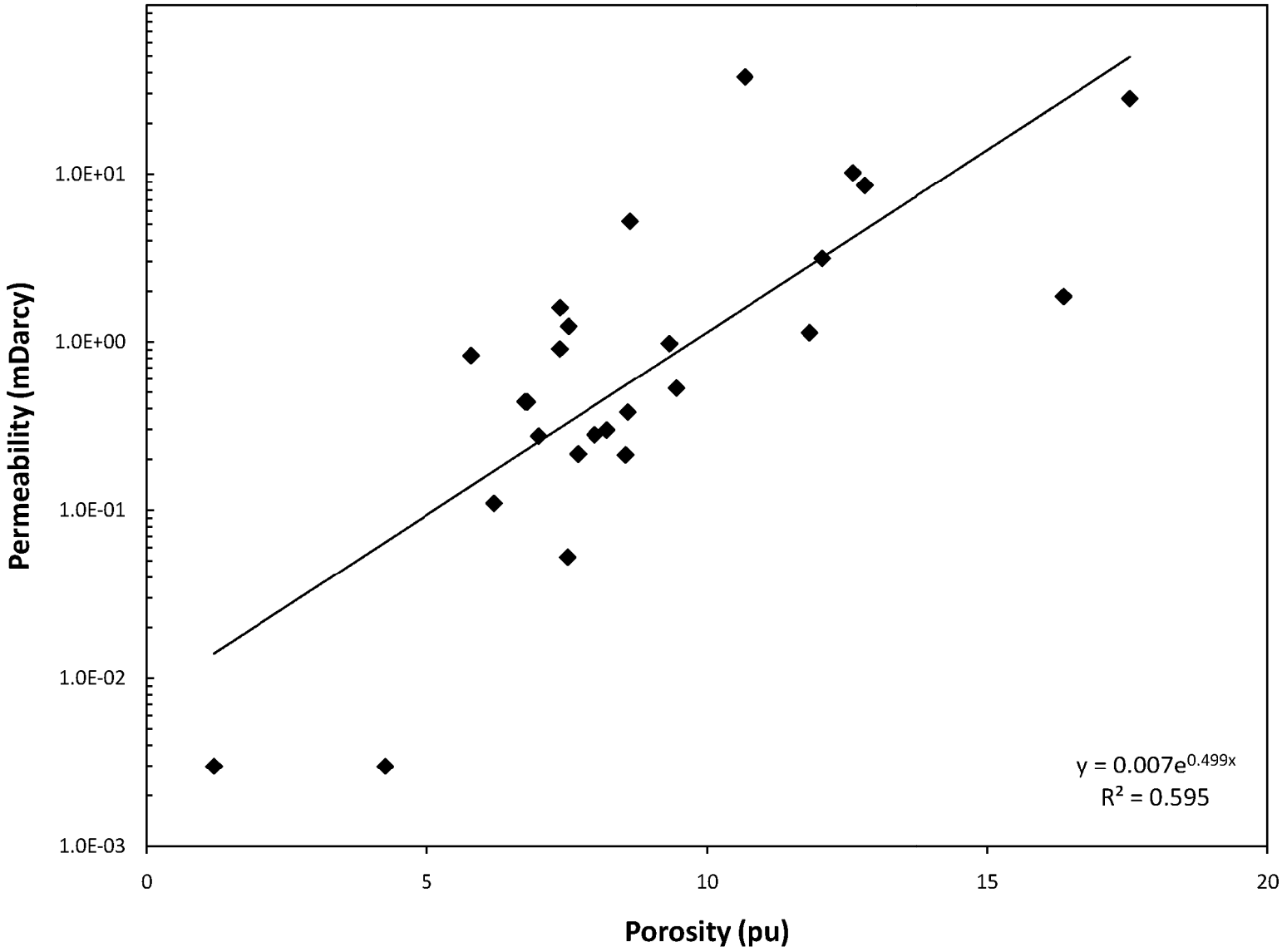

Figure 4.8: Porosity-Air permeability relationship for the Guelph formation. NOTE: Semi-log plot.

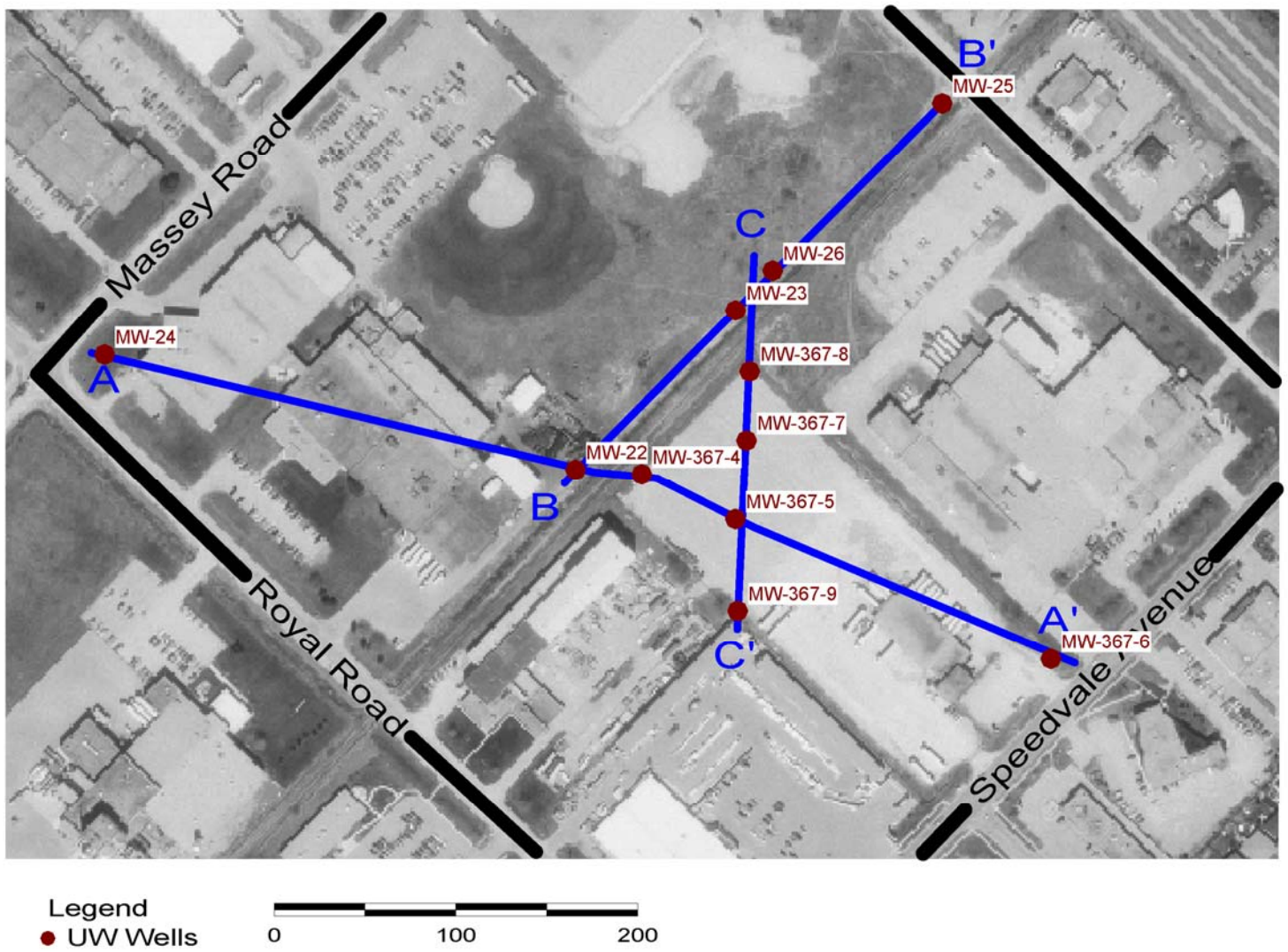

Figure 4.9: Areal site view showing the three cross sections for this study (A-A', B-B', and C-C').

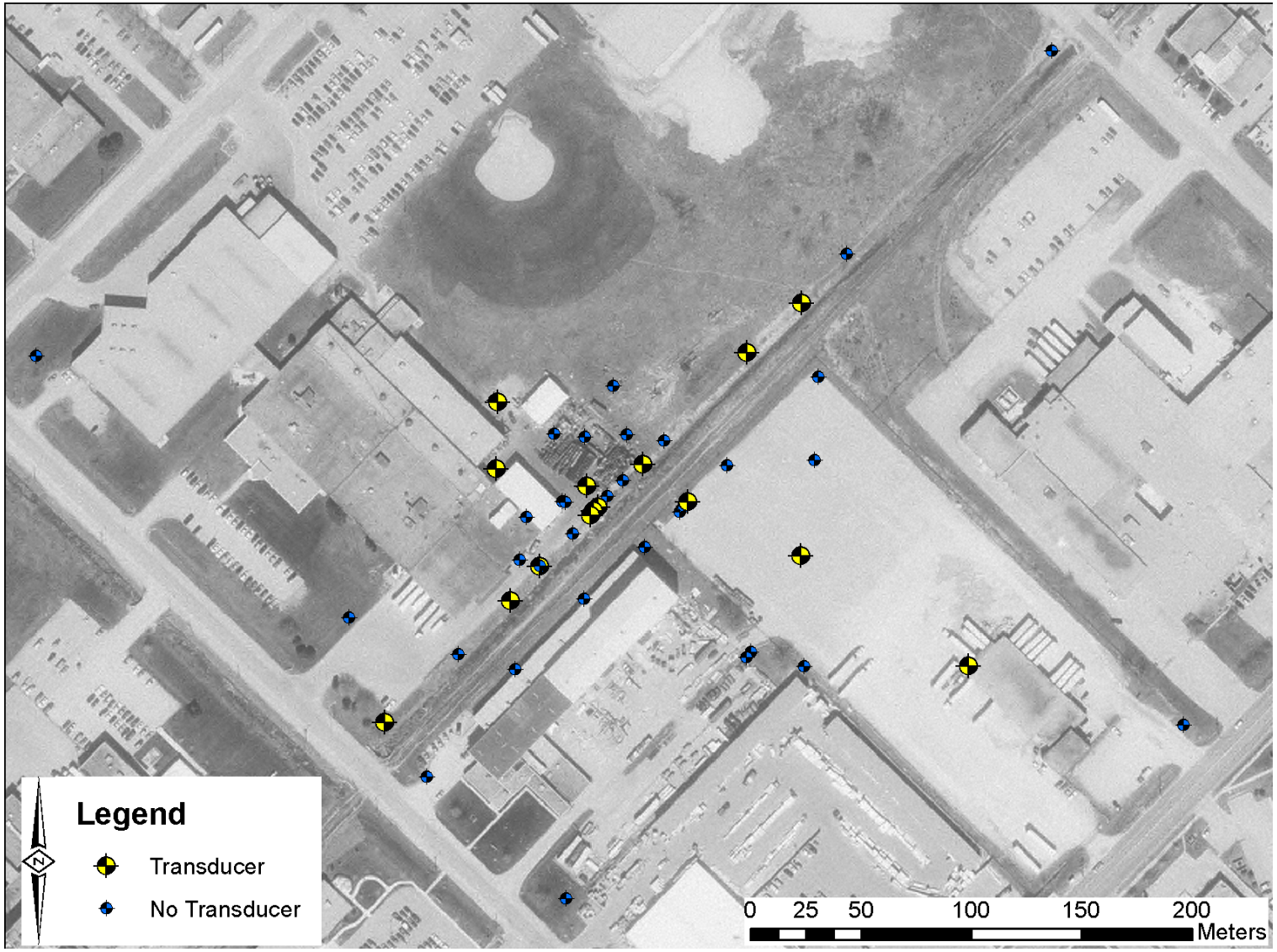

Figure 4.10: Areal site view showing monitoring wells containing dedicated transducers and those not containing transducers.

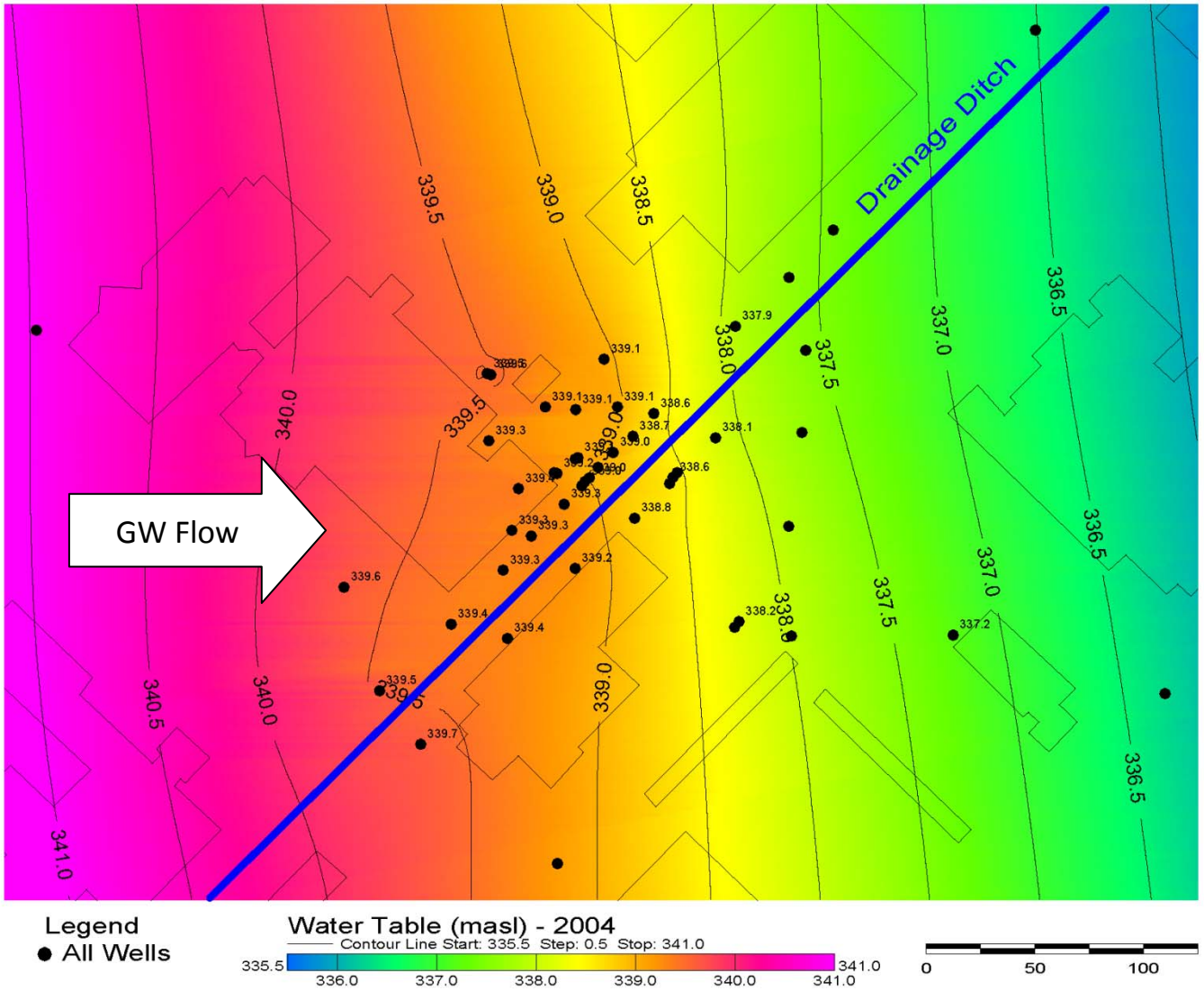

Figure 4.11: Kriged shallow hydraulic heads from 28-5-2004 and inferred flow direction. Groundwater flow is generally to the east. Note the inflection in the contours near the drainage ditch.

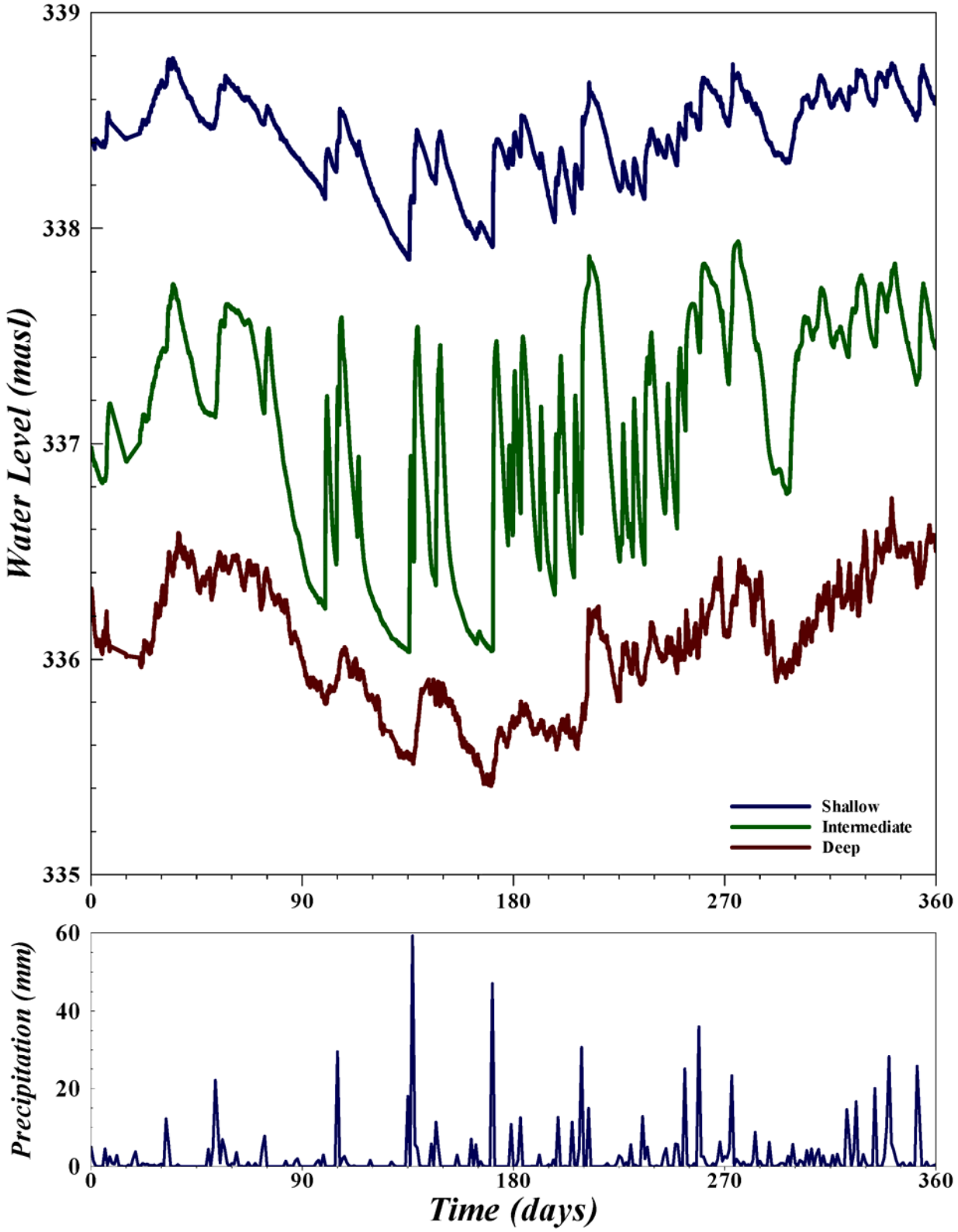

Figure 4.12: Three types of hydrographs found in the Guelph formation at this site (approximately 1 year of data [01-03-05 to 24-02-06]).

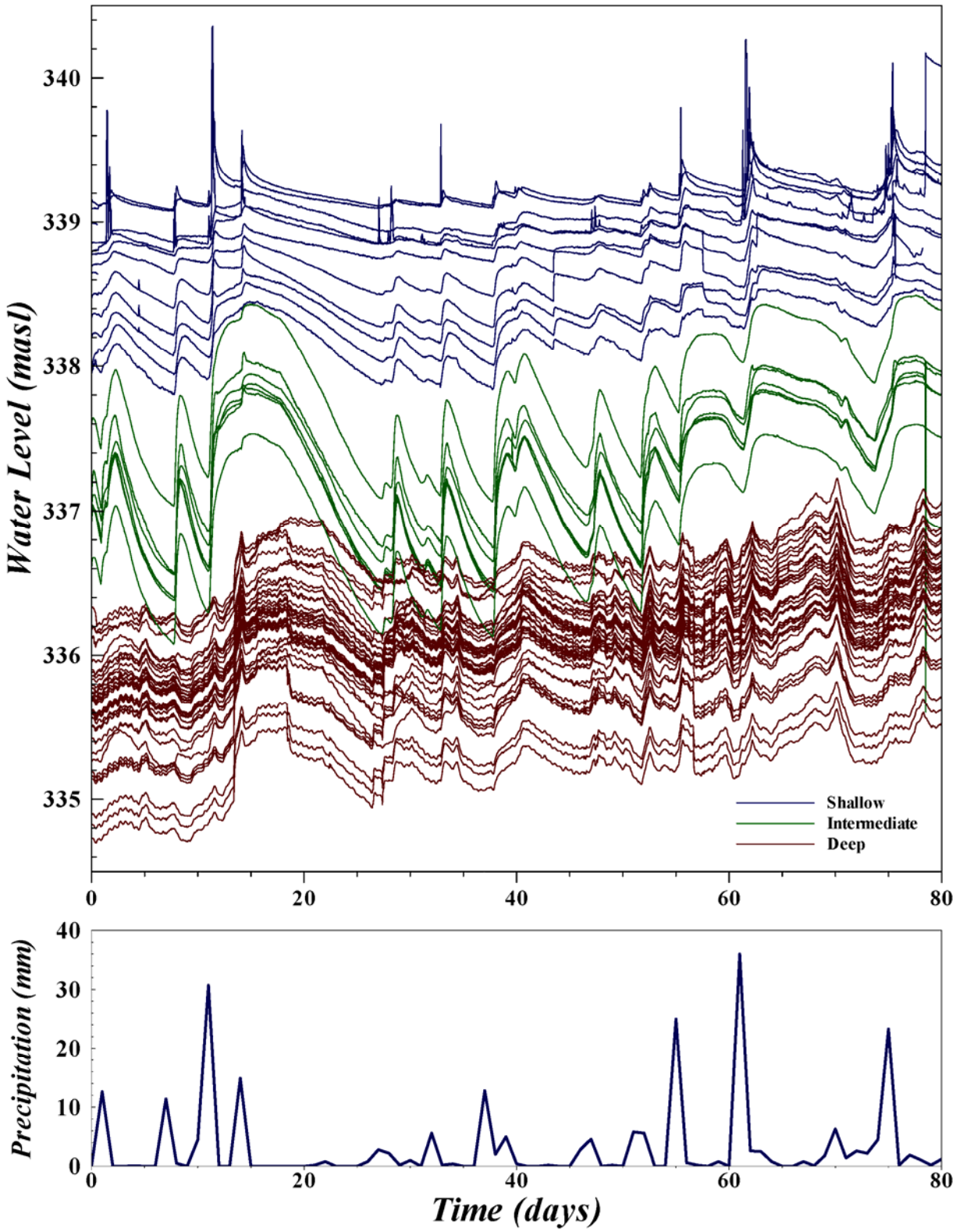

Figure 4.13**: Consistency of the three hydrograph types. Some of the shallow zones show sharp peaks caused by rain events (80 days of data [15-09-05 to 04-12-05]).**

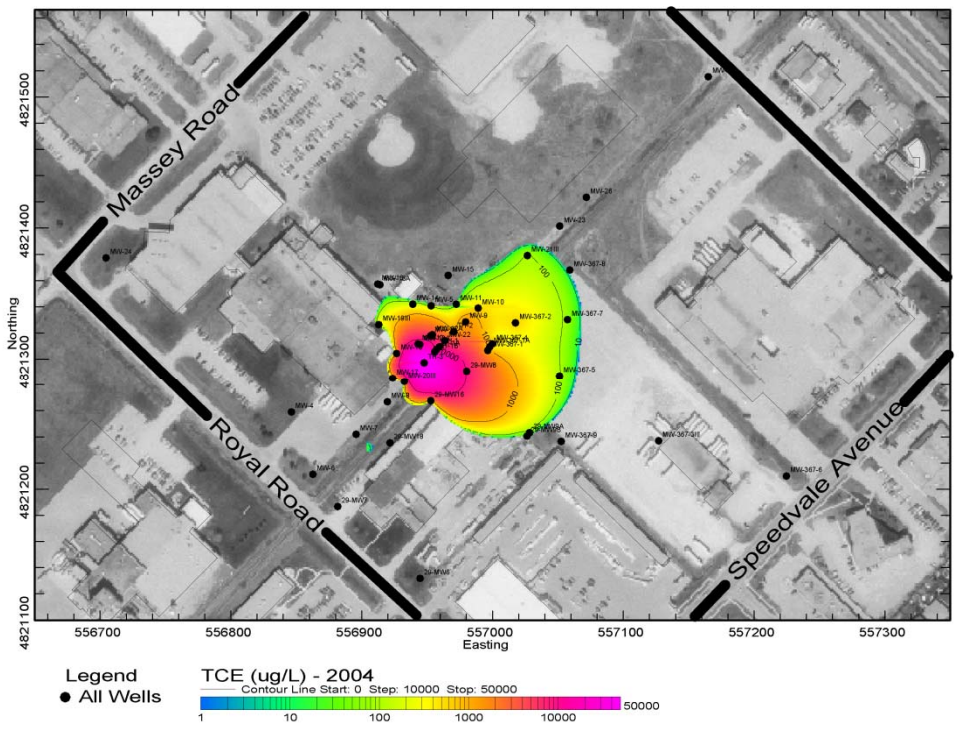

(A)

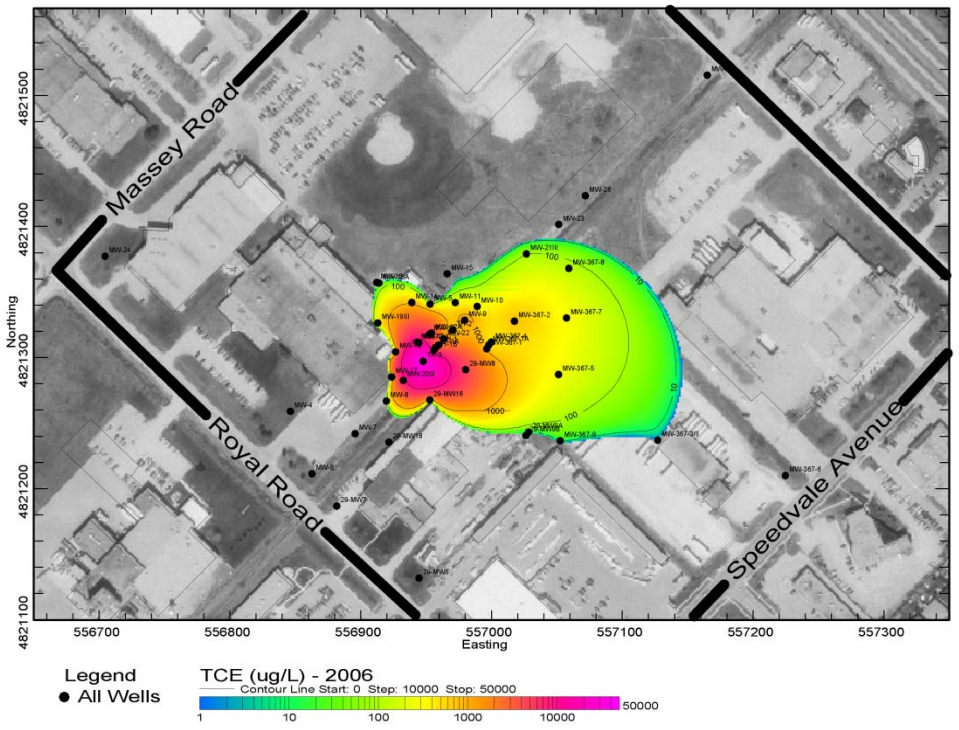

(B)

Figure 4.14: Increasing lateral extent of TCE plume. Kriged TCE groundwater concentrations for 2004 (A). Kriged TCE groundwater concentrations for 2006 (B).

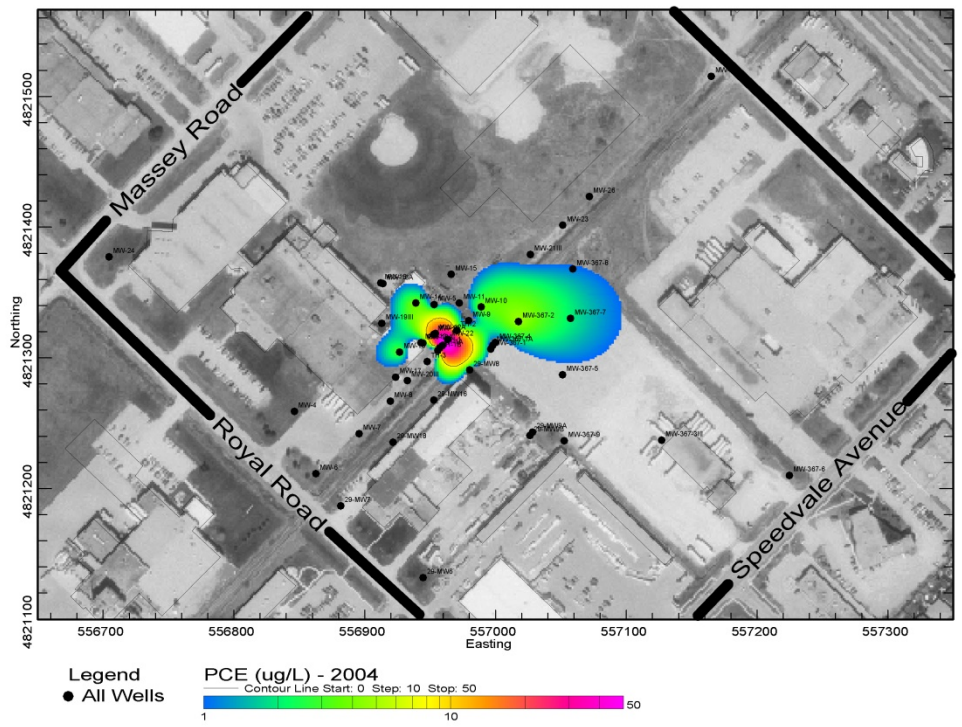

(A)

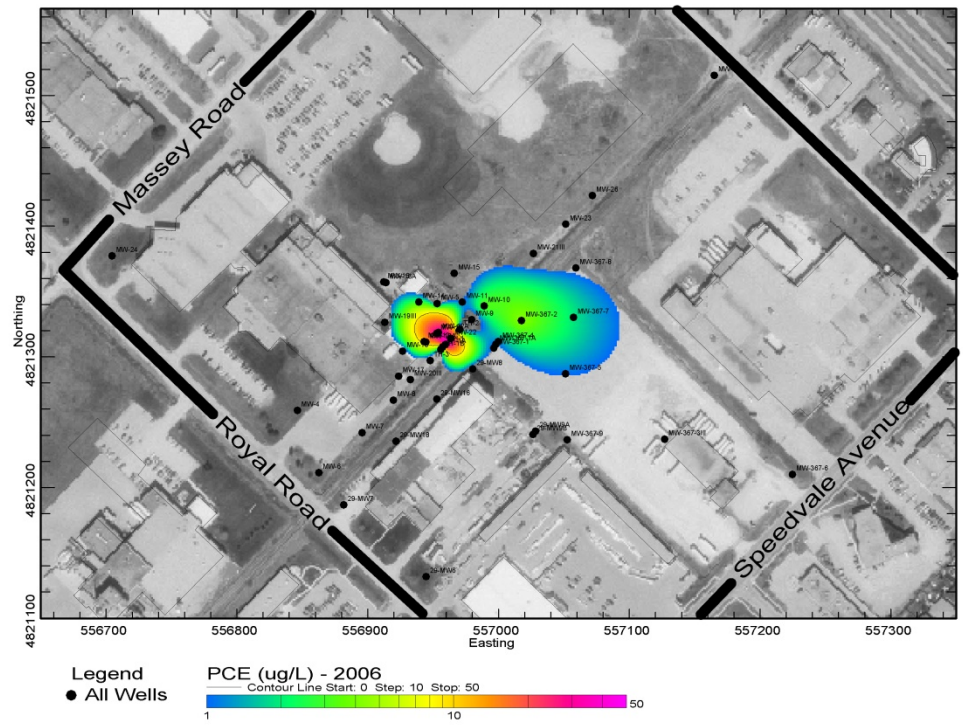

(B)

Figure 4.15: Relatively constant PCE plume. Kriged PCE groundwater concentrations for 2004 (A). Kriged PCE groundwater concentrations for 2006 (B).

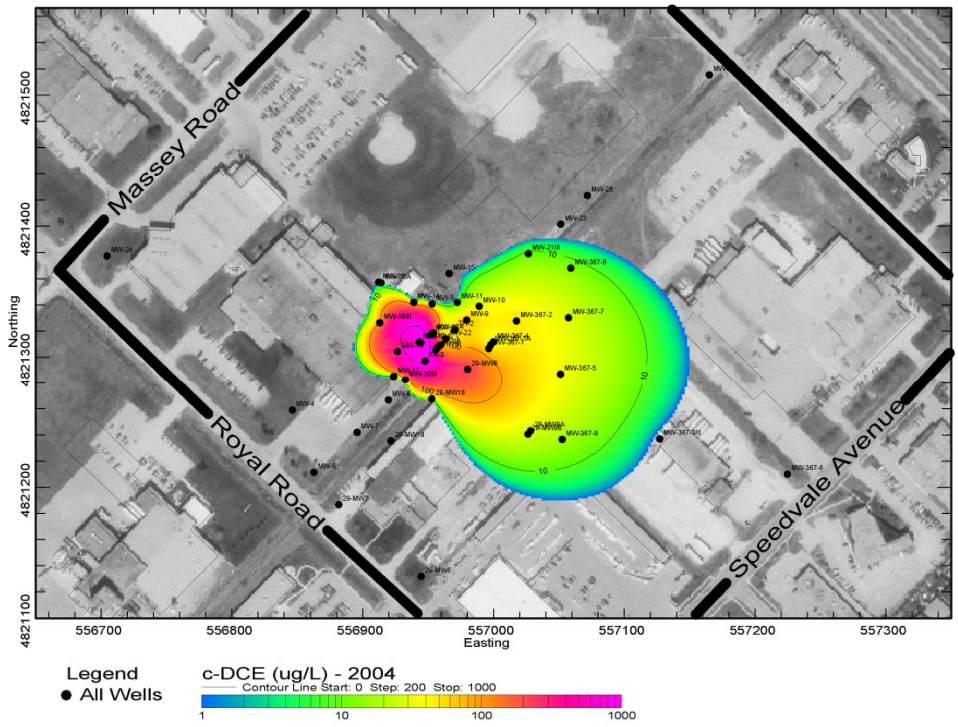

(A)

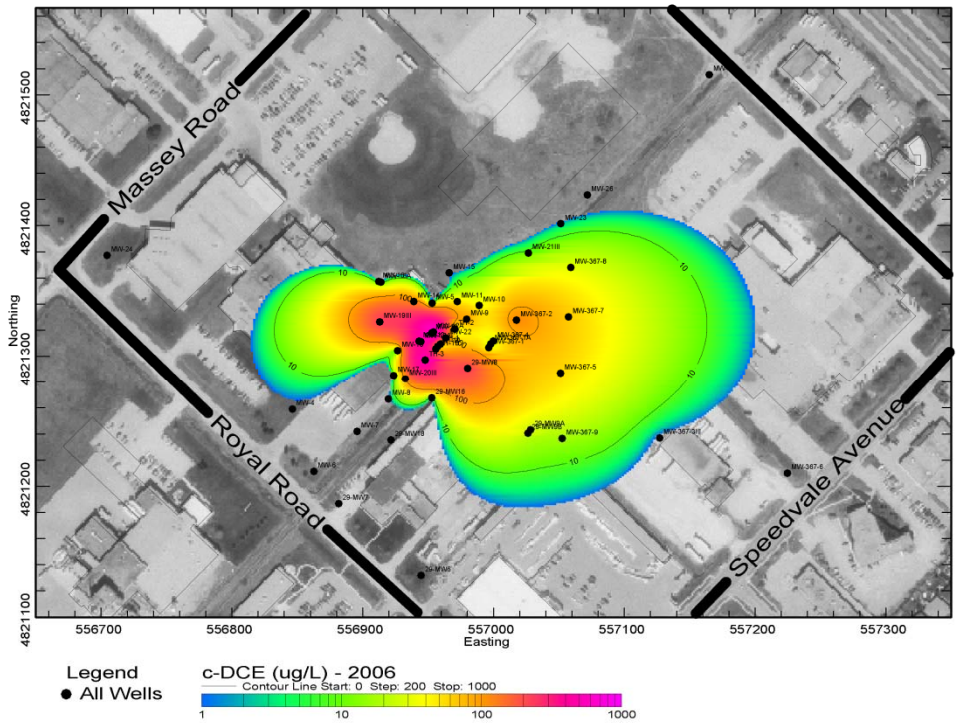

(B)

Figure 4.16: Increasing lateral extent of c-DCE plume. Kriged c-DCE groundwater concentrations for 2004 (A). Kriged c-DCE groundwater concentrations for 2006 (B).

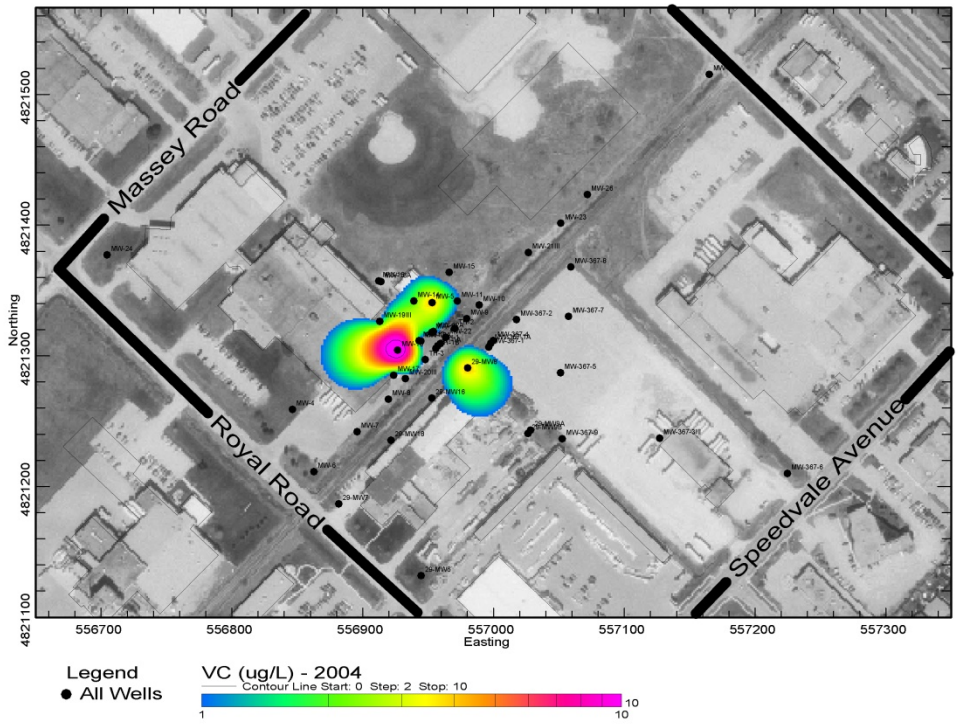

(A)

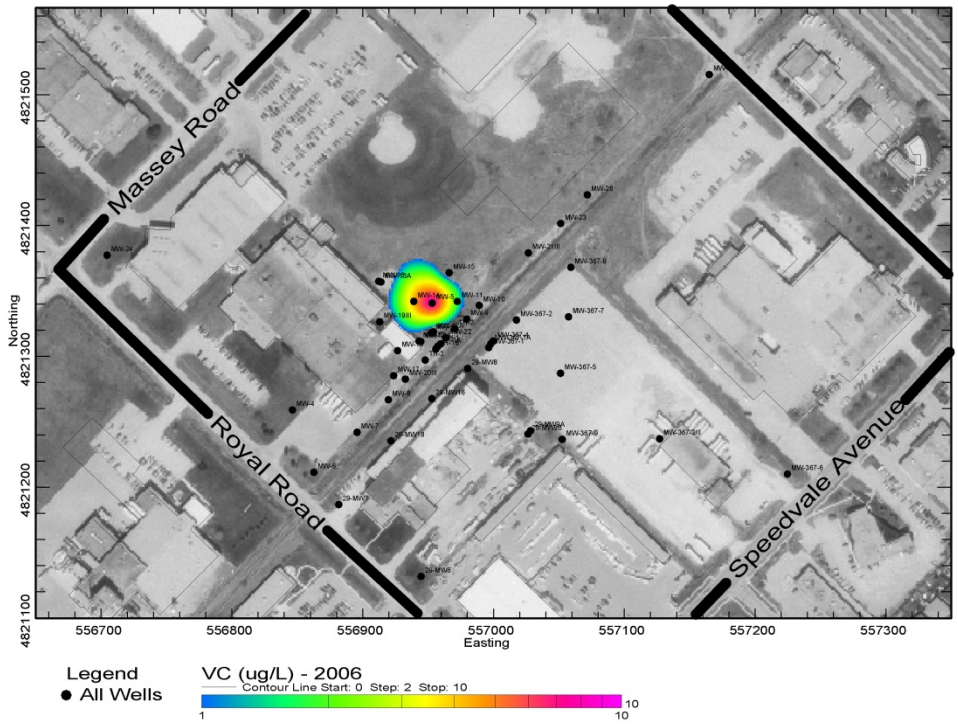

(B)

Figure 4.17: Decreasing lateral extent of VC plume. Kriged VC groundwater concentrations for 2004 (A). Kriged VC groundwater concentrations for 2006 (B).

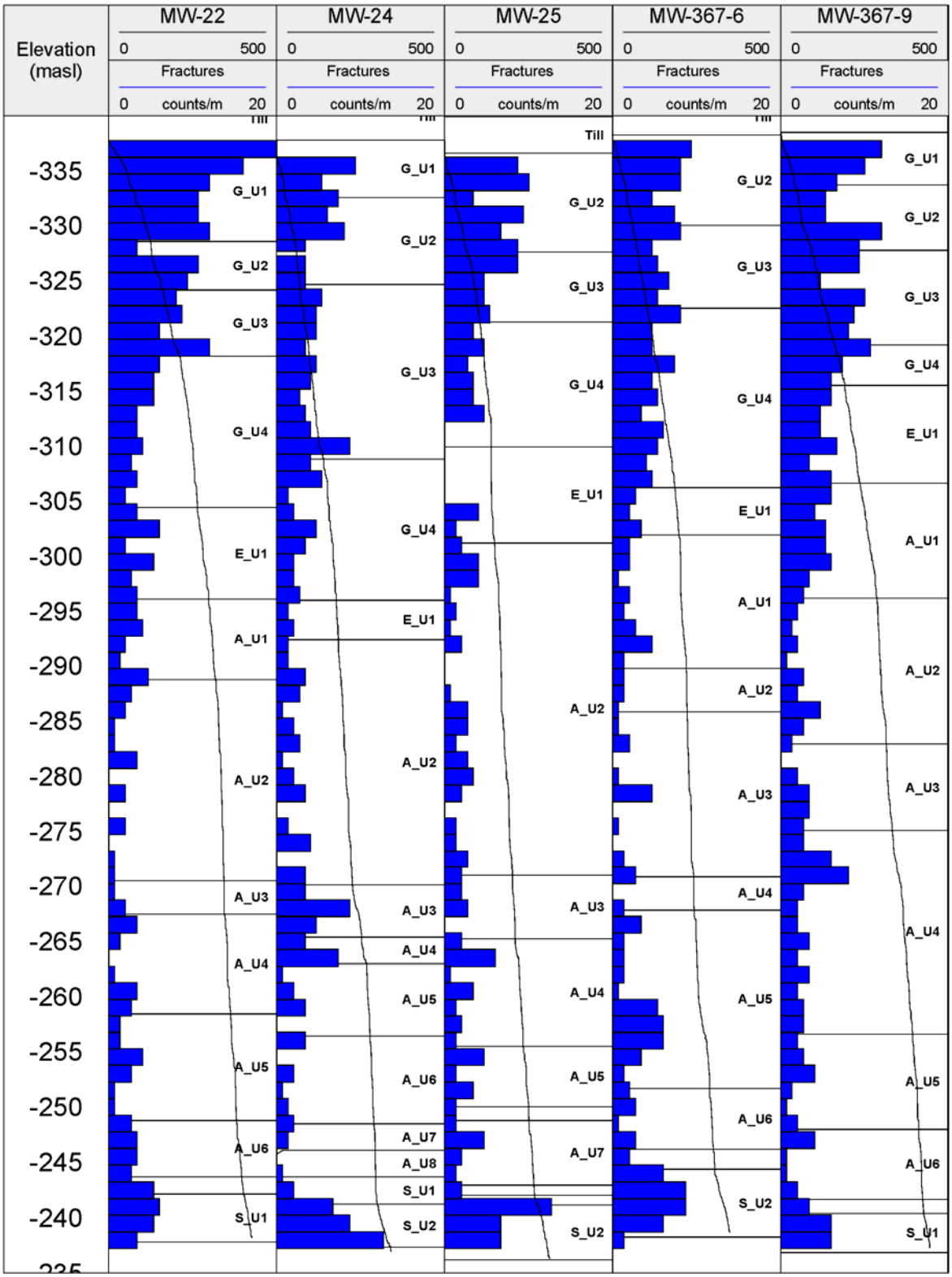

Figure 4.18: Fracture frequencies per meter from rock core and total number of fractures with depth in the hole. Note fracture frequency generally decreases with depth until the shale.

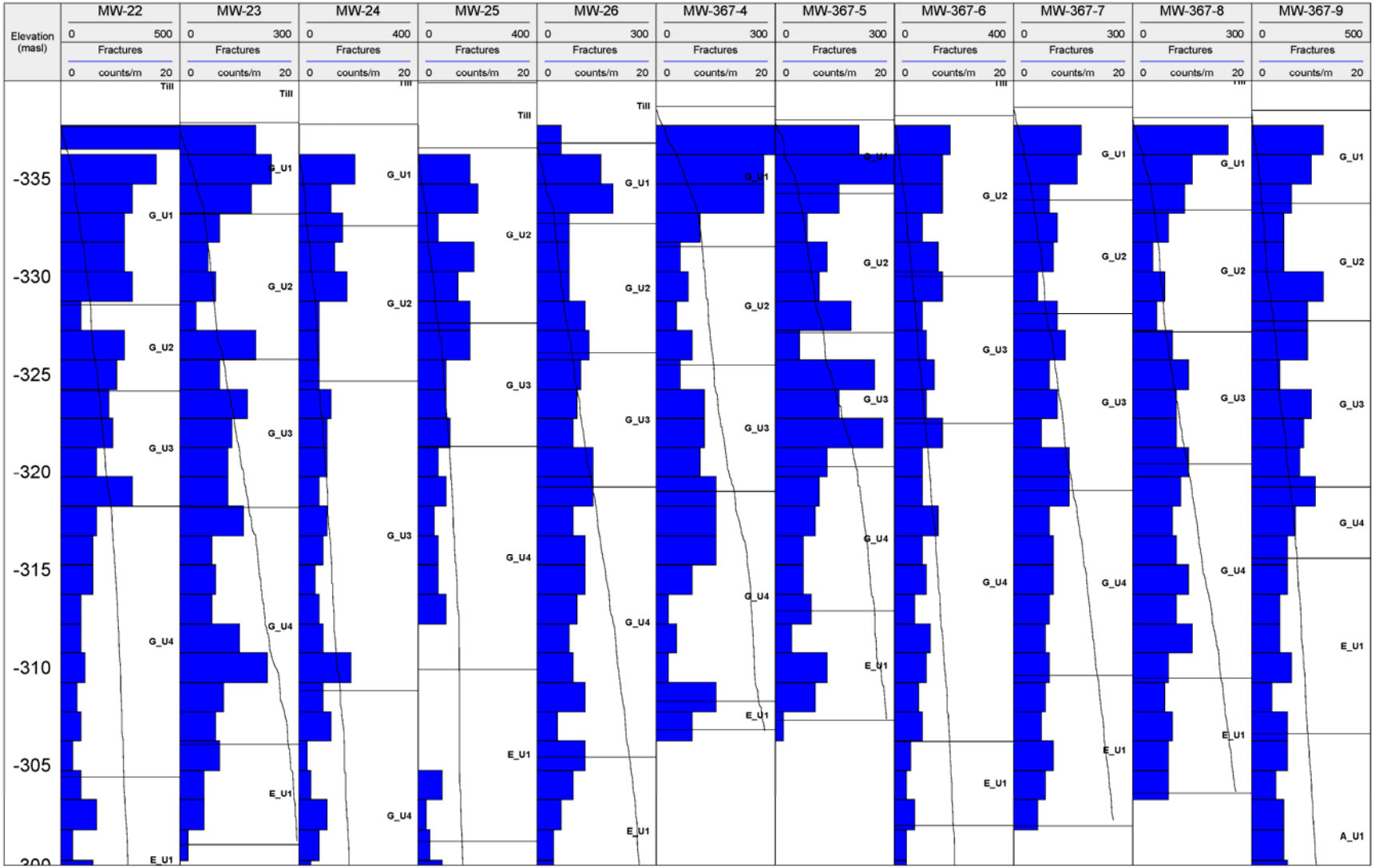

Figure 4.19: Fracture frequency from rock core in the upper 40 m (Guelph formation). The upper five meters generally show the greatest fracture frequency.

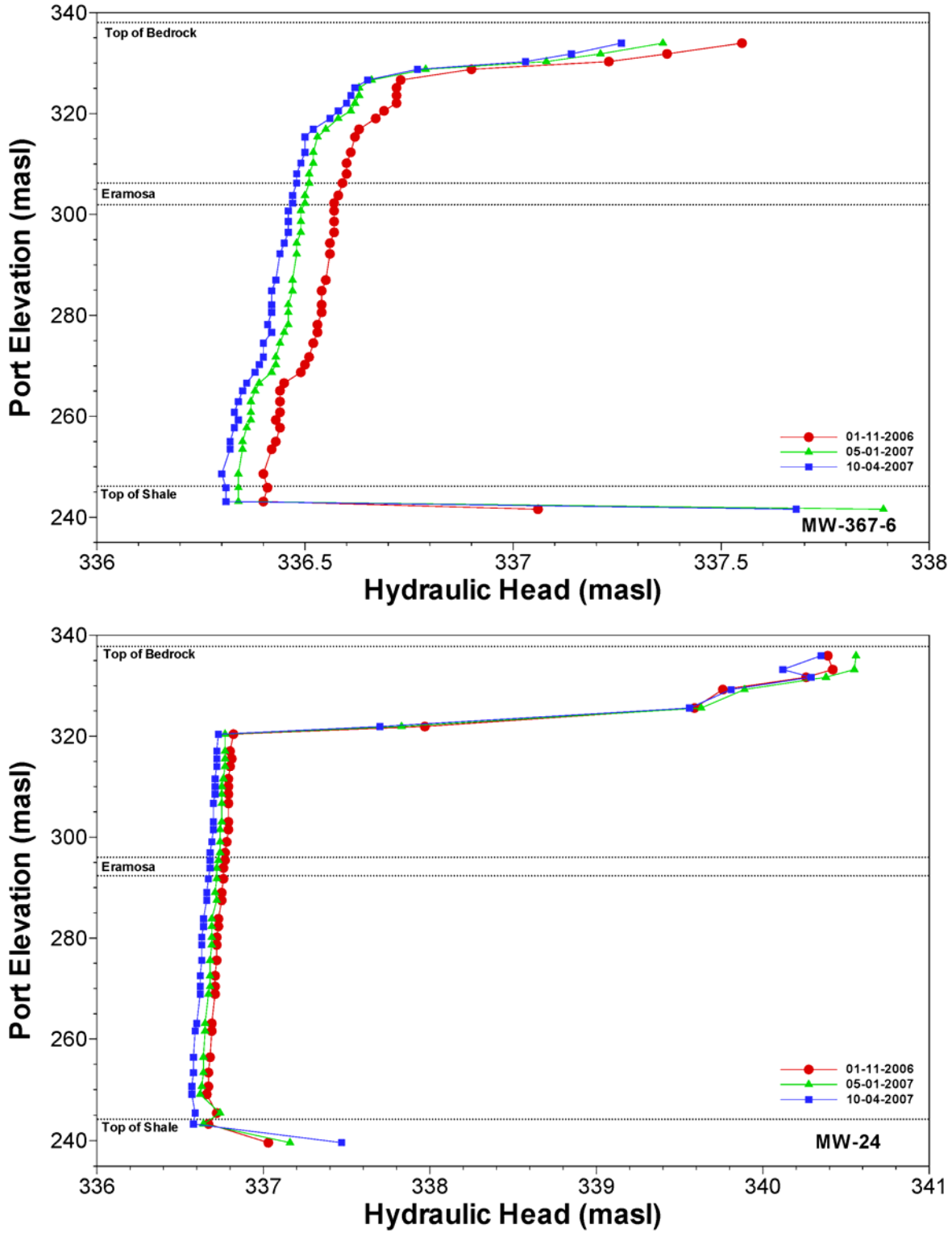

Figure 4.20: Westbay hydraulic head profiles for MW-24 and MW-367-6 showing the temporal stability of the hydraulic gradients. NOTE: Scale difference between wells, the water table for MW-24 is in the overburden, most of the head drop occurs above 320 masl, there is not an inflection point in the head profile at the Eramosa, and the head is higher in the shale.

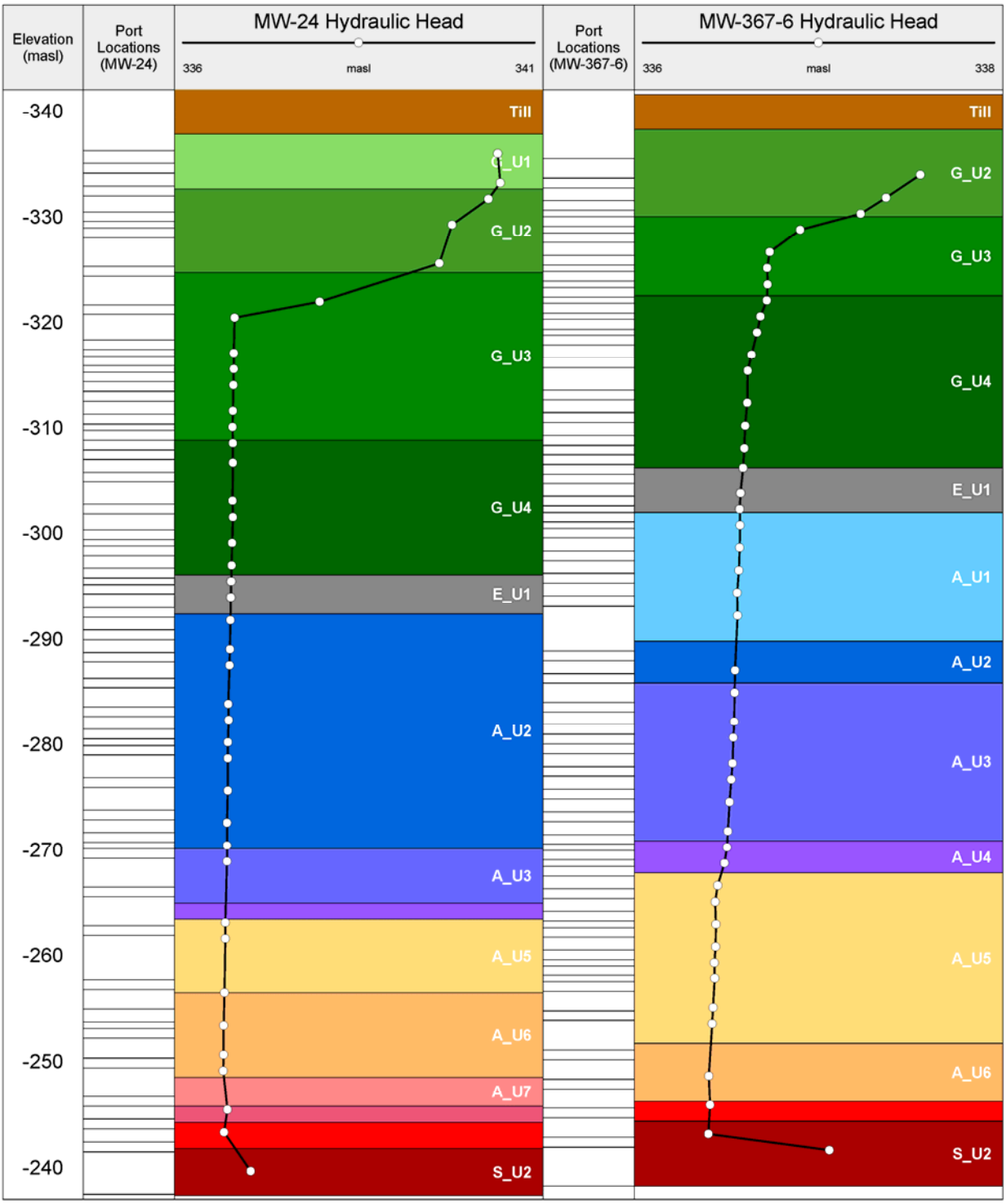

Figure 4.21: Westbay hydraulic head profiles and intervals for MW-24 and MW-367-6 (intervals are indicated as grey).

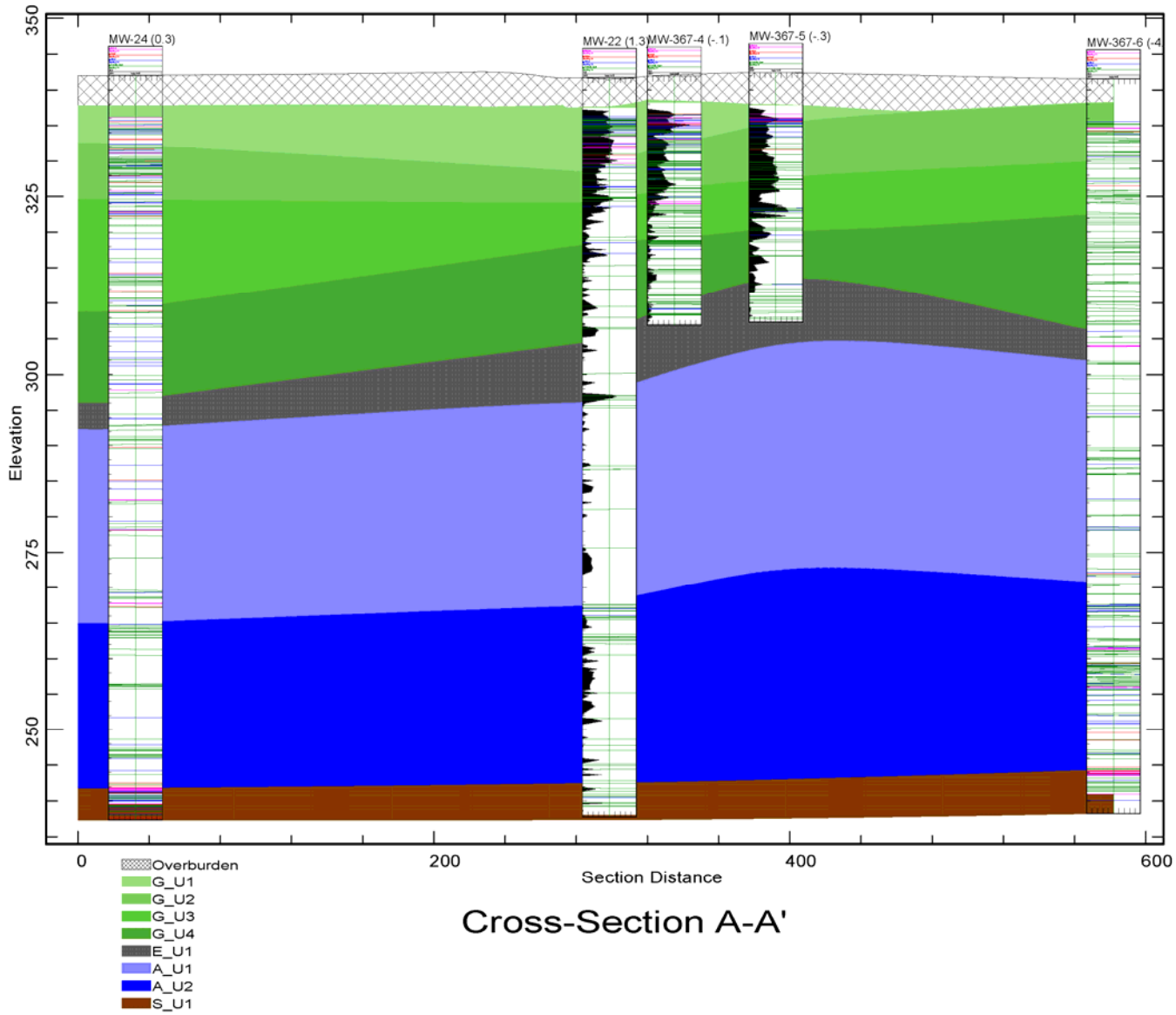

Figure 4.22: Fracture trace and contaminant distribution for A-A'. Note: no rock core VOC data are available for MW-24, and MW-367-6.

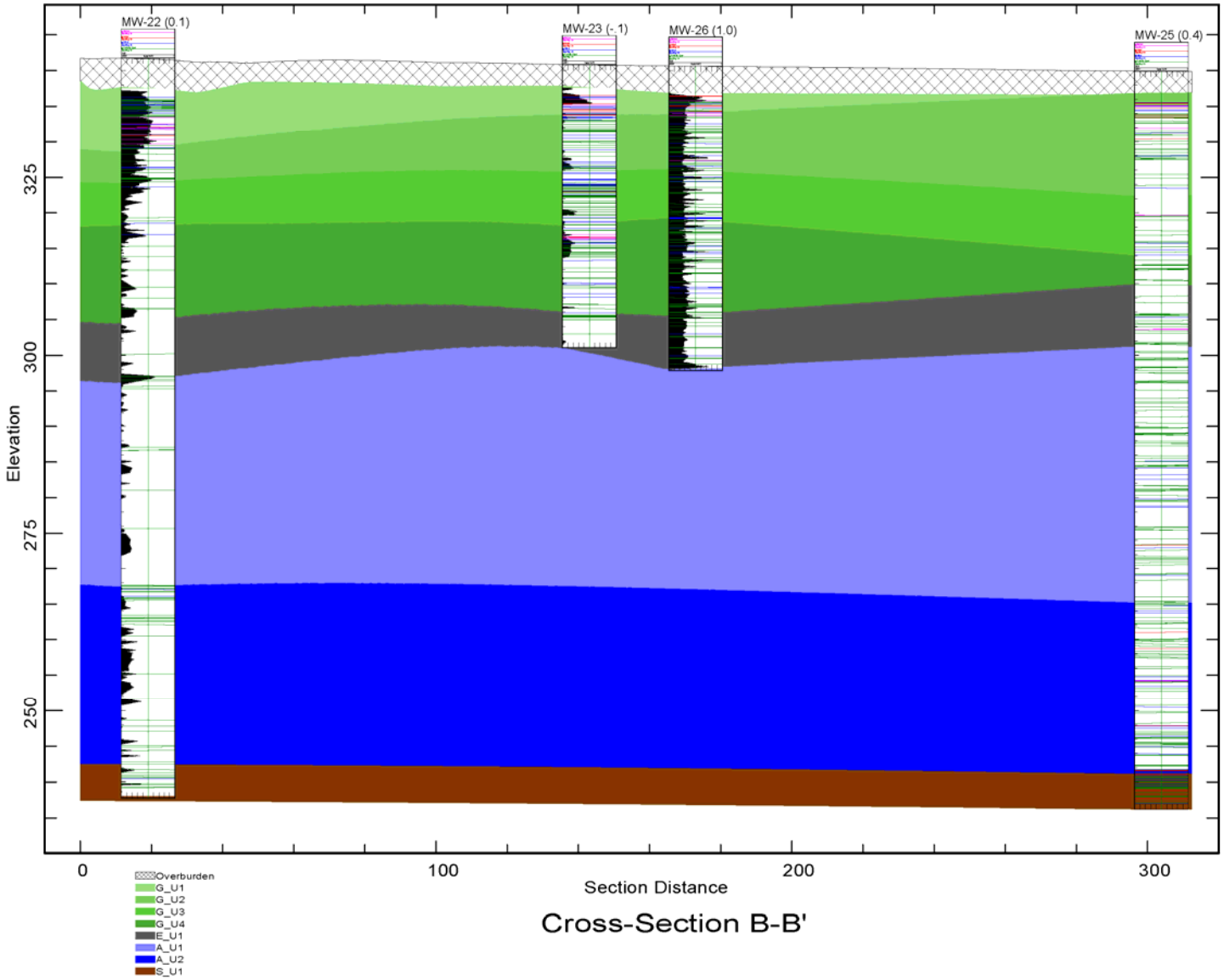

Figure 4.23: Fracture trace and contaminant distribution for B-B'. Note: no rock core VOC data are available for MW-25.

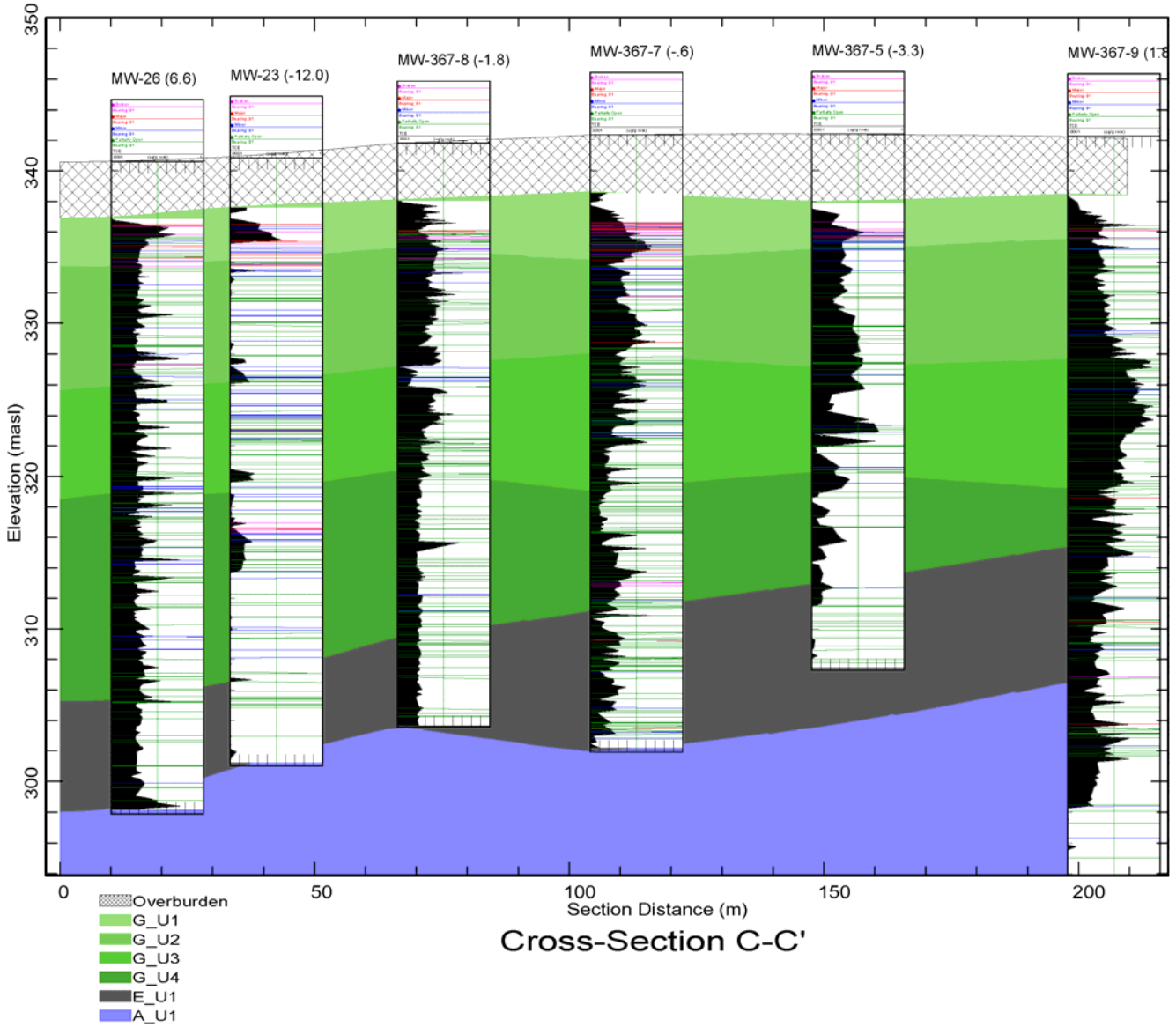

Figure 4.24: Fractures trace and contaminant distribution for C-C'.

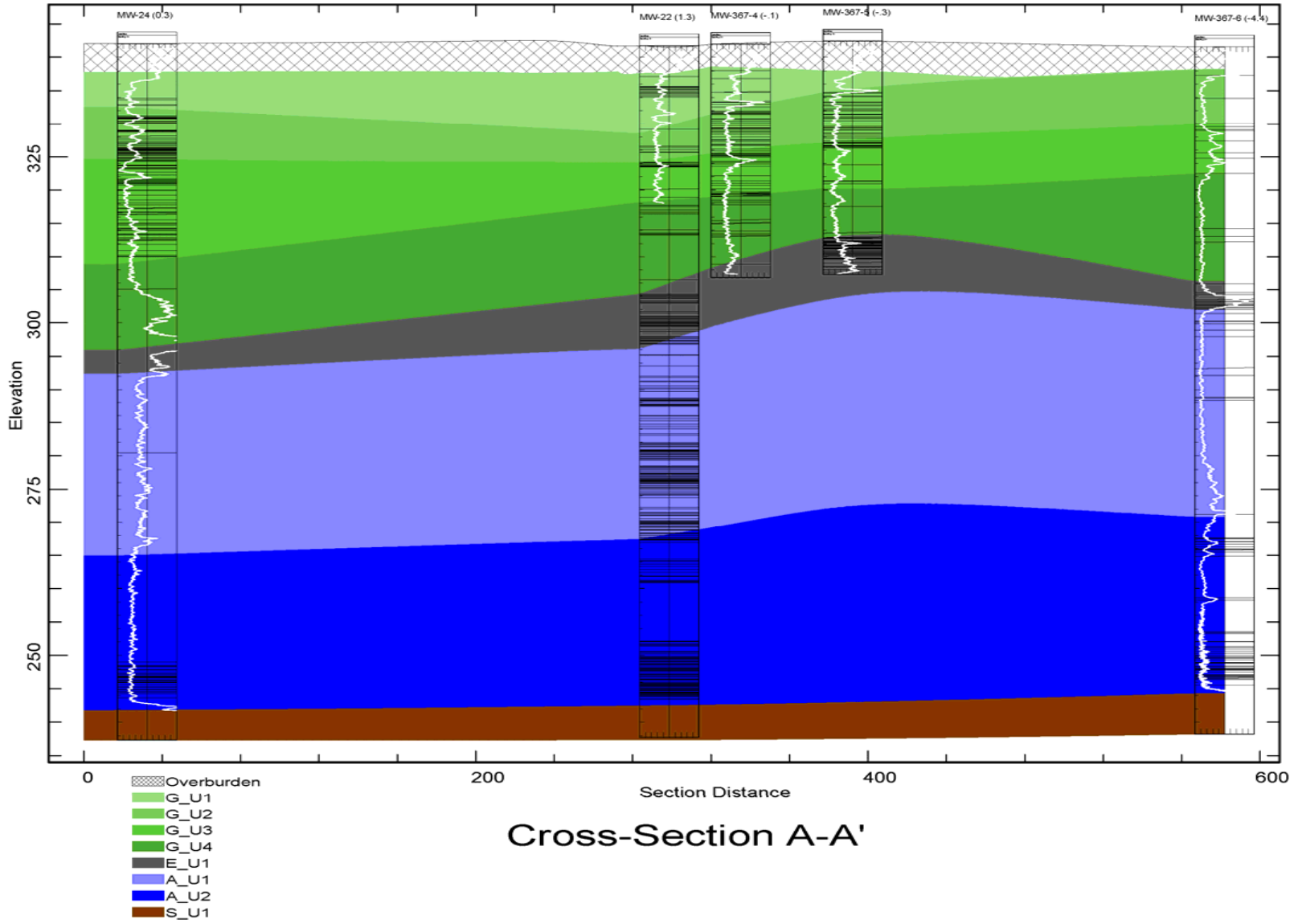

Figure 4.25: Stylolite trace and natural gamma log for A-A'.

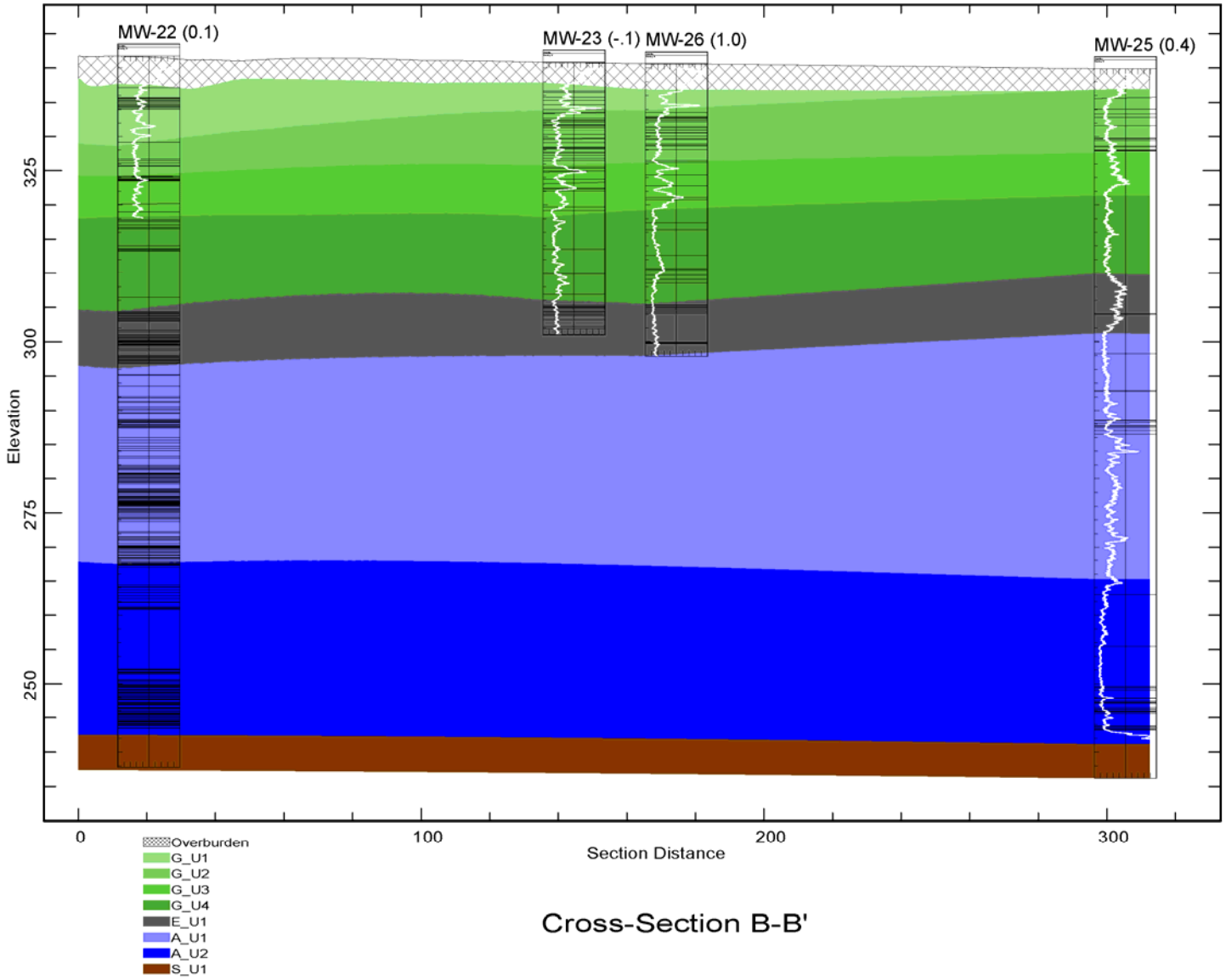

Figure 4.26: Stylolite trace and natural gamma log for B-B'.

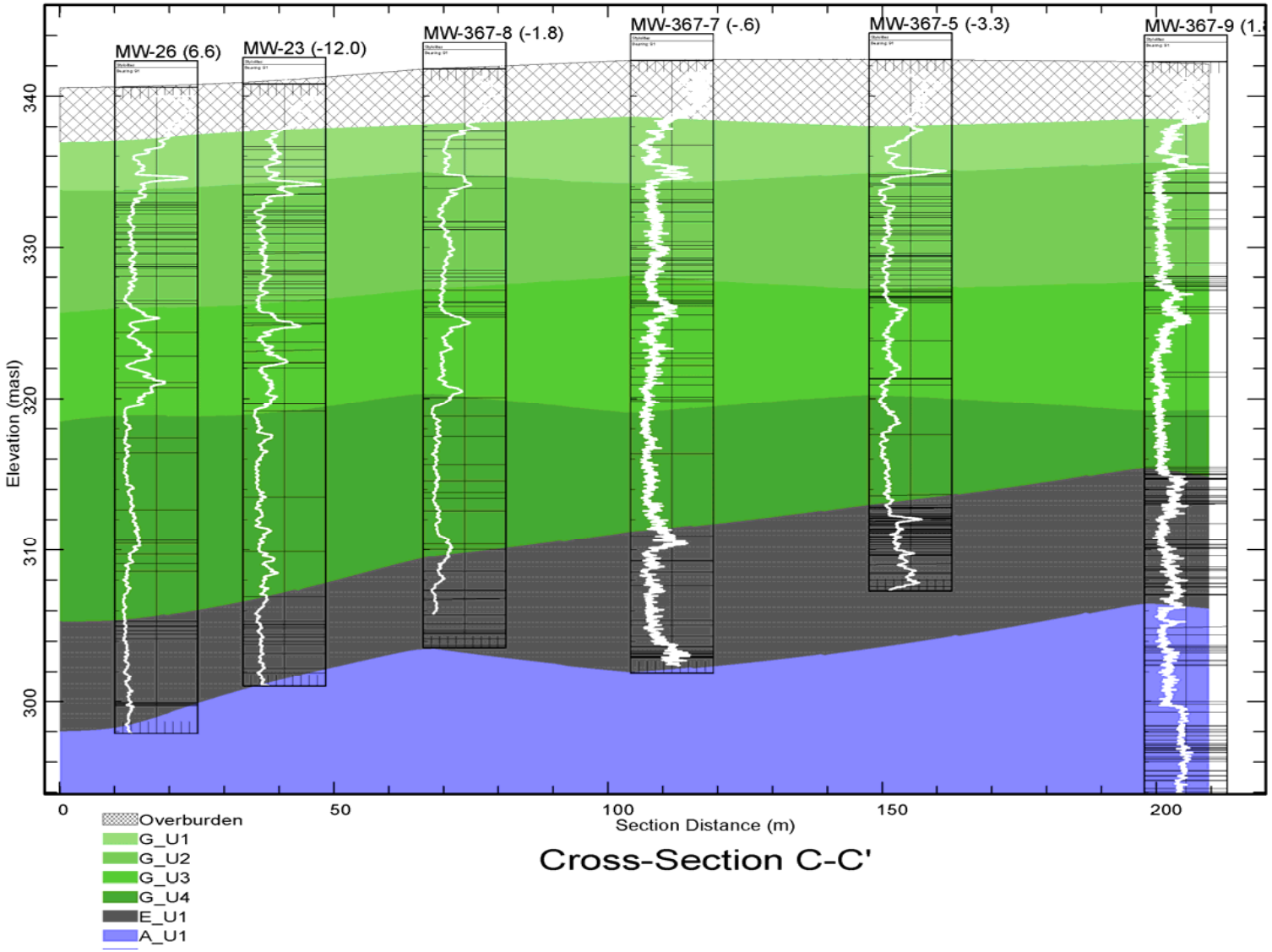

Figure 4.27: Stylolite trace and natural gamma log C-C'.

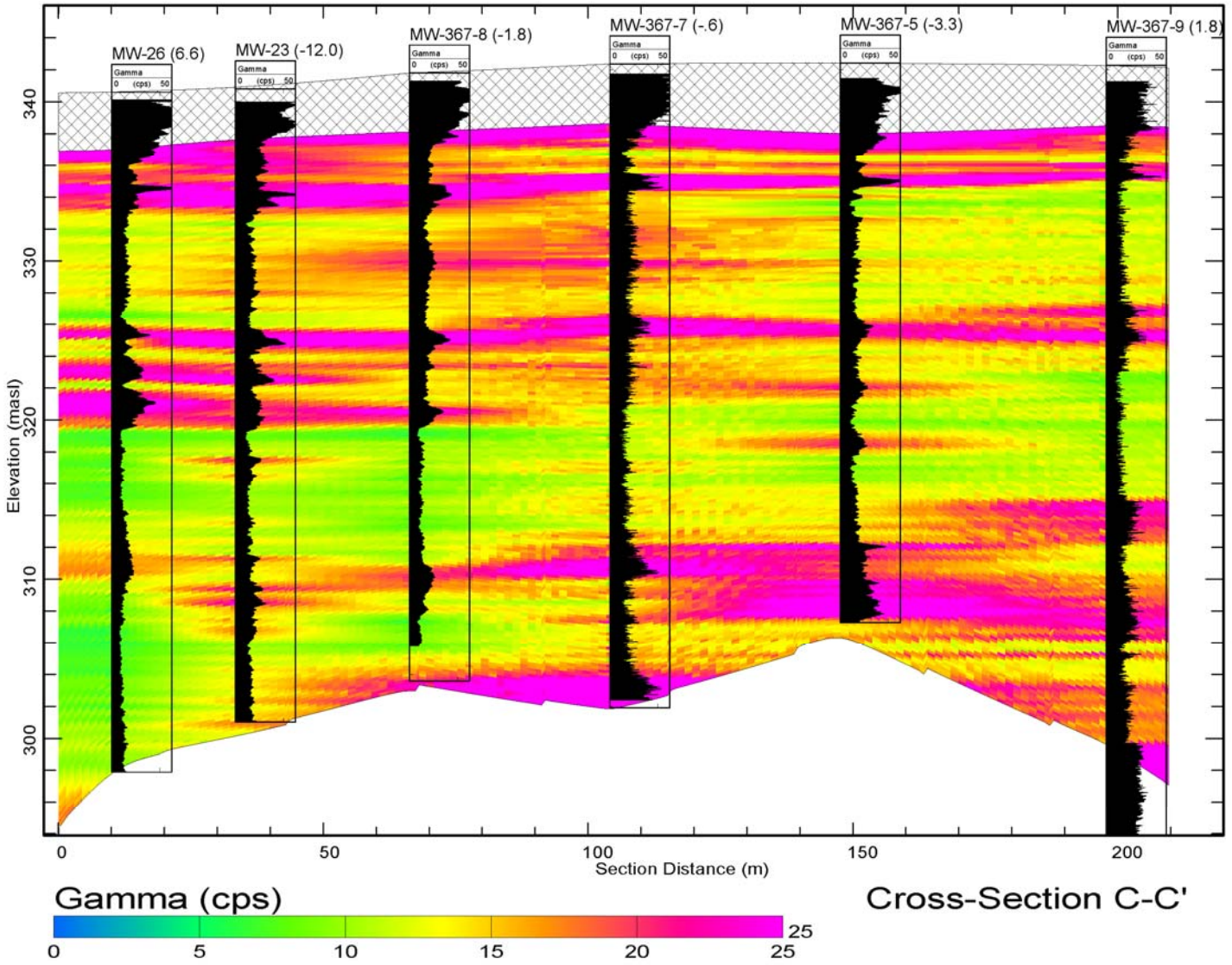

Figure 4.28: Kriged natural gamma response overlain by the natural gamma well logs. Correlateable peaks across the transect are evident.

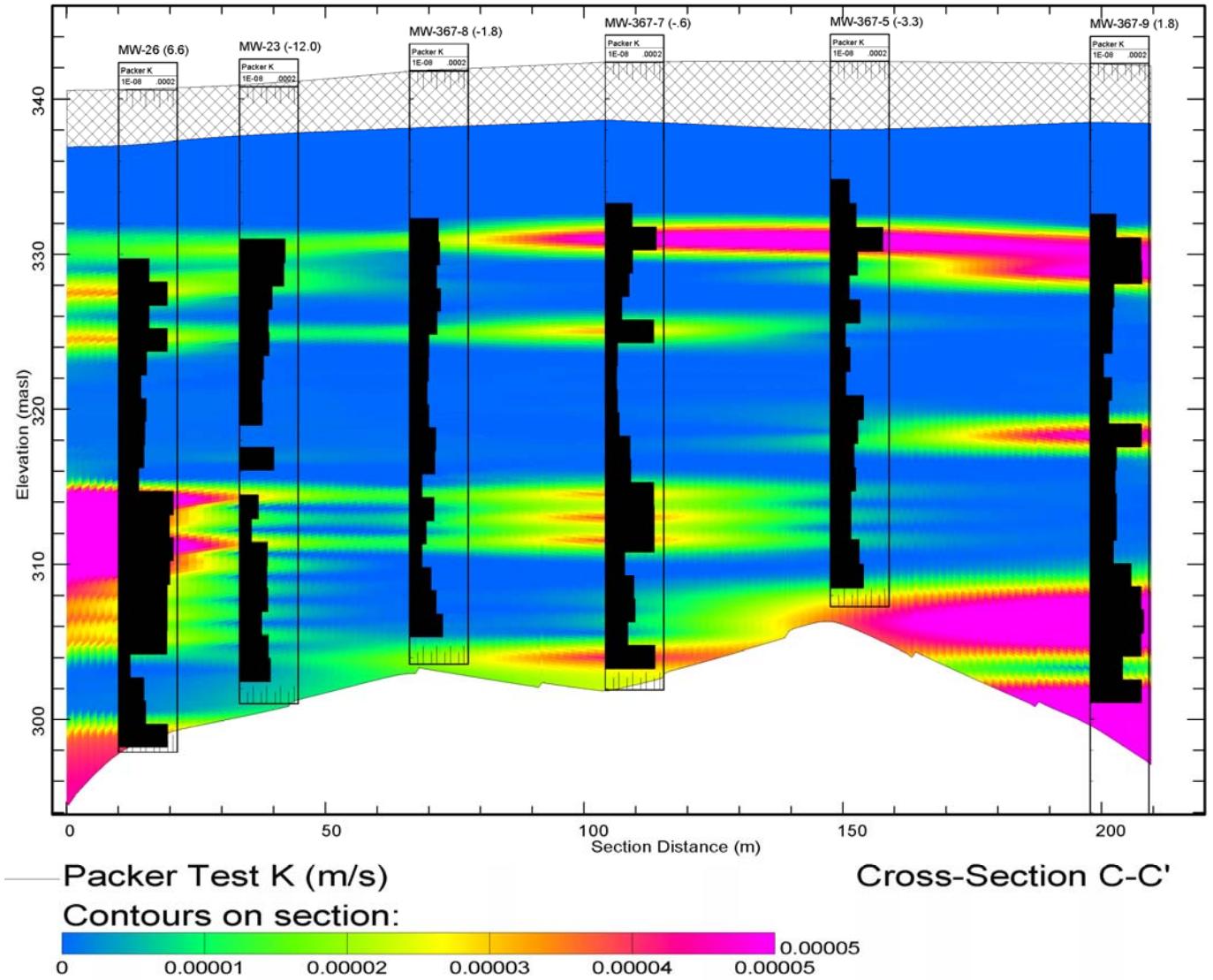

Figure 4.29: Kriged straddle packer hydraulic conductivity distribution across transect overlain by the well straddle packer logs.

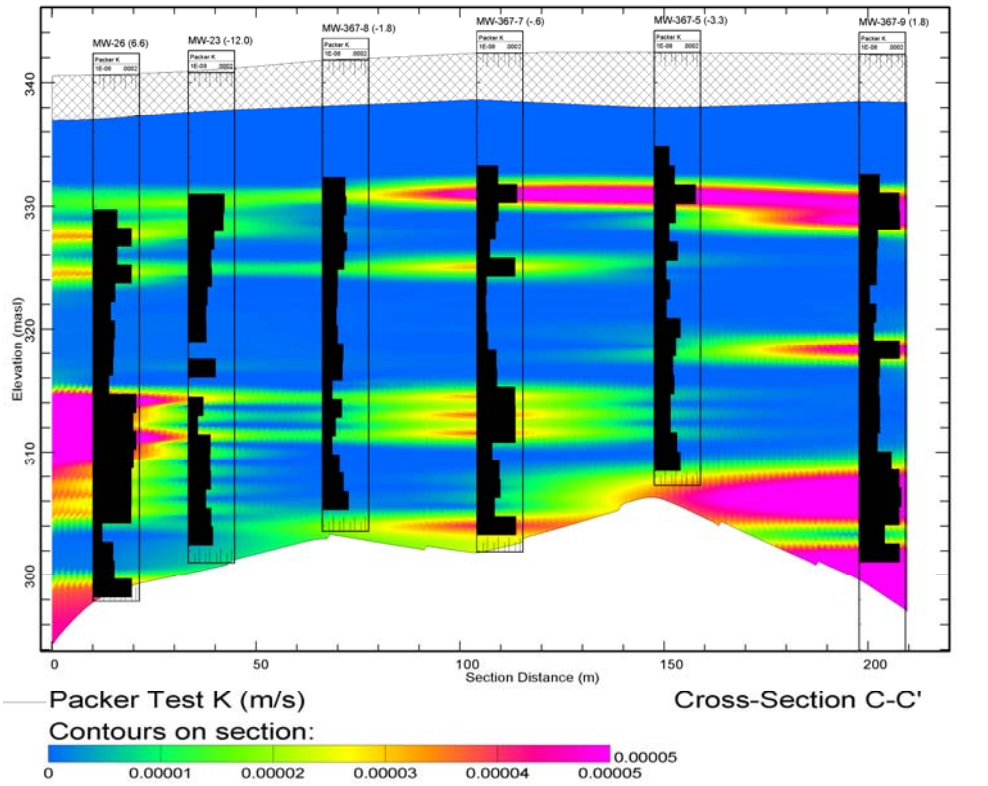

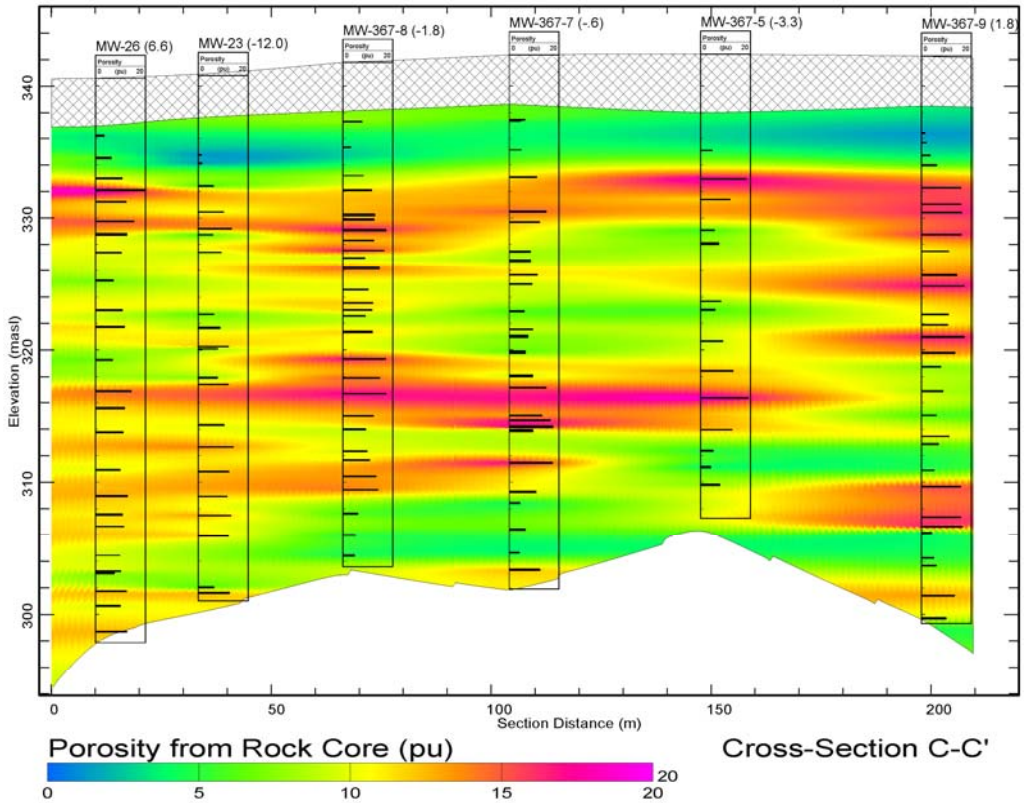

Figure 4.30: Comparison of packer testing and core derived porosity.

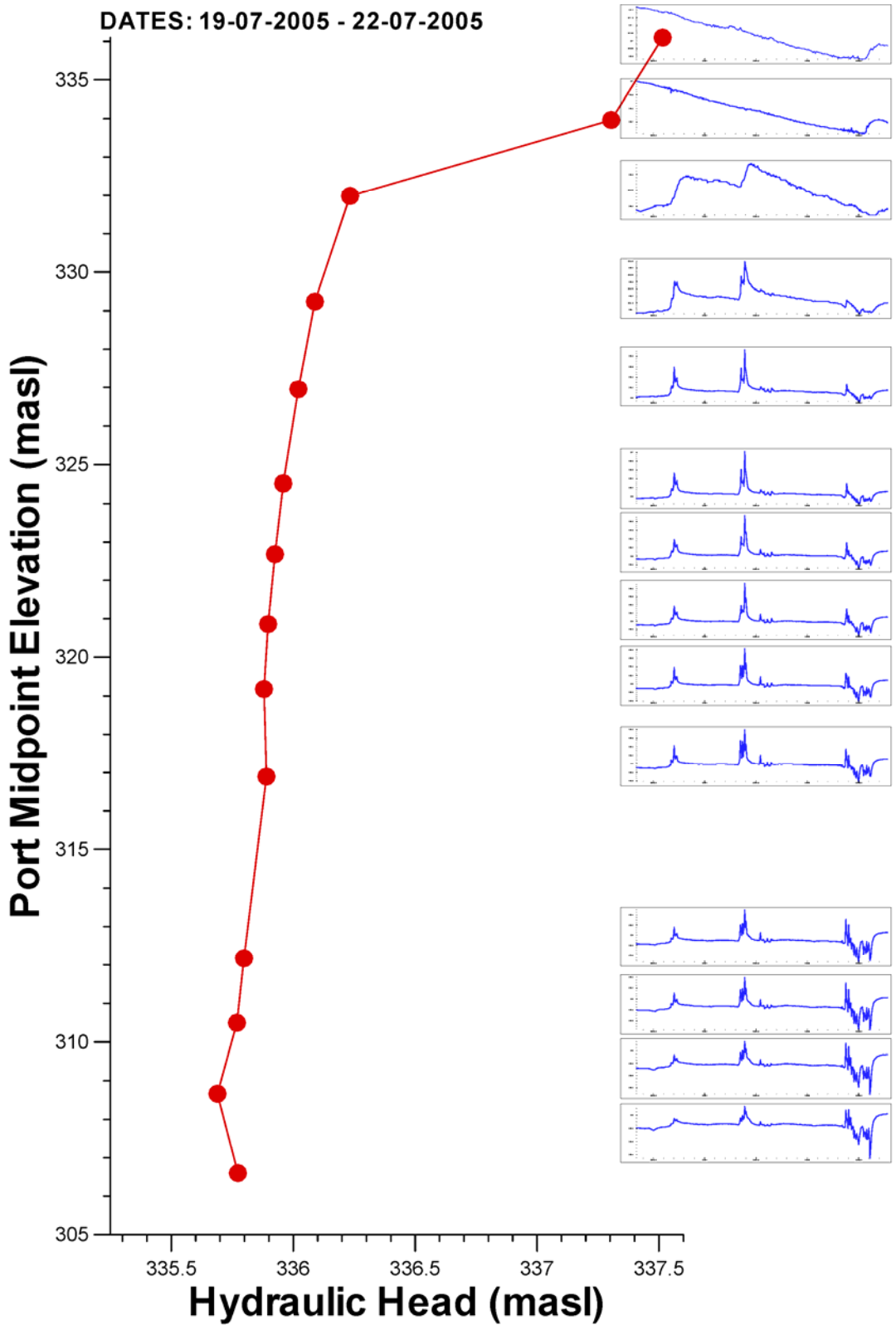

Figure 4.31: MW-23 vertical head profile and hydrographs during the coring of MW-26. Three distinct zones are apparent and some transition regions.

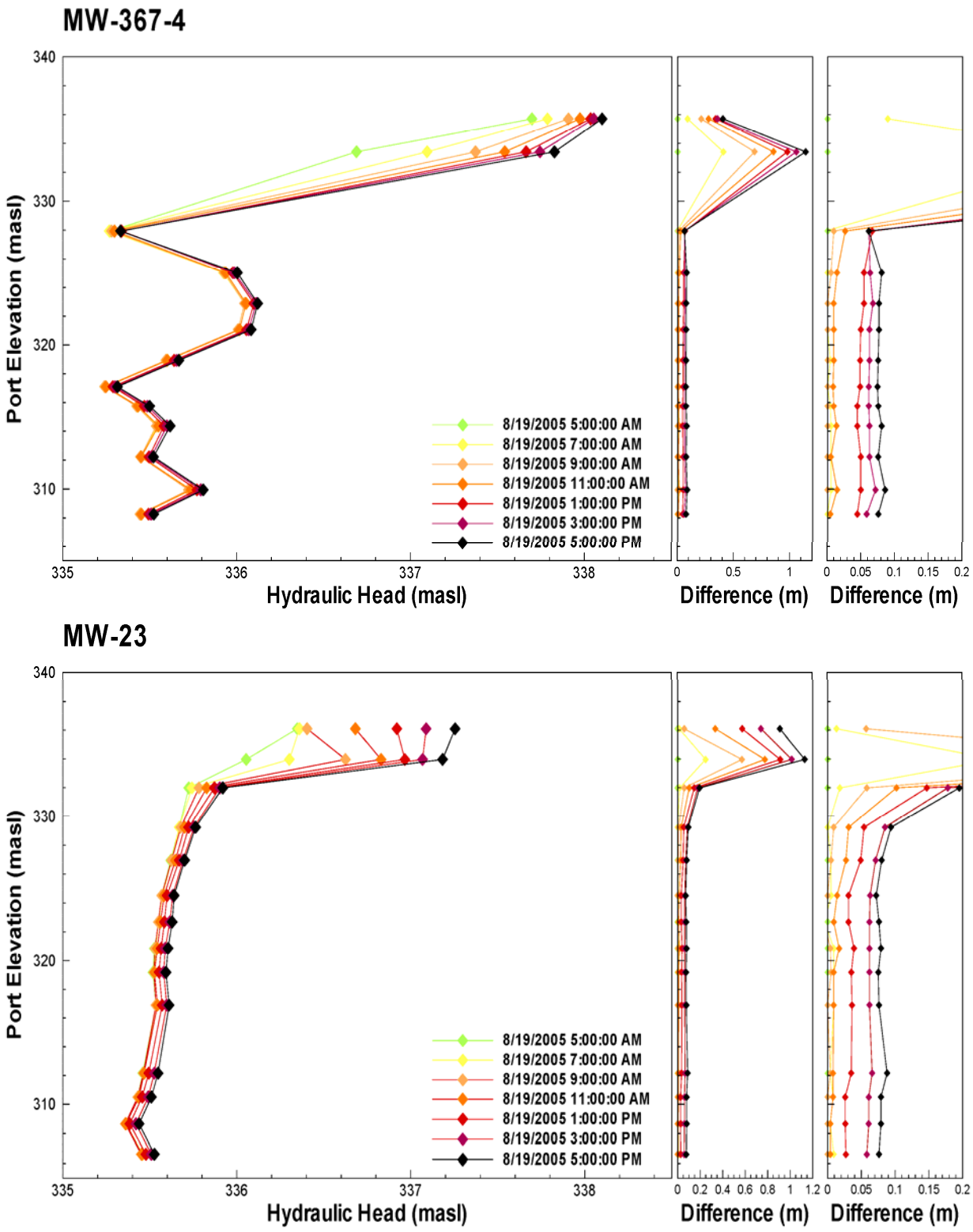

Figure 4.32: Hydraulic head response from FLUTe™ multilevels during an isolated rainfall event (19-Aug-2005). The difference plots show the change in hydraulic head with respect to the static (18-Aug-2005) heads.

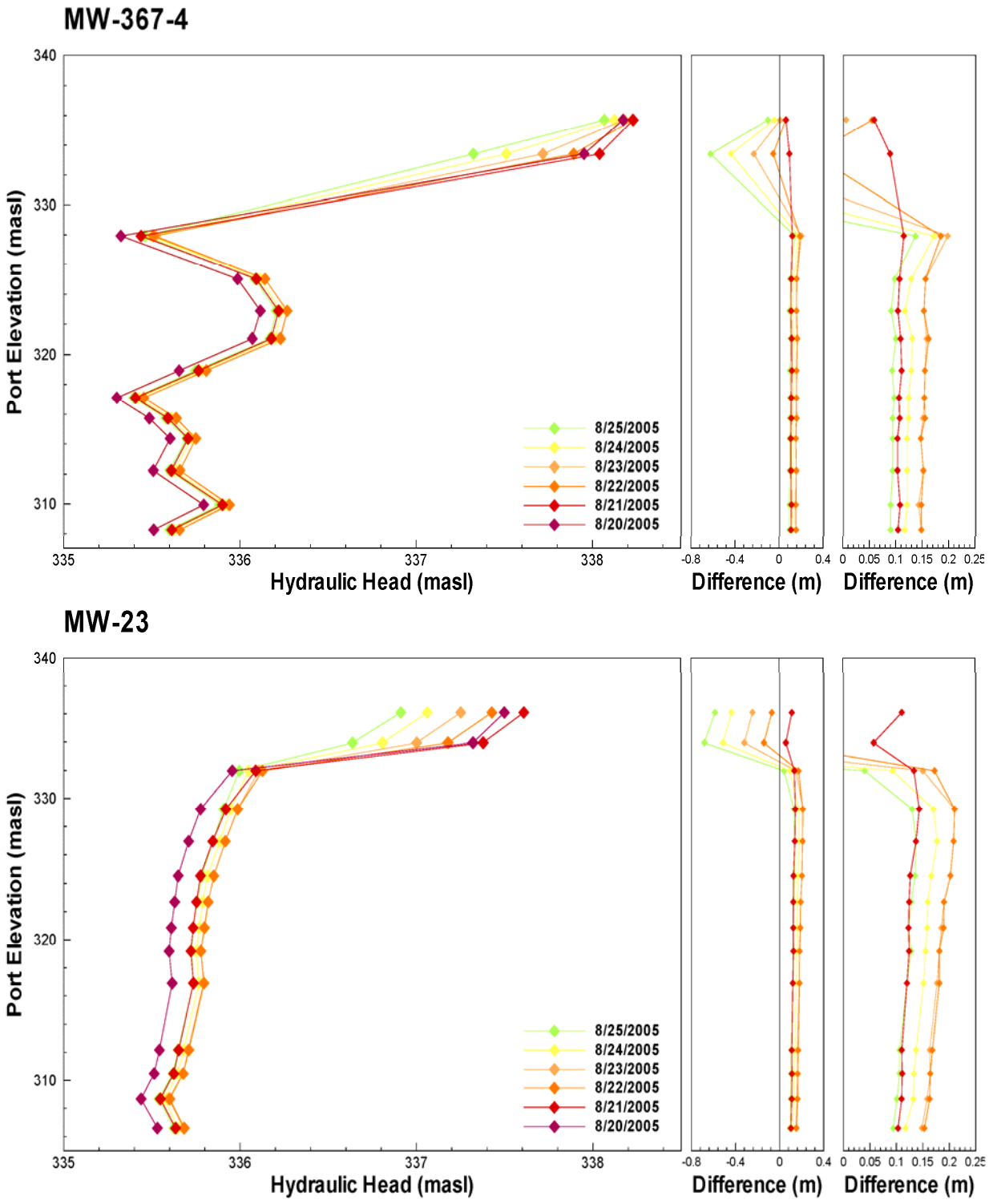

Figure 4.33: Hydraulic head response from FLUTe™ multilevels after the cessation of an isolated rainfall event (19-Aug-2005). The difference plots show the change in hydraulic head with respect to the day after the recharge event (20-Aug-2005) heads.

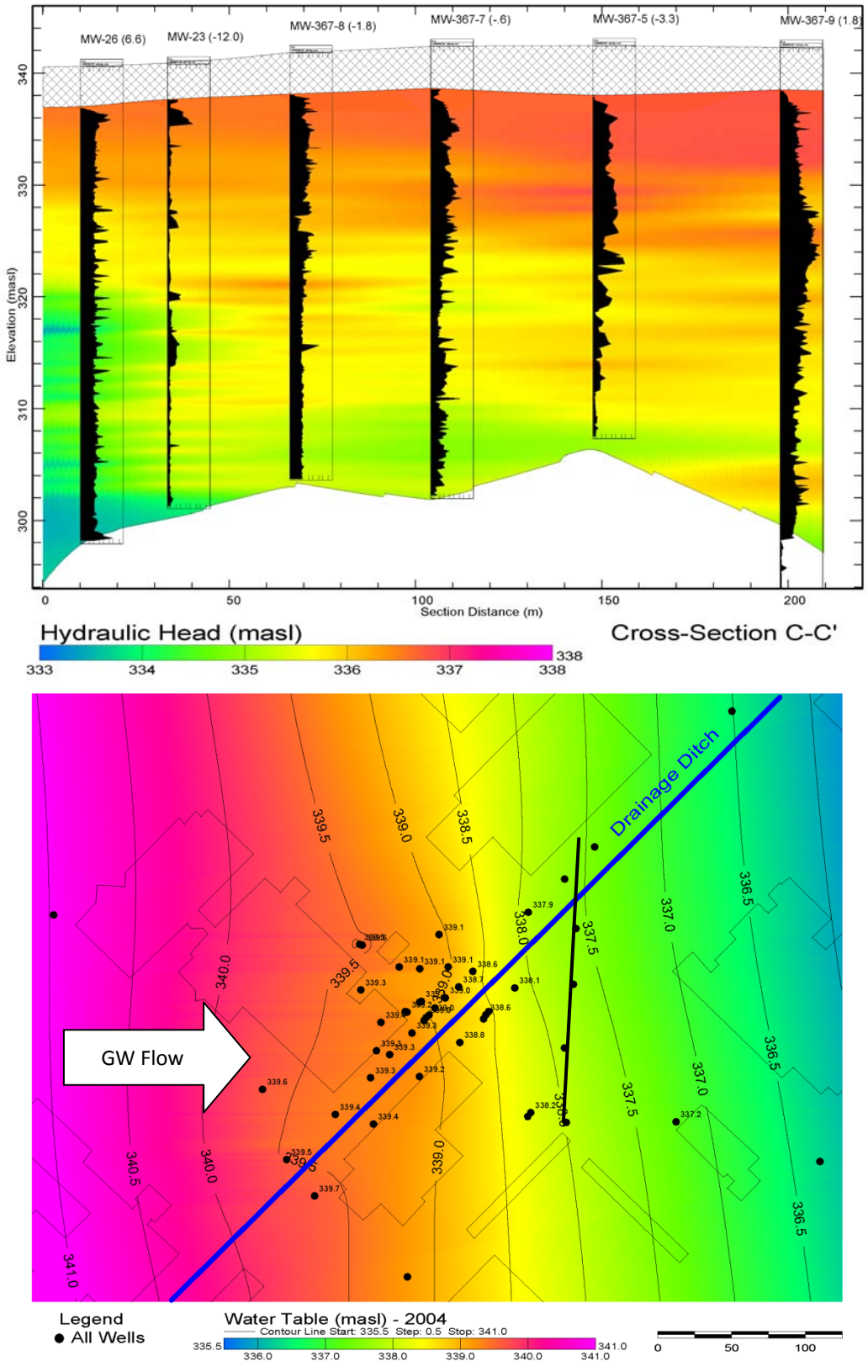

Figure 4.34: Comparison of decreasing heads as you move north and east on the transect.

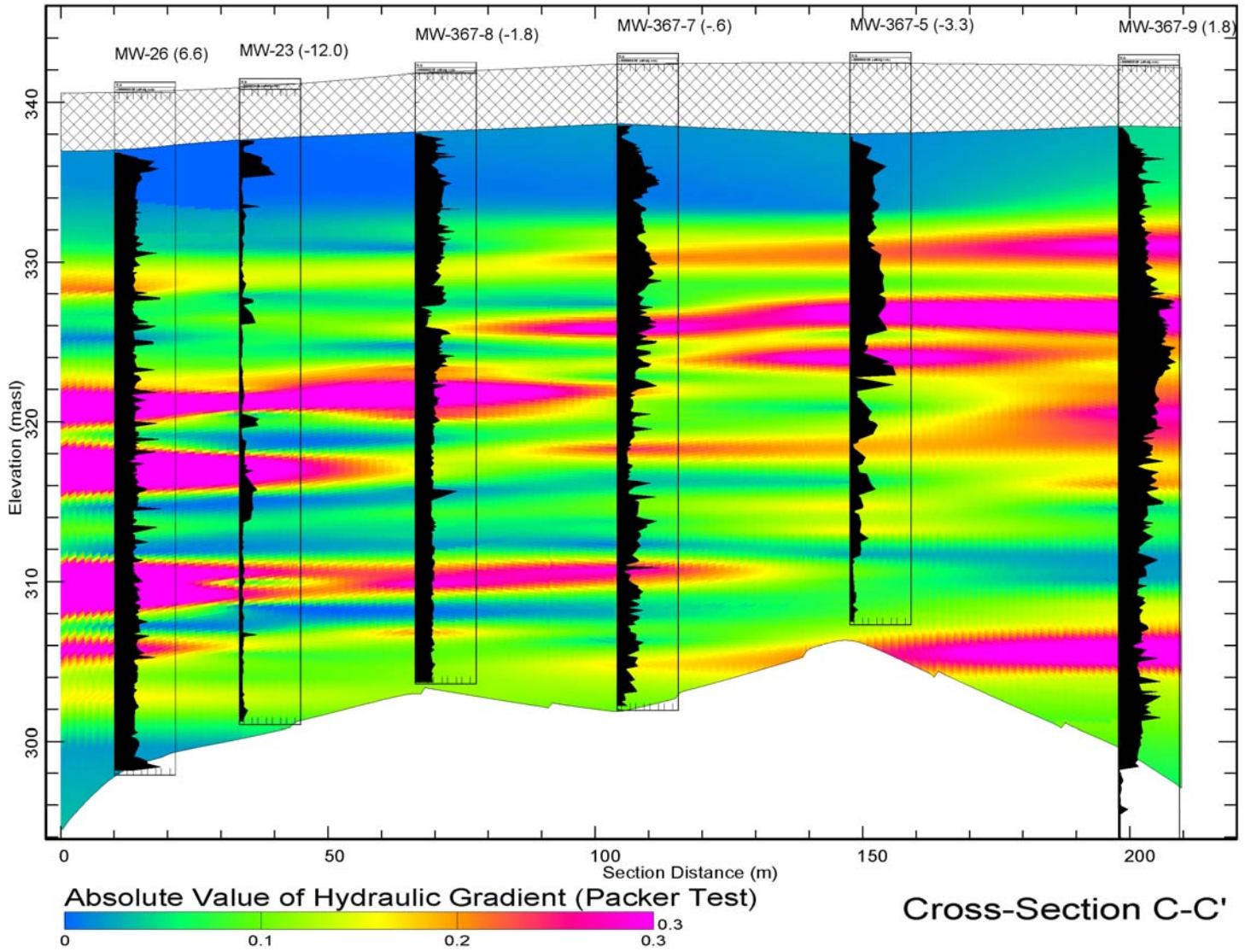

Figure 4.35: Absolute value of hydraulic gradient from packer testing with TCE concentration overlay.

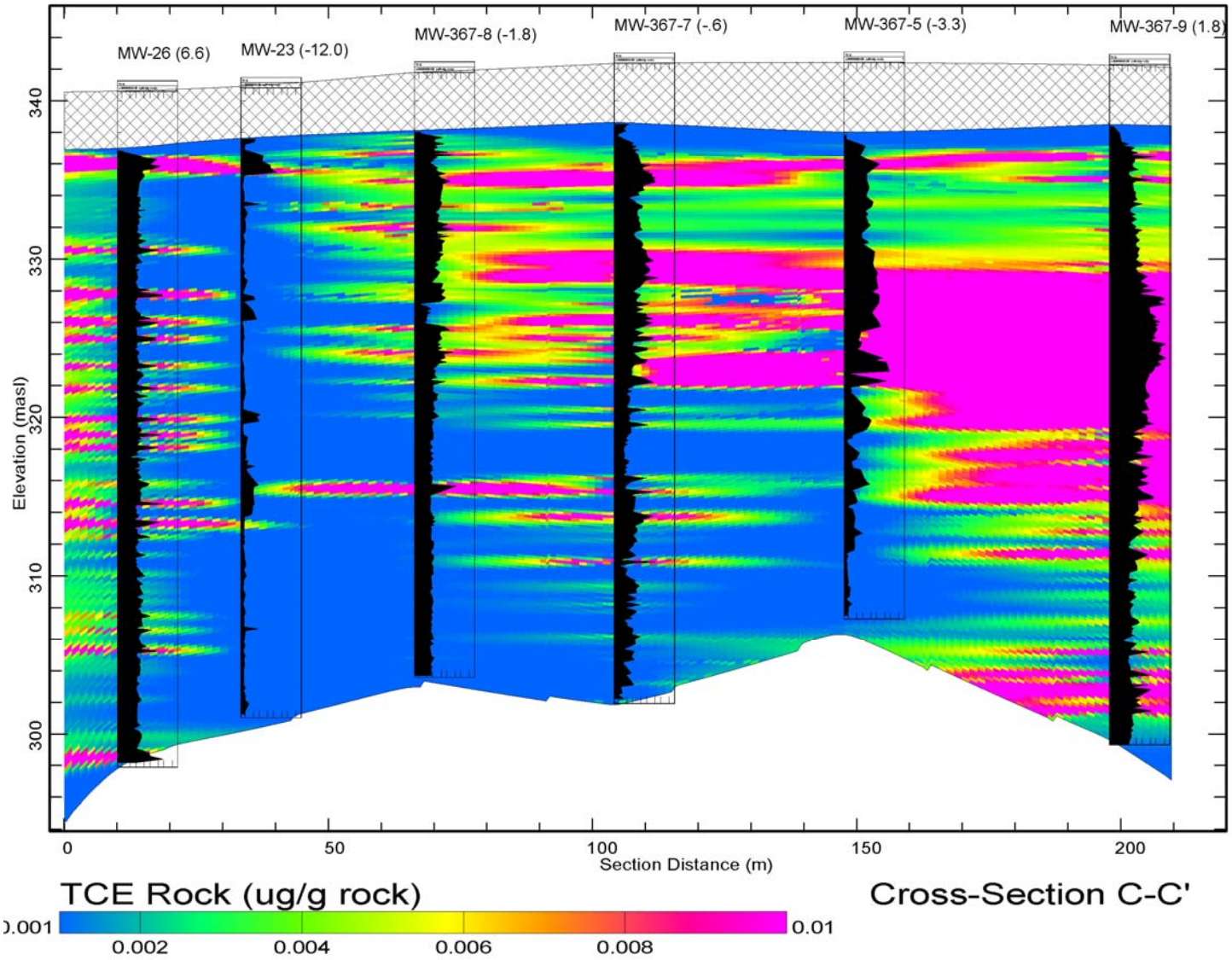

Figure 4.36: Kriged rock core TCE contaminant distribution overlain by the rock core TCE profiles. NOTE: Data from 2005 except wells MW-367-5 and MW-23 were from 2004 and not field preserved in methanol.

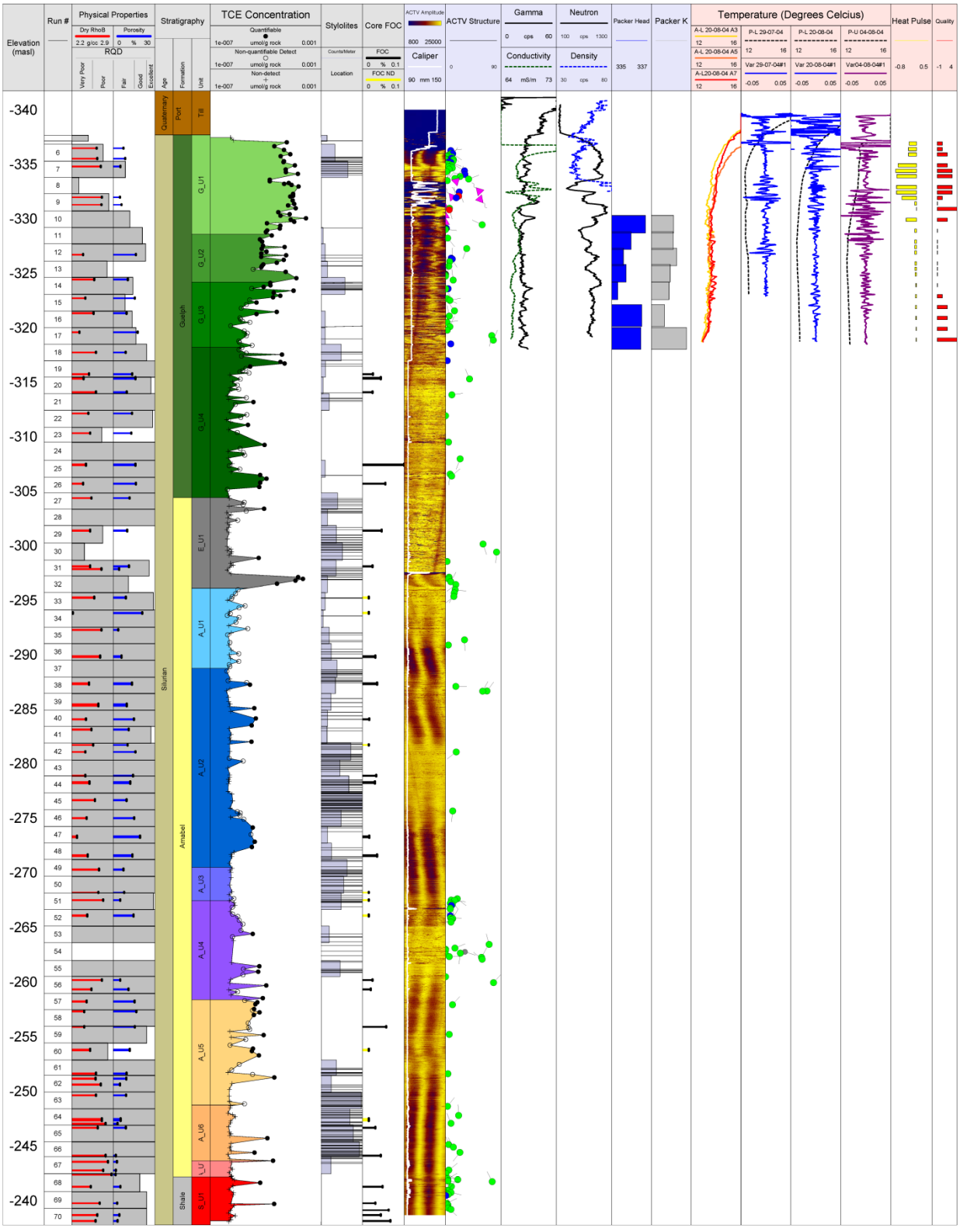

Figure 4.37: MW-22 Summary plot.

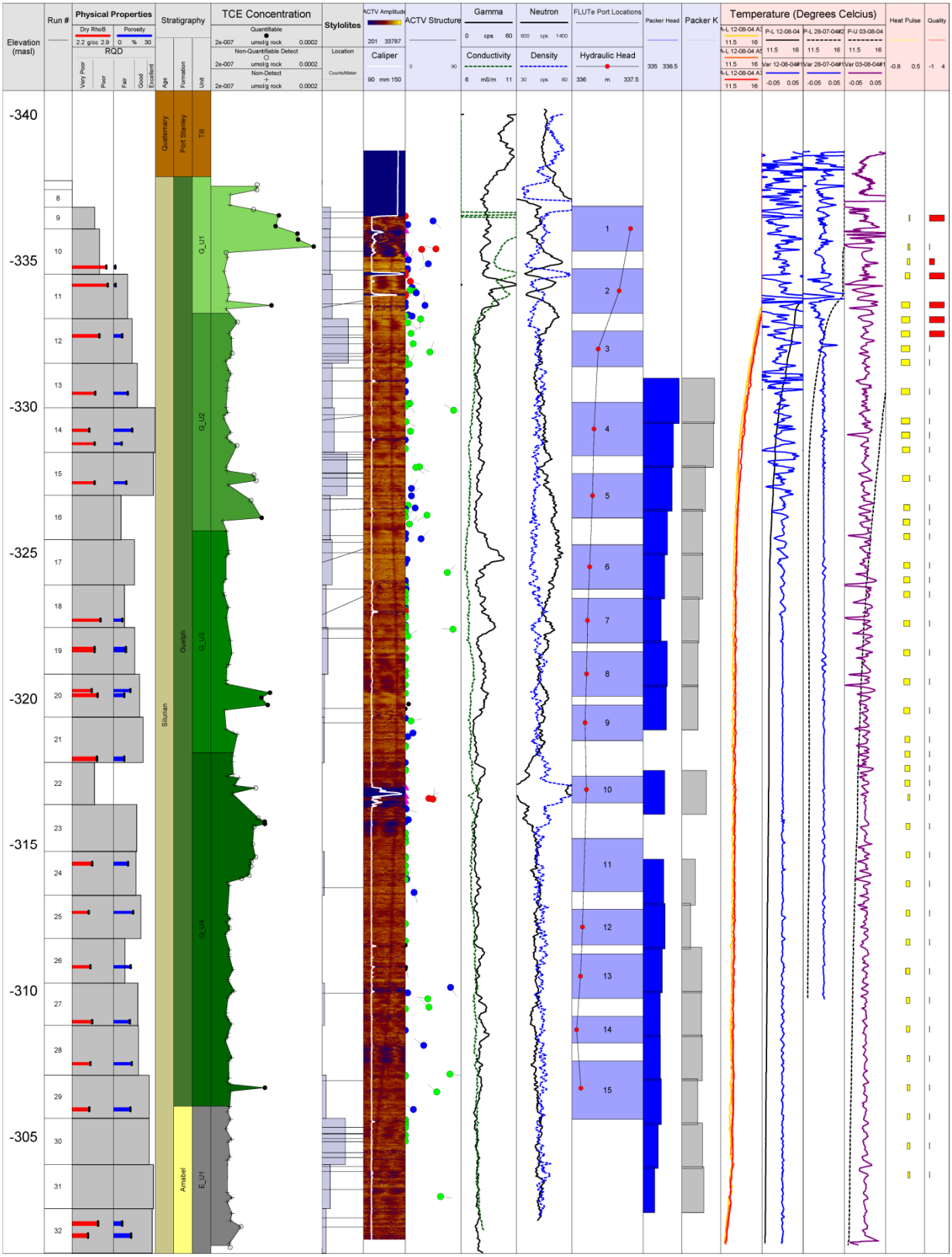

Figure 4.38: MW-23 Summary plot.

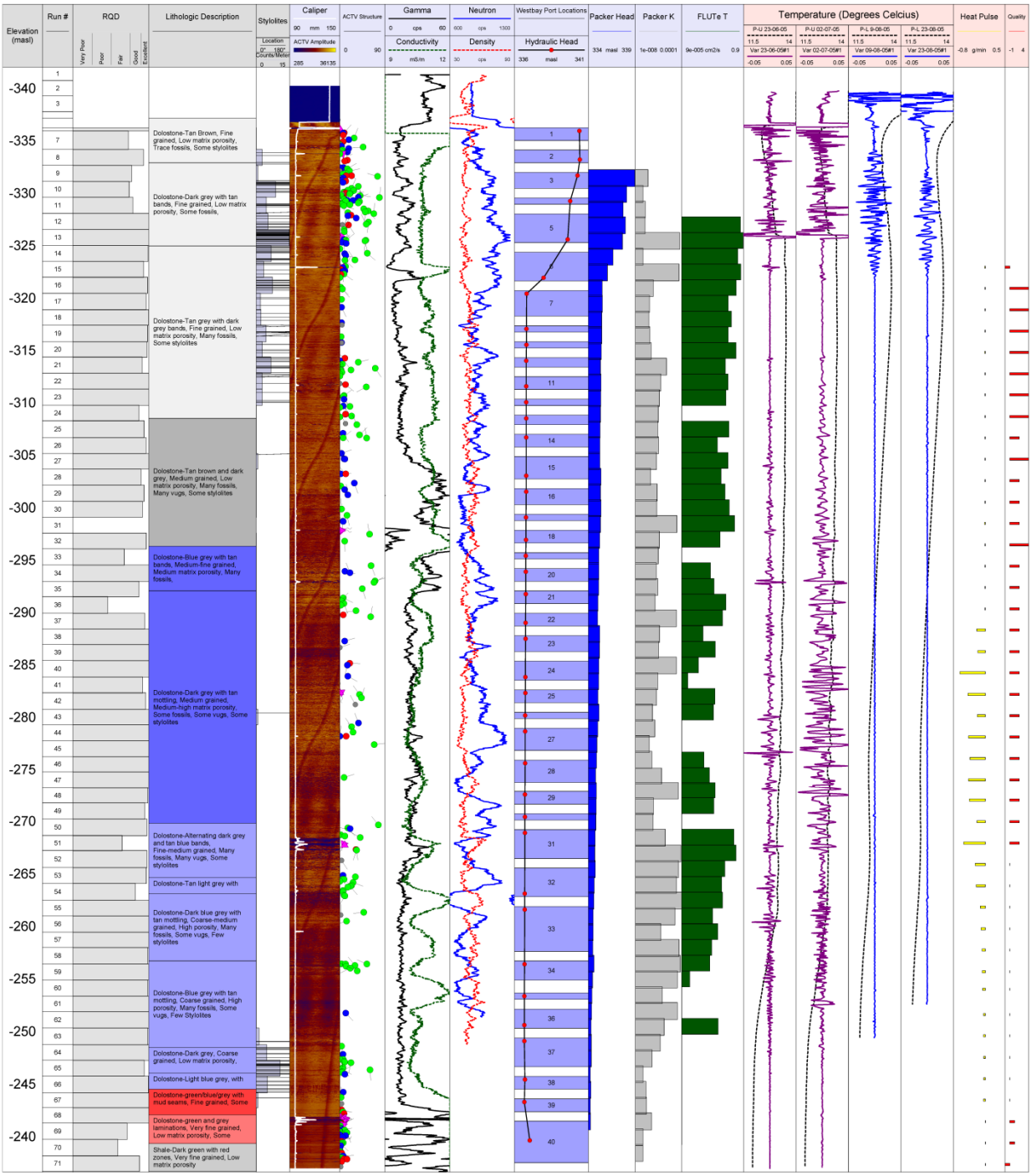

Figure 4.39: MW-24 Summary plot.

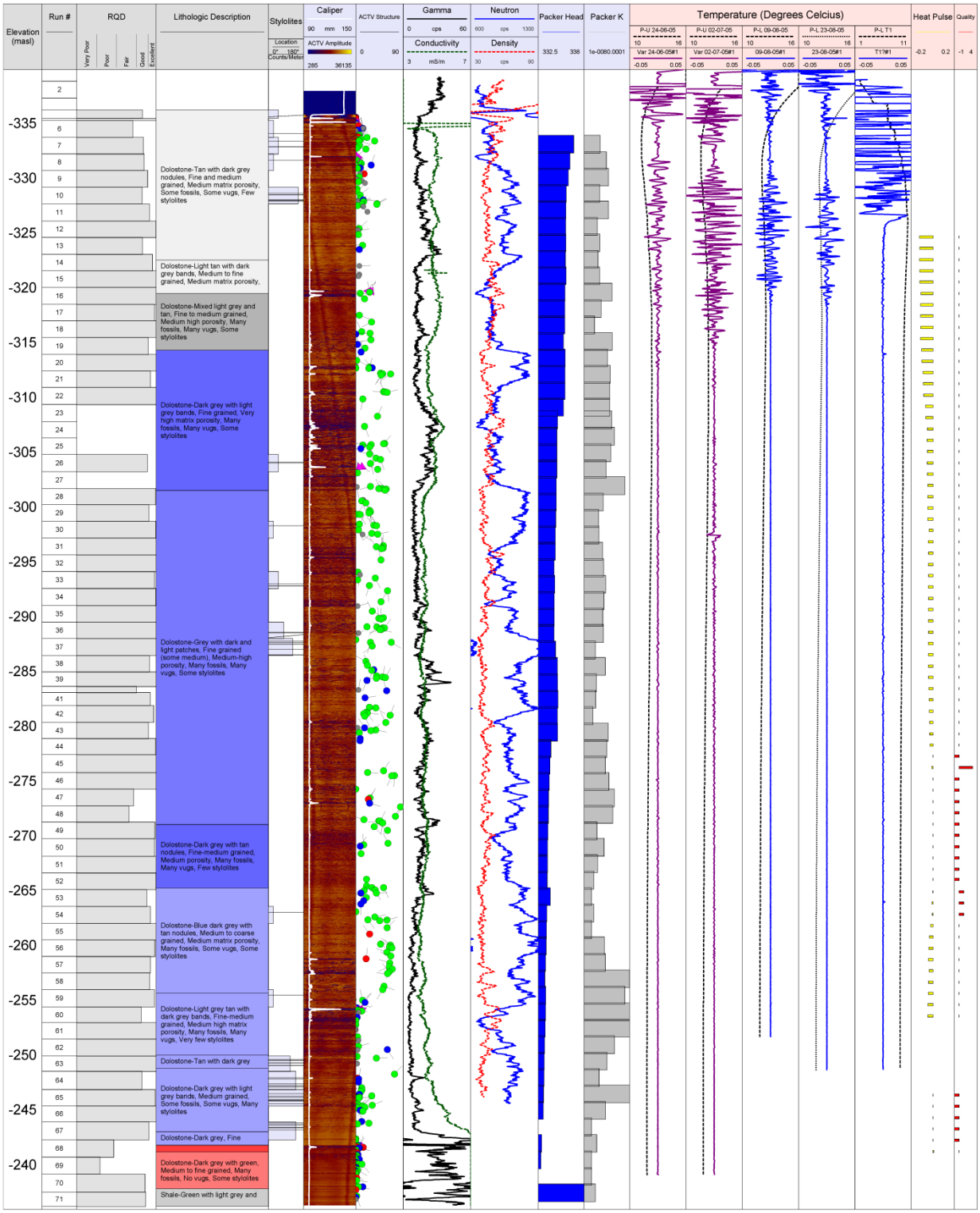

Figure 4.40: MW-25 Summary plot.

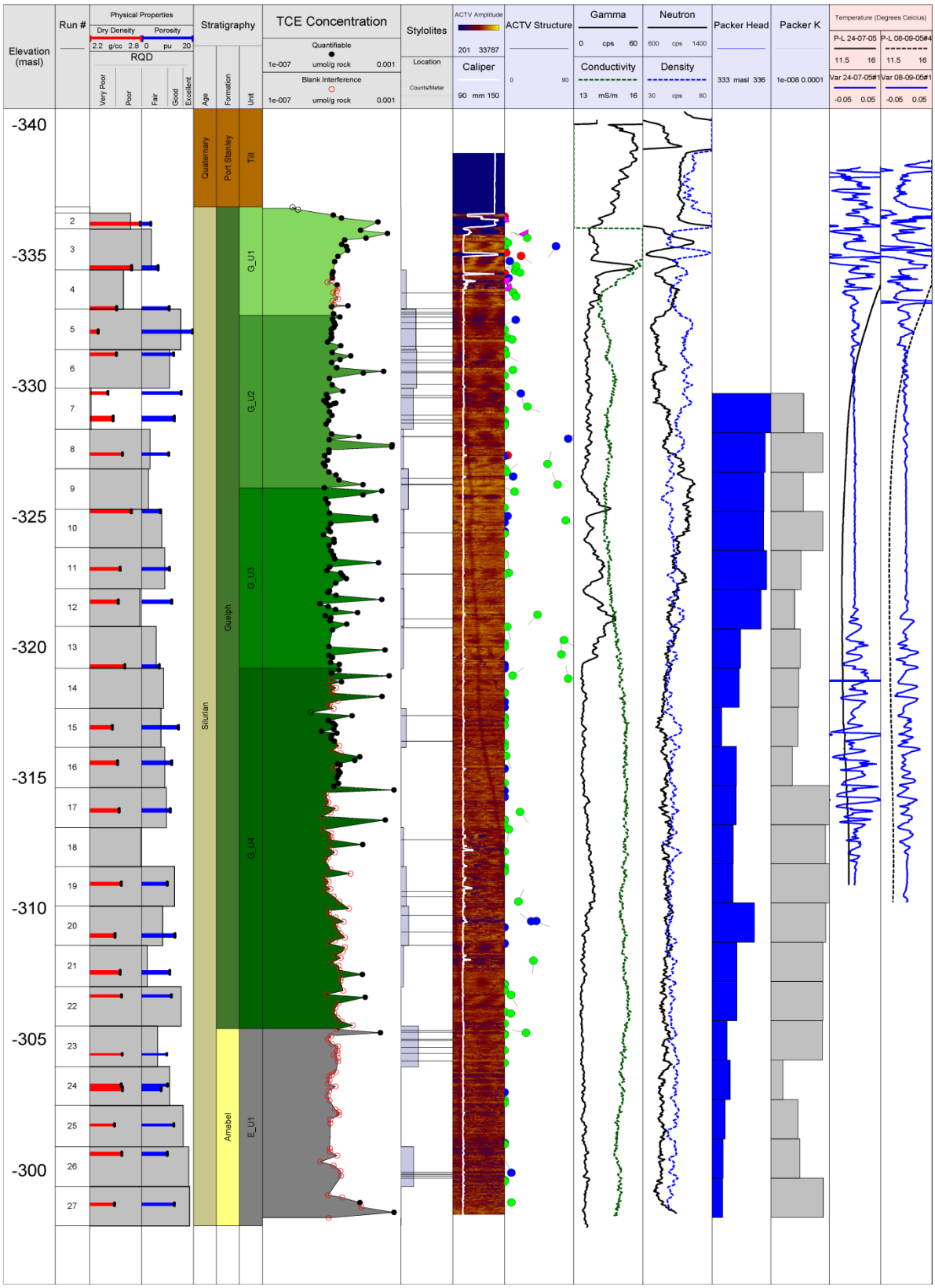

Figure 4.41: MW-26 Summary plot.

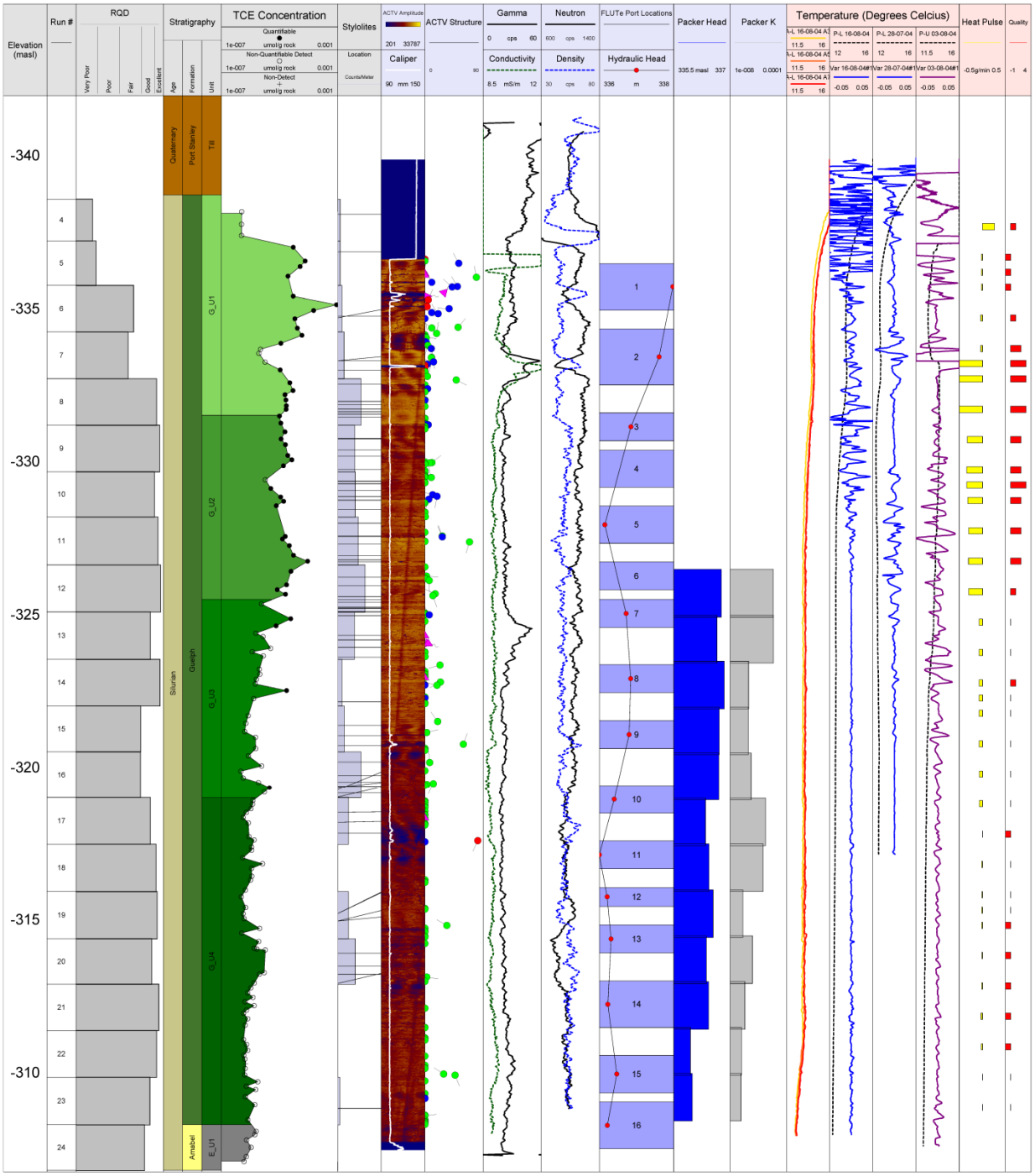

Figure 4.42: MW-367-4 Summary plot.

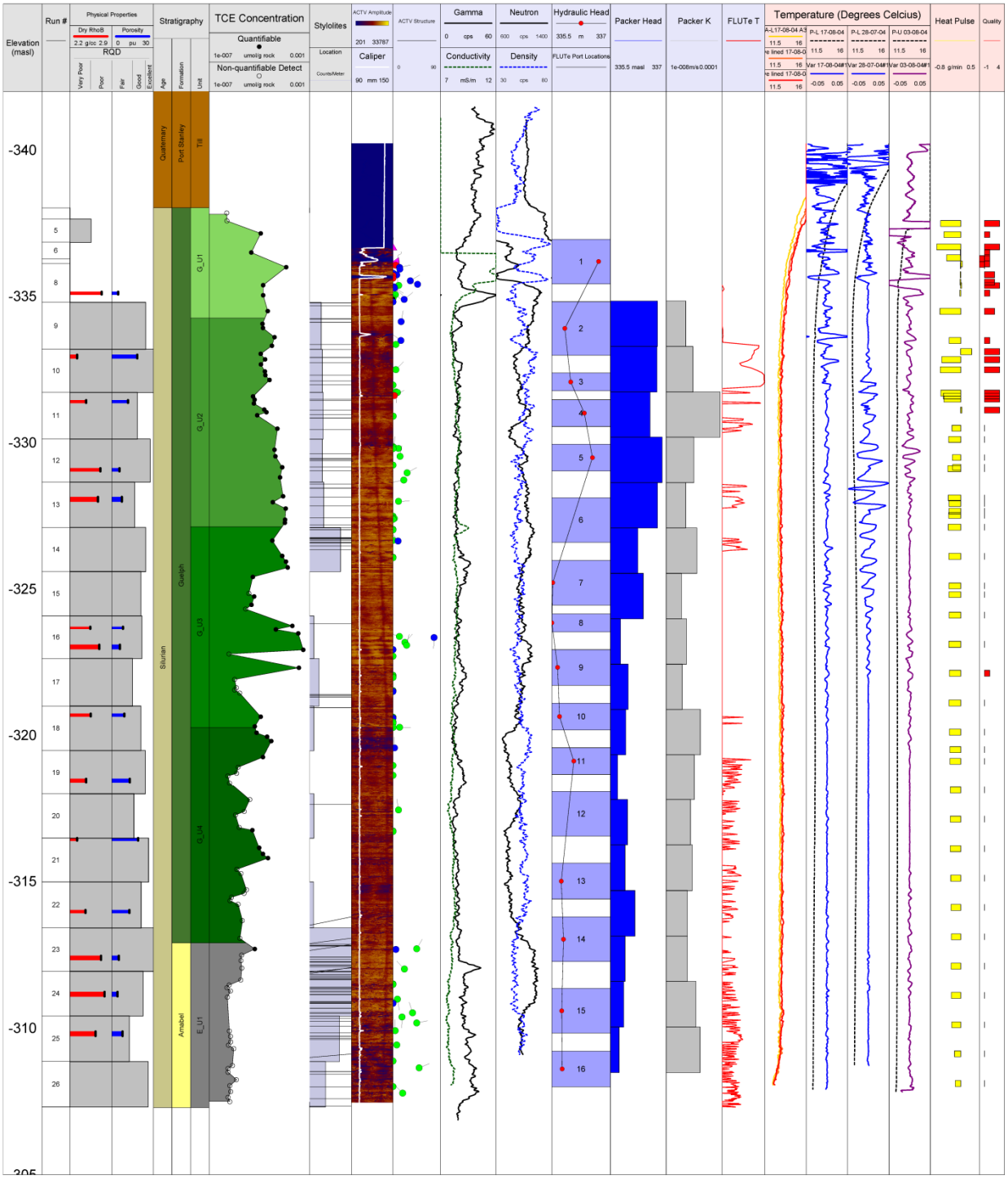

Figure 4.43: MW-367-5 Summary plot.

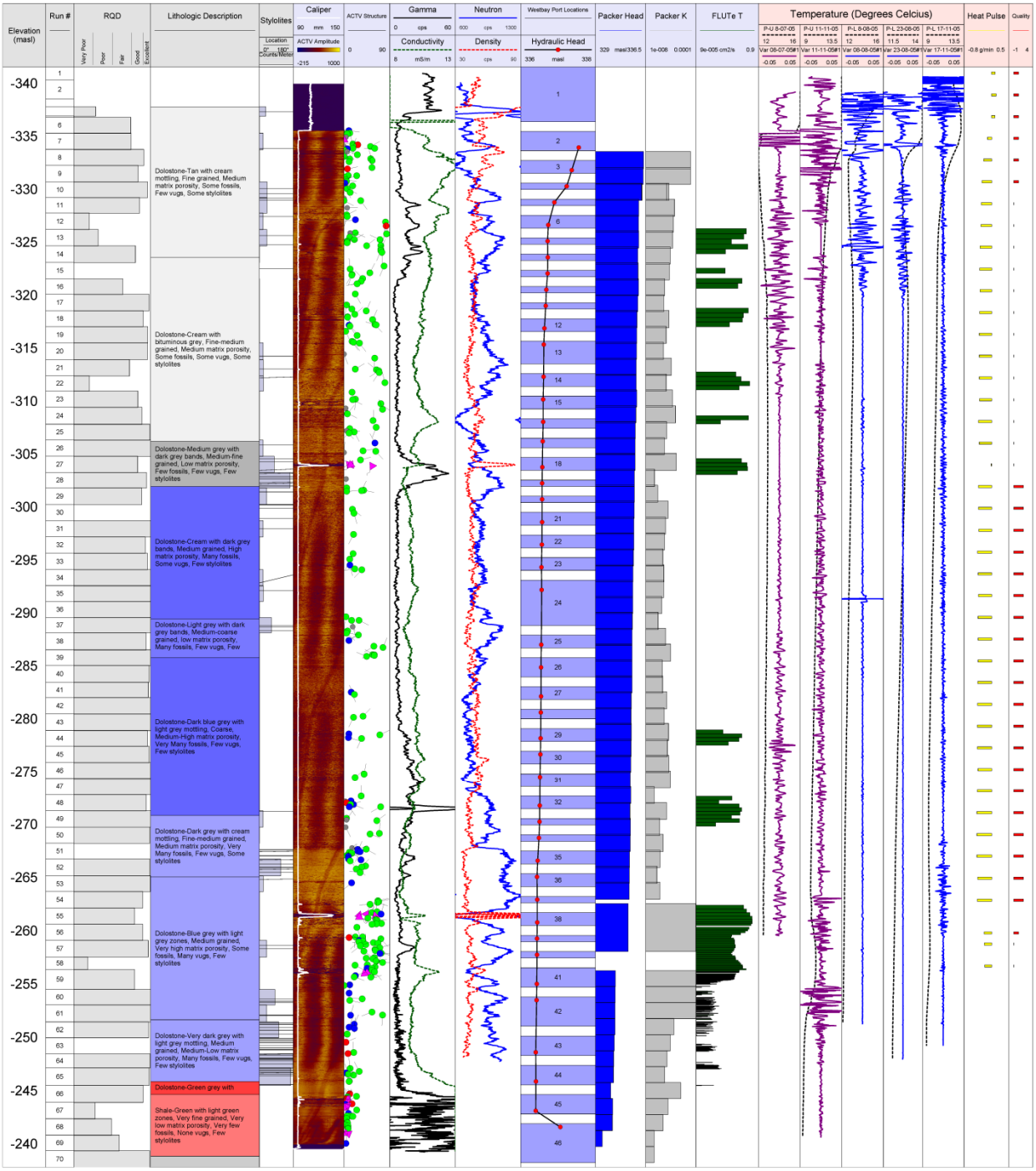

Figure 4.44: MW-367-6 Summary plot.

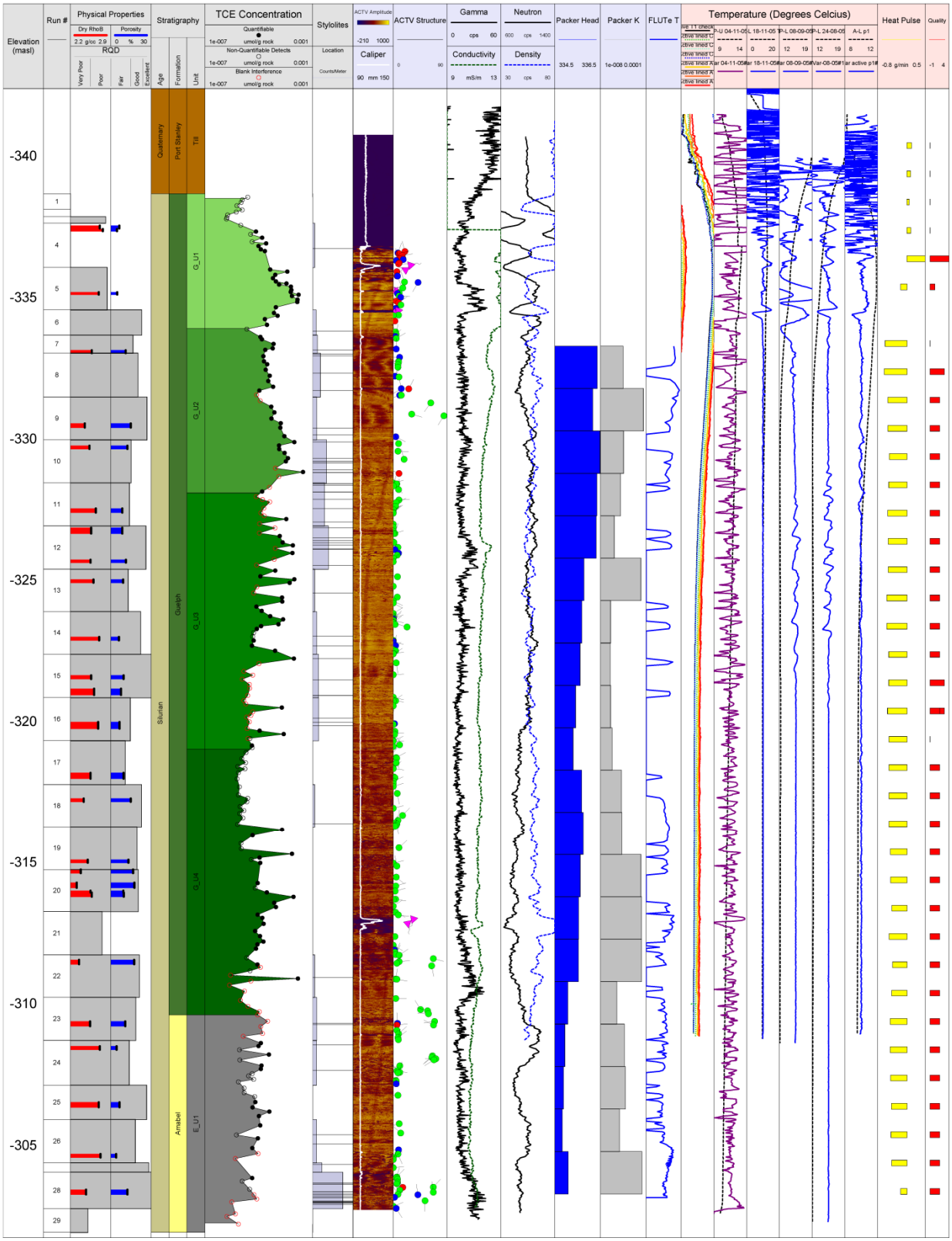

Figure 4.45: MW-367-7 Summary plot.

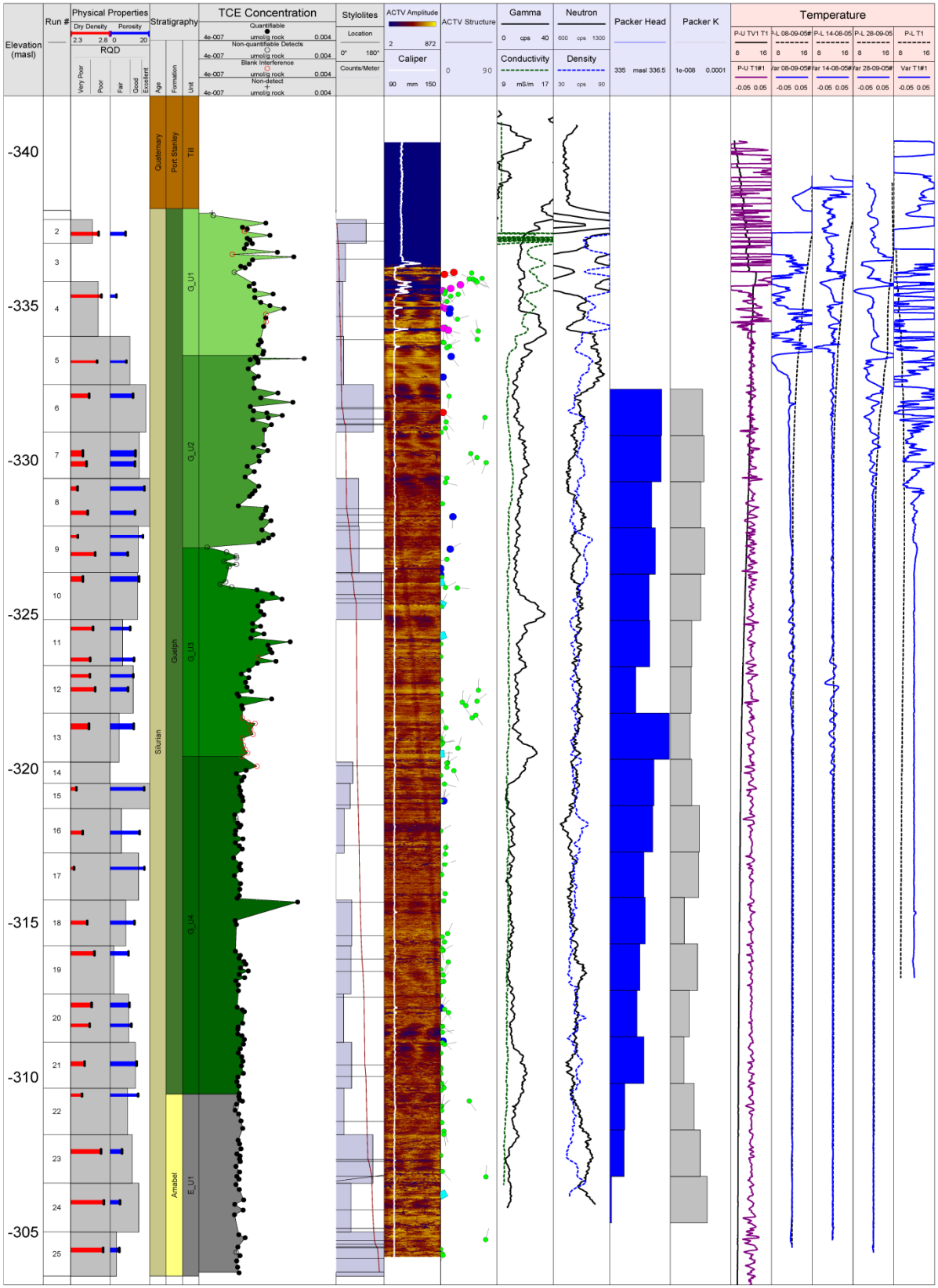

Figure 4.46: MW-367-8 Summary plot.

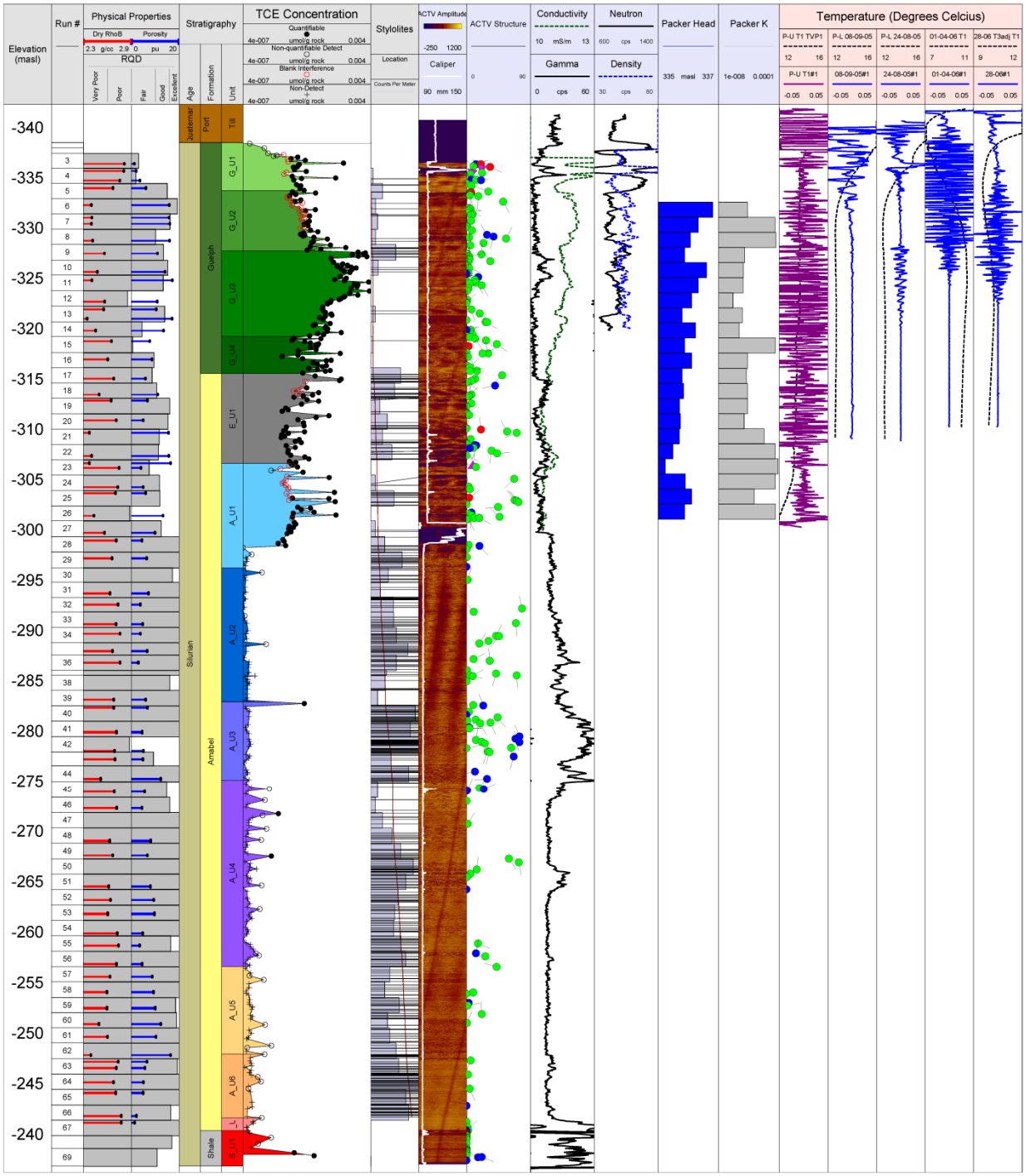

Figure 4.47: MW-367-9 Summary plot.

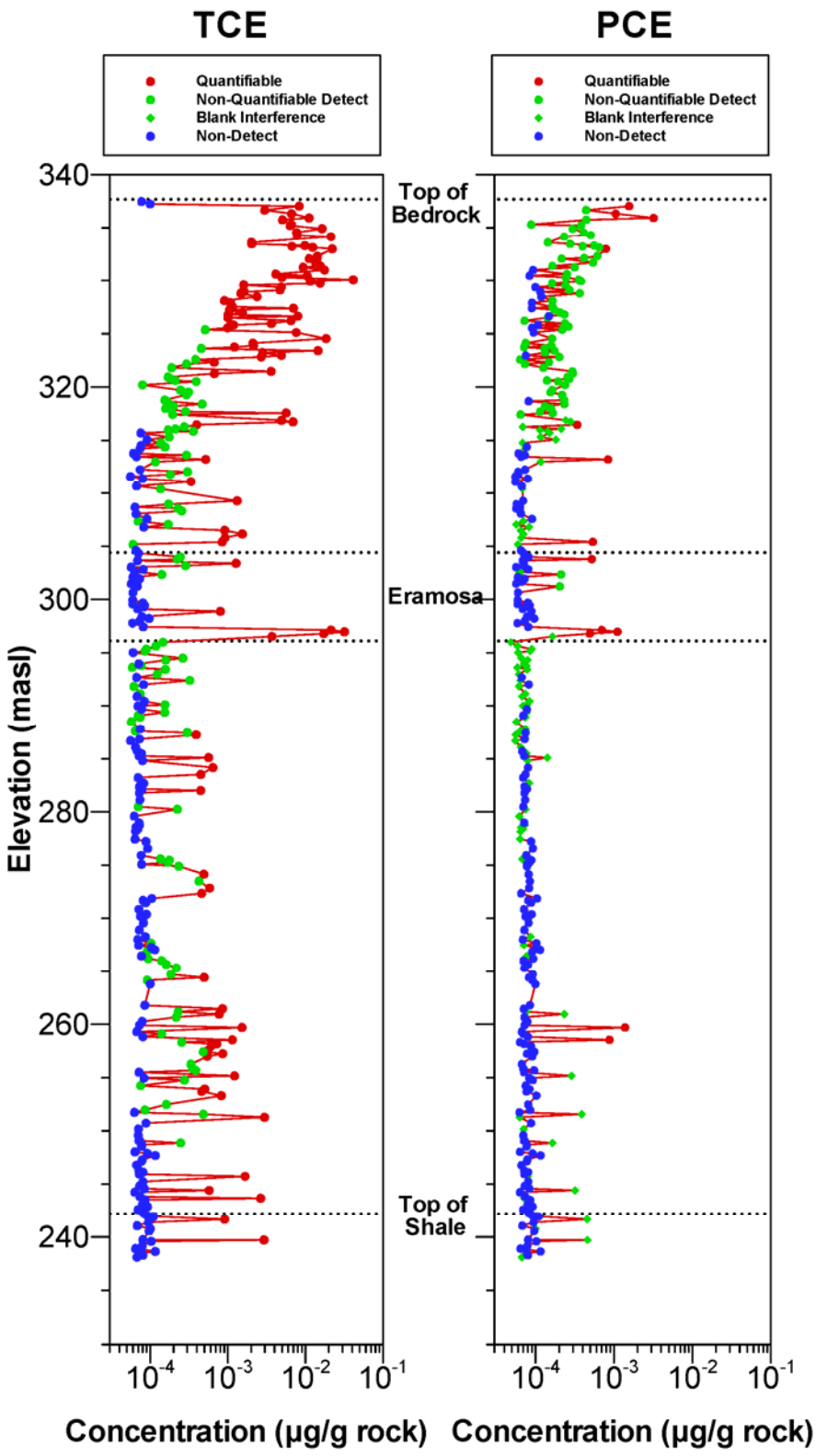

Figure 4.48: MW-22 Concentration profiles (MAE lab preserved – 2004, and MAE field preserved – 2006). Note TCE is found throughout the entire aquifer thickness and into the upper shale.

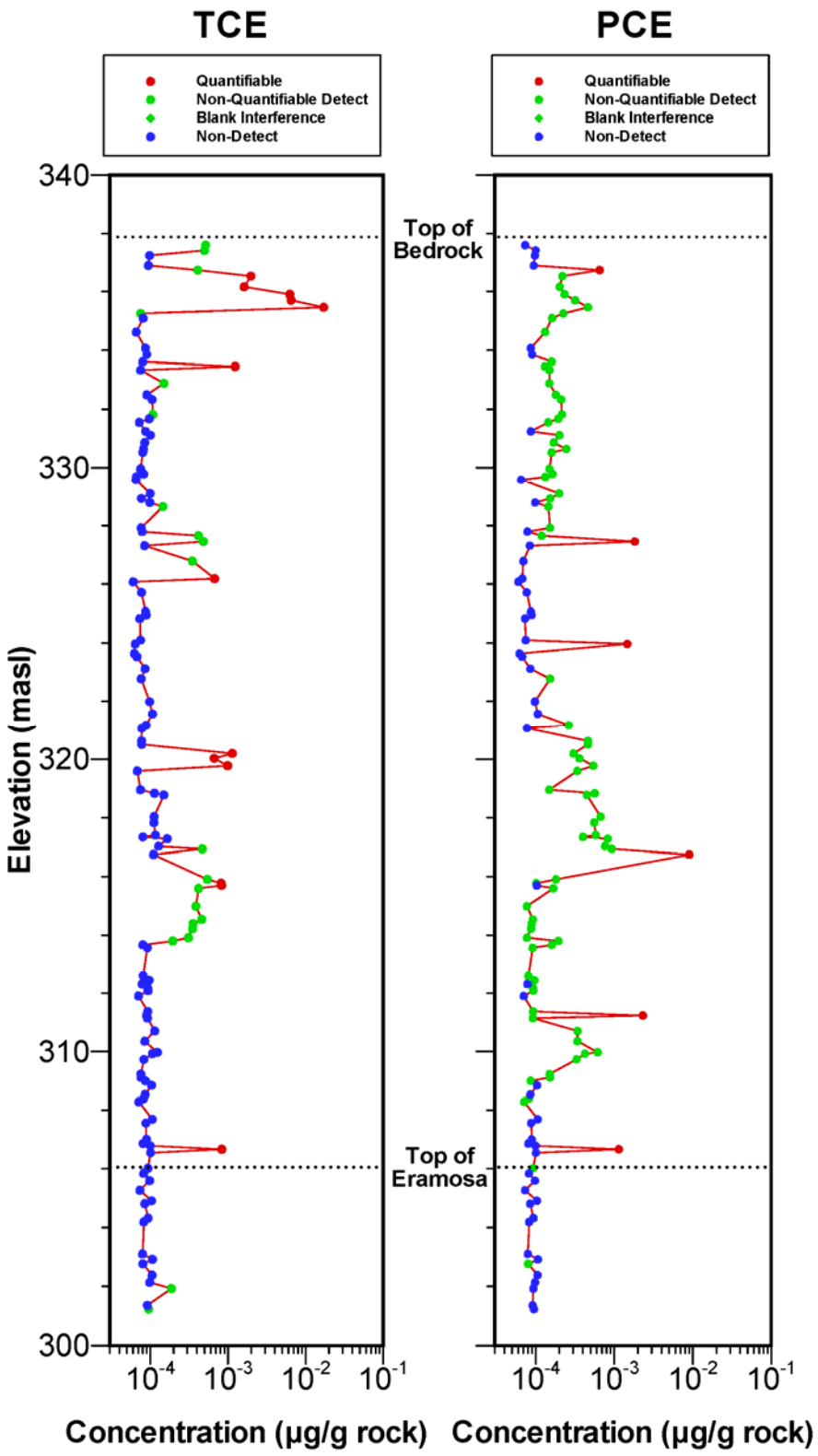

Figure 4.49: MW-23 Concentration profiles (MAE lab preserved – 2004). Low concentrations of TCE were found in this hole with the majority being non-detect values.

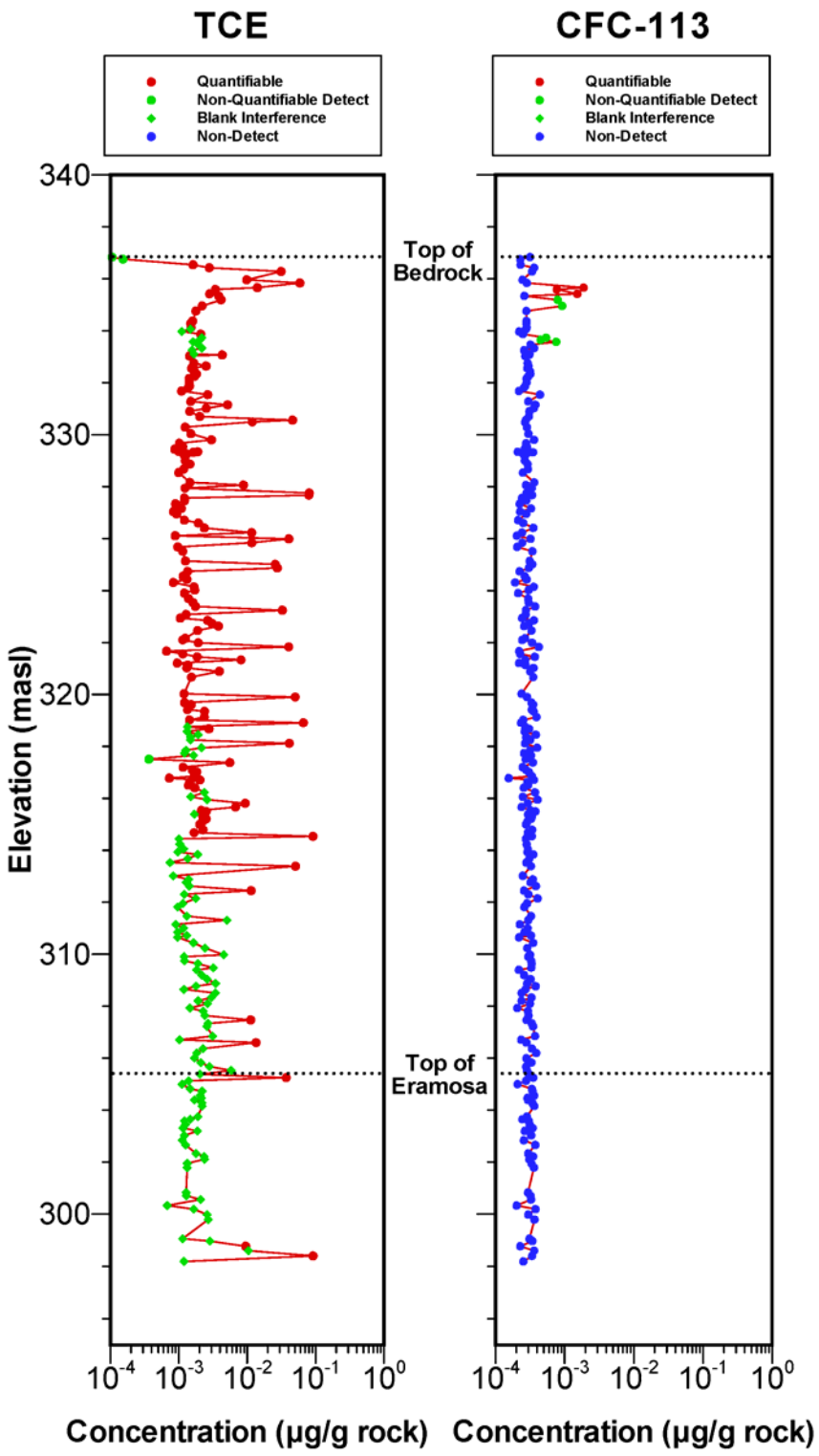

Figure 4.50: MW-26 Concentration profiles (MAE field preserved – 2005). This corehole showed a series of detected values for TCE at relatively low concentrations throughout the hole but did not show many large bulges. This suggests that some form of cross-contamination may have occurred for the TCE results.

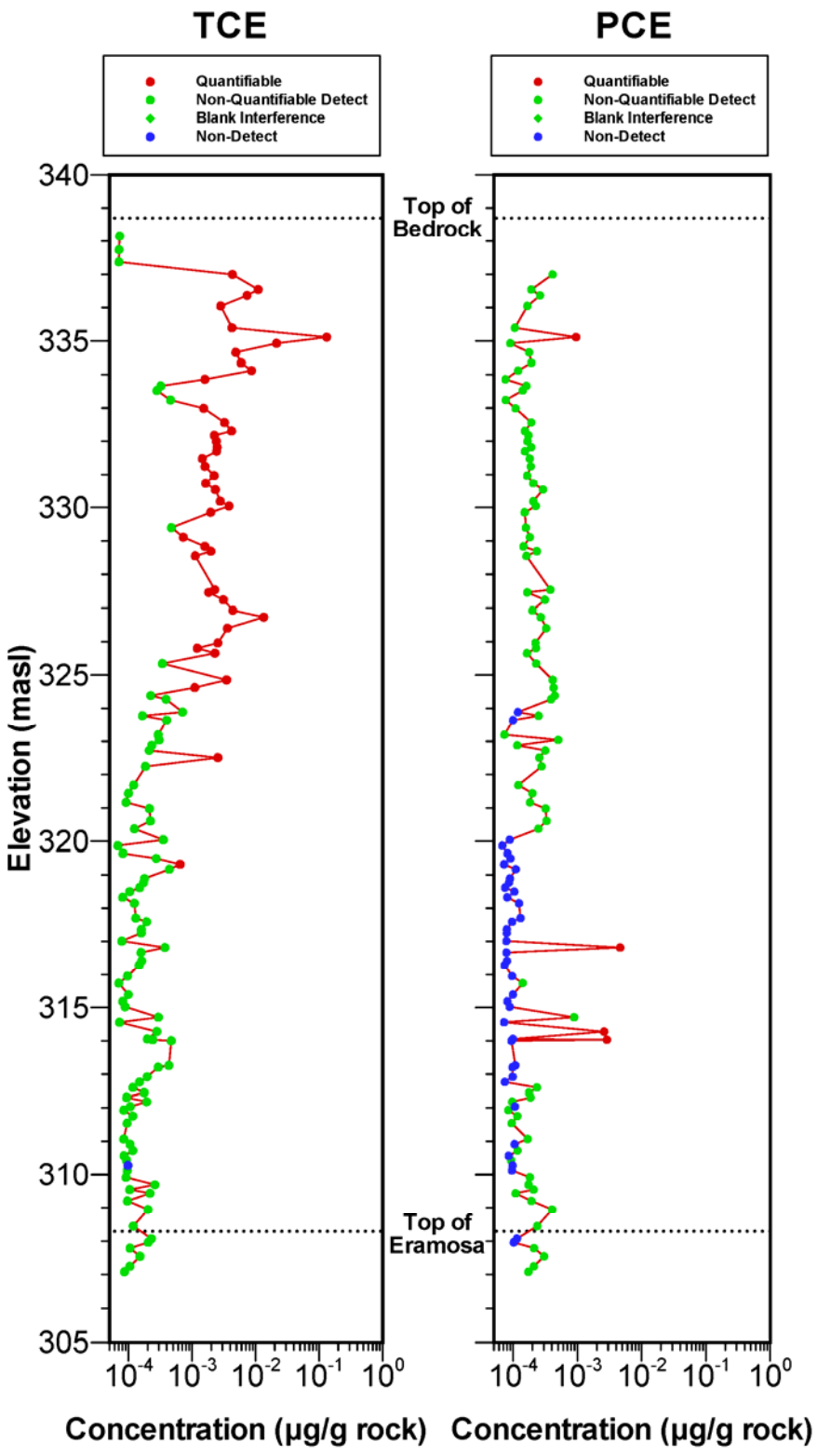

Figure 4.51: MW-367-4 Concentration profiles (MAE lab preserved – 2004). Three TCE bulges are apparent in the upper 15 m followed by a series of low concentration detects. The PCE and TCE concentrations aren't necessarily correlated.

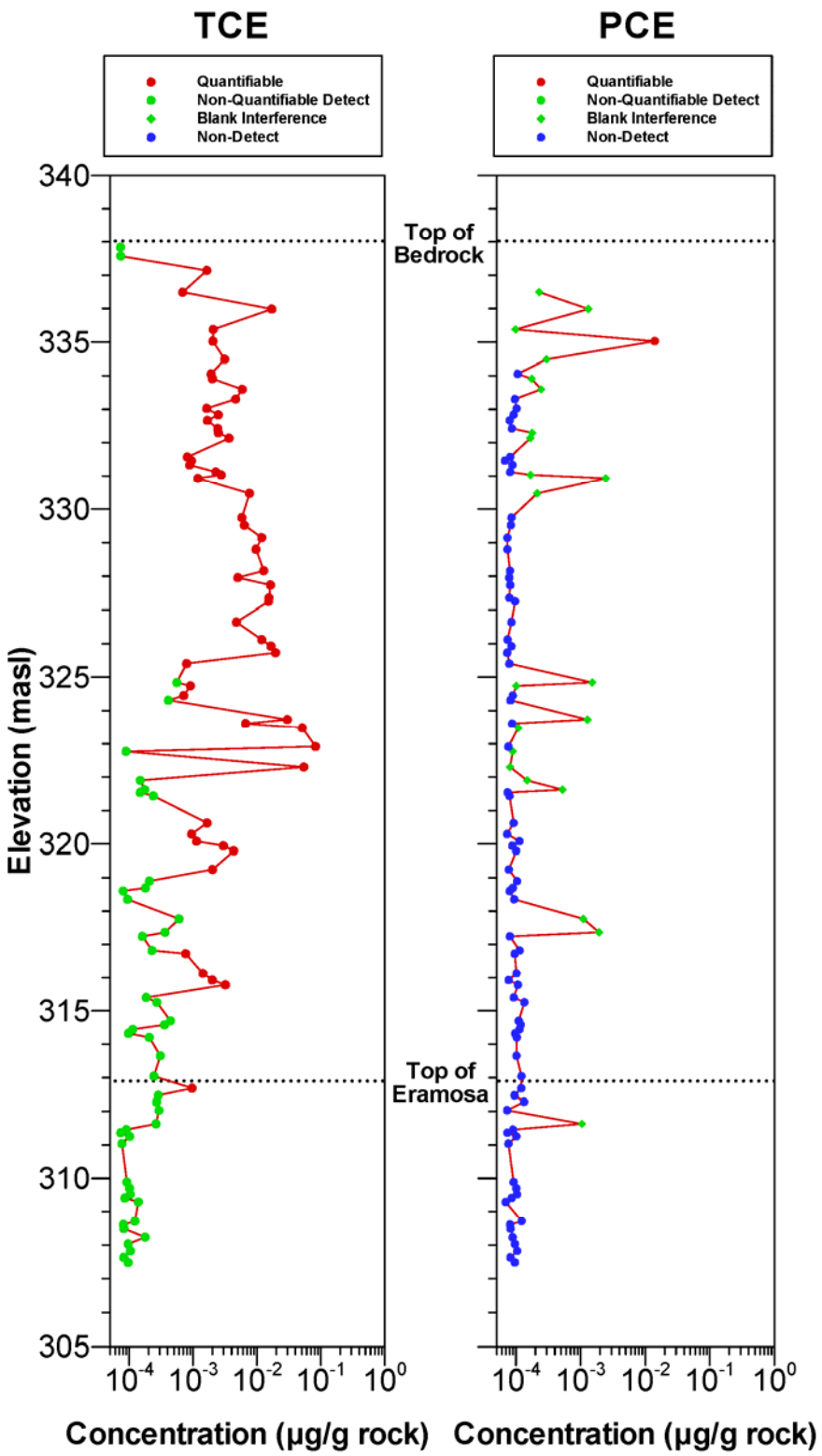

Figure 4.52: MW-367-5 Concentration profiles (MAE lab preserved – 2004). Three TCE bulges are apparent in the upper 20 m followed by a series of low concentration detects. The PCE and TCE concentrations aren't necessarily correlated.

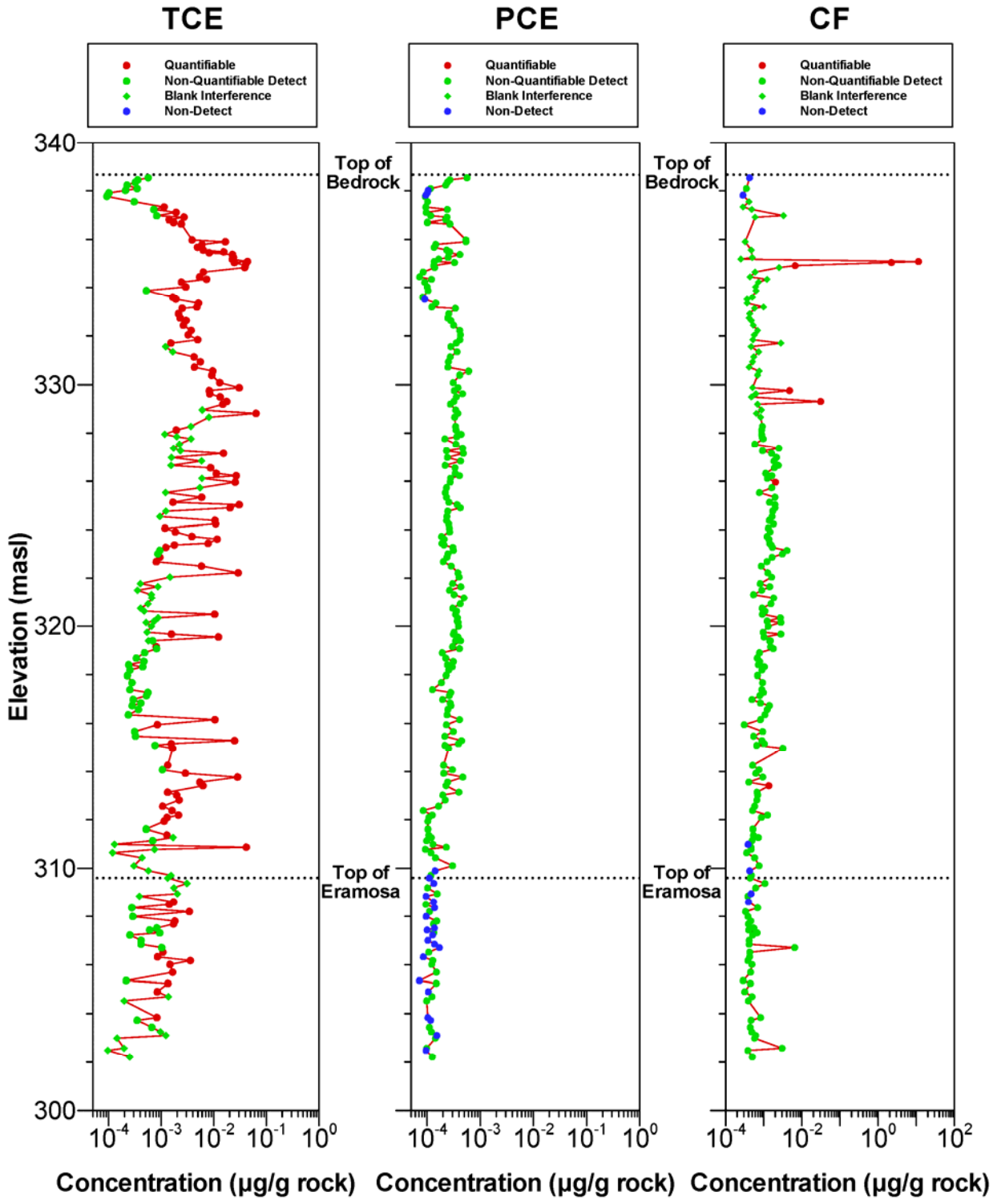

Figure 4.53: MW-367-7 Concentration profiles (MAE field preserved – 2005). The TCE profile shows three bulges in the upper 12 m followed by a series of peaks. NOTE the change in scale for CF.

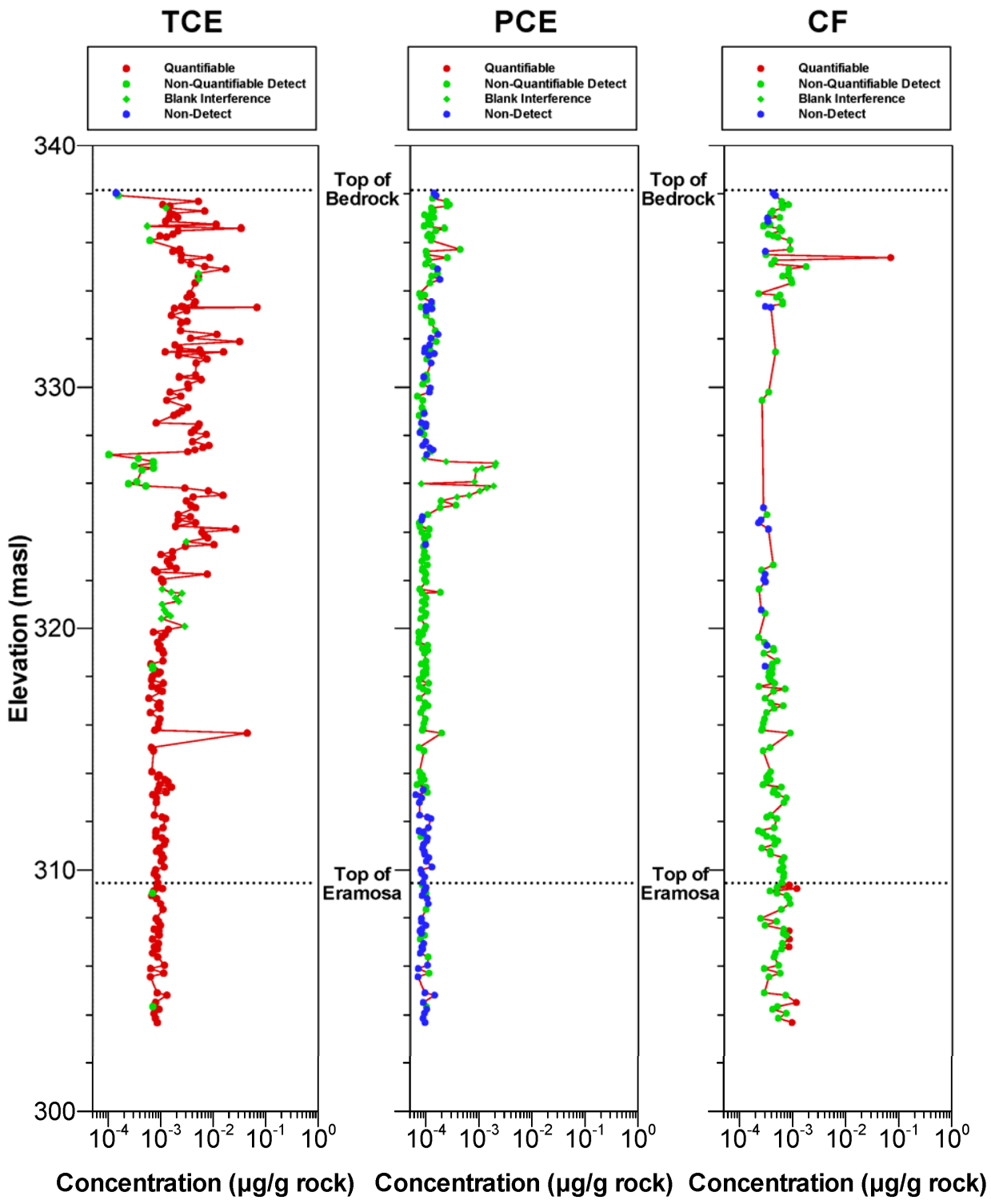

Figure 4.54: MW-367-8 Concentration profiles (MAE field preserved – 2005).

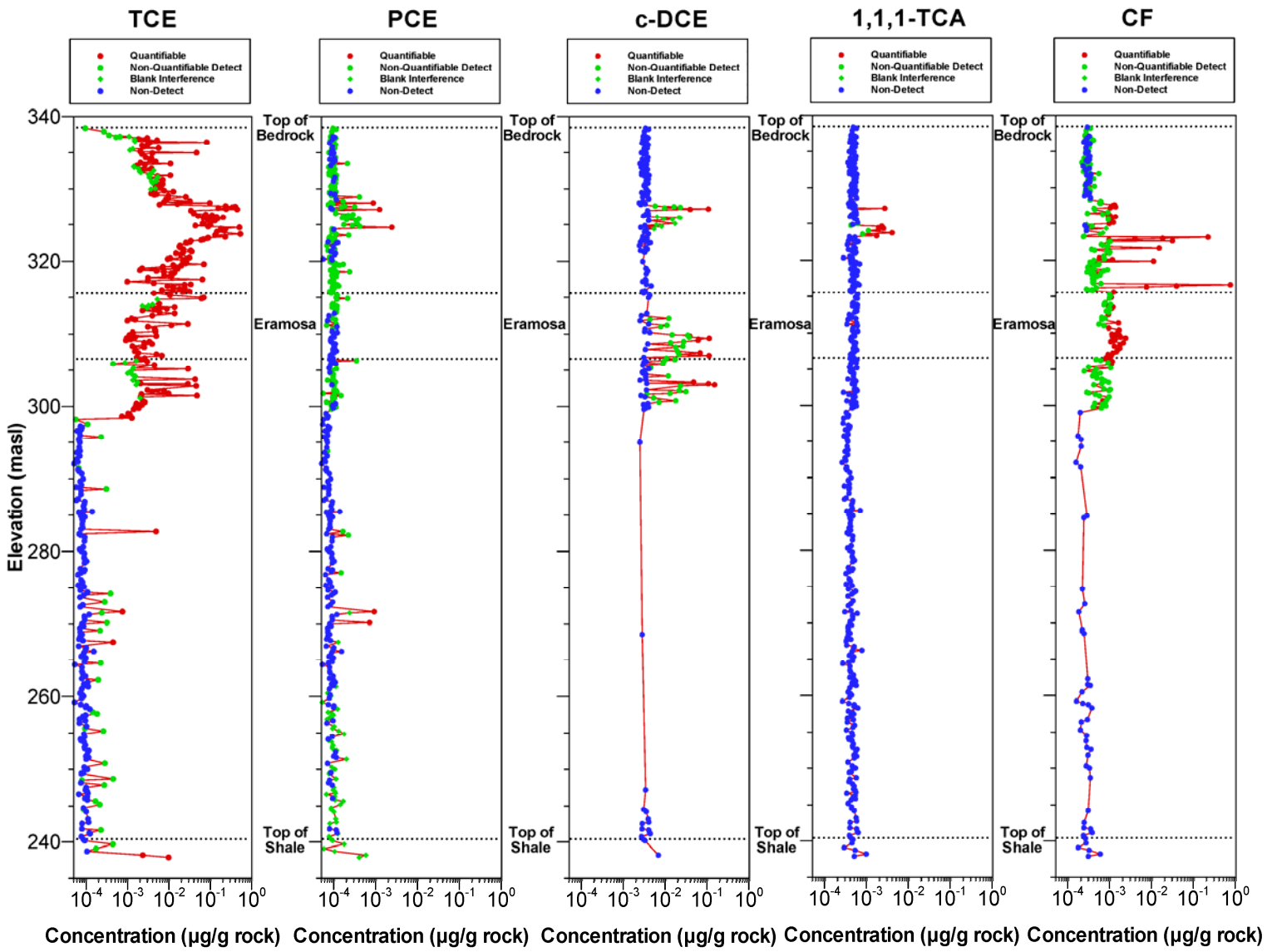

Figure 4.55: MW-367-9 Concentration profiles (MAE field preserved – 2005, and 2006).

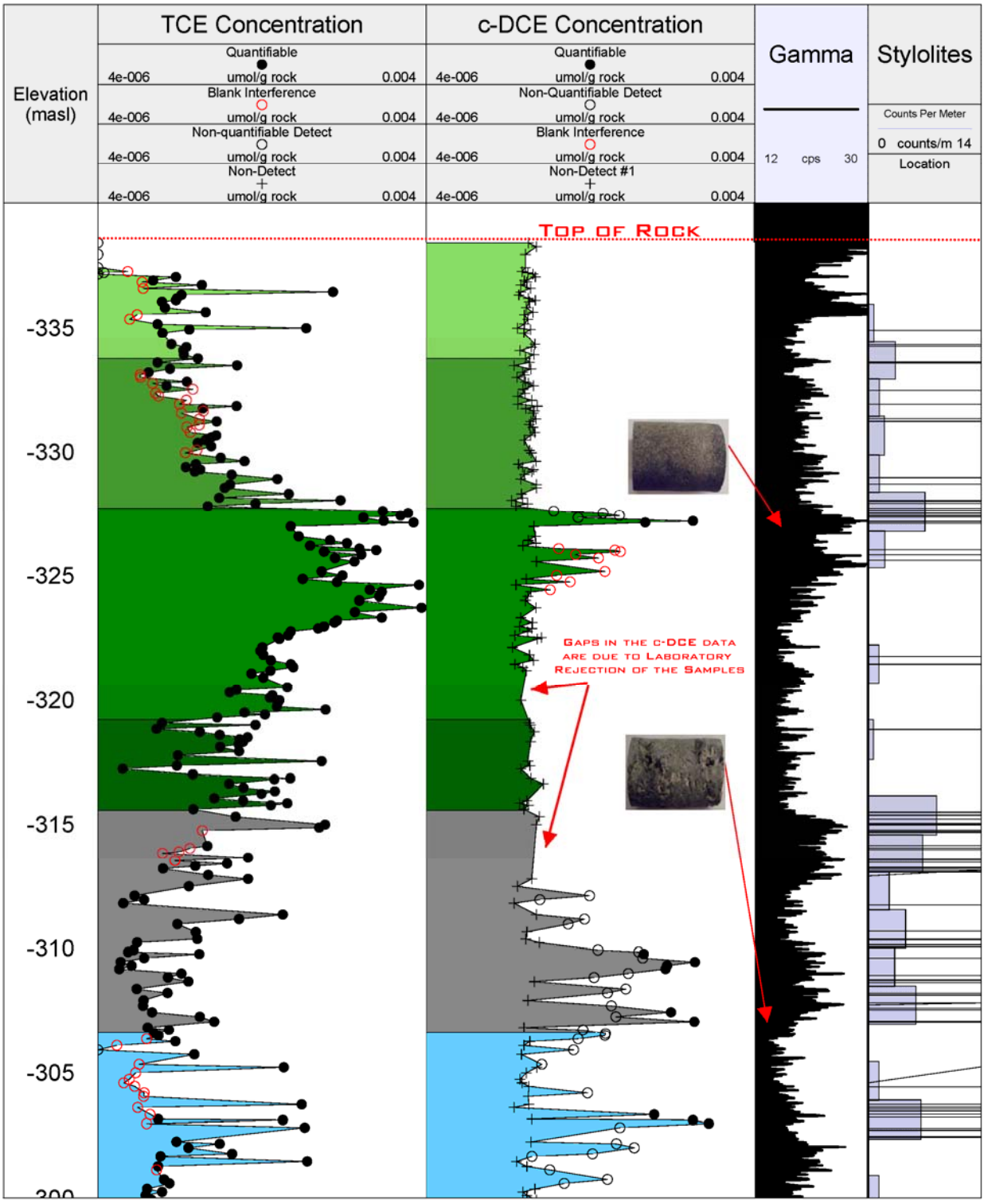

Figure 4.56: Comparison of c-DCE with TCE stylolite and gamma logs. Note that c-DCE concentrations are often greater than TCE concentrations below 312 masl. Portions of the c-DCE profile are missing due to the lab rejection of the samples.

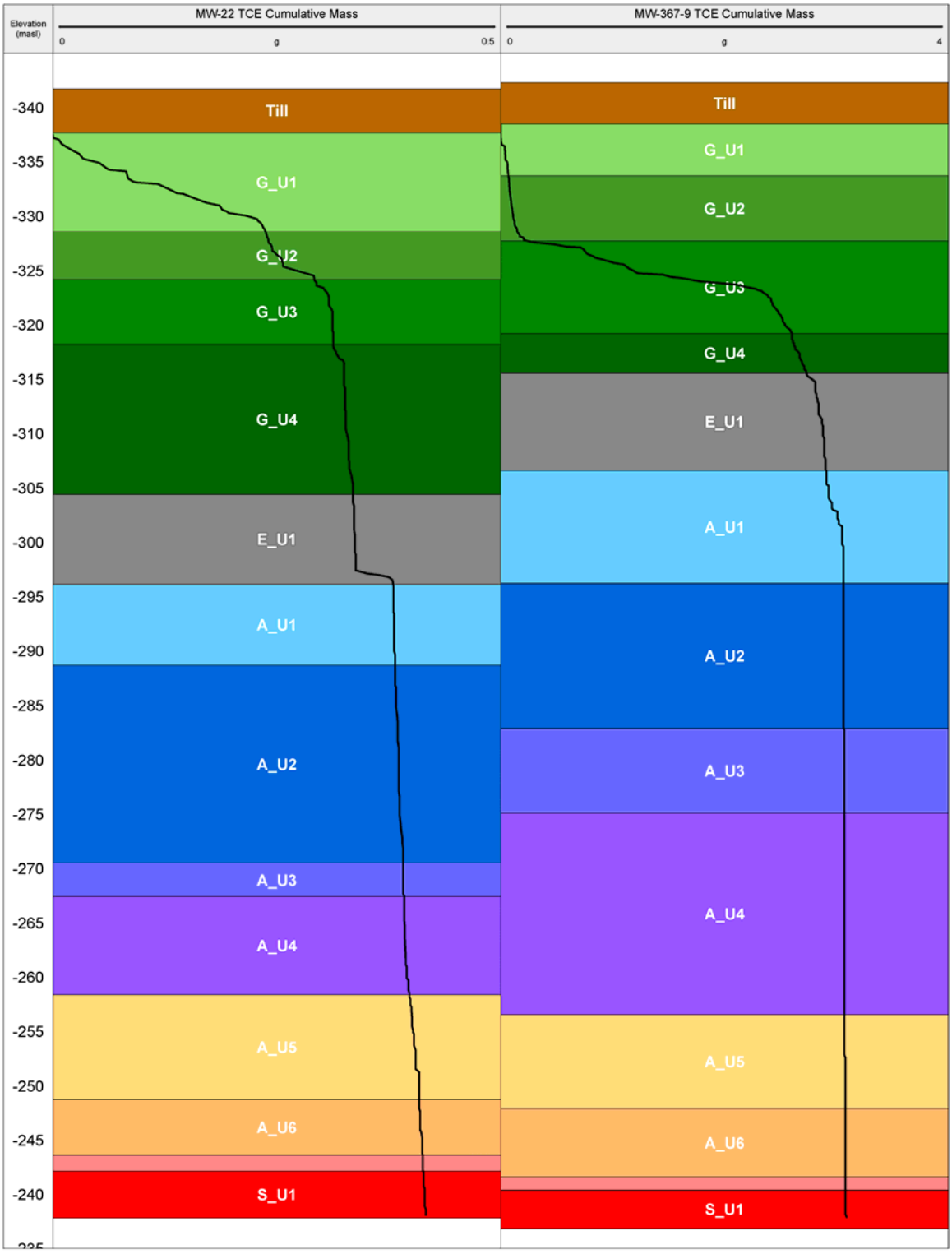

Figure 4.57: Calculated cumulative mass of TCE (based on a 1 m^2 vertical column). Vertical portions indicate low concentrations, horizontal portions indicate high concentrations. The majority of the contaminant mass resides in the Guelph formation.

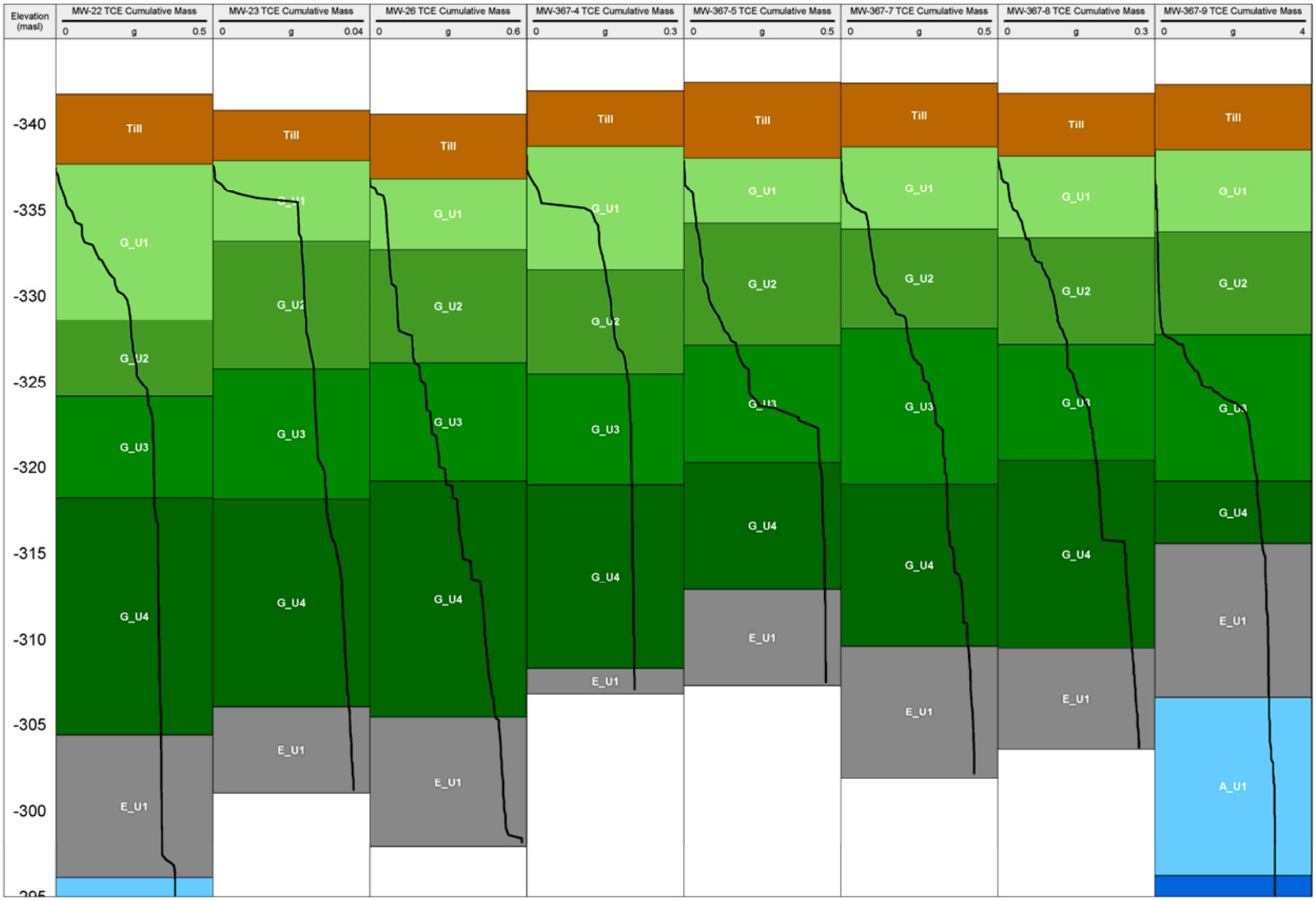

Figure 4.58: Guelph formation calculated cumulative mass for TCE based on a 1 m^2 vertical column. Vertical portions indicate low concentrations, horizontal portions indicate high concentrations.

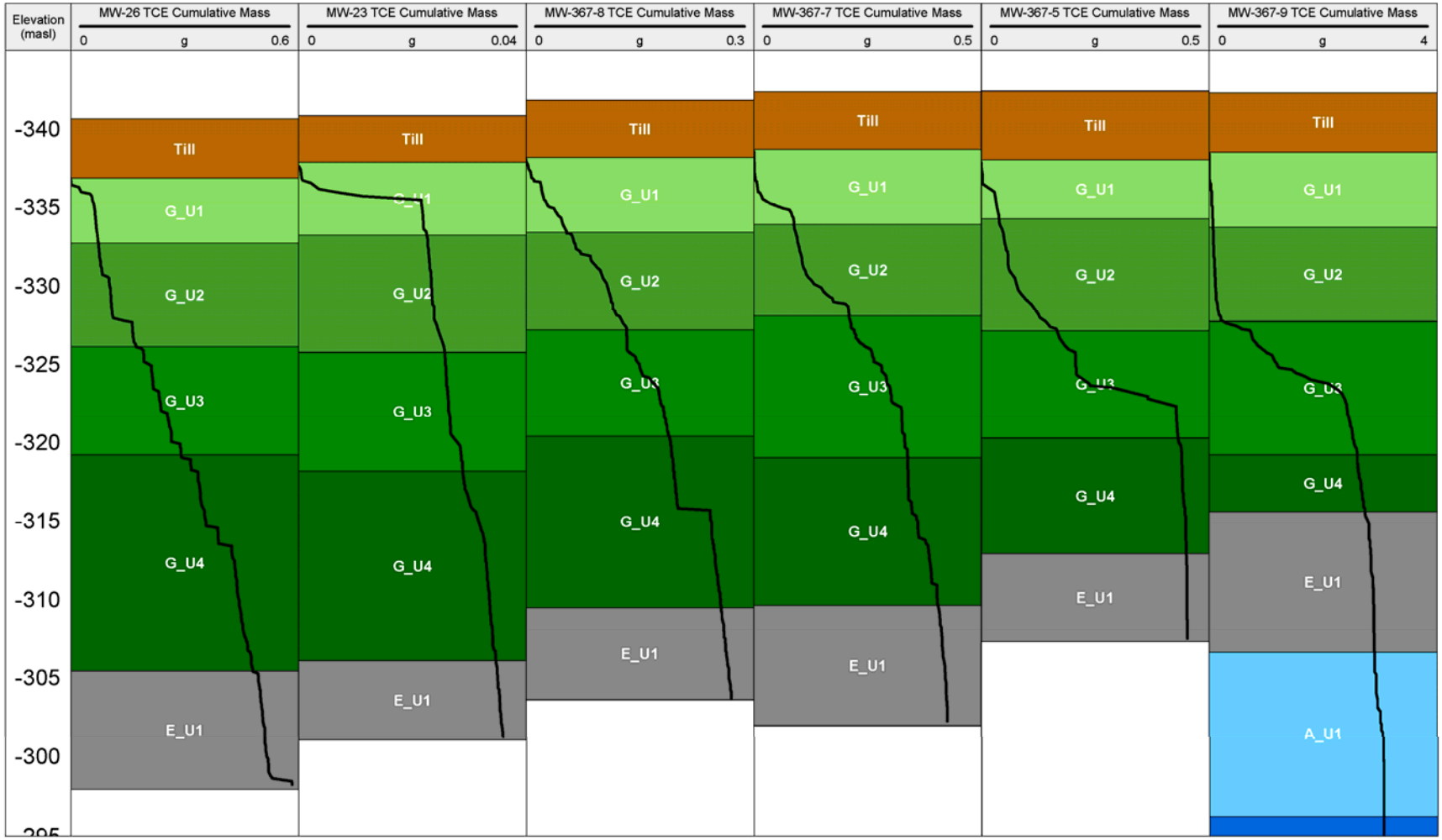

Figure 4.59: Cross Section C-C' calculated cumulative mass for TCE based on a 1 m^2 vertical column. Vertical portions indicate low concentrations, horizontal portions indicate high concentrations.

References

Advanced Logic Technology. ABI 40 Slimhole Acoustic Televiewer. ALT. http://www.alt.lu . 2002. 12-1-2008.
Ref Type: Electronic Citation

Allen, L. S., Tittle, C. W., Mills, W. R., & Caldwell, R. L. 1967, "Dual-Spaced Neutron Logging for Porosity", *Geophysics*, vol. 32, no. 1, p. 60-68.

Amirtharaj, E. 2007, *Manual on Experimental Methods for Physical Property Measurements of Rocks* University of Waterloo.

Austin, D. C. 2005, *Hydrogeologic controls on contaminant distribution within a multi-component DNAPL zone in a sedimentary rock aquifer in south central Wisconsin,* Master's thesis, Earth Sciences Department, University of Waterloo.

Bangkedphol, S., Sakultantimetha, A., Keenan, H. E., & Songsasen, A. 2006, "Optimization of microwave-assisted extraction of polycyclic aromatic hydrocarbons from sediments", *Journal of Environmental Science and Health Part A-Toxic/Hazardous Substances & Environmental Engineering*, vol. 41, no. 6, pp. 1105-1116.

Bear, J., Tsang, C. F., & de Marsily, G. 1993, *Flow and Contaminant Transport in Fractured Rock* Academic Press Inc..

Berkowitz, B. 2002, "Characterizing flow and transport in fractured geological media: A review", *Advances in Water Resources*, vol. 25, no. 8-12, pp. 861-884.

Bolton, T. E. Silurian stratigraphy and palaeontology of the Niagara Escarpment in Ontario. Geological Survey of Canada Memoir 289, 1-145. 1957.
Ref Type: Serial (Book,Monograph)

Bolton, T. E. 1953, "Silurian formations of the Niagara Escarpment in Ontario (preliminary account)", *Geological Survey of Canada, Paper 53-23*.

Burns, L. S. 2005, *Fracture network characteristics and velocities of groundwater, heat and contaminants in a dolostone aquifer in Cambridge, Ontario,* Master's thesis, Earth Sciences Department, University of Waterloo.

Byers, S. C., Mills, E. L., & Stewart, P. L. 1978, "Comparison of Methods of Determining Organic-Carbon in Marine-Sediments, with Suggestions for A Standard Method", *Hydrobiologia*, vol. 58, no. 1, pp. 43-47.

Camel, V. 2001, "Recent extraction techniques for solid matrices-supercritical fluid extraction, pressurized fluid extraction and microwave-assisted extraction: their potential and pitfalls", *Analyst*, vol. 126, no. 7, pp. 1182-1193.

Cameron, F. K. & Patten, H. E. 1907, "The distribution of solute between water and soil", *Journal of Physical Chemistry*, vol. 11, no. 8, pp. 581-593.

Carro, N., Garcia, I., Ignacio, M., & Mouteira, A. 2006, "Microwave-assisted solvent extraction and gas chromatography ion trap mass spectrometry procedure for the determination of persistent organochlorine pesticides (POPs) in marine sediment", *Analytical and Bioanalytical Chemistry*, vol. 385, no. 5, pp. 901-909.

Cherry, J. A., Parker, B. L., & Keller, C. 2007, "A new depth-discrete multilevel monitoring approach for fractured rock", *Ground Water Monitoring and Remediation*, vol. 27, no. 2, pp. 57-70.

Chiba, M. & Morley, H. V. 1968, "Factors Influencing Extraction of Aldrin and Dieldrin Residues from Different Soil Types", *Journal of Agricultural and Food Chemistry*, vol. 16, no. 6, p. 916-922.

Churcher, P. L. & Dickhout, R. D. 1987, "Analysis of Ancient Sediments for Total Organic-Carbon - Some New Ideas", *Journal of Geochemical Exploration*, vol. 29, no. 1-3, pp. 235-246.

City of Guelph. 2006 Water and Wastewater Operating and Capital Budgets. http://guelph.ca/uploads/Finance/Budgets/2006_Water_Waste_Budget.pdf . 2005. 1-23-2008.
Ref Type: Electronic Citation

Dekeyser, L.-K. 2006, *The Silurian Amabel and Guelph formations of the Bruce Peninsula: insights into stratigraphy and diagenesis from petrography and ground-penetrating radar,* Master's thesis, Earth Sciences Department, University of Waterloo.

Dekeyser, L.-K. 2005, *Regional Corehole Geological Logs*, University of Waterloo.

Dincutoiu, I., Gorecki, T., & Parker, B. L. 2006, "Microwave-assisted extraction of trichloroethylene from clay samples", *International Journal of Environmental Analytical Chemistry*, vol. 86, no. 15, pp. 1113-1125.

Doherty, R. E. 2000, "A history of the production and use of carbon tetrachloride, tetrachloroethylene, trichloroethylene and 1,1,1-trichloroethane in the United States: Part 2 - Trichloroethylene and 1,1,1-trichloroethane", *Environmental Forensics*, vol. 1, no. 2, pp. 83-93.

Ellis, D. V. 1990, "Some Insights on Neutron Measurements", *IEEE Transactions on Nuclear Science*, vol. 37, no. 2, pp. 959-965.

Ellis, D. V. & Singer, J. M. 2007, *Well Logging for Earth Scientists*, 2nd edn, Springer, Dordrecht.

Foster, S. S. D. 1975, "Chalk Groundwater Tritium Anomaly - Possible Explanation", *Journal of Hydrology*, vol. 25, no. 1-2, pp. 159-165.

Freeze, R. A. & Cherry, J. A. 1979, *Groundwater* Prentice-Hall, Englewood Cliffs, N.J.

Friedman, I. 1965, "Interstitial Water from Deep Sea Sediments", *Journal of Geophysical Research*, vol. 70, no. 16, p. 4067.

Galle, C. 1994, "Neutron Porosity Logging and Core Porosity Measurements in the Beauvoir Granite, Massif-Central Range, France", *Journal of Applied Geophysics*, vol. 32, no. 2-3, pp. 125-137.

Gamsby and Mannerow Limited 2006, *Hydrogeological Investigation and Monitoring Report Guelph Tool Inc.*

Garbarini, D. R. & Lion, L. W. 1986, "Influence of the Nature of Soil Organics on the Sorption of Toluene and Trichloroethylene", *Environmental Science & Technology*, vol. 20, no. 12, pp. 1263-1269.

Gartner Lee Limited 2004, *Guelph/Eramosa Township Regional Groundwater Characterization and Wellhead Protection Study*.

Goldstein, K. J., Vitolins, A. R., Navon, D., Parker, B. L., Chapman, S. W., & Anderson, G. A. 2004, "Characterization and pilot-scale studies for chemical oxidation remediation of fractured shale", *Remediation Journal*, vol. 14, no. 4, pp. 19-37.

Grisak, G. E. & Pickens, J. F. 1980, "Solute Transport Through Fractured Media .1. the Effect of Matrix Diffusion", *Water Resources Research*, vol. 16, no. 4, pp. 719-730.

Hadermann, J. & Heer, W. 1996, "The Grimsel (Switzerland) migration experiment: Integrating field experiments, laboratory investigations and modelling", *Journal of Contaminant Hydrology*, vol. 21, no. 1-4, pp. 87-100.

Hatzinger, P. B. & Alexander, M. 1995, "Effect of Aging of Chemicals in Soil on Their Biodegradability and Extractability", *Environmental Science & Technology*, vol. 29, no. 2, pp. 537-545.

Hewitt, A. D. 1998, "Comparison of sample preparation methods for the analysis of volatile organic compounds in soil samples: Solvent extraction vs vapor partitioning", *Environmental Science & Technology*, vol. 32, no. 1, pp. 143-149.

Hinsby, K., Mckay, L. D., Jorgensen, P., Lenczewski, M., & Gerba, C. P. 1996, "Fracture aperture measurements and migration of solutes, viruses, and immiscible creosote in a column of clay-rich till", *Ground Water*, vol. 34, no. 6, pp. 1065-1075.

Hurley, J. C. 2003, *Rock core investigation of DNAPL penetration and persistence in fractured sandstone,* Master's thesis, Earth Sciences Department, University of Waterloo.

Jagger Hims Limited 1998, *Aquifer Performance Evaluation, Volume 1, Northwest Quadrant: Prepared for the City of Guelph*.

Johnsen, R. E. & Starr, R. I. 1967, "Ultrasonic Extraction of Insecticides in Soil .I. Comparison of Extraction Methods and Solvent Systems Over 3 Time Intervals", *Journal of Economic Entomology*, vol. 60, no. 6, p. 1679-1682.

Karickhoff, S. W. 1981, "On the Sorption of Neutral Organic Solutes in Soils", *Journal of Agricultural and Food Chemistry*, vol. 29, no. 2, pp. 424-425.

Keller, C. 2007, "Liners and Packers: Similarities and Differences", in *NGWA EPA Fractured Rock Conference*.

Keller, C., Cherry, J. A., & Parker, B. L. 2006, "Comparison of the FLUTe™ Hydraulic Conductivity: Profiling results with Straddle Packer measurements"", in *Geologic Society of America*.

Kennedy, B. A. 1990, *Surface Mining*, 2nd edition edn, Society for Mining, Metallurgy and Exploration, Inc., Littleon, Colorado.

Keys, W. S. 1997, *A practical guide to borehole geophysics in environmental investigations* CRC/Lewis Publishers, Boca Raton, Fla.

Kinniburgh, D. G. & Miles, D. L. 1983, "Extraction and Chemical-Analysis of Interstitial Water from Soils and Rocks", *Environmental Science & Technology*, vol. 17, no. 6, pp. 362-368.

Langer, V. W., Novakowski, K. S., & Woodbury, A. D. 1999, "Sorption of trichloroethene onto stylolites", *Journal of Contaminant Hydrology*, vol. 40, no. 1, pp. 1-23.

Lapcevic, P., Novakowski, K., & Sudicky, E. A. 1999, "Groundwater Flow and Solute Transport in Fractured Media," in *The Handbook of Groundwater Engineering*, CRC Press, Florida, p. 17.1-17.39.

Lawrence, A., Stuart, M., Cheney, C., Jones, N., & Moss, R. 2006, "Investigating the scale of structural controls on chlorinated hydrocarbon distributions in the fractured-porous unsaturated zone of a sandstone aquifer in the UK", *Hydrogeology Journal*, vol. 14, no. 8, pp. 1470-1482.

Lawrence, A. R., Chilton, P. J., Barron, R. J., & Thomas, W. M. A method for determining volatile organic solvents in chalk pore waters (southern and eastern England) and its relevance to the evaluation of groundwater contamination. Journal of Contaminant Hydrology 6[4], 377-386. 1990.
Ref Type: Journal (Full)

Lawrence, A. R., Geol, C., Stuart, M. E., Barker, J. A., & Tester, D. J. 1996, "Contamination of chalk groundwater by chlorinated solvents: Case study of deep penetration by non-aqueous phase liquids", *Journal of the Chartered Institution of Water and Environmental Management*, vol. 10, no. 4, pp. 263-272.

Letellier, M., Budzinski, H., Bellocq, J., & Connan, J. 1999, "Focused microwave-assisted extraction of polycyclic aromatic hydrocarbons and alkanes from sediments and source rocks", *Organic Geochemistry*, vol. 30, no. 11, pp. 1353-1365.

Liberty, B. A. B. T. E. Paleozoic geology of the Bruce Peninsula area, Ontario: Geological Survey of Canada, Memoir 360. 1-163. 1971. Geological Survey of Canada.
Ref Type: Serial (Book,Monograph)

Liikala, T. L., Olsen, K. B., Teel, S. S., & Lanigan, D. C. 1996, "Volatile organic compounds: Comparison of two sample collection and presentation methods", *Environmental Science & Technology*, vol. 30, no. 12, pp. 3441-3447.

Liu, Y. 2005, *Microwave Assisted Rapid Extraction of VOCs from Low Permeability Media,* Master's thesis, Chemistry Department, University of Waterloo.

Lopezavila, V., Young, R., & Beckert, W. F. 1994, "Microwave-Assisted Extraction of Organic-Compounds from Standard Reference Soils and Sediments", *Analytical Chemistry*, vol. 66, no. 7, pp. 1097-1106.

Manheim, F. T. 1968, "Disposable Syringe Techniques for Obtaining Small Quantities of Pore Water from Unconsolidated Sediments", *Journal of Sedimentary Petrology*, vol. 38, no. 2, p. 666-668.

Mazurek, M., Jakob, A., & Bossart, P. 2003, "Solute transport in crystalline rocks at Aspo - I: Geological basis and model calibration", *Journal of Contaminant Hydrology*, vol. 61, no. 1-4, pp. 157-174.

Mcglamery, M. D., Slife, F. W., & Butler, H. 1967, "Extraction and Determination of Atrazine from Soil", *Weeds*, vol. 15, no. 1, p. 35-38.

Mckay, L. D., Gillham, R. W., & Cherry, J. A. 1993, "Field Experiments in A Fractured Clay Till .2. Solute and Colloid Transport", *Water Resources Research*, vol. 29, no. 12, pp. 3879-3890.

Meyer, J. R. 2005, *Migration of a mixed organic contaminant plume in a multilayer sedimentary rock aquifer system,* Master's thesis, Earth Sciences Department, University of Waterloo.

Miles, J. & Shevlin, M. 2001, *Applying regression & correlation : a guide for students and researchers* Sage Publications, London.

Moran, M. J., Zogorski, J. S., & Squillace, P. J. 2007, "Chlorinated solvents in groundwater of the United States", *Environmental Science & Technology*, vol. 41, no. 1, pp. 74-81.

Mutch, R. D., Scott, J. I., & Wilson, D. J. 1993, "Cleanup of Fractured Rock Aquifers - Implications of Matrix Diffusion", *Environmental Monitoring and Assessment*, vol. 24, no. 1, pp. 45-70.

Neretnieks, I. 1980, "Diffusion in the Rock Matrix - An Important Factor in Radionuclide Retardation", *Journal of Geophysical Research*, vol. 85, no. NB8, pp. 4379-4397.

O'Hara, S. K., Parker, B. L., Jorgensen, P. R., & Cherry, J. A. 2000, "Trichloroethene DNAPL flow and mass distribution in naturally fractured clay: Evidence of aperture variability", *Water Resources Research*, vol. 36, no. 1, pp. 135-147.

Oliver, B. G. 1985, "Desorption of Chlorinated Hydrocarbons from Spiked and Anthropogenically Contaminated Sediments", *Chemosphere*, vol. 14, no. 8, pp. 1087-1106.

Pare, J. R. J., Belanger, J. M. R., Lesnik, B., Turpin, R., & Singhvi, R. 2001, "Final evaluation of US EPA method 3546: Microwave extraction, a microwave-assisted process (MAP (TM))

method for the extraction of contaminants under closed-vessel conditions", *Soil & Sediment Contamination*, vol. 10, no. 4, pp. 375-386.

Pare, J. R. J., Belanger, J. M. R., Li, K., Llompart, M. P., Singhvi, R., & Turpin, R. D. 1997, "Gas-phase extraction method using the microwave-assisted process (MAP(TM)) for the determination of aromatic contaminants in soil", *Spectroscopy-An International Journal*, vol. 13, no. 1, pp. 89-98.

Parker, B. L. 2007, "Investigating Contaminated Sites on Fractured Rock Using the DFN Approach", Portland, Maine.

Parker, B. L., Cherry, J. A., & Chapman, S. W. 2004, "Field study of TCE diffusion profiles below DNAPL to assess aquitard integrity", *Journal of Contaminant Hydrology*, vol. 74, no. 1-4, pp. 197-230.

Parker, B. L., Gillham, R. W., & Cherry, J. A. 1994, "Diffusive Disappearance of Immiscible-Phase Organic Liquids in Fractured Geologic Media", *Ground Water*, vol. 32, no. 5, pp. 805-820.

Parker, B. L., McWhorter, D. B., & Cherry, J. A. 1997, "Diffusive loss of non-aqueous phase organic solvents from idealized fracture networks in geologic media", *Ground Water*, vol. 35, no. 6, pp. 1077-1088.

Pavlostathis, S. G. & Mathavan, G. N. 1992, "Desorption-Kinetics of Selected Volatile Organic-Compounds from Field Contaminated Soils", *Environmental Science & Technology*, vol. 26, no. 3, pp. 532-538.

Pehme, P., Cherry, J. A., Parker, B. L., & Greenhouse, J. P. "The Potential for Compromised Interpretations When Based on Open Borehole Geophysical Data in Fractured Rock.", in *NGWA EPA Fractured Rock Conference*.

Perrin, J. 2007, *MW 367-9 and MW 22 Geological Report*, University of Waterloo.

Plett, J. H. 2006, *Metolachlor and TCE plume characteristics in a Dolostone aquifer using a transect,* Master's thesis, Earth Sciences Department, University of Waterloo.

Polak, A., Grader, A. S., Wallach, R., & Nativ, R. 2003, "Chemical diffusion between a fracture and the surrounding matrix: Measurement by computed tomography and modeling", *Water Resources Research*, vol. 39, no. 4.

Rawa-Adkonis, M., Wolska, L., & Namiesnik, J. 2003, "Modern techniques of extraction of organic analytes from environmental matrices", *Critical Reviews in Analytical Chemistry*, vol. 33, no. 3, pp. 199-248.

Resident Geologist Program, M. Geology of the Southwestern District. http://www.mndm.gov.on.ca . 5-21-2004. Government of Ontario, Canada. 1-12-0008. Ref Type: Electronic Citation

Rice, S. L. & Mitra, S. 2007, "Microwave-assisted solvent extraction of solid matrices and subsequent detection of pharmaceuticals and personal care products (PPCPs) using gas chromatography-mass spectrometry", *Analytica Chimica Acta*, vol. 589, no. 1, pp. 125-132.

Richards, L. A. 1941, "A pressure-membrane extraction apparatus for soil solution", *Soil Science*, vol. 51, no. 1, pp. 377-386.

Rider, M. 1996, *The Geological Interpretation of Well Logs*, 2nd edn, Gulf Publishing Company, Houston.

Rolston, D. E. 2007, "Historical development of soil-water physics and solute transport in porous media", *Water Science & Technology: Water Supply*, vol. 7, no. 1, pp. 59-66.

Siegrist, R. L. & Jenssen, P. D. 1990, "Evaluation of Sampling Method Effects on Volatile Organic-Compound Measurements in Contaminated Soils", *Environmental Science & Technology*, vol. 24, no. 9, pp. 1387-1392.

Singer, S. N., Cheng, C. K., & Scafe, M. G. 2003, *The Hydrogeology of Southern Ontario, Second Edition*, Ontario Ministry of the Environment, Toronto, 1.

Smith, A. L. & Legault, J. A. 1985, "Preferred orientations of Middle Silurian Guelph-Amabel reefs of southern Ontario", *Bulletin of Canadian Petroleum Geology*, vol. 33, pp. 421-426.

Smith, M. P. 1986, "Calibration, Checking and Physical Corrections for a New Dual-Spaced Neutron Porosity Tool", in *SPWLA Twenty-seventh Annual Logging Symposium*.

Spence, M. J., Thornton, S. F., Bottrell, S. H., & Spence, K. H. 2005, "Determination of interstitial water chemistry and porosity in consolidated aquifer materials by diffusion equilibrium-exchange", *Environmental Science & Technology*, vol. 39, no. 4, pp. 1158-1166.

Sporring, S., Bowadt, S., Svensmark, B., & Bjorklund, E. 2005, "Comprehensive comparison of classic Soxhlet extraction with Soxtec extraction, ultrasonication extraction, supercritical fluid extraction, microwave assisted extraction and accelerated solvent extraction for the determination of polychlorinated biphenyls in soil", *Journal of Chromatography A*, vol. 1090, no. 1-2, pp. 1-9.

Statistics Canada. Guelph, Ontario (table). *2006 Community Profiles,* 2006 Census, Statistics Canada Catalogue no.92-591-XWE. Ottawa. 2007. Ottawa.
Ref Type: Generic

Sterling, S. N. 1999, *Comparison of Discrete Depth Sampling Using Rock Core and a Removable Multilevel System in a TCE Contaminated Fractured Sandstone,* Master's thesis, Earth Sciences Department, University of Waterloo.

Sterling, S. N., Parker, B. L., Cherry, J. A., Williams, J. H., Lane, J. W., & Haeni, F. P. 2005, "Vertical cross contamination of trichloroethylene in a borehole in fractured sandstone", *Ground Water*, vol. 43, no. 4, pp. 557-573.

Stiles, W. & Jorgensen, I. 1914, "The nature and methods of extraction of the soil solution", *Journal of Ecology*, vol. 2, pp. 245-250.

Stromswold, D. C., Mills, W. R., Wilson, R. D., & Cook, T. K. 1989, "Formation Porosity Measurement Using Epithermal Neutron Lifetime", *Ieee Transactions on Nuclear Science*, vol. 36, no. 1, pp. 1210-1214.

Sudicky, E. A. & Frind, E. O. 1982, "Contaminant Transport in Fractured Porous-Media - Analytical Solutions for A System of Parallel Fractures", *Water Resources Research*, vol. 18, no. 6, pp. 1634-1642.

Sudicky, E. A. & Mclaren, R. G. 1992, "The Laplace Transform Galerkin Technique for Large-Scale Simulation of Mass-Transport in Discretely Fractured Porous Formations", *Water Resources Research*, vol. 28, no. 2, pp. 499-514.

Tang, D. H., Frind, E. O., & Sudicky, E. A. 1981, "Contaminant Transport in Fractured Porous-Media - Analytical Solution for A Single Fracture", *Water Resources Research*, vol. 17, no. 3, pp. 555-564.

Therrien, R. & Sudicky, E. A. 1996, "Three-dimensional analysis of variably-saturated flow and solute transport in discretely-fractured porous media", *Journal of Contaminant Hydrology*, vol. 23, no. 1-2, pp. 1-44.

Tittle, C. W. & Allen, L. S. 1966, "Theory of Neutron Logging .2", *Geophysics*, vol. 31, no. 1, p. 214-224.

Turner, C. M. 2001, *Origin and behaviour of TCE and metolachlor contamination in a fractured dolostone water supply aquifer,* Master's thesis, Earth Sciences Department, University of Waterloo.

US EPA 1996, *Test Methods for Evaluating Solid Waste, Physical/Chemical Methods: method 8260B volatile organic compounds by gas chromatography/mass spectrometry (GC/MS)*, US EPA, Washington, DC, Technical Report SW-846 Chapter 4.3.2.

UW Weather Station. 15 Minute Data, Preciption, Temperature. http://weather.uwaterloo.ca/data.html . 2005.
Ref Type: Electronic Citation

Walkley, A. & Black, I. A. 1934, "An examination of the Degtjareff method for determining soil organic matter, and a proposed modification of the chromic acid titration method", *Soil Science*, vol. 37, no. 1, pp. 29-38.

Westbay Instruments Inc. 1994, *Multi-level Groundwater Monitoring System with the MP System*.

Wilcoxon, F. 1945, "Individual Comparisons by Ranking Methods", *Biometrics Bulletin*, vol. 1, no. 6, pp. 80-83.

Williams, I. H. 1968, "Note on Effect of Water on Soxhlet Extraction of Some Organochlorine Insecticides from Soil and Comparison of This Method with 3 Others", *Journal of the Association of Official Analytical Chemists*, vol. 51, no. 3, p. 715-717.